PHYSICALLY AWARE AGILE OPTICAL NETWORKS

by

Wenhao Lin

A dissertation submitted in partial fulfillment
of the requirements for the degree

of

Doctor of Philosophy

in

Engineering

MONTANA STATE UNIVERSITY
Bozeman, Montana

July 2008

©COPYRIGHT

by

Wenhao Lin

2008

All Rights Reserved

APPROVAL

of a dissertation submitted by

Wenhao Lin

This dissertation has been read by each member of the dissertation committee and has been found to be satisfactory regarding content, English usage, format, citations, bibliographic style, and consistency, and is ready for submission to the Division of Graduate Education.

Dr. Richard S. Wolff

Approved for the Department of Electrical and Computer Engineering

Dr. Robert C. Maher

Approved for the Division of Graduate Education

Dr. Carl A. Fox

STATEMENT OF PERMISSION TO USE

In presenting this dissertation in partial fulfillment of the requirements for a doctoral degree at Montana State University, I agree that the Library shall make it available to borrowers under rules of the Library. I further agree that copying of this dissertation is allowable only for scholarly purposes, consistent with "fair use" as prescribed in the U.S. Copyright Law. Requests for extensive copying or reproduction of this dissertation should be referred to ProQuest Information and Learning, 300 North Zeeb Road, Ann Arbor, Michigan 48106, to whom I have granted "the exclusive right to reproduce and distribute my dissertation in and from microform along with the non-exclusive right to reproduce and distribute my abstract in any format in whole or in part."

Wenhao Lin

July 2008

ACKNOWLEDGEMENTS

I am grateful to acknowledge and thank all of those who assisted me in my graduate study at Montana State University.

First, I would like to express my deepest gratitude to my advisor, Dr. Wolff, for his excellent guidance, caring, patience, and providing me with an excellent condition for doing research. Without his guidance and help, I would never have been able to finish my dissertation.

I would also like to express my thanks and appreciation to Dr. Mumey for his assistance and support in my research. The contributions and expertise provided by Dr. Mumey have improved the quality of my research.

Special thanks are given to my other graduate committee members for their valuable suggestions and comments. Special thanks also go to my colleague students, Trent Jackson, Timothy Hahn, and Sriharsha K. Pavan, in the optical research group. I enjoy the meetings and discussions we had on optical communication research.

At last, I would like to thank my parents and wife for their support and encouragement throughout these years, and take this opportunity to thank my daughter, Michelle, for all the happiness she has brought to us. She will come to this world very soon and we are willing to send her all our loves and good wishes.

TABLE OF CONTENTS

1. INTRODUCTION 1

Evolution of Optical Networks 1
Overview of All-Optical Routing 3
Motivation and Outline of the Dissertation 7

2. FIBER OPTIC COMMUNICATION NETWORKS 11

Introduction 11
Network Components 12
Transmitters 12
Multiplexers and Demultiplexers 14
Fiber Properties 15
Optical Amplifiers 20
Optical Switches 21
Receivers 22
Signal Propagation and Physical Impairments 24
Linear Effects 26
Attenuation 26
Dispersion 27
ASE Noise 28
Gain Non-Flatness of EDFA 28
MEMS Switch Transients 29
OXC Crosstalk 29
Non-Linear Effects 30
Self-Phase Modulation 31
Cross-Phase Modulation 31
Four-Wave Mixing 31
Stimulated Inelastic Scattering 31
Temporal Effects 32
Detector Effects 34

3. MODELING ALL-OPTICAL NETWORKS 37

Introduction 37
Simulating the Physical Layer 39
Modeling the Physical Layer 39
Simulating Pulse Propagation and the Split-Step Fourier Method 41
The Nonlinear Schrödinger Equation 41
The Coupled Nonlinear Schrödinger Equations 42
The Split-Step Fourier Method 43
Improving Simulation Efficiency by Grid Computing 46

TABLE OF CONTENTS – CONTINUED

Introduction to PHOTOSS™ and OptSim™ 48
PHOTOSS™ 48
OptSim™ 55
Simulating the Network Layer 58
Modeling the Network Layer 59
Architecture of the OPNET™ Simulation System 62

4. ANALYTICAL MODELS FOR THE ASSESSMENT OF FIBER NONLINEAR EFFECTS 64

Introduction 64
Analytical Model for the Assessment of XPM 66
XPM in A Single Fiber 67
The Incremental Transfer Function 67
Power Evolution of the Pump Channel 70
The XPM Transform Function 71
XPM in Optical Links 73
FOCS Links 73
DUCS Links 74
XPM in Optical Lightpaths 76
Numerical Simulation of XPM 78
Analytical Model for the Assessment of FWM 83
FWM in A Single Fiber 83
FWM in Optical Links 86
FWM in Optical Lightpaths 88
Numerical Simulation of FWM 89
Analytical Model for the Assessment of Multiple Nonlinear Effects 96
Case 1: FWM dominates 97
Case 2: XPM dominates 98
Case 3: Equally dominate 98
Discussion 100

5. SUPPRESSION OF NETWORK TRANSIENTS 102

Introduction 102
Suppression of Switch Transients 104
Experiment on MEMS transients 104
Method for Eliminating Switch Transients 106
Suppression of In-Line Amplifier Transients 108
Working Principle 109
Performance of Power Shaping in Circuit/Burst-Switched Networks 111
Performance of Power Shaping in Packet-Switched Networks 114

TABLE OF CONTENTS – CONTINUED

Scenario A 117
Scenario B 118
Sensitivity to the Shaping-Period 121
Experimental Validation 122
Discussion 124
Suppression of In-Line Amplifier Transients at Network Failures 127
System Design 128
Numerical Simulation 130
Discussion 133

6. ADAPTIVE RWA ALGORITHMS FOR TRAFFIC ENGINEERING ... 137

Introduction 137
A Lexicographically Optimized Routing Algorithm (LORA) for All-Optical Networks 139
Network Model 140
The Design of LORA 142
Dynamically Changing β 145
Numerical Simulation and Analysis 146
A Markov-Based Reservation Algorithm (MBR) for Wavelength Assignment in All-Optical Networks 149
Markov Modeling of Optical Links 151
Detecting Interfering Connection Requests 157
Signaling Procedures of MBR 158
Numerical Simulation and Analysis 160
The Poisson Traffic Model 162
The Pareto Traffic Model 165
Discussion 167

7. QoS FRAMEWORK FOR All-OPTICAL NETWORKS 170

Introduction 170
Network Model 174
QoS Framework for All-Optical Networks 178
Physically Aware Routing Algorithm (PAR) 179
Link Cost Function 179
Pruning the Search Space 179
Physically Aware Backward Reservation Protocol (PABR) 181
Signaling Procedures of PABR 181
Estimation of Lightpath Signal Quality 185
Preserve Lightpath Signal Quality 189
Numerical Simulation and Analysis 192

TABLE OF CONTENTS – CONTINUED

The NSF Network Topology 195
The Mesh Network Topology 204
Discussion 206

8. CONCLUSIONS AND FUTURE WORK 209

Conclusions 209
Future Work 212

REFERENCES CITED 214

APPENDICES 223

APPENDIX A - Matlab Code for Simulating Pulse Propagation 224
APPENDIX B - XML Configuration File for the NSF Network 228
APPENDIX C - Matlab Code for Counting FWM Mixing Terms 233

LIST OF TABLES

Table Page

2.1. Different physical impairments in optical networks 26

3.1. Global variables of a PHOTOSS^{TM} simulation 53

3.2. Global variables of an OptSim^{TM} simulation 59

5.1. Power shaping simulation parameters 116

5.2. The controlling table of generator controller used in a simulation 132

6.1. Results of sensitivity experiments using the Poisson traffic model 165

6.2. Results of sensitivity experiments using the Pareto traffic model . 166

7.1. Physical characteristics of an optical span 193

7.2. PABR simulation parameters 194

LIST OF FIGURES

Figure Page

1.1. Structure of an ASON network 3

2.1. Structure of a point-to-point WDM transmission system 12

2.2. Structure of a DFB laser 13

2.3. Structure of an optical demultiplexer 14

2.4. Structure of an add-drop multiplexer 15

2.5. Structure of a single-mode fiber and the geometrical optics theory of wave guiding 16

2.6. Dispersion of a typical single-mode fiber 19

2.7. Structure of an EDFA using the co-propagating pumping scheme 20

2.8. The general structure of an optical switch 22

2.9. Structure of a MEMS wavelength routing switch 23

2.10. Structure of a *pin* detector 24

2.11. Gain profile of an EDFA 29

2.12. Transient behavior of output power due to MEMS switch closure 30

2.13. Transient response of a gain-clamped EDFA chain 33

3.1. PHOTOSS^{TM} model of a lightpath 40

3.2. Architecture of Grid_sim 47

3.3. Main window of PHOTOSS^{TM} 49

3.4. Property window of PPG 51

3.5. The structure of a span defined in the *Iterator* component 51

LIST OF FIGURES – CONTINUED

Figure Page

3.6. Property window of an optical fiber 53

3.7. PHOTOSS^{TM} simulation configuration 55

3.8. OptSim^{TM} simulation model for investigating the performance of power shaping 56

3.9. OptSim^{TM} model of AOGC_EDFA 58

3.10. OPNET^{TM} model for the control plane of the NSF network 60

3.11. Structure of an optical workstation sub-network 61

3.12. Logical relationship between processes created for a connection .. 63

4.1. Example eye-diagram 66

4.2. Lightpath1 and co-propagating lightpaths 76

4.3. XPM simulation setup 79

4.4. Comparison of the Q factor of a probe channel in a FOCS link ... 80

4.5. Comparison of the Q factor of a probe channel in a DUCS link ... 81

4.6. Sensitivity of the XPM analytical model to the increase of channel power 82

4.7. Comparison of XPM-generated noise waveforms on CW and dynamic probe channels 83

4.8. Illustration of FWM 84

4.9. FWM simulation setup for a single fiber segment 90

4.10. Comparison of the Q factor of a powered-off probe channel in a fiber segment with 5 channels 91

LIST OF FIGURES – CONTINUED

Figure Page

4.11. Comparison of the Q factor of a powered-on probe channel in a fiber segment with 5 channels 92

4.12. Comparison of the Q factor of a powered-on probe channel in a fiber segment with 21 channels 93

4.13. FWM simulation setup for an optical link 94

4.14. Comparison of the Q factor of a powered-off probe channel in an optical link 95

4.15. Comparison of the Q factor of a powered-on probe channel in an optical link 95

4.16. Simulation setup for investigating signal quality when both XPM and FWM are active 97

4.17. Comparison of the Q factor of a probe channel at the output of each span (case 1) 98

4.18. Comparison of the Q factor of a probe channel at the output of each span (case 2) 99

4.19. Comparison of the Q factor of a probe channel at the output of each span (case 3) 100

5.1. Working principle of EDFA amplifiers 103

5.2. Experiment setup for the observation of MEMS switch transients 104

5.3. Temporal behavior of MEMS switch output power when cross-connection is closed 105

5.4. Temporal behavior of MEMS switch output power when cross-connection is opened 106

5.5. Working principle of power shaping 110

LIST OF FIGURES – CONTINUED

Figure Page

5.6. OptSim™ model for simulating the application of power shaping in circuit-switched networks 112

5.7. Comparison of power transients on CW2 with and without power shaping in circuit-switched networks 113

5.8. Comparison of power transients on channel 10 with and without power shaping using the self-similar traffic pattern 117

5.9. Comparison of power transients on channel 10 with and without power shaping using the Poisson traffic pattern 118

5.10. Comparison of power transients on channel 10 with and without power shaping using the self-similar traffic pattern in a mixed scenario 119

5.11. Comparison of power transients on channel 10 with and without power shaping using the Poisson traffic pattern in a mixed scenario 121

5.12. Power transients on channel 10 with varying shaping-period 122

5.13. Experiment setup for testing the effectiveness of power shaping .. 123

5.14. Transients on the probe channel when no power shaping is applied 124

5.15. Comparison of transient amplitudes for linear shaping profile 125

5.16. Design of TPC 130

5.17. OptSim™ simulation model for TPC 132

5.18. Power evolution of each wavelength in TPC simulation 133

5.19. Comparison of transients with and without TPC when different numbers of channels are dropped in a network failure 134

5.20. Comparison of TPC performance with varying TP_{cmp} 134

LIST OF FIGURES – CONTINUED

Figure Page

6.1. Two paths between S and D with different wavelength utilizations 144

6.2. The NSF network topology 147

6.3. Optimal value of β versus traffic load with hill climbing step resolution 0.1 147

6.4. Performance comparison of LORA and benchmark algorithms 148

6.5. An example of reservation confliction 149

6.6. The C-T Markov chain of an optical link with N wavelengths..... 153

6.7. Prediction of the behavior of a C-T Markov chain 156

6.8. Example of interfering connection requests 158

6.9. The mesh network topology 161

6.10. Comparison of MBR and benchmark algorithms on the NSF and mesh networks using the Poisson traffic model 162

6.11. Comparison of the performance of MBR on the NSF and mesh networks 163

6.12. Comparison of the performance of MBR on the NSF network in two wavelength configurations 164

6.13. Comparison of MBR and benchmark algorithms on the NSF and mesh networks using the Pareto traffic model 166

7.1. Lightpath3 and co-propagating lightpaths 191

7.2. Structure of an optical span 193

7.3. The NSF network topology with numbers of spans for edges 196

LIST OF FIGURES – CONTINUED

Figure Page

7.4. Comparison of the blocking probabilities of different algorithms on the NSF network with $N = 5$ 197

7.5. Comparison of the blocking probabilities due to 'None_resource' of different algorithms on the NSF network with $N = 5$ 198

7.6. Comparison of the blocking probabilities due to 'Bad_quality' of different algorithms on the NSF network with $N = 5$ 198

7.7. Comparison of the blocking probabilities of different algorithms on the NSF network with $N = 10$ 199

7.8. Comparison of the blocking probabilities due to 'None_resource' of different algorithms on the NSF network with $N = 10$ 200

7.9. Comparison of the blocking probabilities due to 'Bad_quality' of different algorithms on the NSF network with $N = 10$ 200

7.10. Comparison of the blocking probabilities of different algorithms on the NSF network when varying N 202

7.11. Comparison of the blocking probabilities due to 'None_resource' of different algorithms on the NSF network when varying N .. 203

7.12. Comparison of the blocking probabilities due to 'Bad_quality' of different algorithms on the NSF network when varying N .. 203

7.13. The mesh network topology with numbers of spans for edges 204

7.14. Comparison of the blocking probabilities of different algorithms on the mesh network with $N = 10$ 205

7.15. Comparison of the blocking probabilities due to 'None_resource' of different algorithms on the mesh network with $N = 10$ 205

7.16. Comparison of the blocking probabilities due to 'Bad_quality' of different algorithms on the mesh network with $N = 10$ 206

ABSTRACT

With the development of new laser sources, fiber amplifiers, and other optical components, optical communication systems have undergone enormous growth and evolution in recent decades. The current trend of optical networking is to move towards dynamic, all-optical networks. In all-optical networks, information signals are transmitted from source to destination totally in the optical domain, without the usual optical-electrical-optical conversions at intermediate nodes. New challenges and opportunities emerge in different layers of the optical network architecture in this transition process.

This research work explores several interesting topics in both the physical layer and the network layer of all-optical networks. Our studies examine physical impairments which can adversely influence network performance. Both novel proactive and reactive approaches are proposed to improve network performance and provide quality of service (QoS) for users.

In the physical layer, network transients, including switch transients and amplifier transients, can pose a serious threat to signal quality in dynamic networks. In all-optical networks, these transients can escalate along a lightpath. In this research, a new functionality is added to the backward reservation protocol to eliminate switch transients and a power shaping technique implemented at the link layer is proposed to decrease in-line amplifier transients. Compared to other approaches in the literature, our designs are more general, economical, and can seamlessly cooperate with other solutions.

In the network layer, a new QoS framework is proposed to provide QoS assurance in all-optical networks. The framework has two parts: the Physically Aware Routing algorithm (PAR) and the Physically Aware Backward Reservation protocol (PABR). Analytical models are incorporated into the QoS framework to predict lightpath signal quality with fiber nonlinear effects and ASE noise. For a connection request, the source node executes PAR to select a set of candidate paths which can possibly satisfy the user QoS requirement, and then starts PABR to probe candidate paths in parallel. The destination node selects a satisfactory lightpath from candidate paths. New functionality is designed in PABR to guarantee the signal quality of a lightpath during its life time. The proposed QoS framework is more efficient, scalable, and flexible compared to other benchmark algorithms.

1

INTRODUCTION

Evolution of Optical Networks

Optical networks are the infrastructure of our information society. In less than 25 years, optical systems have undergone a tremendous evolution. Starting from the unrepeated point-to-point transmission in the 1980s, the inventions of wavelength division multiplexing (WDM) and optical amplifiers have led to an explosion of system capacity, system reach, and network architecure.

The currently deployed optical networks use point-to-point links between switch nodes and repeaters, and are called opaque networks. Electrical signals are converted to the optical domain for transmission at the edge of a network. At intermediate nodes (e.g. switches, add-drop multiplexers, and repeaters) signals are converted back to the electrical domain for processing and are converted to the optical domain again for transmission along the next hop, the so called OEO (optical-electrical-optical) conversion. Multiple channels, each using a different wavelength, can be used for transmitting multiple information signals at the same time in a fiber. For state of the art transmission systems, a fiber can have 100 channels each with a transmission rate of 10Gbps. Optical amplifiers can be deployed along an optical link to extend transmission distance. Multiple channels passing through an optical amplifier are amplified simultaneously. However, opaque networks have the shortcomings of being

inflexible, un-scalable, and expensive. For example, if the optical modulation format or transmission speed is to be changed, then all the regenerators may need to be replaced.

The trend in optical network development is to move towards dynamic all-optical networks, also called transparent networks, including circuit-switched, burst-switched, and packet-switched networks. In all-optical networks, information is transmitted from source to destination totally in the optical domain without the OEO conversions at intermediate points. The advantages are multifold. The large number of devices for OEO conversion are not required and greatly decreases deployment costs. The decreased number of components in a network can also reduce the administration effort and the probability of network-element failure. Furthermore, the offering of dynamic bandwidth provisioning can bring new revenue to carrier companies.

The architecture of the next-generation dynamic all-optical networks, also named the automatically switched optical network (ASON) in the literature, is shown in Figure 1.1 [1]. The network has three layers: the transport plane, the control plane, and the management plane. In the transport plane, user information is transmitted from the source to the destination in the optical domain along a lightpath. The control plane plays a crucial role and supports the functionalities of managing and allocating network resources, signaling the creation of a lightpath, providing network-network interfaces (NNI) to facilitate the exchange of relevant data with neighboring domains,

and providing user-network interfaces (UNI) to enable automated bandwidth provisioning on demand [1]. In Figure 1.1, the centralized management plane is shown only as an example, and distributed management planes can also be applied in optical networks.

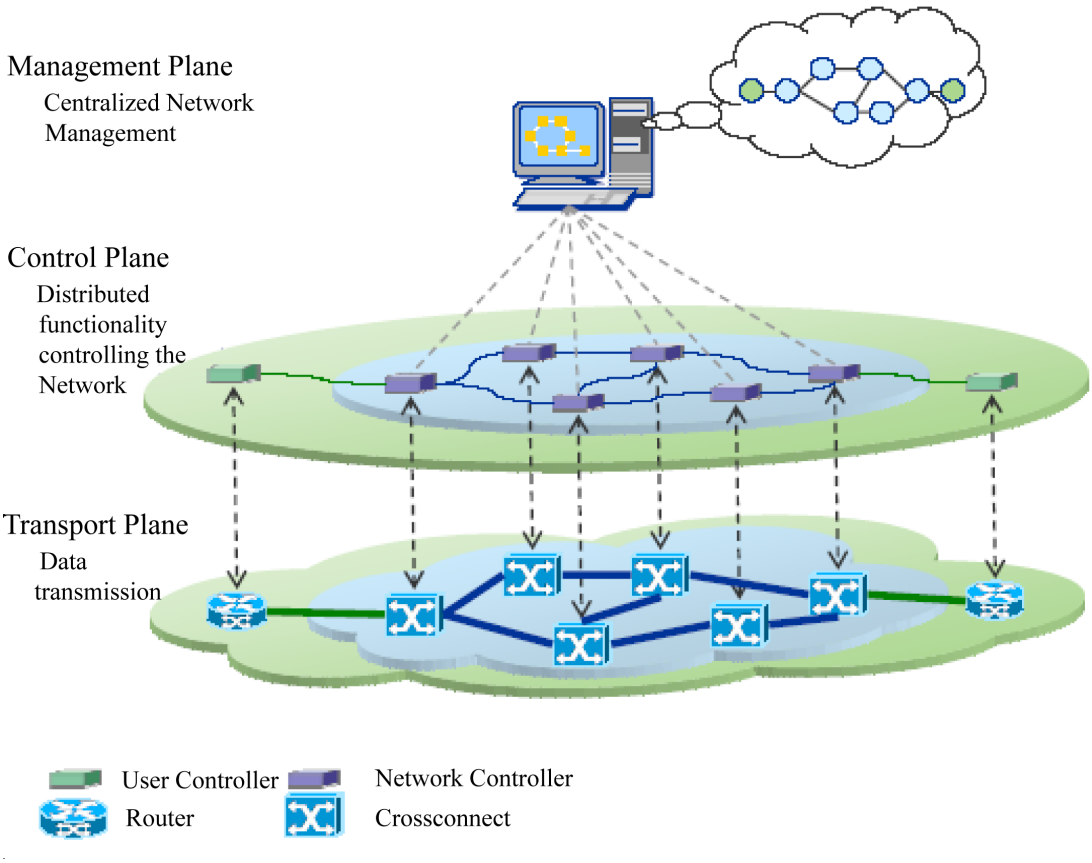

Figure 1.1. Structure of an ASON network [1].

4

Overview of All-Optical Routing

One basic problem of all-optical routing is to find a path and a free wavelength for a source-destination pair such that traffic data can be transmitted along the lightpath (path+wavelength) without the need to convert to electrical signal or change wavelength at intermediate points. This is referred to in the literature as the routing and wavelength assignment (RWA) problem of optical routing. Traditionally, the RWA problem is addressed by a two-step process to decrease complexity: first find a path from the source to the destination using a routing algorithm, and then pick a free wavelength on the chosen path using a wavelength-assignment algorithm. The constraints of the RWA problem may include wavelength continuity, physical impairments, and traffic engineering considerations. The wavelength-continuity constraint requires a connection to use the same wavelength along a lightpath. In some networks, wavelength converters are deployed at switch nodes and the wavelength-continuity constraint can be relaxed. However, wavelength converters are expensive and we assume no converter exists in networks for our research. The traffic engineering constraints aim to improve resource-usage efficiency and decrease connection blocking probability. The physical impairment constraints are used to guarantee signal quality to some level.

A large number of routing and wavelength-assignment algorithms designed to efficiently use network resources and provide satisfactory service to network users have

been proposed for all-optical networks. These routing algorithms can be classified in two categories: static and adaptive. In static routing algorithms (e.g. fixed routing [2], fixed-alternative routing [2]), one or several paths are pre-computed for each source-destination pair. Static routing can decrease the connection provisioning time, but can't respond to dynamic traffic conditions in a network. Adaptive routing algorithms (e.g. shortest-path [2], shortest-cost-path [3], and least-congested-path [4]) usually use the Dijkstra algorithm to compute a minimal cost path from source to destination. The definition of the link cost function is critical for such algorithms.

There are also several wavelength-assignment algorithms in the literature. In the Random algorithm [2], one free wavelength is randomly selected from among the unused wavelengths on the chosen path. In the First-fit algorithm [2], the free wavelength with the smallest index is selected. In the Most-used algorithm [2], the free wavelength which is used most often in the network is selected. In the Least-used algorithm [2], the free wavelength which is used least in the network is selected. The Min-product [5], Least-loaded [6], Max-sum [7], and Relative-capacity-loss [8] algorithms have been proposed for multi-fiber networks. The performance of different wavelength-assignment algorithms were compared in [3]. It was reported that when the network is lightly loaded, the Most-used algorithm is the best and the Least-used algorithm is the worst, where 'best' and 'worst' are defined in terms of connection blocking probability. When the network is heavily loaded, there are no big differences among the performance of these wavelength-assignment algorithms. We notice that in

the Most-used algorithm, free wavelengths in a network are less segmented than with other algorithms (i.e. the free wavelengths are more continuous in the wavelength index space). Hence connections with large hop count have a larger chance of being accepted.

Two routing-and-assignment architectures have been proposed for all-optical networks: centralized and distributed [2]. The centralized architecture is similar to the approach used in a circuit-switched telephone network, whereas the distributed approach is similar to a packet data network such as the Internet. In the centralized architecture, a controlling node monitors the network state and controls all resource allocation. Upon receiving a connection request, an edge node sends a message to the controlling node. The controlling node executes the routing algorithm and the wavelength-assignment algorithm. Upon deciding a path and a free wavelength, the controlling node will reserve resources on all nodes along the path. This architecture poses problems such as performance bottleneck, single point of failure, and scalability. In the distributed control architecture, information about network state is broadcast periodically and each edge node can compute the path upon receipt of a connection request. Distributed control is more scalable and robust. Upon receiving a connection request, an edge node first executes the routing algorithm to compute a path. It then starts the wavelength-reservation protocol. The wavelength-assignment algorithm can be executed by either the destination node or the source node to pick a free wavelength.

In the distributed control architecture, two wavelength reservation approaches can be applied: the forward reservation protocol and the backward reservation protocol. In the forward reservation, a 'resv' (reservation) message (specifying the path and wavelength computed by an edge node) is sent from source to destination on the specified path. When an intermediate node receives 'resv', it executes the resource reservation operation. When the destination node receives 'resv', a 'conf' (confirmation) message is sent upstream. In the backward reservation, a 'probe' (probe) message (specifying the path computed by an edge node) is sent from source to destination. The message collects wavelength-state information on the relevant optical links from intermediate nodes as it propagates on the specified path. After receiving the 'probe' message, the destination node picks one free wavelength using one of the wavelength-assignment algorithms and a 'resv' message is sent upstream to finish the actual resource reservation.

In currently deployed commercial optical networks, traffics are rather static and the duration of a connection can be in the scale of weeks or months (e.g. IP over WDM). However, with the emergence of new applications and services, traffics are becoming more dynamic and lightpaths need to be created and torn down dynamically under request. The development of optical networks (including circuit-switched, burst-switched, and packet-switched all-optical networks) requires highly efficient routing and wavelength assignment (RWA) algorithms.

Motivation and Outline of the Dissertation

Most papers about optical routing assume that all the physical links and network components are perfect. That is, the links are equal in performance and introduce no impairments to optical signal. This is not true in practical networks. When an optical signal is propagated in a fiber, it will experience linear and nonlinear impairments. These impairments will accumulate along a lightpath, resulting in degraded performance, evidenced by the increased bit-error-rate (BER) and other factors. This problem is of particular concern in an all-optical network, as there are no intermediate OEO conversions or regenerators, where the impairments would be removed. Other factors such as non-ideal components, traffic-dependent behavior, how the facilities are used (number of wavelengths, channel power, etc.), and temporal effects that are transient in nature induced by changes such as switching will further complicate the scenario and degrade network performance. To meet end-to-end service requirements, efficient strategies need to be designed to mitigate these impairments. Network routing algorithms need to be aware of signal quality and intelligently choose an appropriate lightpath.

Several routing algorithms that consider physical impairments were recently proposed [9][12]. Each paper considered two or three types of impairments in an example network configuration. Estimations of the end-to-end OSNR (optical signal to noise

ratio) or BER (bit error rate) were provided. In the proposed algorithms, one lightpath which satisfies the OSNR or BER requirements is picked from a set of candidate lightpaths. The difficulty of such routing algorithms is how to make them efficient and scalable.

In this dissertation, some important types of physical impairments are examined in detail and new solutions are designed to mitigate their effects. New analytical models are designed to predict the effects of some of the most important nonlinear phenomena on signal quality in a complex network environment. Finally, a new framework of QoS routing for dynamic all-optical networks is proposed, implemented, and studied. The proposed QoS framework is shown to be efficient, modular and scalable.

The remainder of this dissertation is organized as follows. Chapter 2 provides a review and additional background of optical networks. Chapter 3 focuses on how to model the physical layer and the network layer of all-optical networks. Three commercial simulation programs, including PHOTOSS^{TM},OptSim^{TM}, and OPNET^{TM}, are also briefly introduced. In Chapter 4, analytical models for predicting the effects of nonlinear phenomena on signal quality are developed. These mathematical models are used in the proposed QoS framework for predicting lightpath signal quality. In Chapter 5, network transients, including switch transients and amplifier transients, are studied. Unique solutions to mitigate the effects of network transients are also proposed and verified through simulations and experiments. In Chapter 6, two new

RWA algorithms for traffic engineering are proposed and discussed. In Chapter 7, the data structure, algorithms, implementation, and application of the new framework of QoS routing in all-optical networks are explained and investigated in detail. Conclusions are given in Chapter 8.

FIBER OPTIC COMMUNICATION NETWORKS

Introduction

Optical transmission systems have evolved through five generations. The present generation systems use low-attenuation single-mode fibers (SMFs) or dispersion-shifted fibers (DSFs) as the transmission medium. Attenuation is periodically compensated using optical amplifiers such as erbium doped fiber amplifiers (EDFAs). One optical amplifier can amplify all the input channels (i.e. wavelengths) at the same time. Dispersion is periodically compensated using dispersion-compensation fibers (DCFs). In one fiber, multiple channels can be used for transmitting traffic data simultaneously (e.g. wavelength division multiplexing (WDM)), each with transmission rate of 10Gbps or greater. With periodic amplification, an optical link can extend across thousands of kilometers without regeneration. Figure 2.1 schematically shows the structure of a point-to-point optical transmission system [13]. The functions of its components will be described later.

Communication networks using state of the art optical transmission technologies constitute the backbone of today's information infrastructure. In recent years, these communication networks have begun to evolve towards all-optical networks.

In this chapter, first, some basic components in optical networks are briefly reviewed. Next, the concept of optical pulse propagation is introduced. Finally, different

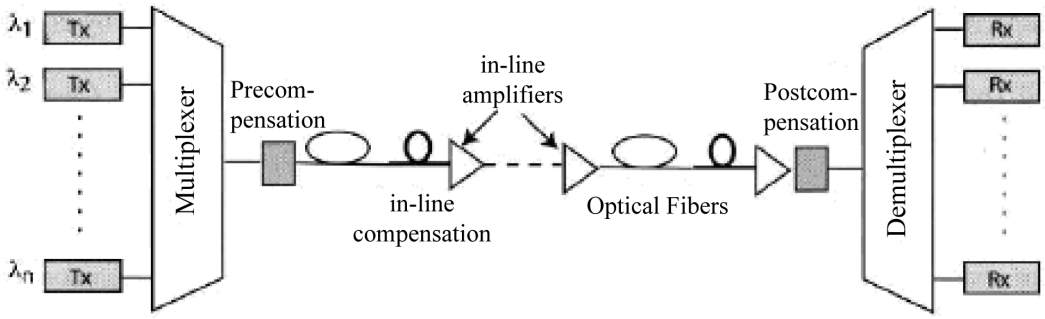

Figure 2.1. Structure of a point-to-point WDM transmission system [13].

physical impairments, such as loss, chromatic dispersion, polarization-mode dispersion, and switch crosstalk, are explained in detail. These impairments can degrade signal quality and potentially cause nework performance outage. They are the major concerns in the research of this dissertation.

Network Components

Transmitters

Optical transmitters usually use a semiconductor laser diode as light source. Its working principle is based on the physical phenomenon of stimulated emission. As an example, Figure 2.2 shows the structure of a DFB (distributed feed-back) laser diode [14].

The p-n junction in Figure 2.2 is forward-biased. Electrons are pumped into the excited state by drive circuits and the 'population inversion' is achieved. A given wavelength from the ASE (amplified spontaneous emission) spectrum is amplified by

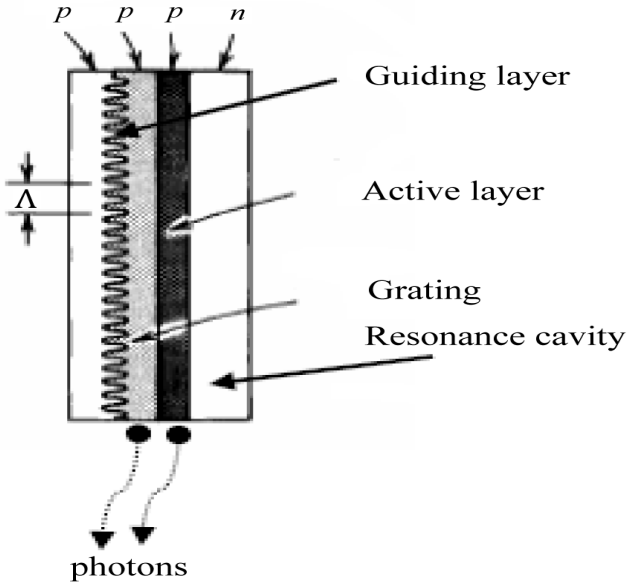

Figure 2.2. Structure of a DFB laser [14]. The periodic grating structure works as a distributed reflective mirror, thus the name DFB.

the active medium and reflected back and forth in the laser cavity. Single longitude-mode operation is achieved by using the grating structure shown in Figure 2.2. Such a semiconductor laser diode is called the distributed feedback (DFB) laser diode, and is commonly used in the optical communication industry. The output optical beam of a laser diode has the properties of high output power and narrow spectral width (several MHz).

Two modulation methods can be applied. One is called the direct modulation, where current or voltage input of the laser diode is modulated by data signal. A major drawback of direct modulation is the generation of phase noise, which is caused by variation of the refractive index induced by the changes of carrier density. Another

modulation method is called the external modulation. The output beam of a laser diode, which is operated at constant output power, is coupled to an optical modulator. The transmissivity of the modulator is controlled by a data signal. The laser diode works in the continuous-wave (CW) mode, and thus can has much lower noise compared to the direct modulation method.

Most optical systems use an intensity modulated signal format (sometimes called the on-off keying (OOK)), where the intensity of optical pulses represents the signal information. In the discussion of this dissertation it is assumed that the optical networks are digital communication systems and use intensity modulation.

Multiplexers and Demultiplexers

Multiplexers and demultiplexers are important components for WDM optical networks. They are used to multiplex several channels onto one fiber for transmission and demultiplex signals into separate channels for routing and detection, respectively. Figure 2.3 shows the structure of a simple optical demultiplexer [15].

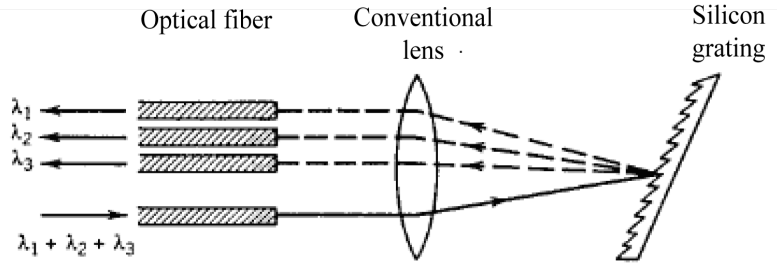

Figure 2.3. Structure of an optical demultiplexer [15]. Input wavelengths are directed to different output fibers by the diffraction grating.

Notice that optical multiplexers and demultiplexers are bidirectional devices. In Figure 2.3, the demultiplexer becomes a multiplexer if the input and output are exchanged. Multiplexers and demultiplexers are usually used in end terminals of WDM networks. They can also be used as constituent components in other devices, for example optical switches.

Figure 2.4 shows two other types of multiplexer and demultiplexer [16]. They are used to add one channel onto or drop one channel from an optical fiber, and thus are called the add-drop multiplexers. They are usually used in metro or local optical networks.

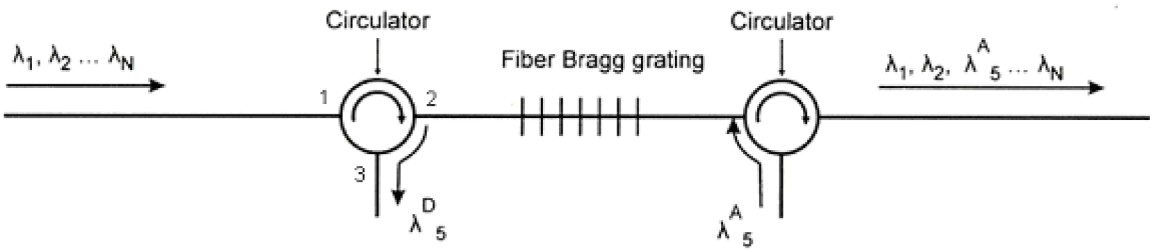

Figure 2.4. Structure of an add-drop multiplexer [16].

In Figure 2.4, the input channels λ_1, λ_2, ..., and λ_N go into the circulator from port 1 and out of it from port 2. However, the wavelength λ_5 is reflected back by the fiber Bragg grating and go out of the circulator via port 3, thus this channel is dropped. Similarly, a channel can be added as shown on the right side of the figure.

Fiber Properties

Single-mode fiber is widely used in today's optical communication networks. Such fibers have attenuations as low as 0.2dB/Km in the 1550nm wavelength range and are made of silica glass, which is much cheaper than other transmission mediums like copper coax cable. Figure 2.5 shows the cross-sectional structure of an optical fiber and the geometrical optics view of wave propagation in a single-mode fiber [17].

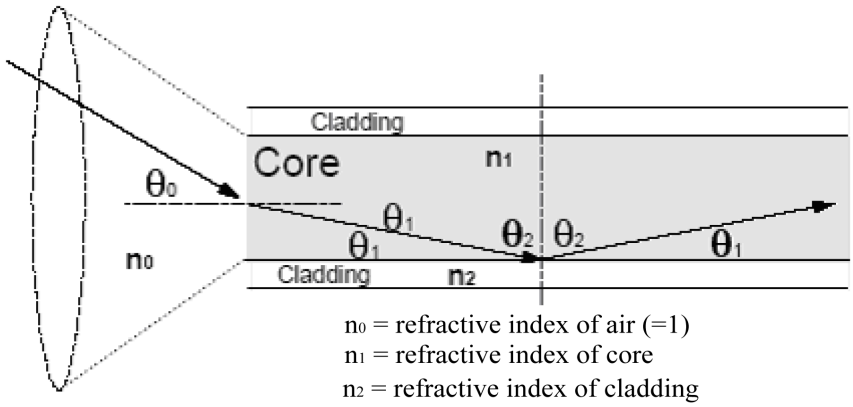

Figure 2.5. Structure of a single-mode fiber and the geometrical optics theory of wave guiding [17].

In Figure 2.5, the fiber has a cylindrical geometry. It has a core with refractive index n_1, and an outer cladding layer with a smaller refractive index n_2. Outside of the cladding are plastic protective layers, not shown in the figure. The working principle that guides the light in the optical fiber is total internal reflection. When the incident angle is smaller then the critical angle (θ_0 in Figure 2.5), light in the fiber will incur total internal reflection, and all the signal energy will be confined in the core.

To further understand wave guiding in fibers, a wave theory needs to be applied. The light is an electromagnetic wave. For a monochromatic wave propagating in a fiber with a small core dimension, only one (in a single-mode fiber, SMF) or several modes (in a multi-mode fiber, MMF) can propagate. A mode is a specific distribution of fields in the fiber. In a SMF fiber, only one mode can propagate, and all the energy in the higher order modes leaks into the cladding. When the output of a laser diode is coupled to a SMF fiber, many modes can be triggered, including the leaking modes. However, only the major mode remains after a short distance. Long distance communication systems mainly use single-mode fibers. A monochromatic wave travels in a SMF fiber with a propagation constant β which is the phase velocity of the wave. The propagation constant β varies when the wavelength or frequency of a monochromatic wave changes. We denote it as $\beta(w)$ to emphasize that it is a function of frequency and call it the propagation-constant function, in a bulk material $\beta(w) = n(w) * \frac{2\pi}{w}$, where $n(w)$ is the refractive index and λ is the wavelength. But in a fiber, the wave actually propagates partially in the core and partially in the cladding. For a given frequency w, the propagation constant $\beta(w)$ in a fiber is a complex function of $\beta^1(w)$ and $\beta^2(w)$, where $\beta^1(w)$ and $\beta^2(w)$ are the propagation constants in the core and in the cladding respectively.

When an optical pulse is modulated on a carrier frequency w, it propagates with the group velocity v_g, which is defined as

$$v_g = \frac{dw}{d\beta}. \tag{2.1}$$

Three important parameters characterizing the properties of a fiber are the attenuation coefficient α in units of dB/Km, the dispersion parameter D in units of $\frac{\text{ps}}{\text{Km*nm}}$, and the nonlinear coefficient γ in units of $\frac{1}{\text{W*Km}}$. Parameter D is defined as

$$\begin{cases} D = \frac{d\tau_g}{d\lambda} \\ \tau_g = \frac{1}{v_g} = \frac{d\beta}{dw}. \end{cases} \tag{2.2}$$

The parameter D is a measure of chromatic dispersion and has two contributing factors. The first is that different monochromatic waves propagate in a material with different phase velocities and the resulting dispersion (i.e. material dispersion) is denoted as D_m. The other factor is that in a fiber the waves propagate in two materials, the core and the cladding. The effective propagation constant $\beta(w)$ depends on the proportion of wave power that is contained in the core and in the cladding. For waves with different wavelengths, this power proportion is also different and the resulting dispersion (i.e. waveguide dispersion) is denoted as D_w. The chromatic dispersion is given by $D = D_m + D_w$. Figure 2.6 shows D as a function of wavelength [18].

After propagation along a fiber with large dispersion, defined by $D * L$ where L is the fiber length, an optical pulse is spread in the time domain which can result in inter-symbol interference (ISI). Propagation in fibers is also polarization sensitive. The two polarization states of an optical pulse propagate at different group velocities and results in pulse spread in the time domain, called the polarization-mode dispersion (PMD). Details of PMD are provided later.

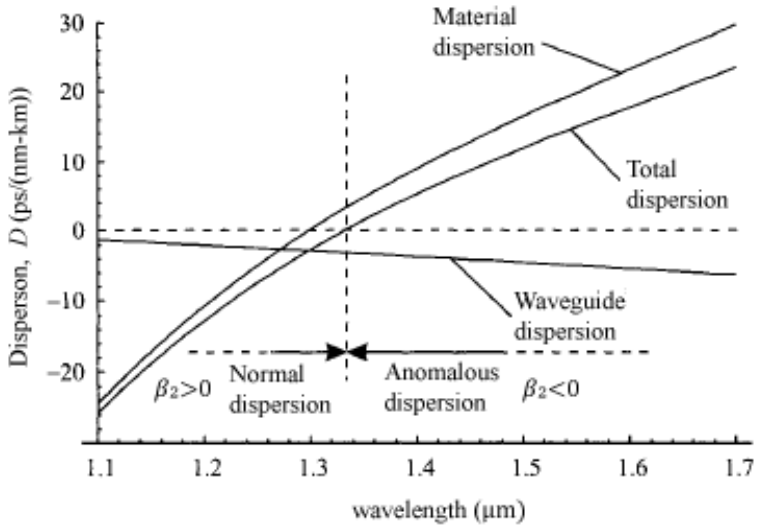

Figure 2.6. Dispersion of a typical single-mode fiber [18]. We notice that the zero-dispersion wavelength is at about 1.34μm while there is still large dispersion value at about 1.55μm, which is the wavelength typically used for long distance communication and called the C-band. β_2 is defined as $\frac{d^2w}{dw^2}$.

The coefficient γ is a measure of the power of nonlinear effects and we will discuss it in detail in Chapter 3 and Chapter 4.

Besides single-mode fibers and multi-mode fibers, there are also many other types of fibers used in the communication industry. In dispersion shifted fibers (DSFs), the zero-dispersion wavelength is shifted to about 1.55μm in the C-band. In non-zero dispersion shifted fibers (NZDSFs), the zero-dispersion wavelength is shifted to be close to but different from 1.55μm to avoid the build up of nonlinear effects. Dispersion compensation fibers (DCFs) are used to compensate dispersion and the parameter D is negative. The negative dispersion of a DCF fiber can cancel that of

a normal single-mode fiber, which is positive. Optical fibers are also used in other components, such as EDFAs and fiber lasers.

Optical Amplifiers

There are several different types of optical amplifiers, including semiconductor optical amplifiers (SOAs), erbium doped fiber amplifiers (EDFAs), erbium doped waveguide amplifiers (EDWAs), and Raman amplifiers. EDFAs are the most commonly used amplifiers in current generation optical networks, especially for long distance networks. EDFAs provide impressive performance, including high gain (up to 30dB), wide bandwidth, and low noise. The structure of an EDFA is shown in Figure 2.7 [19].

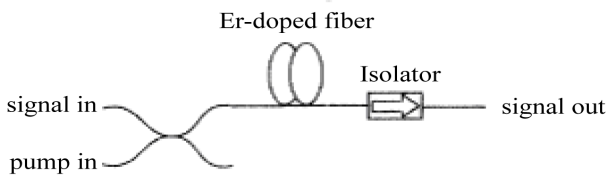

Figure 2.7. Structure of an EDFA using the co-propagating pumping scheme [19].

In Figure 2.7, the input signal and the pump are coupled into an Er-doped fiber. In the fiber, the signal is amplified by the process of stimulated emission while the pump is attenuated due to the energy transfer from pump photons to erbium ions. Another process called spontaneous emission generates the ASE noise. The isolator

is used to prevent reflection from the output port entering the amplifier and causing unwanted optical feedback.

Two parameters are used to characterize an EDFA, the gain G and the noise figure F_n which is defined as the output noise to input noise ratio. The working principle of EDFA will be discussed in more detail in Chapter 5.

Optical Switches

Optical switches are important components for all-optical networks. Its basic function is to switch signals on one wavelength of an input fiber to another output fiber. If no wavelength converters are deployed in the switch, then the input wavelength and the output wavelength are the same. This is the origin of the wavelength-continuity constraint in the RWA problem of optical routing. Through optical switches, wavelengths on different links can be connected and a lightpath constructed. There are different types of optical switches. Figure 2.8 shows the general structure of an optical switch [9]. In Figure 2.8, all the wavelengths of an input fiber are first demultiplexed and connected to an array of wavelength routing switches (WRSs). Each WRS is responsible for switching one specific wavelength of all input fibers. A wavelength on an input fiber can be switched to any output fiber. There are different technologies to implement the WRSs, and thus different types of optical switches.

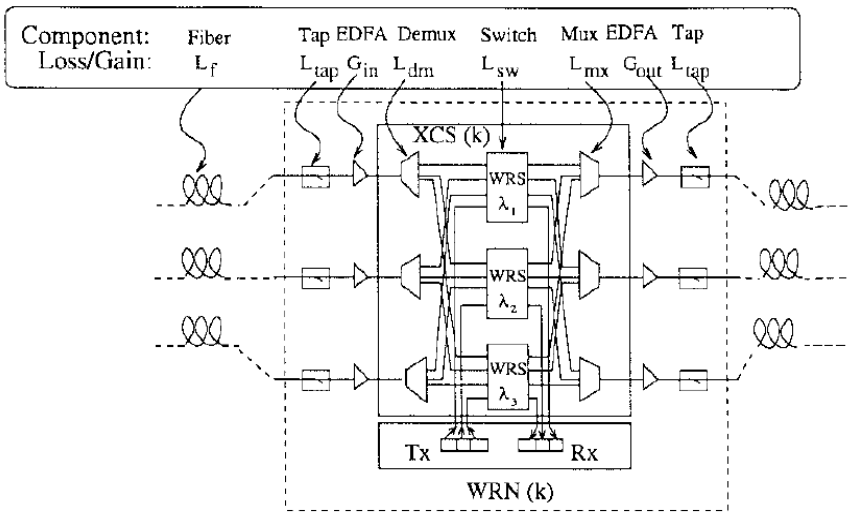

Figure 2.8. The general structure of an optical switch [9].

A parameter describing the performance of an optical switch is the *switching time*, which measures its response speed to a controlling signal. Other parameters include loss and crosstalk.

In the research discussed in this dissertation, A MEMS (Microelectromechanical Systems) optical switch is used, with the structure of its WRSs schematically shown in Figure 2.9 [20]. Compared to other types of switches, the MEMS switch has the shortcoming of long switching time (in the scale of ms compared to μs or ns of fast switches) and the advantage of being economical. The MEMS switch is suitable for circuit-switched networks.

Receivers

Optical signals are converted to the electrical domain using a photo-detector. Figure 2.10 shows the structure and working principle of a simple *pin* detector [21].

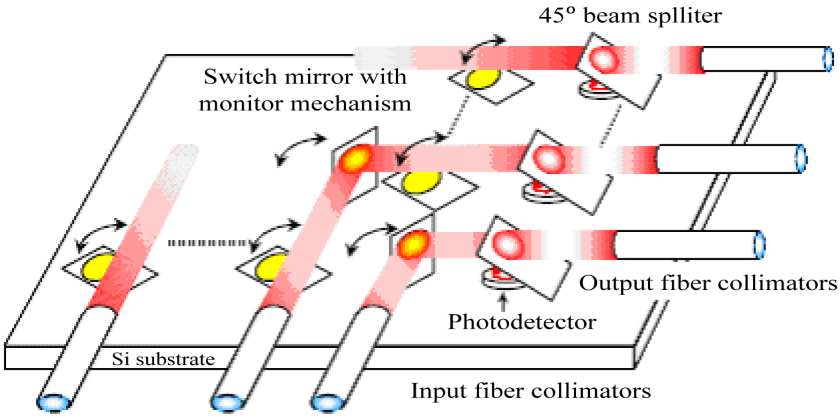

Figure 2.9. Structure of a MEMS wavelength routing switch. Micro-mirrors are used to guide input beam to different outputs [20].

In Figure 2.10, the *p-i-n* junction is reversely biased. The intrinsic layer (i.e. *i* layer in the figure) is used to increase the width of depletion region. When a signal photon heats the depletion region, an electron-hole pair is generated and swept across the depletion region, and hence current is generated. The variation of V_{out} represents the transmitted information.

Two parameters characterizing the performance of a *pin* detector are the responsivity R and the quantum efficiency η. The following relationships hold

$$\begin{cases} I_p = R * P \\ \eta = \frac{N_e}{N_p} \\ R = \frac{\eta * \lambda}{1248}, \end{cases} \tag{2.3}$$

where P is the power of incoming light, I_p is the induced photo-current in a *pin* detector, N_e is the number of generated free electrons in the depletion region per second, N_p is the number of incoming photons per seconds, and λ is the wavelength of the incoming light in units of nm. There are also other types of detectors, for example

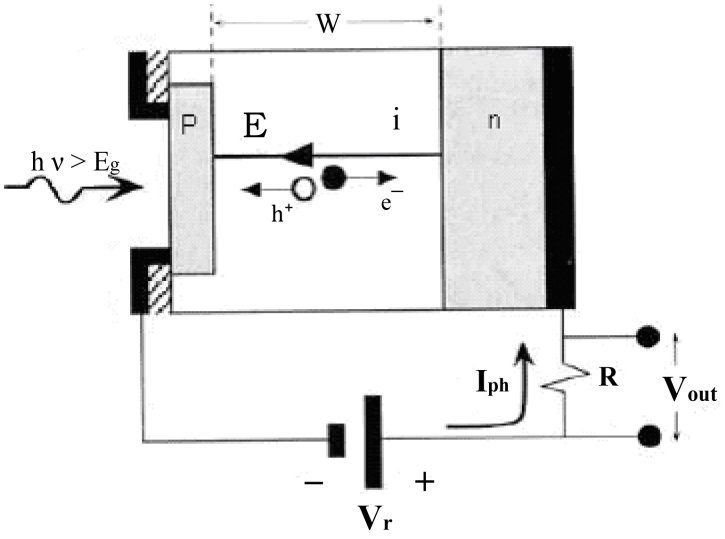

Figure 2.10. Structure of a *pin* detector [21].

the avalanche photo-detector (APD), which has larger responsivity but generates more noise than a *pin* detector. In this research, *pin* photo-detectors, which are widely used in optical networks, are assumed.

Signal Propagation and Physical Impairments

This section gives an overview of what happens when an optical pluse on one channel propagates in an all-optical network consisting of semiconductor lasers, single-mode fibers, MEMS switches and EDFAs. By channel, we mean a single wavelength in a fiber. The laser source with a specific wavelength is modulated (using either direct or external modulation) by an information signal to generate an intensity modulated pulse train. The light is collected into and propagates in a fiber. During its propagation, the signal is attenuated by the effects of absorption and scattering. At

the same time, the pulse spreads in the time domain because of the effects of chromatic dispersion and polarization-mode dispersion. If the power of the signal is high enough, then nonlinear effects such as self-phase modulation, cross-phase modulation, stimulated Brillouin scattering, stimulated Raman scattering, and four-wave mixing also influence the signal, adding noise, attenuating signal power, and spreading the pulse. These different nonlinear effects will be defined shortly. When the signal goes through an EDFA, it is amplified, but this amplification process also introduces ASE noise to the signal. If the total input power to the EDFA is high, then it works in the saturation mode and signals on different channels may affect each other through cross-gain modulation. In a switch, the signal is transferred from an input fiber to an output fiber. However, in some switching fabrics, crosstalk may be generated in this process. At the destination, the optical signal is converted to an electrical signal by a detector. Each of the components in a network can degrade the signal, resulting in a potentially unacceptable level of performance.

To sum up, Table 2.1[a] lists the different types of physical impairments. These are discussed in detail below.

In Table 2.1, we have categroized the impairments as independent impairments and dependent impairments. Independent impairments are generated by a channel itself, while dependent impairments are generated by the interactions among several channels. For example, the self-phase modulation will occur if the power of a channel

[a]Impairments marked by '*' are considered important in the literature.

Table 2.1. Different physical impairments in optical networks.

Independent impairments	*Dependent impairments*
Attenuation*	OXC crosstalk*
Material dispersion*	EDFA transients
Waveguide dispersion*	Cross-phase modulation*
Polarization-mode dispersion*	Four-wave mixing*
ASE noise*	Stimulated Brillouin scattering
MEMS switch transients	Stimulated Raman scattering
Self-phase modulation	
Gain non-flatness of EDFA	

is high enough and it is an independent impairment. The cross-phase modulation is due to the interference among several channels and it is a dependent impairment.

Linear Effects

Attenuation. A signal is attenuated by scattering, absorption, and other mechanical effects such as fiber bending. Absorption is due to impurities (such as OH^- ions) in fibers, which will absorb optical power. Scattering can deflect an optical ray and cause power leakage out of the core. The most important scattering effect in optical fibers is due to Rayleigh scattering. The total attention A_{db} of a fiber with length L kilometers is

$$A_{db} = L * \alpha, \tag{2.4}$$

where α is the attenuation coefficient in units of dB/Km. Attenuation is wavelength dependent [22]. The low attenuation window at 1.55μm is used for long distance optical communication and called the C-band.

Dispersion. There are four dispersion effects: material dispersion, waveguide dispersion, polarization-mode dispersion, and multi-mode dispersion. The combined effect of material dispersion and waveguide dispersion is called chromatic dispersion and has been discussed before. In long distance optical communication systems, single-mode fibers are used and the multi-mode dispersion is not relevant.

The spectral width of a laser source is not zero, although it is very narrow (a few MHz). A pulse generated at the laser source can be modeled as a sequence of pulses each modulated on a carrier with slightly different wavelengths, overlapping in the time domain. At the receiving side, the pulse will be spread in the time domain because each of its components propagates at a different velocity due to the chromatic dispersion. The spreading of a pulse (in the time domain) due to chromatic dispersion, $\triangle T_{chromatic}$, after propagating a distance L is

$$\triangle T_{chromatic} = D(\lambda) * L * \triangle\lambda, \tag{2.5}$$

where λ is the carrier wavelength, $\triangle\lambda$ is the channel spectrum width, and D is the dispersion parameter of the fiber.

The optical wave in a single-mode fiber is approximately a TEM wave. One polarization state is along the X axis, and the other is along the Y axis, while the wave propagates along the Z axis. If the shape of the fiber is not perfectly cylindrical, waves with different polarization states will propagate at different velocities, resulting in pulse spreading in the time domain and called the polarization-mode dispersion (PMD). The polarization-mode dispersion parameter D_{pmd} of a fiber is expressed

in units of ps/$\sqrt{\text{km}}$. The spreading of a pulse due to polarization-mode dispersion, $\triangle T_{pmd}$, after propagating a distance L is

$$\triangle T_{pmd} = D_{pmd} * \sqrt{L}. \tag{2.6}$$

The total pulse spreading, $\triangle T$, considering both the chromatic dispersion and the polarization-mode dispersion is

$$\triangle T = \sqrt{\triangle T^2_{chromatic} + \triangle T^2_{pmd}}. \tag{2.7}$$

Attenuation and dispersion are called linear effects.

ASE Noise

The ASE noise of an EDFA is due to the spontaneous emission of atoms at the excited state. The power spectral density of ASE noise is

$$S(f) = 2n_{sp}(G-1)hf, \tag{2.8}$$

where n_{sp} is the spontaneous emission factor, h is the Planck constant, f is the frequency and G is the amplification gain. For a given signal channel, the ASE noise on this channel is usually treated as white noise.

Gain Non-Flatness of EDFA

Different channels going through an EDFA experience different gains. Figure 2.11 shows the gain profile of an EDFA [23]. This is an undesirable effect. Equalization filters can be used to provide a flatter gain profile.

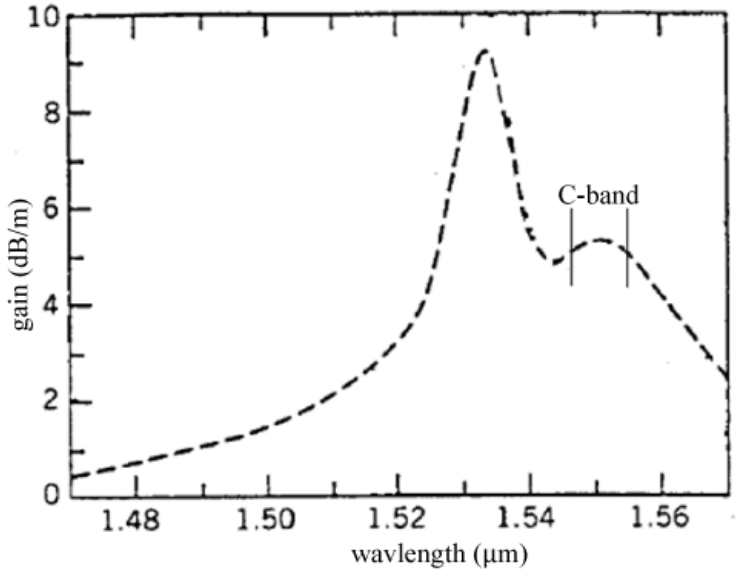

Figure 2.11. Gain profile of an EDFA [23].

MEMS Switch Transients

MEMS switch transients are dependent on several factors, including the physical characteristics of mirrors and the drive-signal waveform. Figure 2.12 shows the transients when a switch from an input port to an output port is suddenly closed [24]. We notice that the output waveform has a settling time in the range of tens of milliseconds (ms). Both the switch loss and the resonant frequencies of ouptput ringing are characterisitcs of an optical switch, indepdent of channel frequency.

In Figure 2.12, the output optical power reaches the 90% level in about 2 ms, but considerable ringing (up to 23% of mean power) persists for 10 ms and damps to a few percent of the mean power in 20 ms.

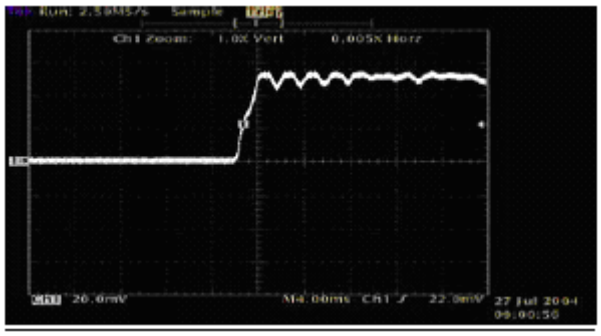

Figure 2.12. Transient behavior of output power due to MEMS switch closure [24]. The X axis is time and the Y axis is the output optical power.

OXC Crosstalk

OXC (optical switch crosstalk) can be generated while demultiplexing or multiplexing WDM signals. For example, λ_1 on input fiber 1 is switched to output fiber 1. However, some fraction of the power of λ_1 on input fiber 2 is also switched to the output fiber 1 due to imperfect hardware operation, causing crosstalk. The crosstalk power on a signal channel λ_k is

$$P_{oxc}^{k} = \sum_{i=1}^{N} x_{k,i} P_i, \tag{2.9}$$

where N is the number of co-propagating channels, $x_{k,i}$ is the crosstalk ratio of co-propagating channel i relative to k, and P_i is the power of channel i.

Non-Linear Effects

Non-linear effects occur when the optical power in a fiber exceeds a threshold associated with the particular phenomenon. In WDM and DWDM (dense wavelength division multiplexing, which uses smaller channel spacing and more channels for signal

transmission compared to WDM) networks, the combination of multiple wavelengths with high power per channel can make the non-linear effects a serious problem. In Chapter 4, we will discuss the most important nonlinear effects in more detail.

Self-Phase Modulation. Self-phase modulation (SPM) arises because the refractive index of a signal channel has an intensity-dependent component. This nonlinear refractive index causes a phase shift, resulting in chirping (modulation of the carrier frequency) of a pulse. This will further cause temporal spreading of the pulse by dispersion.

Cross-Phase Modulation. Cross-phase modulation (XPM) arises because the refractive index of a signal channel can be influenced by the intensities of other co-propagating channels, causing a phase shift and chirping of a pulse, and as a result, the spreading of the pulse by dispersion.

Four-Wave Mixing. In four-wave mixing (FWM), a spurious channel is generated in the presence of three other channels (pump channels). This can cause trouble if the spurious channel has the same wavelength as another signal channel, causing crosstalk and increased noise.

Stimulated Inelastic Scattering. The stimulated inelastic scattering includes two phenomena: stimulated Brillouin scattering (SBS) and stimulated Raman scattering (SRS). In a simple quantum-mechanical picture applicable to both SBS and SRS, an

incident photon is annihilated to create a photon at a lower frequency (belonging to the Stokes wave) and a phonon with the right energy and momentum to conserve the energy and the momentum [25]. A higher-energy photon at the so-called anti-Stokes frequency can also be created if a phonon of right energy and momentum is available.

In the stimulated Brillouin scattering, a signal channel generates a Stokes wave propagating in the opposite direction. This can deplete power of the signal channel [26].

In the stimulated Raman scattering, power from a signal channel with shorter wavelength is transferred to co-propagating channels with longer wavelengths. Although SRS is not a significant problem in systems with only a small number of channels due to its relatively high power threshold, it can pose a serious problem in systems with a large number of signal channels.

Temporal Effects

When the temporal behavior of network traffic is considered, as in circuit-switched, burst-switched, and packet-switched networks, physical impairments may become more complex. In packet switching, the duration of a packet can be in the range from nanoseconds to microseconds. In burst switching, the duration of a burst can be in the range from microseconds to milliseconds. In circuit switching, the duration of a connection is usually greater than milliseconds. With fast traffic dynamics, some types of physical impairments are dependent on the instantaneous power of a channel

and its co-propagating channels. This means that the impairments are dynamically changing dependent on network state.

As an example, the transient response of a gain-clamped EDFA chain is shown in Figure 2.13 [27].

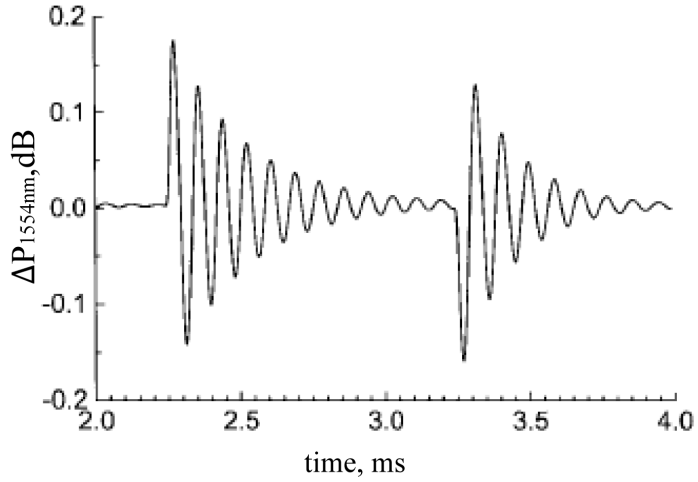

Figure 2.13. Transient response of a gain-clamped EDFA chain [27]. Eight channels ranging from 1547nm to 1554nm with spacing 1nm go through a cascade of 6 gain-clamped EDFAs. This figure shows the power dynamics of the channel at wavelength 1554nm when other six channels are periodically turned on and off.

The data in Figure 2.13 show that the dropping/adding of channels can induce gain oscillation of other channels. This phenomenon has detrimental effects. First, if the gain is too high or too low, the received power can fall beyond the working range of a detector. Second, these excursions can adversely affect the bit decision process by closing the eye-diagram (an oscilloscope display in which pulse shapes from a receiver are repetitively sampled and stacked together)and increasing the BER during the transient periods. It was reported in [28] that as the number of switched channels

(i.e. added/dropped channels) is increased, both the frequency and the amplitude of the power excursions experienced by surviving channels increase. It was also reported in [29] that the transient speed in one EDFA is in the range of several hundreds of microseconds (μs), but the transient speed in a cascade of EDFAs is proportional to 1/N (N is the number of EDFAs in the cascade), making the transients difficult to suppress, and the transients caused by channel dropping are more serious than those by channel adding.

The relationship between EDFA transients and traffic is complex. When a channel is dropped from an EDFA, another channel can also be dropped or a new channel can be added shortly after this event. The dropping of another channel will increase the transients, while the adding of a new channel will decrease the transients. For a given signal channel, the dropping and adding of other channels may be random events. The instantaneous power of a signal channel can be treated as a random variable with a mean equal to its steady state value. A probability distribution function (PDF) can be used to describe the power of a signal channel as in [30][31]. It was reported in [31] that the standard deviation of the power of a signal channel increases as the network traffic load and the burstiness level of network traffic increase.

Detector Effects

At a detector, optical signals are converted to the electrical domain. Because the detector is not linear, the output will include several beating terms that contribute to the output noise level. This is demonstrated by the following simple example. A

signal channel without any noise goes through an EDFA and is detected by a *pin* photo-detector. The detector output photo-current can be expressed as [32]

$$I = \bar{I} + i_n \tag{2.10}$$

$$\sigma_n^2 = \sigma_{shot}^2 + \sigma_{sig-spon}^2 + \sigma_{spon-spon}^2 \tag{2.11}$$

$$\sigma_{shot}^2 = 2eR[GP_i + P_n(G-1)B_o]B_e \tag{2.12}$$

$$\sigma_{sig-spon}^2 = 4R^2GP_iP_n(G-1)B_e \tag{2.13}$$

$$\sigma_{spon-spon}^2 = R^2[P_n(G-1)]^2(2B_o - B_e)B_e \tag{2.14}$$

$$P_n = n_{sp}hf_c, \tag{2.15}$$

where $\bar{I}$ is the average photo-current, i_n is the noise current, σ^2s are the variances of different noise terms, B_o is the optical bandwidth, B_e is the electrical bandwidth, G is the gain of the EDFA, P_i is the signal power before amplification, and R is the responsivity of the *pin* detector. Considering these noise terms, the quality of the signal channel is characterized by the Q factor, which is a metric defined as [33]

$$Q = 10\log_{10}(\frac{I_1 - I_0}{\sigma_1 + \sigma_0}), \tag{2.16}$$

where $I_{1/0}$ and $\sigma_{1/0}$ are the photo-current and the current standard deviation at the mark/space state respectively.

The above discussions illustrate the characteristics of physical impairments: they are varied, originating from different physical phenomena, and some are independent while others can be related. Of course, not all impairments are important at the same time. For a given network configuration, some of them will dominate. The proposed

routing framework should be flexible and scalable to take into account different physical impairments. A combination of proactive and reactive strategies is applied in our research in handling physical impairments. For some types of impairments, proactive solutions can be designed to decrease or eliminate their effects. These solutions are usually implemented at the physical or link layer. While for others, a reactive strategy is used, in which the routing algorithm can predict their effects using simplified analytical models and select lightpaths that result in minimal effects in a network.

MODELING ALL-OPTICAL NETWORKS

Introduction

Numerical simulation plays a crucial role for the study and design of optical networks. Researchers and engineers use simulation software to study the performance of networks before field deployment. In our research, we have used the PHOTOSS™ software to investigate the influence of fiber linear and nonlinear effects on signal quality. The performance of our proposed new RWA algorithms were studied using the OPNET™ software.

The propagation of optical signals along an optical fiber is described by the nonlinear Schrödinger equation (NLSE). In the case of WDM systems, a set of partial differential equations, each describing the propagation of one channel and their interactions, are required. The Split-step Fourier method (SSFM) is the most popular algorithm for solving the NLSE equation because of its good accuracy and moderate computation time. In the physical layer simulation, we are mainly concerned with the distortion of pulse shapes when signals are propagated along a lightpath. The input signals are represented as arrays of field samples. During simulation, the influences of network components (e.g. optical amplifiers, switches, etc.) and transmission medium (i.e. optical fibers) are considered. These will introduce different noises on signal channels. Signal quality is quantitatively determined at the end of a lightpath.

Degradations can accumulate along a lightpath, as there is no signal regeneration. QoS routing algorithms at the network layer need to be aware of signal quality and choose an appropriate lightpath. Routing algorithms use simplified analytical models to estimate signal quality, measured by the Q factor. In our research, we use physical layer simulation to validate the analytical models developed for predicting signal quality under the influence of fiber linear and nonlinear effects.

Control plane is important for the operation of an optical network. For the network layer, we have developed OPNET^{TM} models to simulate the working of a GMPLS (generalized multiprotocol label switching) control plane for the establishment and release of connections. Using this simulation system, we have studied the performance of our proposed routing algorithms and other benchmark algorithms.

In this chapter, we first review the nonlinear Schrödinger equation and the coupled nonlinear Schrödinger equations which describe signal propagation along optical fibers. The simulation of the physical layer is time-consuming. We have implemented a new simulation system (Grid_sim) built on grid computing technology. The parallelism in computations of the Split-step Fourier method is exploited to divide a large simulation into parallel components and distribute them to free CPUs across an organization. The design of the Grid_sim system will then be explained in more detail. Two commercial software packages, including PHOTOSS^{TM} and OptSim^{TM}, are also briefly introduced. We use PHOTOSS^{TM} in Chapter 4 to study the influence of fiber nonlinear effects on signal quality and use OptSim^{TM} in Chapter 5 to

investigate the effectivenss of the proposed power shaping technique on suppressing amplifier transients. The architecture of our network layer simulation system will then be discussed.

Simulating the Physical Layer

Modeling the Physical Layer

Figure 3.1 shows the model of an all-optical lightpath generated using PHOTOSS^{TM}. Each span includes a NZDSF fiber, a DCF fiber, and an in-line EDFA which exactly compensates for the attenuation of a span. The dispersions of the NZDSF and DCF fibers can be tuned to achieve the best performance for an optical link. Two compensation schemes can be used. In the DUCS (distributed under-compensation scheme) scheme [34], each span is under-compensated. Link pre-compensation and post-compensation can also be applied. The amounts of span residual dispersion, pre-compensation, and post-compensation need to be tuned. In the FOCS (full-inline and optimized post compensation scheme) scheme [34], the span residual dispersion is zero and the amount of link post-compensation needs to be tuned. The compensation schemes used by optical links can have a significant influence on the noise generated by different nonlinear effects.

For an all-optical lightpath, it is assumed in this research that either FOCS or DUCS is applied for each link, with the link residual dispersion equal to zero. This

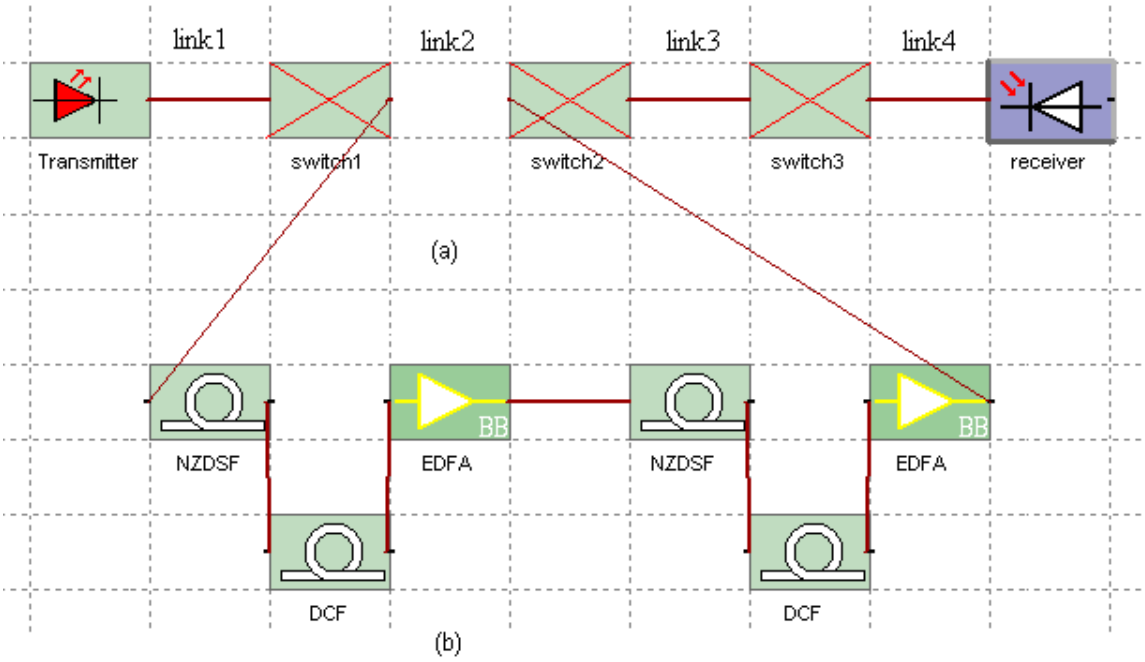

Figure 3.1. PHOTOSS^{TM} model of a lightpath. (a) A lightpath consisting of 4 links. (b) Model of a link consisting of 2 spans.

assumption will influence the analytical models used to predict the effects of non-linear phenomena in a dynamic network environment and the complexity of routing algorithm design. This point will be further clarified in Chapter 4 and Chapter 7.

In our research, we have also assumed that the noise and signal distortion due to optical switches are negligible. The linear and nonlinear effects of optical fibers and the ASE noise are taken into account when determining signal quality at the end of a lightpath.

Simulating Pulse Propagation and the Split-Step Fourier Method

The Nonlinear Schrödinger Equation. Assuming the electric field of a signal channel to be $A(z,t)f(x,y)e^{-jw_0t+j\beta(w_0)z}$,where $A(z,t)$ is the compex amplitude, $f(x,y)$ is the normalized transversal profile of the field mode, w_0 is the carrier frequency, and $\beta(w_0)$ is the propagation constant of the carrier frequnecy, the partial differential equation describing the propagation of a pulse on the single channel along a fiber segment is defined by the nonlinear Schrödinger equation (NLSE)[a] [35]

$$\begin{aligned}
\frac{\partial A}{\partial z} = & -\frac{\alpha}{2}A && \text{(Attenuation)}\\
& -\beta_1\frac{\partial A}{\partial t} && \text{(Delay)}\\
& -\frac{j\beta_2}{2}\frac{\partial^2 A}{\partial t^2} && \text{(First Order Dispersion)}\\
& +\frac{\beta_3}{6}\frac{\partial^3 A}{\partial t^3} && \text{(Second Order Dispersion)}\\
& +j\gamma[|A|^2A && \text{(Self Phase Modulation, SPM)}\\
& \quad +\frac{j}{w_0}\frac{\partial|A|^2A}{\partial t} && \text{(Self Steepening Effect)}\\
& \quad -T_RA\frac{\partial|A|^2}{\partial t}], && \text{(Stimulated Raman Scattering, SRS)}
\end{aligned} \tag{3.1}$$

where α is the attenuation coefficient, $\beta_1 = \frac{1}{v_g}$ with v_g the group velocity, $\beta_2 = \frac{d^2\beta}{dw^2}$, $\beta_3 = \frac{d^3\beta}{dw^3}$, γ is the nonlinear coefficient, and T_R is the slope of the Raman gain.

[a] If the field is assumed to be $A(z,t)f(x,y)e^{jw_0t-j\beta(w_0)z}$, then both Equation 3.1 and Equation 3.4 need to be changed accordingly as in [36][37][38].

For networks using low channel power and only one channel, the SPM effect is considered important. Using the transformation

$$T = t - \frac{z}{v_g}, \tag{3.2}$$

a time coordinate system moving at the channel group velocity v_g, Equation 3.1 can be simplified as

$$\frac{\partial A}{\partial z} + \frac{\alpha}{2}A + \frac{j\beta_2}{2}\frac{\partial^2 A}{\partial T^2} - \frac{\beta_3}{6}\frac{\partial^3 A}{\partial T^3} = j\gamma|A|^2 A. \tag{3.3}$$

The Coupled Nonlinear Schrödinger Equations. To simulate a WDM system, the coupled NLSE equations need to be used. They are actually a set of partial differential equations, given by [39]

$$\begin{cases} \frac{\partial A_1}{\partial z} &= -\frac{\alpha}{2}A_1 + (\frac{1}{v_c} - \frac{1}{v_1})\frac{\partial A_1}{\partial T} - \frac{j\beta_2(w_1)}{2}\frac{\partial^2 A_1}{\partial T^2} + \frac{\beta_3(w_1)}{6}\frac{\partial^3 A_1}{\partial T^3} + j\gamma(2\sum_{i=2}^{N}|A_i|^2 + |A_1|^2)A_1 \\ &\quad + \frac{j\gamma}{3}\sum_{m,n\neq p, w_m+w_n-w_p=w_1} d_{m,n,p}A_m A_n A_p^* e^{j\triangle K_1 z} \\ \vdots & \\ \frac{\partial A_c}{\partial z} &= -\frac{\alpha}{2}A_c - \frac{j\beta_2(w_c)}{2}\frac{\partial^2 A_c}{\partial T^2} + \frac{\beta_3(w_c)}{6}\frac{\partial^3 A_c}{\partial T^3} + j\gamma(2\sum_{i=1, i\neq c}^{N}|A_i|^2 + |A_c|^2)A_c \\ &\quad + \frac{j\gamma}{3}\sum_{m,n\neq p, w_m+w_n-w_p=w_c} d_{m,n,p}A_m A_n A_p^* e^{j\triangle K_c z} \\ \vdots & \\ \frac{\partial A_N}{\partial z} &= -\frac{\alpha}{2}A_N + (\frac{1}{v_c} - \frac{1}{v_N})\frac{\partial A_N}{\partial T} - \frac{j\beta_2(w_N)}{2}\frac{\partial^2 A_N}{\partial T^2} + \frac{\beta_3(w_N)}{6}\frac{\partial^3 A_N}{\partial T^3} \\ &\quad + j\gamma(2\sum_{i=1}^{N-1}|A_i|^2 + |A_N|^2)A_N + \frac{j\gamma}{3}\sum_{m,n\neq p, w_m+w_n-w_p=w_N} d_{m,n,p}A_m A_n A_p^* e^{j\triangle K_N z}, \end{cases} \tag{3.4}$$

where A_is, $\beta_2(w_i)$s, and $\beta_3(w_i)$s are the complex amplitudes, the first order dispersions, and the second order dispersions of signal channels respectively, $d_{m,n,p}$ is the degeneracy factor of a FWM mixing term ($d_{m,n,p} = 6$ when $m = n$, else $d_{m,n,p} = 3$), and $\triangle K_i = \beta_2(w_m) + \beta_2(w_n) - \beta_2(w_p) - \beta_2(w_i)$ for each FWM mixing term on signal

channel i. In Equation 3.4, a time coordinate system moving at the group velocity v_c of channel w_c is used, and only SPM, XPM, and FWM are considered. The terms $(\frac{1}{v_c} - \frac{1}{v_i})$ manifest the pulse shifting of other channels relative to the channel w_c due to their different group velocities.

In studying the influence of fiber nonlinear effects on signal quality, the 'probe and pump' approach is commonly used and discussed in the literature [40]. In Equation 3.4, we call w_c the *probe* channel and all the other channels the *pump* channels. The Q factor of the probe channel is investigated at the end of a link or lightpath.

The Split-Step Fourier Method. The numerical solution to the NSLE equation is obtained by the Split-step Fourier Method (SSFM), shown in the operator form as [41]

$$A(z + dz, T) = e^{\frac{dz}{2}\hat{L}} e^{\int_z^{z+dz} \hat{N}(z')dz'} e^{\frac{dz}{2}\hat{L}}, \tag{3.5}$$

where the linear operator $\hat{L}$ includes the linear terms in Equation 3.4 (i.e. attenuation and dispersion) and the nonlinear operator $\hat{N}$ includes all the nonlinear terms. An important observation of Equation 3.5 is that the influence of nonlinear effects is lumped at the point $z + \frac{dz}{2}$. Algorithm 3.1 can be used to solve Equation 3.4 in a small step $[z_0, z_0 + dz]$.

Algorithm 3.1 SSFM in a small step $[z_0, z_0 + dz]$

1: Compute the $\vec{A}(z_0 + \frac{dz}{2}, T)$ by linearlly propagating the field vector $\vec{A}(z, T)$ from z_0 to $z_0 + \frac{dz}{2}$. $\vec{A}(z, T)$ is a vector of the complex amplitudes of all channels and the linear operator is defined as

$$\begin{cases} \frac{\partial A_1}{\partial z} & = -\frac{\alpha}{2}A_1 + (\frac{1}{v_c} - \frac{1}{v_1})\frac{\partial A_1}{\partial T} - \frac{j\beta_2(w_1)}{2}\frac{\partial^2 A_1}{\partial T^2} + \frac{\beta_3(w_1)}{6}\frac{\partial^3 A_1}{\partial T^3} \\ \vdots & \\ \frac{\partial A_c}{\partial z} & = -\frac{\alpha}{2}A_c - \frac{j\beta_2(w_c)}{2}\frac{\partial^2 A_c}{\partial T^2} + \frac{\beta_3(w_c)}{6}\frac{\partial^3 A_c}{\partial T^3} \\ \vdots & \\ \frac{\partial A_N}{\partial z} & = -\frac{\alpha}{2}A_N + (\frac{1}{v_c} - \frac{1}{v_N})\frac{\partial A_N}{\partial T} - \frac{j\beta_2(w_N)}{2}\frac{\partial^2 A_N}{\partial T^2} + \frac{\beta_3(w_N)}{6}\frac{\partial^3 A_N}{\partial T^3}. \end{cases} \tag{3.6}$$

2: Solve the following set of nonlinear equations using the Runga-Kutta method in the interval $[z_0, z_0 + dz]$, using the initial condition $\vec{A}'(z_0, T) = \vec{A}(z_0 + \frac{dz}{2}, T)$. The result is still denoted as $\vec{A}(z_0 + \frac{dz}{2}, T)$.

$$\begin{cases} \frac{\partial A_1'}{\partial z} & = j\gamma(2\sum_{i=2}^{N}|A_i'|^2 + |A_1'|^2)A_1' + \frac{j\gamma}{3}\sum_{m,n\neq p, w_m+w_n-w_p=w_1} d_{m,n,p}A_m'A_n'A_p'^* e^{j\triangle K_1 z} \\ \vdots & \\ \frac{\partial A_c'}{\partial z} & = j\gamma(2\sum_{i=1,i\neq c}^{N}|A_i'|^2 + |A_c'|^2)A_c' + \frac{j\gamma}{3}\sum_{m,n\neq p, w_m+w_n-w_p=w_c} d_{m,n,p}A_m'A_n'A_p'^* e^{j\triangle K_c z} \\ \vdots & \\ \frac{\partial A_N'}{\partial z} & = j\gamma(2\sum_{i=1}^{N-1}|A_i'|^2 + |A_N'|^2)A_N' + \frac{j\gamma}{3}\sum_{m,n\neq p, w_m+w_n-w_p=w_N} d_{m,n,p}A_m'A_n'A_p'^* e^{j\triangle K_N z} \end{cases} \tag{3.7}$$

3: Linearly propagate the field vector $\vec{A}(z, T)$ from $z_0 + \frac{dz}{2}$ to $z_0 + dz$ and obtain $\vec{A}(z_0 + dz, T)$.

If using the field definition of $A(z,t)f(x,y)e^{jw_0 t - j\beta(w_0)z}$, then the linear operator in Algorithm 3.1 is changed to

$$\begin{cases} \frac{\partial A_1}{\partial z} & = -\frac{\alpha}{2}A_1 + (\frac{1}{v_c} - \frac{1}{v_1})\frac{\partial A_1}{\partial T} + \frac{j\beta_2(w_1)}{2}\frac{\partial^2 A_1}{\partial T^2} + \frac{\beta_3(w_1)}{6}\frac{\partial^3 A_1}{\partial T^3} \\ \vdots & \\ \frac{\partial A_c}{\partial z} & = -\frac{\alpha}{2}A_c + \frac{j\beta_2(w_c)}{2}\frac{\partial^2 A_c}{\partial T^2} + \frac{\beta_3(w_c)}{6}\frac{\partial^3 A_c}{\partial T^3} \\ \vdots & \\ \frac{\partial A_N}{\partial z} & = -\frac{\alpha}{2}A_N + (\frac{1}{v_c} - \frac{1}{v_N})\frac{\partial A_N}{\partial T} + \frac{j\beta_2(w_N)}{2}\frac{\partial^2 A_N}{\partial T^2} + \frac{\beta_3(w_N)}{6}\frac{\partial^3 A_N}{\partial T^3}, \end{cases} \tag{3.8}$$

and the nonlinear operator (i.e. the set of nonlinear equations) in Algorithm 3.1 is changed to

$$\begin{cases} \frac{\partial A_1^{'}}{\partial z} & = -j\gamma(2\sum\limits_{i=2}^{N}|A_i^{'}|^2+|A_1^{'}|^2)A_1^{'}-\frac{j\gamma}{3}\sum\limits_{m,n\neq p,w_m+w_n-w_p=w_1} d_{m,n,p}A_m^{'}A_n^{'}A_p^{'*}e^{-j\triangle K_1 z} \\ \vdots & \\ \frac{\partial A_c^{'}}{\partial z} & = -j\gamma(2\sum\limits_{i=1,i\neq c}^{N}|A_i^{'}|^2+|A_c^{'}|^2)A_c^{'}-\frac{j\gamma}{3}\sum\limits_{m,n\neq p,w_m+w_n-w_p=w_c} d_{m,n,p}A_m^{'}A_n^{'}A_p^{'*}e^{-j\triangle K_c z} \\ \vdots & \\ \frac{\partial A_N^{'}}{\partial z} & = -j\gamma(2\sum\limits_{i=1}^{N-1}|A_i^{'}|^2+|A_N^{'}|^2)A_N^{'}-\frac{j\gamma}{3}\sum\limits_{m,n\neq p,w_m+w_n-w_p=w_N} d_{m,n,p}A_m^{'}A_n^{'}A_p^{'*}e^{-j\triangle K_N z}. \end{cases} \tag{3.9}$$

We have used these equations[b] [c] [d] for the Matlab implementation of simulating pulse propagation, given in Appendix A.

The idea of Alogirthm 3.1 was applied in [39]. In the above discussion, the step size is assumed given. Different approaches have been proposed to decide the correct step size in the literature [42] [43]. Usually, a small step size is used at the beginning of a fiber segment and then dynamically adjusted in the simulation. Given the complex amplitude $A_c(z,T)$ and the step size dz at a point $z=z_0$, the LEM (Least Error Method) algorithm can be used to adaptively adjust the step size as shown in Agorithm 3.2 [42][e].

[b] Refer to function *ssprop_linear* in Appendix A for the Matlab implementation of linear propgation.

[c] Refer to function *part_solve* in Appendix A for the Matlab implementation of solving Equation 3.9 using the Runga-Kutta method.

[d] Refer to function *ssprop_incremtal* in Appendix A for the Matlab implementation of SSFM in a small interval.

[e] Refer to function *ssprop* in Appendix A for the Matlab implementation of the LEM algorithm.

Algorithm 3.2 the Least Error Method

1: Compute $A_c(z_0 + dz, T)$ using Algorithm 3.1 with step size dz and denote the result as $A_{coarse}(T)$.
2: Compute $A_c(z_0 + dz, T)$ using Algorithm 3.1 with step size $\frac{dz}{2}$ and denote the result as $A_{fine}(T)$. This computation requires two consecutive steps.
3: Compute the relative local error $\sigma = \frac{||A_{coarse} - A_{fine}||}{||A_{fine}||}$,with the norm operator defined as $||A|| = \sqrt{\int_{-\infty}^{\infty} |A(T)|^2 dT}$.
4: Adjust the step size according to the following policy
- $\sigma > 2\sigma_G$: the solution is discarded. The step size is halved and run LEM again
- $\sigma \in (\sigma_G, 2\sigma_G]$: the step size is divied by $\sqrt[3]{2}$
- $\sigma \in [\frac{\sigma_G}{2}, \sigma_G]$: the step size is unchanged
- $\sigma < \frac{\sigma_G}{2}$: the step size is multiplied by $\sqrt[3]{2}$,

where σ_G is a system parameter specifying precision. In cases when $\sigma \leq 2\sigma_G$, $A_c(z_0 + dz, T) = \frac{1}{3}(4A_{fine} - A_{coarse})$.

The LEM algorithm is more general, robust, and yields satisfactory accuracy in different simulation configurations, compared to other step size controlling algorithms (e.g. the Fix-Step-Size, the Logarithmic-Step-Size-Distribution, and the Walk-Off-Method [43]).

Improving Simulation Efficiency by Grid Computing

The Split-step Fourier method can become rather slow when simulating some nonlinear effects, because a very small step size has to be used. Some nonlinear effects (e.g. FWM) are sensitive to signal initial phases. To estimate the signal quality of a probe channel w_c, the Q factor of the received signal needs to be averaged over tens of iterations to achieve statistical confidence. For each iteration, the initial phase and bit pattern of each channel need to be randomized.

In the literature, different approaches have been proposed to parallelize and improve the efficiency of SSFM. In current WDM networks, low channel power (in the range of several mW) is used, and the nonlinear effects are small. In [44], the pump channels were decoupled from the probe channel by assuming that their propagation only cause attenuation and pulse shifting in the time domain relative to the probe channel. In [45][46], the Fast Fourier Transform (FFT) based and IIR based methods were combined to improve simulation performance. In [47][48], parallel algorithms for FFT were proposed for multiprocessor machines.

We have built a prototype simulation system (named Grid_sim) based on grid computing technology to improve simulation efficiency. The system was implemented using *Matlab distributed computing toolbox 3.1.* The architecture of the prototype system is shown in Figure 3.2.

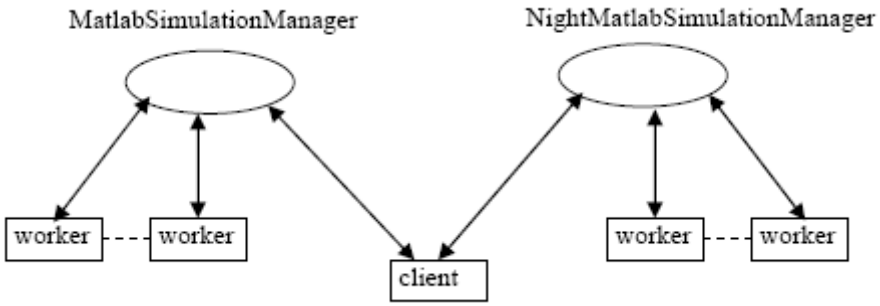

Figure 3.2. Architecture of Grid_sim. Workers are distributed across the MSU campus. The MatlabSimulationManager and NightMatlabSimulationManager are two jobmanagers. The Client controls the whole simulation, submitting simulation jobs to jobmanagers according to a scheduling policy and collecting simulation results.

According to the requirement of multi-iterations, Algorithm 3.1, and Algorithm 3.2, we can identify three levels of parallelism. First, all the iterations are independent and can be run by workers independently. Second, from z_0 to $z_0 + dz$, the LEM algorithm compares the results computed by using step size dz and by using step size $\frac{dz}{2}$. These two computations can be executed in parallel. Third, when running Algorithm 3.1, Equation 3.7 or Equation 3.9 needs to be solved for each sample of time T, and these computations can be executed in parallel.

The scheduling policy for the prototype system is given by Algorithm 3.3.

Algorithm 3.3 Scheduling policy of Grid_sim

1: Submit a job to the jobmanager MatlabSimulationManager if any worker is free;
2: Submit jobs to the jobmanager NightSimulationManager only at midnight;

Introduction to PHOTOSS™ and OptSim™

PHOTOSS™. In our research, PHOTOSS™ is used to investigate fiber nonlinear effects. Figure 3.3 shows the main window of PHOTOSS™ when we investigated the FWM noise generated on a probe channel in an optical link.

We use this example to illustrate the important concepts and components in PHOTOSS™ used in our research. In studying FWM, both the probe channel and the pump channels are CW signals. We have used the *Pulse generator* component (PPG) as signal source for each channel, with its property window shown in Figure 3.4. In Figure 3.4, the parameter *Pulse_Shaping_Mode* is set to be 'Power' to

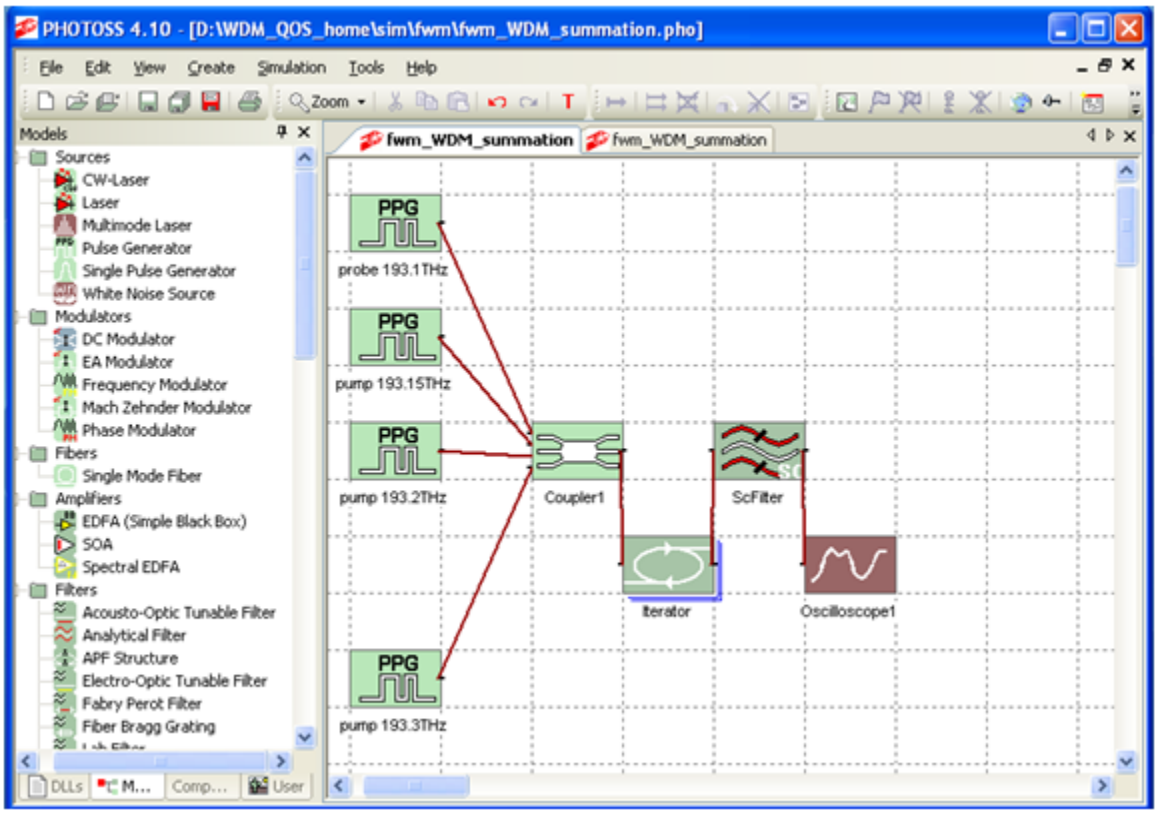

Figure 3.3. Main window of PHOTOSS^{TM}.

tell PHOTOSS^{TM} that the parameter *A_Min* is the minimal power and the parameter *A_Max* is the maximal power of the generated optical pulses. The parameter *Pulse_Shape* is set to be 'Rectangle' to define the pulse shape. Other pulse shapes (including Squared-cosine, Sine, Sech, Gaussian, etc.) are also available. The frequency of channel carrier is specified by the parameter *f0*, which is set to 193.1THz for the probe channel. The bit pattern is defined by the parameter *Pattern generation*, which is set to be 'Sequence of 1's' to mimic a CW source. Other patterns (including Random, Single pulse, etc.) can also be used. For example, by setting the parameter *Pattern generation* to be 'Create random sequence' and setting the

parameter *PRBS length* (not available in Figure 3.4 when *Pattern generation* is set to be 'Sequence of 1's') to be '10', a random bit stream of length 2^{10} can be generated. When 'Create random sequence' is used, the parameter *Calc.bit shift* should also be checked. For each iteration of a simulation, PHOTOSS^{TM} only generates one random bit pattern with exactly equal numbers of 1's and 0's. All random pulse generators (i.e. those with parameter *Pattern generation* set to be 'Create random sequence') generate their own random patterns by shifting this common pattern. The parameter *Calc.bit shift*, shown in Figure 3.4, is unchecked because the probe channel is a CW source. The parameter *initial_phase* is set to be 'Random'. For one iteration, if the random initial phase of a channel has value Φ (a constant), then the waveform of the channel is represented as $\sqrt{P(t)}e^{j\Phi}$, where $P(t)$ is the power of the channel given by the bit pattern.

In Figure 3.3, the four channels are coupled onto the optical link through *Coupler1*. The *Iterator* component is used to save space and repeat the structure defined in the component for several times (given by the parameter *size* of the *Iterator* component and is set to 6 for this example). The structure of a span defined in *Iterator* is shown in Figure 3.5. The DCF fiber in the figure is used to cancel the dispersion accumulated in the NZDSF fiber.

Figure 3.6 shows the property window of the NZDSF fiber. In Figure 3.6(a), the parameter *Mode* is set to be 'Nonlinear' to tell PHOTOSS^{TM} that nonlinear effects need to be considered in the propagation along the NZDSF fiber. Because

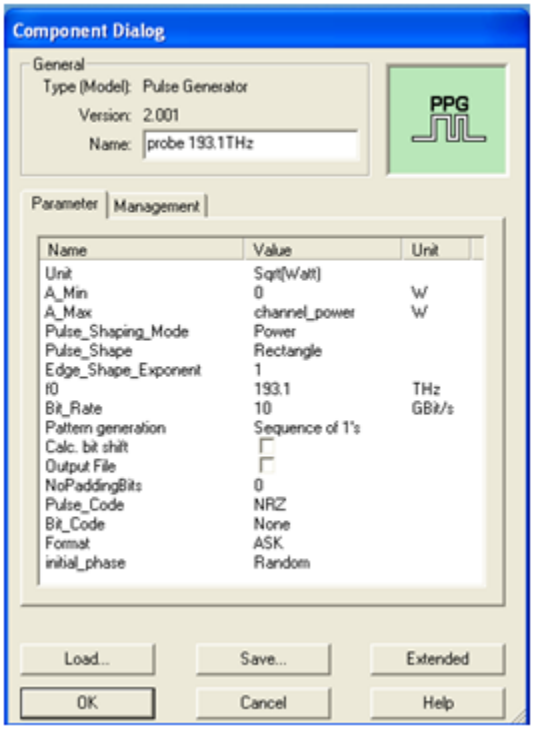

Figure 3.4. Property window of PPG.

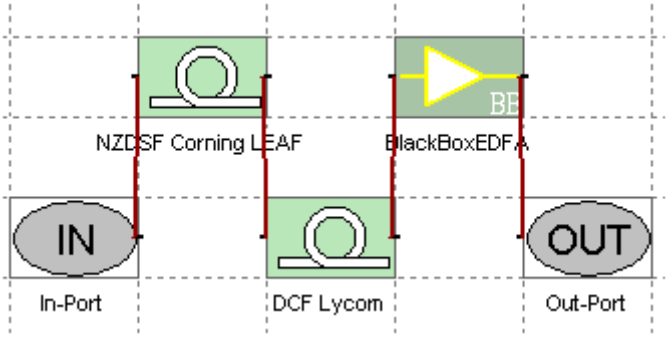

Figure 3.5. The structure of a span defined in the *Iterator* component.

only the parameter *FWM* is checked, only the effect of FWM is considered in this simulation. We can study nonlinear effects individually or in combination by turning these parameters corresponding to different nonlinear effects on and off. For the DCF fiber, we have set the parameter *Mode* to be 'Linear' to save simulation time, because nonlinear effects in the DCF fiber are negligible due to large attenuation of the NZDSF fiber. In this case, PHOTOSS^{TM} will only consider attenuation and dispersion in the propagation along the DCF fiber. In Figure 3.6(b), the parameters *Alpha*, *D*, *S*, *length*, and *gamma*, specify the attenuation coefficient, dispersion parameter, dispersion slope, length, and nonlinear coefficient of the NZDSF fiber respectively. By unchecking the parameter *Use D and S*, we can then input β_2 and β_3 directly. The parameter f_0 is used to specify the reference frequency ($w_0 = 2\pi f_0$) for making a Taylor expansion of $\beta(w)$. The inputted β_2 and β_3 are the values of $\beta_2(w)$ and $\beta_3(w)$ evaluated at the reference frequency respectively (i.e. $\beta_2 = \frac{d^2\beta(w)}{dw^2}|_{w=w_0}$ and $\beta_3 = \frac{d^3\beta(w)}{dw^3}|_{w=w_0}$).

The *BlackBoxEDFA* component in Figure 3.5 is a simplified model of EDFA and models amplification without any distortion except ASE noise. The parameter *NF* (noise figure) of *BlackBoxEDFA* is set to be a negative value to disable ASE noise in the example.

Using the *Iterator* component, we have defined an optical link with 6 identical spans. At the end of the link, the probe channel is filtered out using the *ScFilter* component. This filter is ideal, with the waveform of the probe channel outputted

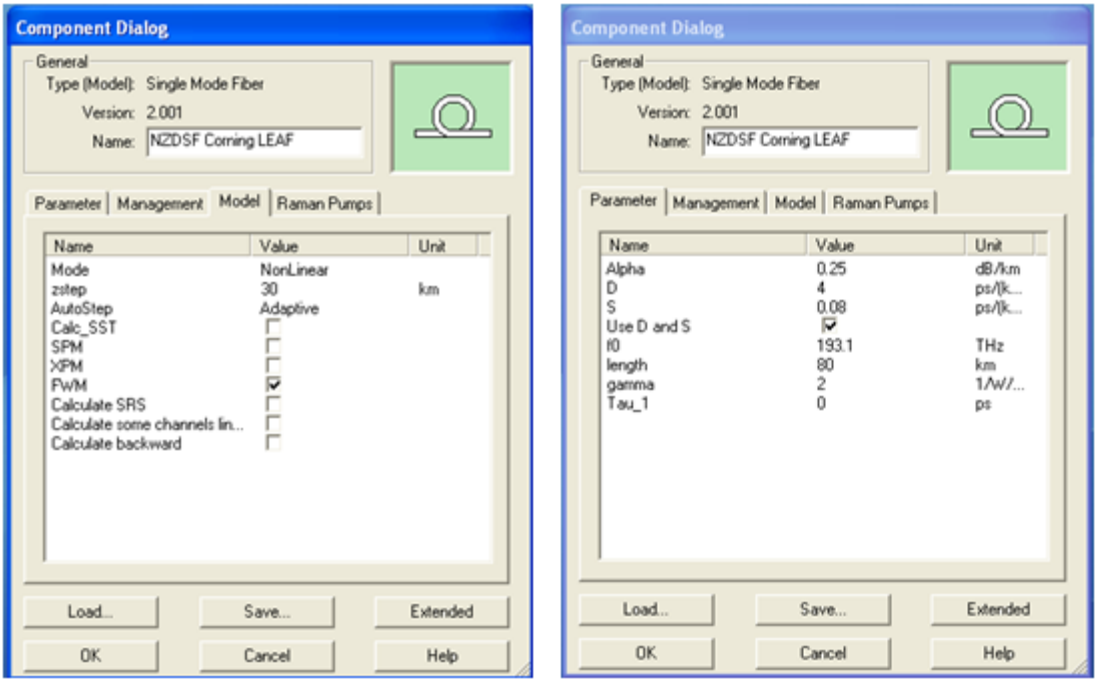

(a) The Model tab (b) The Parameter tab

Figure 3.6. Property window of an optical fiber.

without any change and all other channels blocked. The *Oscilloscope1* component is used to analyze the waveform of the probe channel, including the average, min, max, and variance of its power.

The global variables of the simulation are shown in Table 3.1.

Table 3.1. Global variables of a PHOTOSS^{TM} simulation.

Variable name	Value
p_tmp	1mW
channel_power	4*p_tmp
iter	1:80

The desired peak power (*p_tmp*) of optical pulses at the input of the link is 1mW. The *Coupler1* component in Figure 3.3 can influence signal power by [49]

$$A_{out} = \frac{\alpha}{\sqrt{N_{in} * N_{out}}} \sum_{i=0}^{i=N} A_i, \tag{3.10}$$

where α is the additional loss of the coupler (set to 0dB in the simulation), N_{in} and N_{out} are the number of inputs and number of outputs of the coupler respectively ($N_{in} = 4$ and $N_{out} = 1$ in the simulation), and A_{out} and A_i's are the output and the input amplitudes of the coupler respectively. By setting the parameter *A_Max* in Figure 3.4 to be 'channel_power = 4*p_tmp' for all *pulse generator* components, optical pulses on each channel will have 1mW peak power after the *Coupler1* component and at the input of the *Iterator* component.

PHOTOSS^{TM} sweeps the variable *iter* for 80 times from 1 to 80, thus running 80 iterations. In PHOTOSS^{TM}, a simulation run can have multiple iterations and these iterations are independent. Sweeping variable provides a good mechanism for optimizing link design. For example, by setting the length of a link post-compensation DCF fiber to be a sweeping variable, we can find its optimal length for achieving the best signal quality.

The simulation parameters of PHOTOSS^{TM} are shown in Figure 3.7. The parameter *Signal representation* is set to be 'Sampled', so the waveforms of signal channels are represented as samples of complex amplitude. The parameter *Method* is set to be 'Separated channels' to indicate that samples of each channnel are stored in a separate array. This is required if nonlinear effects shown in Figure 3.6(a) need to

be turned on and off individually. The parameter *Convolution* is set to be 'Cyclic' to avoid waveform edge effects. With this setting, the channel samples are treated as periodic signal. The parameter *Rnd. gener. initializtions* is set to be 'Random', so the random number generator of PHOTOSS^{TM} will start with a different seed each time when the program is restarted. The parameters defining *Sampled signal representation*, shown in Figure 3.7, cause the pulse generator to send out one block of 128 bits in each iteration, with 64 samples per bit. The parameter *Reference bitrate* is set to 10Gbps to specify the bit transmission rates of all the pulse generators.

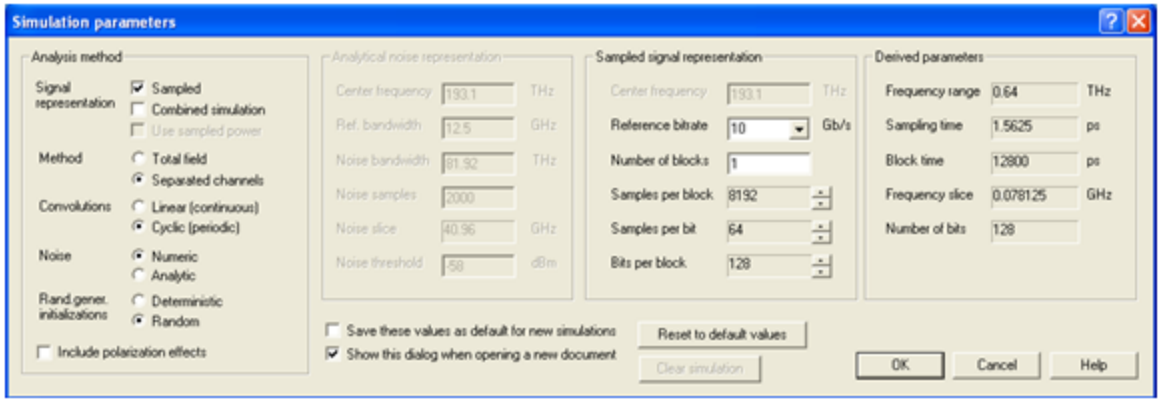

Figure 3.7. PHOTOSS^{TM} simulation configuration.

OptSim^{TM}. In our research, we have used OptSim^{TM} to study the behavior of EDFA amplifiers. The simulation model in Figure 3.8 will be used in Chapter 5 to verify the effectiveness of the proposed power shaping technique. We use this example to explain the important concepts and components of OptSim^{TM} used in our research.

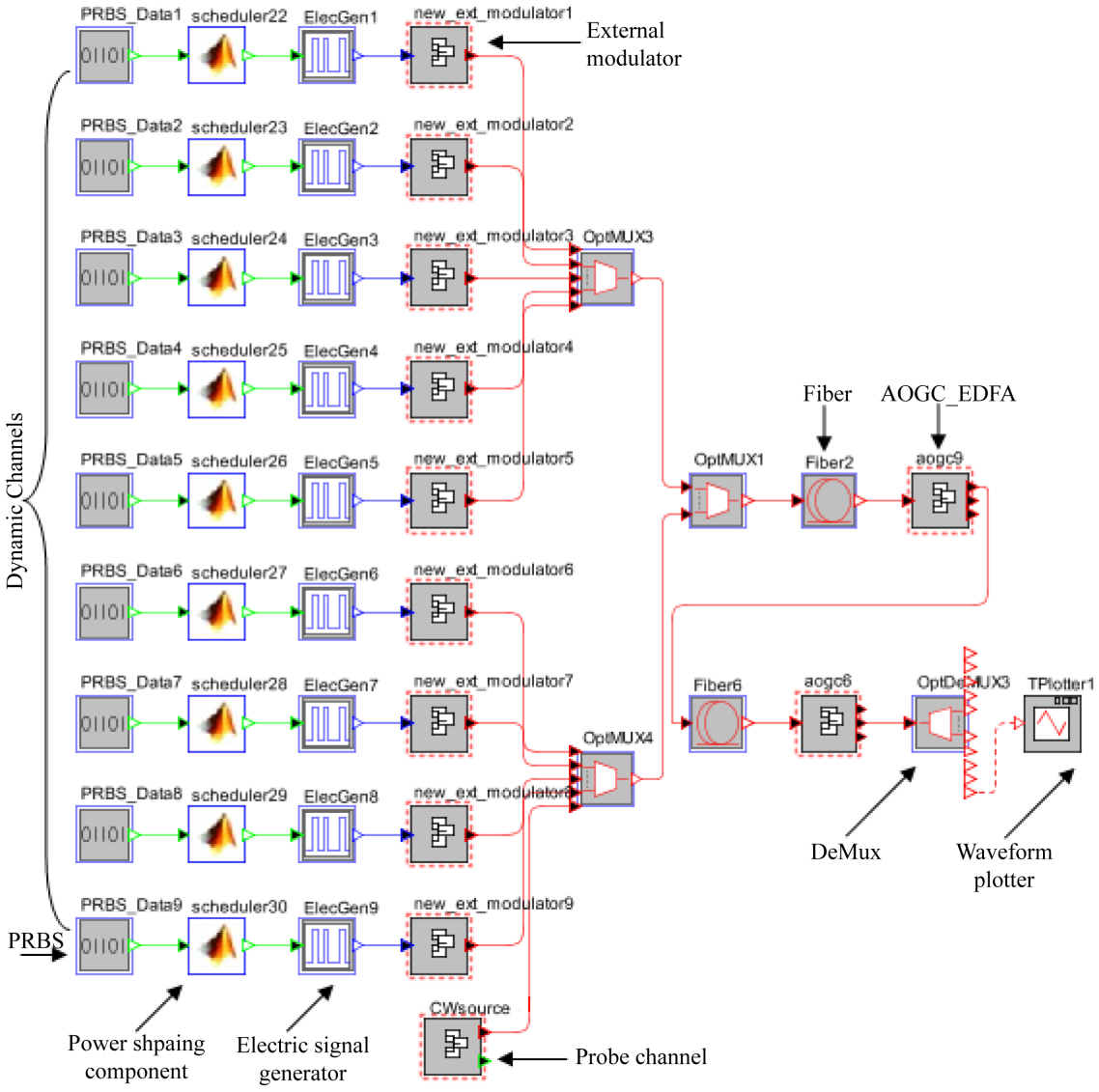

Figure 3.8. OptSim^{TM} simulation model for investigating the performance of power shaping.

In Figure 3.8, 10 channels (including 9 dynamic channels and the probe channel) co-propagate along an optical link. For each dynamic channel, the simulation time is divided into a series of alternating "on" and "off" periods. In an "on" period, the *PRBS* (pseduo-random binary sequence generator) component sends out random bit streams and in an "off" period it is silent. The *PRBS* component has a data transmission rate of 1Gbps. The *Power shaping* component is used to add a *head* before and a *tail* after the traffic block of an "on" period. The output of the *Electric signal generator* is connected to the *External modulator* to generate intensity modulated optical signals. At the end of the link, the probe channel is demultiplexed and analyzed using the *Waveform plotter*.

The *AOGC_EDFA* component in the link was created according to [50] and has the internal structure shown in Figure 3.9. In Figure 3.9, input signal channels (through *port_6*) and the pump laser are coupled into a loop structure. The *OptSim EDFA* component is for simulating an ordinary EDFA without gain-clamping. A specific wavelength from the ASE spectrum (i.e. the lasing wavelength) is filtered out by the optical filter *OptFilt2* and fed back into the loop. We have tuned the additional loss (controlled by the global variable *FeedbackLoss*) and the pass-band wavelength (controlled by the global variable *Lasingwavelength*) of the optical filter *OptFilt2* such that the lasing wavelength can effectively clamp the amplifier gain. The *DelayBlock* component is a special OptSim^{TM} module for avoiding computation deadlock in a loop structure [51]. The attenuator bank following the output of the loop structure

is used to simulate a comb filter. We tuned the loss of each attenuator in the bank such that all the input signal channels will achieve a 20dB gain.

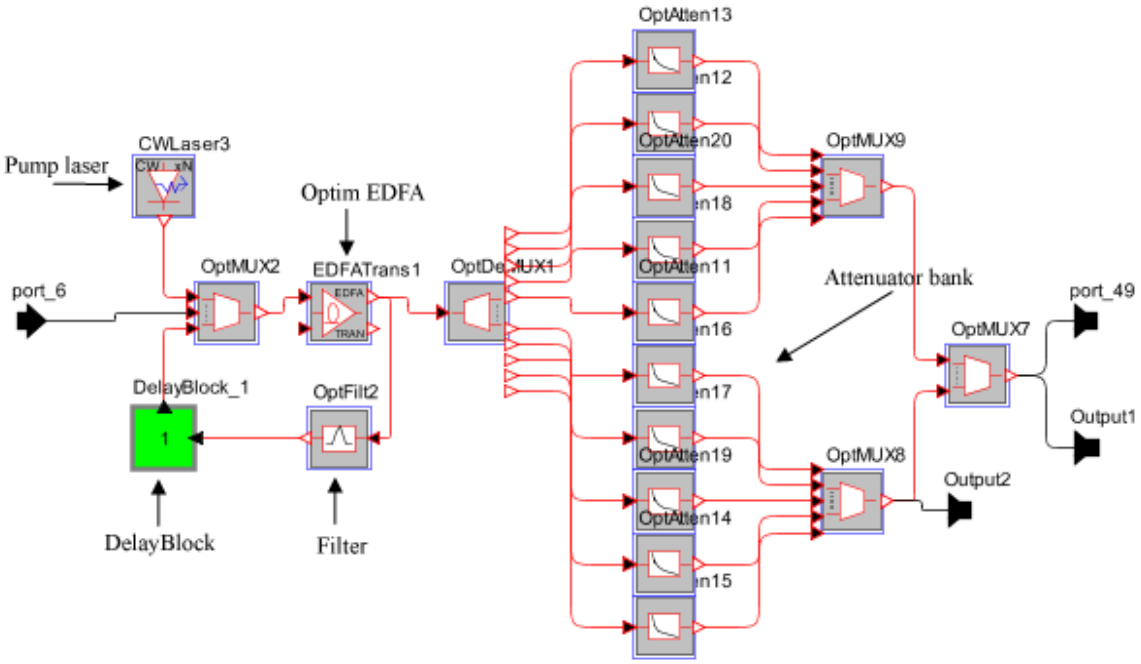

Figure 3.9. OptSim^{TM} model of AOGC_EDFA.

In an OptSim^{TM} block mode simulation, a simulation run is composed of several iterations. These iterations are dependent and OptSim^{TM} simulation components will keep track of status across iterations. The lengths of the "on" and "off" periods and the lengths of the power shaping head and tail are all specified in units of iteration. In each iteration of an "on" period, the *PRBS* component generates a random bit stream sent downstream along the link.

The global variables of the simulation are shown in Table 3.2.

Table 3.2. Global variables of an OptSim™ simulation.

Variable name	Value
iterations	2000
Time step per iteration	0.5120μs
Lasingwavelength	1563.5nm
FeedbackLoss	18dB

Simulating the Network Layer

OPNET™ is a discrete event network level simulator. It simulates the system behavior by modeling each event that occurs and processes it by user-defined procedures. It uses a hierarchical strategy to organize all the models to build a whole network. The hierarchy models entities including physical link transceivers, CPU running processes, queue management and running protocols, devices modeled by nodes with process modules and transceivers, and network models that connect all of the different nodes together. Researchers usually use OPNET™ for investigating network protocols and network performance (e.g. network delay and throughput). At present, OPNET™ has no built-in modules for simulating optical networks. We use OPNET™ to simulate the control plane and RWA algorithms for all-optical networks.

Modeling the Network Layer

The control plane of an optical network can be constructed by reserving one wavelength on the link between each pair of adjacent switch nodes for signaling message transmission. The control plane and the optical network have the same topology.

Alternatively, a separate network can be created for the control and management of an optical network. In this case, the topologies of the control plane and the underlying optical network can be totally different. We have applied this strategy and assume that an IP network is used for the optical network control plane. Figure 3.10 shows the OPNET^{TM} model for the control plane of the NSF network.

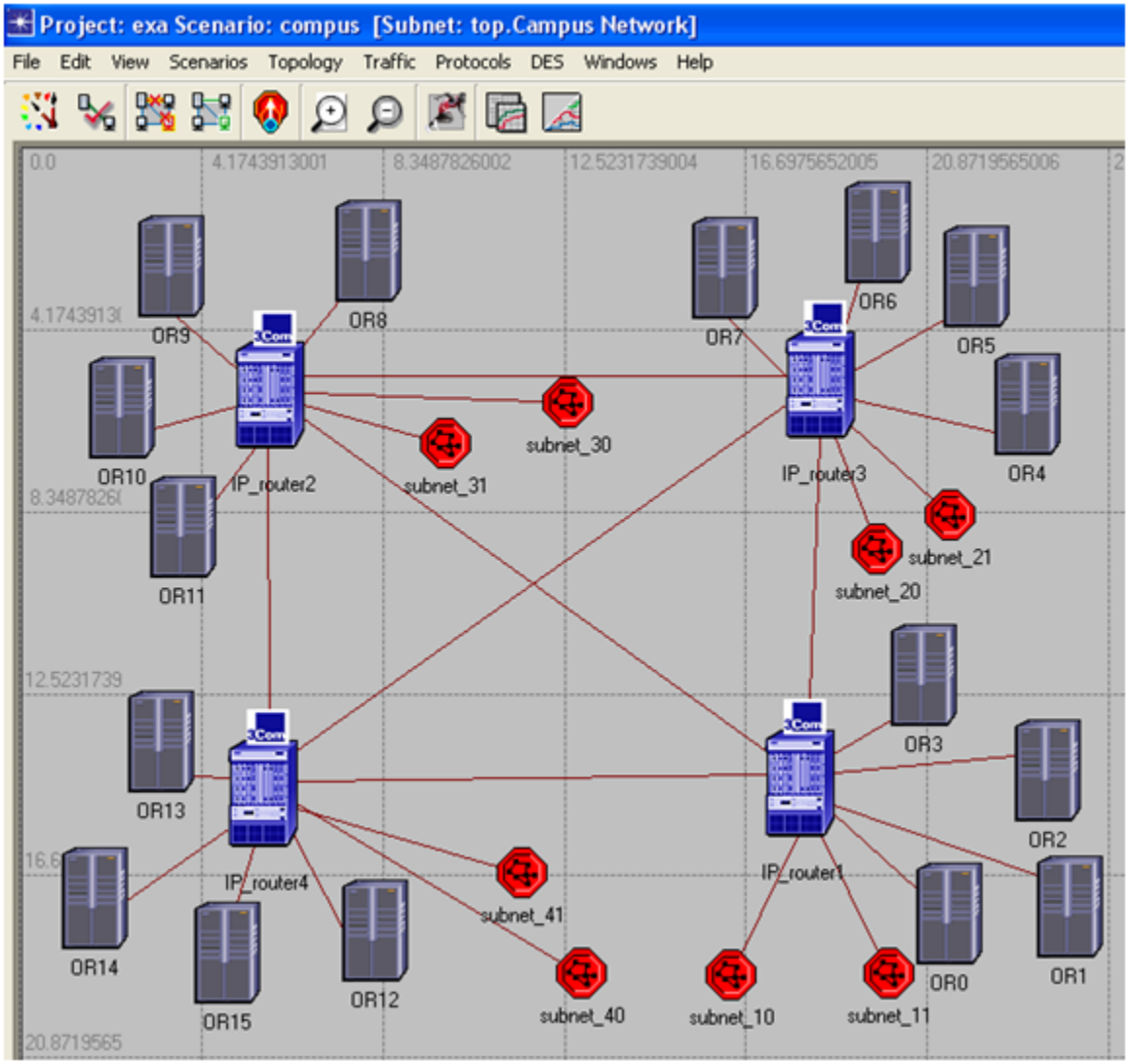

Figure 3.10. OPNET^{TM} model for the control plane of the NSF network.

In Figure 3.10, the links are not optical links, but Ethernet 10BaseT cables. Optical workstations (i.e. OW nodes) are grouped into sub-networks with the internal structure shown in Figure 3.11. The OR nodes are optical routers which represent the signaling processing modules of optical switches and are responsible for handling GMPLS signaling messages and allocating necessary resources for user connections. We have simulated only the signaling functions of the optical-network control plane.

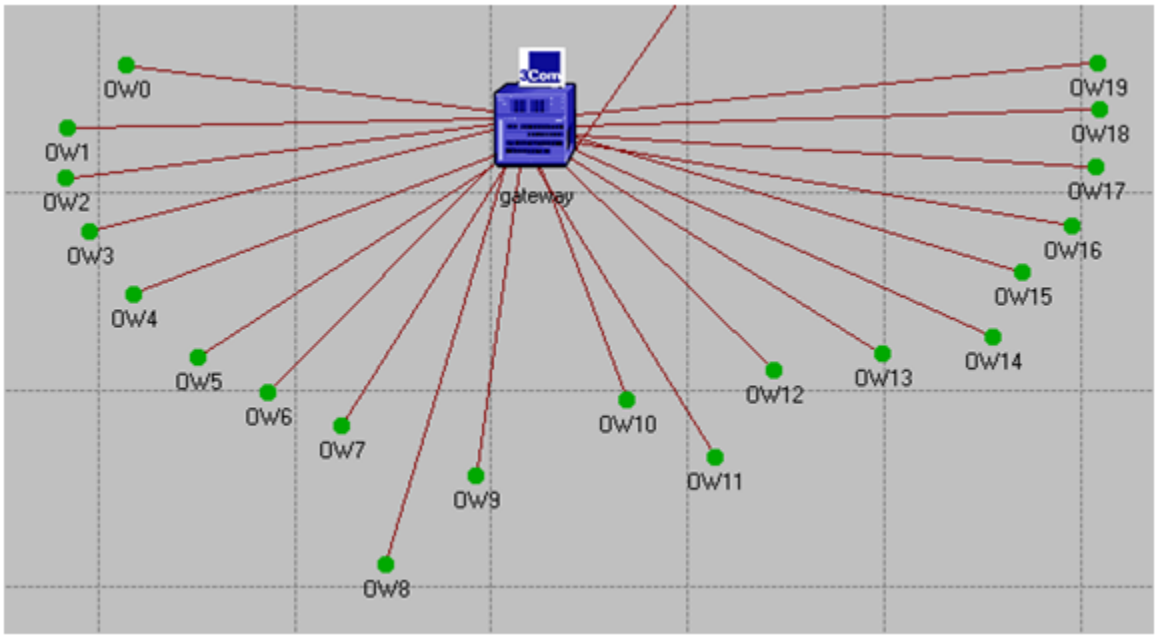

Figure 3.11. Structure of an optical workstation sub-network.

Knowledge of the optical network itself, including the network topology and physical characteristics, is stored in an XML configuration file, which is parsed and read into memory when a simulation starts. Appendix B shows the configuration file we used for the NSF network.

When a simulation starts, OW nodes send out connection requests according to a stochastic traffic pattern (e.g. Poisson and Self-similar). Upon receiving a connection request, the edge OR node computes a path from the source to the destination and starts a reservation protocol to create the connection. For each connection request, the source and the destination are randomly chosen among all OR nodes.

In simulating the network layer, we are mainly concerned with the performance of different RWA algorithms, where the performance of an algorithm is measured by the connection blocking probability under different constraints.

Architecture of the OPNET™ Simulation System

We have developed an OPNET™ simulation system for the implementation of a control plane as shown in Figure 3.10. New node modules and process modules have been designed. A node module usually represents a network component (e.g. the OR nodes and the OW nodes). Process modules defined inside a node module represent tasks running in the node and specify how the node functions.

The OW node in Figure 3.11 has two important process modules: *Cli_mgr* and *O_cli*. The *Cli_mgr* process randomly generates connection requests. The *O_cli* process represents the part of a connection stored in an optical workstation and will handle signaling messages on behalf of the workstation.

The OR node has 3 important process modules: *resource_manager*, *O_calle*, and *O_caller*. The *resource_manager* process is responsible for the management and allocation of resources in an optical router. The *O_callee* process and the *O_caller* process represent the part of a connection stored in an optical switch and are created on the demand of a connection request. Process *O_callee* is created in an OR node when a 'probe' message is received. If the node is not the destination, process *O_caller* is created, which will forward the 'probe' message to the next hop.

Figure 3.12 shows the collection of process modules created on nodes along the lightpath once a connection is established (2 hops in the example of Figure 3.12). When a connection is torn down, the *O_cli*, *O_calle*, and *O_caller* processes on the nodes need to be destroyed to free memory.

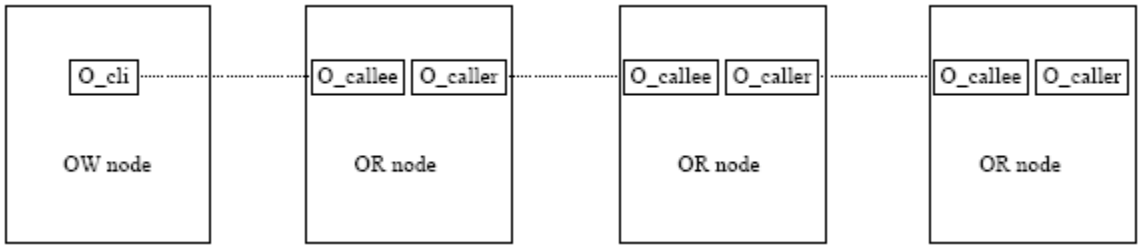

Figure 3.12. Logical relationship between processes created for a connection.

This simulation system has provided us the basic platform for studying, designing, implementing, testing, and comparing different RWA algorithms for all-optical networks.

ANALYTICAL MODELS FOR THE ASSESSMENT OF FIBER NONLINEAR EFFECTS

Introduction

The nonlinearities in optical fibers fall into two categories: stimulated scatterings (including Raman and Brillouin) and optical Kerr effects due to changes in the refractive index with optical power (including SPM, XPM, FWM). For today's standard optical links, the optical Kerr effects are considered more important in influencing signal quality. In this chapter, we focus on the effects of XPM and FWM, which are considered to be important for the current and near-future next-generation optical transmission systems.

Nonlinear effects originate from nonlinear polarizations. When multiple nonlinear effects are active, their interactions are complicated. To create simplified analytical models for predicting noise generated by nonlinear effects, three assumptions are made. First, the powers of signal channels are assumed to be low, such that the small-signal analysis can be applied and nonlinear noises are treated as small perturbations to the signal channels. Second, the electric fields of signal channels existing in a fiber are assumed to be co-linear (i.e. with the same polarization state) and bifringence is not considered. The aggregate influence of polarization-mode dispersion due to bifringence will be considered when computing the Q factor. Third, nonlinear effects

are assumed to be independent, and the power of the total noise generated by different nonlinear effects is simply the sum of the powers of the individual noise terms. Analytical models used to predict noise generated by different nonlinear effects can be developed separately. To be applied in an in-line routing algorithm, these models need to be efficient and scalable. The analytical models developed in this chapter will be used in the algorithms proposed in Chapter 7.

According to [52], the Q factor of a signal channel, considering a variety of physical impairments, can be computed as

$$Q = \frac{1}{EOP_{pmd}} \frac{I_1 - I_0}{\sigma_1 + \sigma_0} \tag{4.1}$$

by factoring out the polarization-mode dispersion effect, where EOP_{pmd} is the eye-openning penalty due to the polarization-mode dispersion, and σ_1^2 and σ_0^2 are the noise powers due to different noise sources at the mark state (i.e. when sending bit '1') and at the space state (i.e. when sending bit '0') respectively. Equation 4.1 can be understood by using the eye-diagram shown in Figure 4.1. Compared to the case when the polarization-mode dispersion is not present, Equation 4.1 assumes that the effect of the polarization-mode dispersion is to decrease the vertical openning of the eye-diagram due to pulse spread in the time domain.

In the derivations and simulations of this chapter, the 'probe and pump' approach is applied. The noise at the mark state can be found by setting the power of a CW probe channel equal to the channel peak power. The noise at the space state can be found by setting the power of a CW probe channel equal to 0.

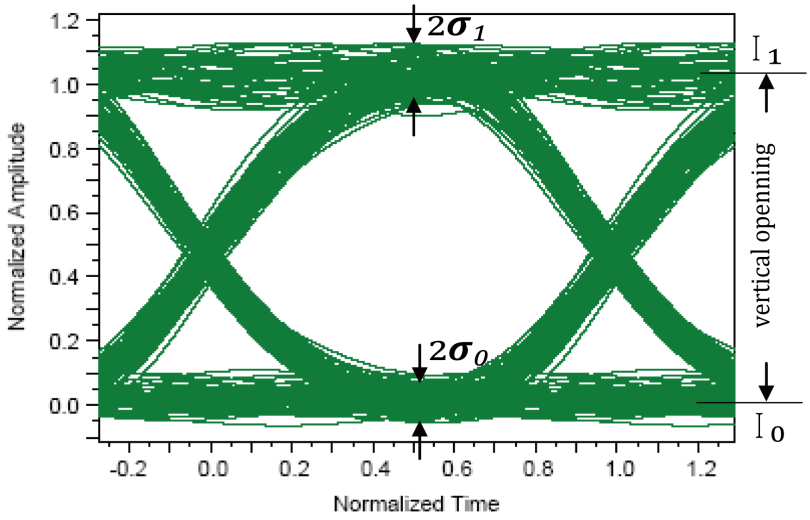

Figure 4.1. Example eye-diagram.

In this chapter, the analytical models for the assessment of XPM and FWM are first derived respectively for different optical link models and for the all-optical network models. Then the simulation results in different scenarios are discussed and compared with theoretical predications. These simulations are used to validate the analytical models.

Analytical Model for the Assessment of XPM

By XPM, the phase of a channel is modulated by the intensity fluctuations on other co-propagating channels. This phase modulation will later be converted to intensity modulation of the channel by fiber dispersion. In the study of XPM, the probe channel is a CW source. Along its propagation path, differential phase changes caused by pump channels can induce differential intensity modulation, behaving as

noise, of the probe channel at the end of an optical link or lightpath. The total noise is the integration of the generated differential noises along the propagation. In the following discussions, we first explain how to predict the noise of XPM effect in a single fiber segment, and then extend the model to more complex situations, including periodically amplified optical links and optical lightpaths.

XPM in A Single Fiber

The Incremental Transfer Function. Using a time coordinate system moving at the group velocity v_c of a probe channel and only considering XPM, the NLSE equation describing the propagation of the probe channel in a fiber segment is given by

$$\frac{\partial A_c}{\partial z} = \frac{-\alpha}{2} A_c(z,T) - \frac{j\beta_2}{2}\frac{\partial^2 A_c}{\partial T^2} + j\gamma 2 P_k(z,T) A_c(z,T), \tag{4.2}$$

where $A_c(z,T)$ is the complex amplitude of the probe channel, $P_k(z,T) = \overline{P_k(z,T)} + p_k(z,T)$ is the power of the only pump channel with $\overline{\quad}$ the average operator, and $p_k(z,T)$ is the power flunctuation of the pump channel.

To derive the XPM noise at the end of a fiber segment, the *incremental method* [53] is applied. Using the same idea as in SSFM, in the small interval $[z, z+dz]$, A_c satisfies the equation

$$\frac{\partial A_c}{\partial z} = j\gamma 2 P_k(z,T) A_c(z,T). \tag{4.3}$$

The solution of Equation 4.3 is

$$A_c(z+dz,T) = A_c(z,T) e^{j\gamma 2 P_k(z,T) dz} = A_c(z,T) e^{j\gamma 2 \overline{P_k(z,T)} dz}(1 + j\gamma 2 p_k(z,T) dz). \tag{4.4}$$

The probe channel is perturbed when it propagates along the fiber segment. According to the *incremental method*, the complex amplitude of the probe channel at the fiber end with length L is

$$A_c(L,T) = \overline{A_c(0,T)}e^{\frac{-\alpha L}{2}} + \int_{z=0}^{z=L} D_{z\to L}\overline{A_c(z,T)}j2\gamma p_k(z,T)dz, \tag{4.5}$$

where $D_{z\to L}$ denotes the linear propagation from point z to the fiber end and is defined in the frequency domain as

$$D_{z\to L} = e^{\frac{-\alpha(L-z)}{2}}e^{\frac{j\beta_2 w^2(L-z)}{2}}. \tag{4.6}$$

The term $e^{j\gamma 2\overline{P_k(z,T)}dz}$ in Equation 4.4 only causes a phase shift to $A_c(L,T)$ and is discarded for convenience.

Assuming that the pump channel is sinusoidally modulated with frequency w, i.e.

$$p_k(z,T) = p_k(z,w)e^{-jwT} + cc, \tag{4.7}$$

where *cc* indicates the complex conjugate, and substituting Equation 4.6 and Equation 4.7 into Equation 4.5, the complex amplitude at the fiber end is

$$\begin{aligned} A_c(L,T) =& \overline{A_c(0,T)}e^{\frac{-\alpha L}{2}} + \int_{z=0}^{z=L} D_{z\to L}\overline{A_c(z,T)}j2\gamma[p_k(z,w)e^{-jwT} + cc]dz \\ =& \overline{A_c(0,T)}e^{\frac{-\alpha L}{2}} + \int_{z=0}^{z=L} \overline{A_c(z,T)}j2\gamma[p_k(z,w)e^{-jwT} + cc]e^{\frac{-\alpha(L-z)}{2}}e^{\frac{j\beta_2 w^2(L-z)}{2}}dz. \end{aligned} \tag{4.8}$$

The power of the probe channel at the fiber end is

$$
\begin{aligned}
|A_c(z,T)|^2 =& \left\{ \overline{A_c(0,T)} e^{\frac{-\alpha L}{2}} + \int_{z=0}^{z=L} \overline{A_c(z,T)} j2\gamma [p_k(z,w) e^{-jwT} + cc] e^{\frac{-\alpha(L-z)}{2}} e^{\frac{j\beta_2 w^2 (L-z)}{2}} dz \right\} * \\
& \left\{ \overline{A_c(0,T)}^* e^{\frac{-\alpha L}{2}} - \int_{z=0}^{z=L} \overline{A_c(z,T)}^* j2\gamma [p_k^*(z,w) e^{jwT} + cc] e^{\frac{-\alpha(L-z)}{2}} e^{\frac{-j\beta_2 w^2 (L-z)}{2}} dz \right\} \\
\approx & |\overline{A_c(0,T)}|^2 e^{-\alpha L} + \\
& \overline{A_c(0,T)}^* e^{\frac{-\alpha L}{2}} \int_{z=0}^{z=L} \overline{A_c(z,T)} j2\gamma [p_k(z,w) e^{-jwT} + cc] e^{\frac{-\alpha(L-z)}{2}} e^{\frac{j\beta_2 w^2 (L-z)}{2}} dz - \\
& \overline{A_c(0,T)} e^{\frac{-\alpha L}{2}} \int_{z=0}^{z=L} \overline{A_c(z,T)}^* j2\gamma [p_k^*(z,w) e^{jwT} + cc] e^{\frac{-\alpha(L-z)}{2}} e^{\frac{-j\beta_2 w^2 (L-z)}{2}} dz \\
= & |\overline{A_c(0,T)}|^2 e^{-\alpha L} + \\
& e^{\frac{-\alpha L}{2}} \int_{z=0}^{z=L} [\overline{A_c(0,T)}^* \overline{A_c(z,T)} e^{\frac{j\beta_2 w^2 (L-z)}{2}} - \overline{A_c(z,T)}^* \overline{A_c(0,T)} e^{\frac{-j\beta_2 w^2 (L-z)}{2}}] * \\
& \qquad j2\gamma p_k(z,w) e^{-jwT} e^{\frac{-\alpha(L-z)}{2}} dz + CC \\
= & |\overline{A_c(0,T)}|^2 e^{-\alpha L} + \\
& \int_{z=0}^{z=L} |\overline{A_c(z,T)}|^2 [e^{\frac{j\beta_2 w^2 (L-z)}{2}} - e^{\frac{-j\beta_2 w^2 (L-z)}{2}}] j2\gamma p_k(z,w) e^{-jwT} e^{-\alpha(L-z)} dz + CC \\
= & |\overline{A_c(0,T)}|^2 e^{-\alpha L} - \\
& \int_{z=0}^{z=L} \overline{P_c(z,T)} 4\gamma p_k(z,w) sin[\frac{\beta_2 w^2 (L-z)}{2}] e^{-jwT} e^{-\alpha(L-z)} dz + CC.
\end{aligned}
\tag{4.9}
$$

In Equation 4.9, we have used the assumption

$$
\overline{A_c(0,T)} = \overline{A_c(z,T)} e^{\frac{\alpha z}{2}}. \tag{4.10}
$$

From Equation 4.9, we see that the probe channel is also sinusoidally modulated. By comparing Equation 4.7 and Equation 4.9, the incremental transfer function $g(z,w)$ is defined as

$$
g(z,w) = -4\gamma \overline{P_c(z,T)} sin(\frac{\beta_2 w^2 (L-z)}{2}) e^{-\alpha(L-z)}, \tag{4.11}
$$

where the term $sin(\frac{\beta_2 w^2(L-z)}{2})$ is due to the dispersion of the amplitude component with frequency w relative to the carrier of the probe channel from point z to the fiber end and we define $\frac{\beta_2 w^2(L-z)}{2}$ as the *phase-lag* of the amplitude component.

Defining $b = \frac{w^2 D_c \lambda_c^2}{4\pi c}$ (c is the speed of light, λ_c is the wavelength of the probe channel, and D_c is the dispersion parameter of the fiber at the wavelength λ_c), Equation 4.11 can be rewritten as

$$g(z,w) = 4\gamma\overline{P_c(z,T)}sin[b(L-z)]e^{-\alpha(L-z)}. \tag{4.12}$$

In Equation 4.12, we see that the phase-lag is proportional to the accumulated dispersion from the point z to the fiber end.

The intensity modulation component $p_k(z,w)$ of the pump channel has caused a corresponding differential intensity modulation $dp_c(L,w)$ of the probe channel at the fiber end, with

$$dp_c(L,w) = p_k(z,w)g(z,w). \tag{4.13}$$

The total intensity modulation component $p_c(L,w)$ is the integration along the whole fiber segment, i.e.

$$p_c(L,w) = \int_{z=0}^{z=L} p_k(z,w)g(z,w)dz. \tag{4.14}$$

Power Evolution of the Pump Channel. When the power of the pump channel is sinusoidally modulated with frequency w, at point z along the fiber this modulation becomes [54]

$$p_k(z,w) = p_k(0,w)cos(qz)e^{-\alpha z}e^{-jwzd_{ck}}, \tag{4.15}$$

where $p_k(0,w)$ is the intensity modulation component at the beginning of the fiber, $q = \frac{w^2 D_k \lambda_k^2}{4\pi c}$ (λ_k is the wavelength of the pump channel and D_k is the dispersion parameter at λ_k), qz is the phase-lag of the amplitude component with frequency w relative to the carrier of the pump channel, and $e^{-jwzd_{ck}}$ ($d_{ck} = \frac{1}{v_c} - \frac{1}{v_k}$) is due to pulse shifting of the pump channel relative to the probe channel.

The XPM Transform Function. Considering the power evolution of the pump channel and the incremental transfer function, the intensity modulation at the fiber end is [55]

$$\begin{aligned}
p_c(L,w) &= \int_{z=0}^{z=L} p_k(z,w) g(z,w) dz \\
&= \int_{z=0}^{z=L} p_k(0,w) cos(qz) e^{-\alpha z} e^{-jwzd_{ck}} 4\gamma \overline{P_c(z,T)} sin[b(L-z)] e^{-\alpha(L-z)} dz \\
&= 4\gamma p_k(0,w) \overline{P_c(0,T)} e^{-\alpha L} \int_{z=0}^{z=L} cos(qz) e^{-(\alpha + jwd_{ck})z} sin([b(L-z)] dz \\
&= 2\gamma p_k(0,w) \overline{P_c(0,T)} e^{-\alpha L} * \\
&\quad \left\{ \frac{asin(bL) - (b+q)cos(bL) + [asin(qL) + (b+q)cos(qL)] e^{-\alpha L}}{a^2 + (b+q)^2} + \right. \\
&\quad \left. \frac{asin(bL) - (b-q)cos(bL) + [-asin(qL) + (b-q)cos(qL)] e^{-\alpha L}}{a^2 + (b-q)^2} \right\},
\end{aligned} \tag{4.16}$$

where $a = \alpha + jwd_{ck}$.

When the fiber is long enough such that $e^{-\alpha L} \approx 0$, which is true in communication applications, Equation 4.16 can be simplified as

$$p_c(L,w) = 2\gamma p_k(0,w) \overline{P_c(0,T)} e^{-\alpha L} [\frac{asin(bL) - (b+q)cos(bL)}{a^2 + (b+q)^2} + \frac{asin(bL) - (b-q)cos(bL)}{a^2 + (b-q)^2}]. \tag{4.17}$$

The intensity modulation in the time domain is the inverse Fourier transform of Equation 4.17.

The XPM transform function of a pump channel on a single fiber segment with length L is then defined as

$$H(w) = 2\gamma\overline{P_c(0,T)}e^{-\alpha L}[\frac{asin(bL) - (b+q)cos(bL)}{a^2 + (b+q)^2} + \frac{asin(bL) - (b-q)cos(bL)}{a^2 + (b-q)^2}]. \tag{4.18}$$

The variance of the noise generated by the XPM effect on the probe channel is [56]

$$\sigma^2_{xpm} = \frac{1}{2\pi}\int_{-\infty}^{\infty} |H(w)|^2 PSD_{pump}(w)dw, \tag{4.19}$$

where $PSD_{pump}(w)$ is the power spectrum of the pump channel at the input of the fiber segment and $H(w)$ is the XPM transform function of the pump channel.

For WDM systems, all the co-propagating channels need to be considered. Assuming that all pump channels are independent, the variance is [56]

$$\sigma^2_{xpm} = \frac{1}{2\pi}\sum_{j\in pumps}\int_{-\infty}^{\infty} |H_j(w)|^2 PSD_j(w)dw, \tag{4.20}$$

where $PSD_j(w)$ and $H_j(w)$ are the power spectrum and the XPM transfer function of the pump channel j respectively.

When computing the Q factor of a signal channel, this channel is treated as the probe channel. When the signal channel is at the space state, the term $\overline{P_c(0,T)}$ in Equation 4.18 should use 0 and the resultant XPM transfer function is zero. So the

variance of XPM noise at the space state is negligible. When the signal channel is at the mark state, the term $\overline{P_c(0,T)}$ should use the peak power of the channel.

XPM in Optical Links

An optical link consists of several periodically amplified spans. In each span, a long transmission fiber (SMF or NZDSF) is followed by a short DCF fiber. The length of the transmission fiber is assumed to be L. We further assume that the in-line amplifier will exactly compensate the span attenuation. However, the span residual dispersion can be tuned to achieve the best link performance. It was reported in [56], that the XPM effect generated in the DCF fiber is negligible due to the large attenuation incurred in the preceding transmission fiber and will not be taken into account in the following derivations.

The XPM transfer function can be defined for optical links using different compensation schemes.

FOCS Links. For a N-span optical link compensated using the FOCS scheme, the XPM transfer function of a pump channel is

$$\begin{aligned} H(w) &= \sum_{n=1}^{N} \int_{z=0}^{z=L} cos(q_n z) e^{-\alpha_n z} e^{-jwzd_{ck,n}} 4\gamma \overline{P_c(0,T)} e^{-\alpha_n z} sin[b_n(L-z) - b_n L] e^{-\alpha_n (L-z)} e^{\alpha_n L} dz \\ &= \sum_{n=1}^{N} -4\gamma \overline{P_c(0,T)} \int_{z=0}^{z=L} cos(q_n z) e^{-a_n z} sin(b_n z) dz \\ &= \sum_{n=1}^{N} -4\gamma \overline{P_c(0,T)} \frac{b_n a_n^2 + b_n^3 - q_n^2 b_n}{[a_n^2 + (q_n + b_n)^2][a_n^2 + (q_n - b_n)^2]}, \end{aligned} \tag{4.21}$$

where a_n, b_n, and q_n are the corresponding parameters of the n$^{\text{th}}$ span. We notice that the dispersions of the amplitude frequency component w relative to the carrier should be 0 from the beginning of the link to the beginning of the n$^{\text{th}}$ span and from the end of the n$^{\text{th}}$ span to the end of the link due to the FOCS compensation scheme, and hence the corresponding phase-lags are also 0. In the derivation of Equation 4.21, we have only considered the first order dispersion. The term $-b_nL$ is due to the dispersion of the DCF fiber and $e^{\alpha_n L}$ is due to the in-line amplifier at the end of each span.

Assuming a_ns=a (i.e., all the spans are identical) and b_ns=q_ns=b (this is true in WDM and DWDM networks due to the small frequecy difference among channels), Equation 4.21 can be simplified as [56]

$$H(w) = -4\gamma N\overline{P_c(0,T)}\frac{b}{a^2+4b^2}. \tag{4.22}$$

DUCS Links. For a N-span optical link compensated using the DUCS scheme, the XPM transfer function of a pump channel is

$$\begin{aligned} H(w) =& \sum_{n=1}^{N}\int_{z=0}^{z=L} cos(Q_n^k + q_n z)e^{-\alpha_n z}e^{-jwzd_{ck,n}}e^{-jwD_n^k\triangle\lambda_{ck}} * \\ & 4\gamma\overline{P_c(0,T)}e^{-\alpha_n z}sin[C - Q_n^c - b_n z]e^{-\alpha_n(L-z)}e^{\alpha_n L}dz \\ =& \sum_{n=1}^{N} 4\gamma\overline{P_c(0,T)}e^{-jwD_n^k\triangle\lambda_{ck}}\int_{z=0}^{z=L} cos(Q_n^k + q_n z)e^{-a_n z}sin(C - Q_n^c - b_n z)dz, \end{aligned} \tag{4.23}$$

where Q_n^k and Q_n^c are the accumulated phase-lags from the start of the link to the beginning of the n$^{\text{th}}$ span for the pump channel and the probe channel respectively,

$\triangle\lambda_{ck} = \lambda_c - \lambda_k$, and

$$Q_n^k = \frac{w^2\lambda_k^2 D_n^k}{4\pi c}, \tag{4.24}$$

$$Q_n^c = \frac{w^2\lambda_c^2 D_n^c}{4\pi c}, \tag{4.25}$$

$$C = \frac{w^2\lambda_c^2 D_R^c}{4\pi c}, \tag{4.26}$$

where D_n^k and D_n^c are the accumulated dispersions from the start of the link to the beginning of the n$^{\text{th}}$ span for the pump channel and the probe channel respectively, C is the accumulated phase-lag of the probe channel on the whole link, and D_R^c is the residual dispersion of the probe channel on the link.

In Equation 4.23, the term $[C - Q_n^c - b_n z]$ is the phase-lag of the probe channel from point z in the n$^{\text{th}}$ span to the link end and is proved by the following lemma.

Lemma 1. *The phase-lag $\phi_{lag,z\rightarrow link\ end}$ of the probe channel from point z in the n^{th} span to the link end is $[C - Q_n^c - b_n z]$.*

Proof. Assuming that the total dispersion from the point z in the n$^{\text{th}}$ span to the link end is D_x, the following relationship holds

$$D_n^c + Dz + D_x = D_R^c, \tag{4.27}$$

where D is the dispersion parameter of the transmission fiber in the n$^{\text{th}}$ span.

Mutiplying both sides of Equation 4.27 by $\frac{w^2\lambda_c^2}{4\pi c}$, we find

$$Q_n^c + b_n z + \phi_{lag,z\rightarrow\text{link end}} = C$$

$$\phi_{lag,z\rightarrow\text{link end}} = C - Q_n^c - b_n z. \tag{4.28}$$

□

In case $Q_n^k \approx Q_n^c$ and $q_n \approx b_n$, Equation 4.23 can be simplified as [56]

$$H(w) = \sum_{n=1}^{N} 4\gamma \overline{P_c(0,T)} e^{-jwD_n^k \triangle\lambda_{ck}} \int_{z=0}^{z=L} cos(Q_n^c + b_n z) e^{-a_n z} sin(C - Q_n^c - b_n z) dz$$
$$= \sum_{n=1}^{N} 2\gamma \overline{P_c(0,T)} e^{-jwD_n^k \triangle\lambda_{ck}} [\frac{a_n sin(C - 2Q_n^c) - 2b_n cos(C - 2Q_n^c)}{a_n^2 + 4b_n^2} + \frac{sin(C)}{a_n}]. \quad (4.29)$$

XPM in Optical Lightpaths

For an optical lightpath, the set of co-propagating lightpaths can change along its route. At a switch node, some lightpaths can diverge from its route and new lightpaths can join it in co-propagating along the next optical link. As an example, the situation is described in Figure 4.2.

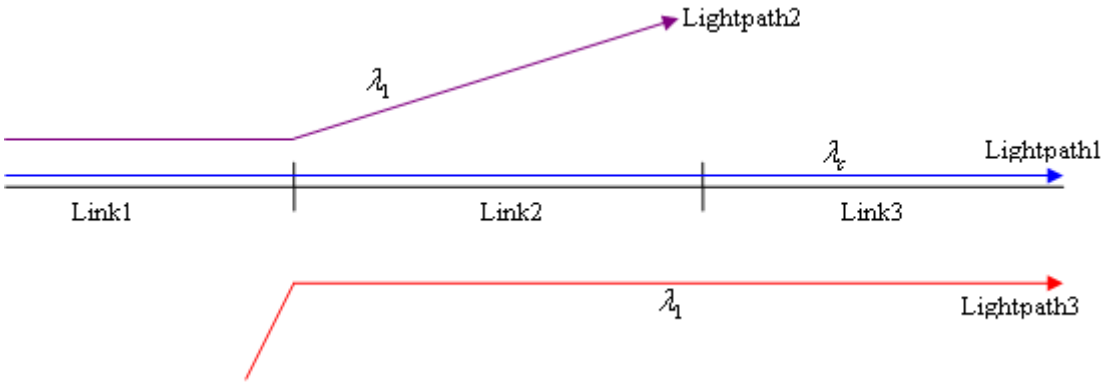

Figure 4.2. Lightpath1 and its co-propagating lightpaths. λ_c is the wavelength used by the probe lightpath Lightpath1.

In Figure 4.2, we are concerned with the signal quality of *Lightpath1* and denote it as the probe lightpath. Its co-propagating lightpaths (e.g. *Lightpath2* and *Lightpath3*) are denoted as pump lightpaths. For each possible pump channel (i.e. wavelength)

on the route along a probe lightpath, the route is divided into *coherent segments*. The same wavelength on a coherent segment belongs to one pump lightpath. In Figure 4.2, the route of *Lightpath1* is divided into two coherent segments for the wavelength λ_1. The first coherent segment, including *Link1*, belongs to *Lightpath2*. The second coherent segment, including *Link2* and *Link3*, belongs to *Lightpath3*. The XPM transfer function of a pump channel on a coherent segment can also be defined. The following algorithm shows how to compute the XPM noise generated on a probe lightpath at the end of the lightpath.

Algorithm 4.1 Computing XPM noise on a probe lightpath

```
1: xpm_noise = 0;
2: for each possible pump channel do
3:    Divide route of the probe lightpath into coherent segments;
4:    for each coherent segment do
5:       seg_noise = compute the XPM noise generated by the segment at the end
         of the lightpath;
6:       xpm_noise+=seg_noise;
7:    end for
8: end for
```

A coherent segment can be treated as a multi-span link and Equation 4.21 and Equation 4.23 can be applied with small modifications (i.e. considering the accumulated phase-lag from the source of the pump lightpath to the position z on the coherent segment and the accumulated phase-lag from the position z to the end of the probe lightpath). An important observation is that if each optical link has 0 residual dispersion, then the XPM transform function of a wavelength on a coherent segment can be determined by only knowing the properties of its consisting links.

Numerical Simulation of XPM

Using the PHOTOSS^{TM} software, we have investigated the influence of XPM on WDM systems. We test the correctness of the derived XPM analytical models by comparing numerical simulation results with theoretical predictions under different link configurations. In the simulation, the pump channels send out pseudo-random bit streams using squared-cosine optical pulses. The definition of a normalized pulse is defined as

$$P(\frac{t}{T}) = \begin{cases} 1 & \text{if } |\frac{t}{T}| < \frac{1-R}{2} \\ cos^2(\frac{\pi}{2R}(|\frac{t}{T}| - \frac{1-R}{2}) & \text{if } \frac{1-R}{2} \leq |\frac{t}{T}| < \frac{1+R}{2} \\ 0 & \text{else,} \end{cases} \tag{4.30}$$

where $P(\frac{t}{T})$ is the optical power profile of the pulse, T is the duration of one bit period , and $R \in [0, 1]$ is the roll-off factor set to 0.5 in our simulations. The power spectrum of a random bit stream using the squared-cosine pulses with peak power P_{max} is defined as

$$PSD(w) = \frac{P_{max}^2}{4}[|\frac{cos(\frac{RTw}{2})}{1-(\frac{RTw}{\pi})^2} sinc(\frac{Tw}{2\pi})|^2 * T + \delta(w)]. \tag{4.31}$$

The PHOTOSS^{TM} simulation setup to simulate a 14-span link is show in Figure 4.3.

The influence of the XPM noises generated by the pump channels on the probe channel (i.e. the CWLaser in Figure 4.3) is investigated at the end of the optical link. In the figure, a post-compensation DCF fiber is used at the end of the link. The length of the post-compensation fiber can be tuned to achieve the best signal quality.

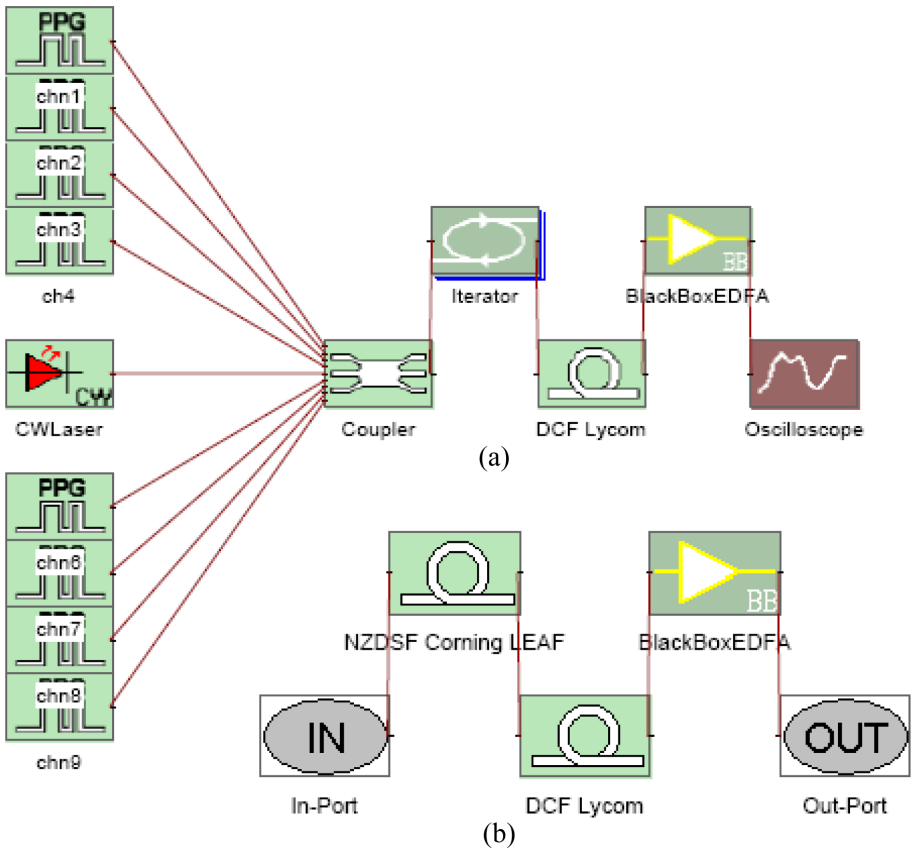

Figure 4.3. XPM simulation setup. The Iterator component includes 14 identical spans, which is show in (b). The frequency comb has spacing 50GHz. The probe channel (i.e. the CW source) is at the center of the comb and has frequency 193.1THz (wavelength 1553.6nm). The pump channels have a data transmission rate of 10Gbps each.

When the link in Figure 4.3 is compensated using the FOCS scheme, Figure 4.4 compares the Q factors obtained using the analytical model developed in this section and using the PHOTOSS^{TM} simulation. Figure 4.4 shows a good match.

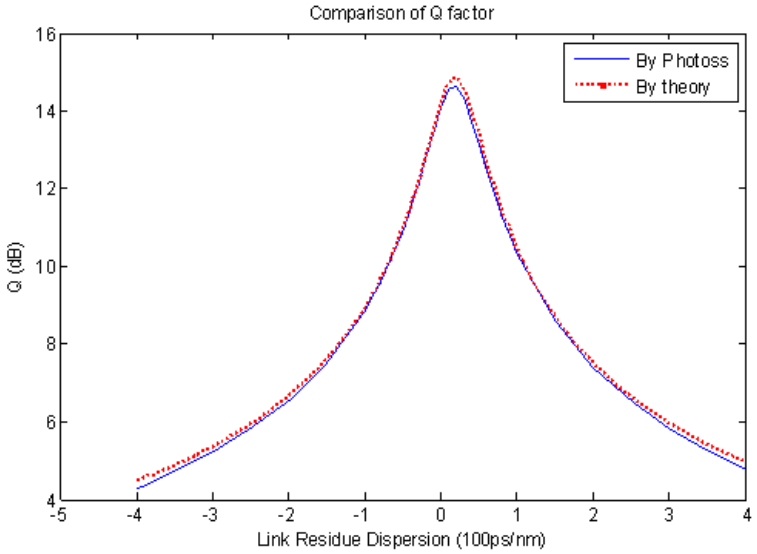

Figure 4.4. Comparison of the Q factor of a probe channel in a FOCS link. The peak powers of the 8 pump channels and the power of the probe channel are set to 1.5632 mW. The NZDSF fiber has configurations: L =80 Km, α =0.25 dB/Km, D=4 $\frac{\text{ps}}{\text{Km*nm}}$, γ =2.0561 $\frac{1}{\text{w*Km}}$. The DCF fiber is linear with L =3.2 Km, α =0.5 dB/Km, D=$-$100 $\frac{\text{ps}}{\text{Km*nm}}$. The gain of the in-line EDFA amplifier is 21.6 dB. The length of the post-compensation fiber is tuned to vary the residual dispersion of the link.

Because in Figure 4.4 a post-compensation fiber is considered, a small modification to Equation 4.21 as

$$H(w) = \sum_{n=1}^{N} \int_{z=0}^{z=L} cos(q_n z) e^{-\alpha_n z} e^{-jwzd_{ck,n}} 4\gamma \overline{P_c(0,T)} e^{-\alpha_n z} * \\ sin[b_n(L-z) - b_n L + Q_p] e^{-\alpha_n (L-z)} e^{\alpha_n L} dz \qquad (4.32)$$

is applied when driving the analytical model of XPM noise in the link, where Q_p is the phase-lag of the probe channel induced in the post-compensation fiber and $Q_p = \frac{w{\lambda_c}^2}{4\pi c} DL$ with DL the accumulated dispersion in the fiber.

Figure 4.5 shows the validity of the analytical model when the link in Figure 4.3 is compensated using the DUCS scheme.

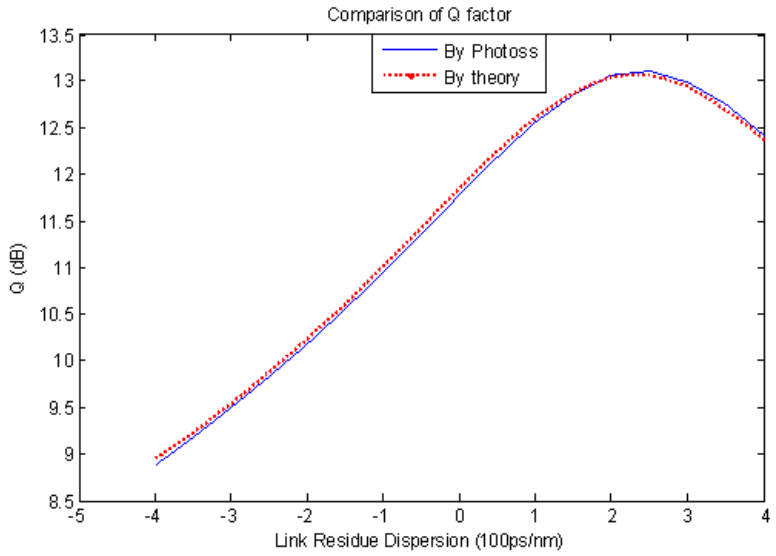

Figure 4.5. Comparison of the Q factor of a probe channel in a DUCS link. The peak powers of the 8 pump channels and the power of the probe channel are set to 1.5632mW. The NZDSF fiber has configurations: L =80 Km, α =0.25 dB/Km, D =4 $\frac{\text{ps}}{\text{Km*nm}}$, γ =2.0561 $\frac{1}{\text{w*Km}}$. The DCF fiber is linear with L =2.9 Km, α =0.4 dB/Km, D =$-$100 $\frac{\text{ps}}{\text{Km*nm}}$. The gain of the in-line EDFA amplifier is 21.16 dB. The length of the post-compensation fiber is tuned to vary the residual dispersion of the link.

The development of the analytical models has assumed that the signal channels have low powers. Figure 4.6 shows the sensitivity of the analytical model to the increase of channel power in a FOCS link. The peak powers of the pump channels and the power of the probe channel are increased from 1 mW to 10 mW.

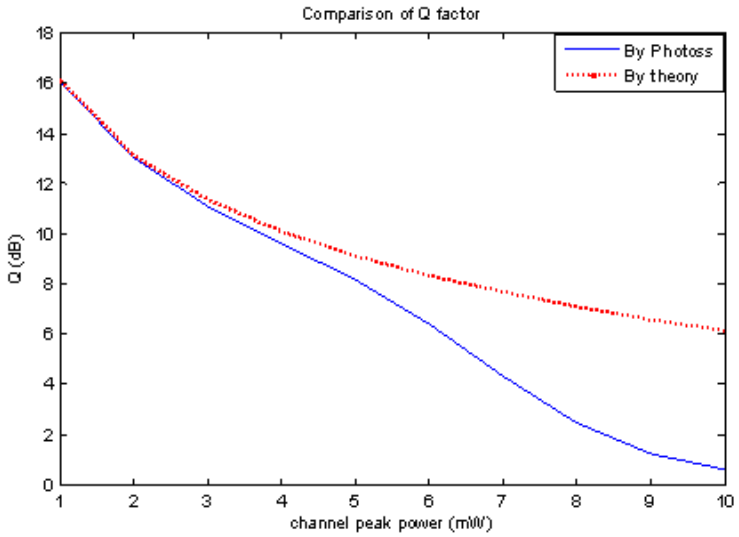

Figure 4.6. Sensitivity of the XPM analytical model to the increase of channel power. The simulation setup is the same as in Figure 4.4, but the length of the post-compensation fiber is fixed to 0.

Figure 4.6 shows that the analytical model works well when the channel power is smaller than 5 mW. The signal power used in communication systems is also in the range of several milliwatts and is limited by a number of factors, including the available laser power.

In practice, the probe channel should also be dynamic, transmitting pulse streams. We argue that the Q factor computed by the above CW method is a good approximation for the dynamic situation. Figure 4.7 shows that the XPM-generated noise waveform on the CW probe channel is similar to the noise waveform on a dynamic probe channel when the dynamic probe is at the mark state.

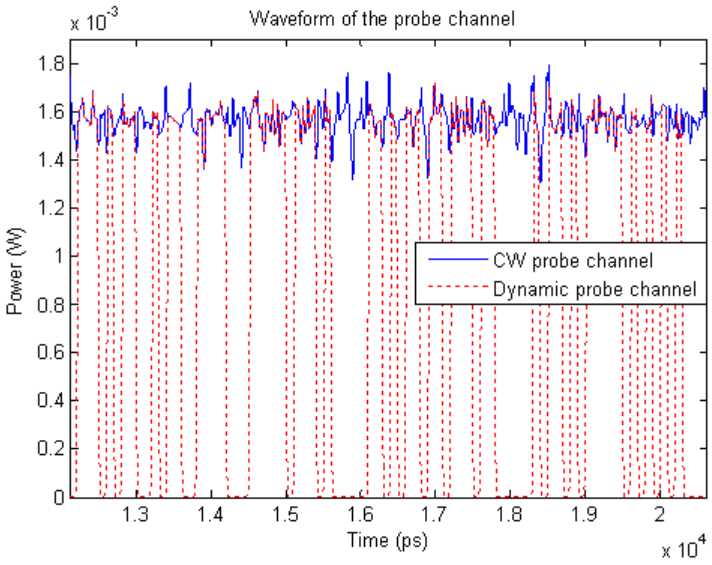

Figure 4.7. Comparison of XPM-generated noise waveforms on CW and dynamical probe channels. The simulation setup is the same as in Figure 4.4, but the length of the post-compensation fiber is fixed to 0. In two cases of the figure, the input of each pump channel is fixed.

Analytical Model for the Assessment of FWM

In FWM, three waves mix and generate a new wave. This poses a problem when the frequency of the generated wave is close to the frequency of another signal channel. The FWM effect is illustrated in Figure 4.8. FWM is an important effect influencing signal quality in WDM and DWDM networks, where channel frequency spacing is small. In the common approaches to study FWM, all the channels are modeled as CW sources [57].

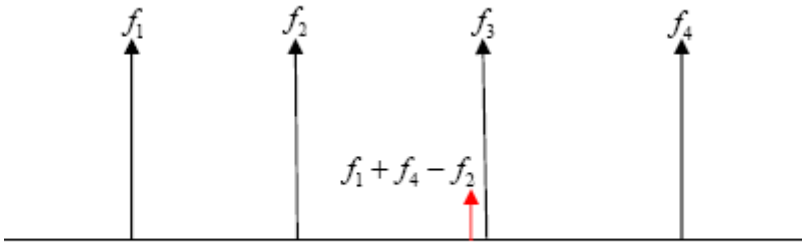

Figure 4.8. Illustration of FWM. Three pump channels (f_1, f_2, and f_4) generate a FWM mixing wave at frequency $f_1 + f_4 - f_2$, close to the channel f_3.

FWM in A Single Fiber

The NLSE equation describing the pulse propagation of a probe channel, considering only one FWM mixing term by three pump channels, is defined as

$$\frac{\partial A_c}{\partial z} = -\frac{\alpha}{2}A_c - \frac{j\beta_2}{2}\frac{\partial^2 A_c}{\partial T^2} + j\gamma\frac{d}{3}A_m A_n A_p^* e^{j\triangle K_c z}, \tag{4.33}$$

where a time coordinate system moving at the probe channel group velocity v_c is used, $A(z,T)$s are the complex amplitudes of signal channels, d is the degeneracy factor, and $\triangle K_c = \beta(w_m) + \beta(w_n) - \beta(w_p) - \beta(w_c)$.

When all the signal channels are CW sources and the probe channel has power 0 at the beginning of a fiber, Equation 4.33 can be simplified as [57]

$$\begin{cases} \frac{\partial A_c}{\partial z} & = -\frac{\alpha}{2}A_c + j\gamma\frac{d}{3}A_m A_n A_p^* e^{j\triangle K_c z} \\ A_c(0) & = 0, \end{cases} \tag{4.34}$$

where $A(z,T)$s in Equation 4.33 are simplified as $A(z)$s due to the fact that they are only functions of position now.

The complex amplitudes of the three pump channels evolve along the fiber as [57]

$$\begin{cases} A_m(z) &= A_m(0)e^{\frac{-\alpha z}{2}} \\ A_n(z) &= A_n(0)e^{\frac{-\alpha z}{2}} \\ A_p(z) &= A_p(0)e^{\frac{-\alpha z}{2}}. \end{cases} \tag{4.35}$$

Substituting Equation 4.35 into Equation 4.34, the evolution of $A_c(z)$ satisfies

$$\begin{cases} \frac{\partial A_c}{\partial z} &= -\frac{\alpha}{2}A_c + j\gamma\frac{d}{3}A_m(0)A_n(0)A_p^*(0)e^{\frac{-3\alpha z}{2}}e^{j\triangle K_c z} \\ A_c(0) &= 0. \end{cases} \tag{4.36}$$

The solution of Equation 4.36 is [57]

$$A_c(z) = j\gamma\frac{d}{3}A_m(0)A_n(0)A_p^*(0)e^{\frac{-\alpha z}{2}}L_{eff}, \tag{4.37}$$

where $L_{eff} = \frac{e^{(j\triangle K_c - \alpha)z}-1}{j\triangle K_c - \alpha}$, and the $\triangle K_c$ can be computed by [57]

$$\triangle K_c = 2\pi\frac{\lambda_c^2}{c}(f_m - f_c)(f_n - f_c)[D - \frac{\lambda_c^2}{c}(\frac{f_m + f_n}{2} - f_c)S], \tag{4.38}$$

where D and S are the dispersion parameter and the dispersion slope of the fiber respectively.

The corresponding electric field of the probe channel is

$$E_c(z) = j\gamma\frac{d}{3}A_m(0)A_n(0)A_p^*(0)e^{\frac{-\alpha z}{2}}L_{eff}e^{j\beta(w_c)z}, \tag{4.39}$$

where the term $f(x,y)e^{-jw_c t}$ in defining electric field is omitted for simplicity, and the power of the probe channel is

$$P_c(z) = |\gamma\frac{d}{3}A_m(0)A_n(0)A_p^*(0)e^{\frac{-\alpha z}{2}}L_{eff}|^2. \tag{4.40}$$

In case of multiple FWM mixing terms, at the end of the fiber segment the power of the total FWM noise generated on the probe channel is computed by

$$\sigma_{fwm}^2 = \sum_{m,n\neq p, w_m + w_n - w_p = w_c} \sigma_{m,n,p}^2, \tag{4.41}$$

where $\sigma^2_{m,n,p}$ is given by Equation 4.40.

FWM in Optical Links

For an optical link as shown in Figure 4.3, the FWM noise generated at the end of the link is the sum of noises generated in all spans. In each span, the noise generated in the DCF fiber is negligible. The post-compensation fiber also has no effects (due to its short length) except attenuation, which is compensated by the amplifier after it, and a constant phase shift.

We define the phase shifts of relevant signal channels in each identical span as

$$\begin{cases} \phi_c & = \phi_c^{NZDSF} + \phi_c^{DCF} \\ \phi_m & = \phi_m^{NZDSF} + \phi_m^{DCF} \\ \phi_n & = \phi_n^{NZDSF} + \phi_n^{DCF} \\ \phi_p & = \phi_p^{NZDSF} + \phi_p^{DCF}, \end{cases} \tag{4.42}$$

where ϕ_c is the phase shift of the probe channel, and ϕ_m, ϕ_n, and ϕ_p are the phase shifts of the three pump channels respectively.

At the beginning of the k$^{\text{th}}$ span, the three pump channels have complex amplitudes $A_m(0)e^{j(k-1)\phi_m}$, $A_n(0)e^{j(k-1)\phi_n}$, and $A_p(0)e^{j(k-1)\phi_p}$ respectively with $A(0)$s the amplitudes of the pump channels at the start of the link. Assuming that the transmission fiber in each span has length L, the electric field of the FWM mixing term generated by the k$^{\text{th}}$ span at the link end is

$$E_c(k^{th}span \rightarrow end) = j\gamma\frac{d}{3}A_m(0)A_n(0)A_p^*(0)e^{j(k-1)(\phi_m+\phi_n-\phi_p)}e^{j\phi_c}e^{j(N-k)\phi_c}L_{eff}, \tag{4.43}$$

where N is the number of spans in the link, the term $e^{j(N-k)\phi_c}$ is due to the propagation from the end of the k$^{\text{th}}$ span to the link end.

The total FWM electric field at the end of the optical link is

$$E_c^{total} = \sum_{n=1}^{N} j\gamma\frac{d}{3}A_m(0)A_n(0)A_p^*(0)e^{j(k-1)(\phi_m+\phi_n-\phi_p)}e^{j\phi_c}e^{j(N-k)\phi_c}L_{eff}$$
$$= j\gamma\frac{d}{3}A_m(0)A_n(0)A_p^*(0)e^{jN\phi_c}L_{eff}\sum_{n=1}^{N}e^{j(k-1)(\phi_m+\phi_n-\phi_p-\phi_c)}. \quad (4.44)$$

The power of the total FWM noise generated on the probe channel then is [59]

$$P_c^{total} = |\gamma\frac{d}{3}A_m(0)A_n(0)A_p^*(0)L_{eff}|^2 * |\sum_{n=1}^{N}e^{j(k-1)(\phi_m+\phi_n-\phi_p-\phi_c)}|^2. \quad (4.45)$$

In Equation 4.45, the term $|\gamma\frac{d}{3}A_m(0)A_n(0)A_p^*(0)L_{eff}|^2$ is the power of the FWM noise generated by just one span, and the term $|\sum_{n=1}^{N}e^{j(k-1)(\phi_m+\phi_n-\phi_p-\phi_c)}|^2$ manifests the accumulation of noise along the link. Equation 4.45 can be rewritten as

$$P_c^{total} = P_c^{1span} * link_factor, \quad (4.46)$$

where $P_c^{1span} = |\gamma\frac{d}{3}A_m(0)A_n(0)A_p^*(0)L_{eff}|^2$ and $link_factor = |\sum_{n=1}^{N}e^{j(k-1)(\phi_m+\phi_n-\phi_p-\phi_c)}|^2 = |\frac{1-e^{jN\triangle\phi}}{1-e^{j\triangle\phi}}|^2$ with $\triangle\phi = \phi_m + \phi_n - \phi_p - \phi_c$. The $\triangle\phi$ can be computed as

$$\triangle\phi = \triangle K_c^{NZDSF}L_{NZDSF} + \triangle K_c^{DCF}L_{DCF}$$
$$= 2\pi\frac{\lambda_c^2}{c}(f_m - f_c)(f_n - f_c)[D_{NZDSF} - \frac{\lambda_c^2}{c}(\frac{f_m+f_n}{2} - f_c)S_{NZDSF}]L_{NZDSF} +$$
$$2\pi\frac{\lambda_c^2}{c}(f_m - f_c)(f_n - f_c)[D_{DCF} - \frac{\lambda_c^2}{c}(\frac{f_m+f_n}{2} - f_c)S_{DCF}]L_{DCF}$$
$$= 2\pi\frac{\lambda_c^2}{c}(f_m - f_c)(f_n - f_c)[D_{NZDSF}L_{NZDSF} + D_{DCF}L_{DCF} -$$
$$\frac{\lambda_c^2}{c}(\frac{f_m+f_n}{2} - f_c)(S_{NZDSF}L_{NZDSF} + S_{DCF}L_{DCF})]. \quad (4.47)$$

When the link is compensated using the FOCS scheme, the term $D_{NZDSF}L_{NZDSF}+D_{DCF}L_{DCF}=0$ and Equation 4.47 can be simplified as

$$\triangle\phi = 2\pi\frac{\lambda_c^2}{c}(f_m - f_c)(f_n - f_c)[-\frac{\lambda_c^2}{c}(\frac{f_m + f_n}{2} - f_c)(S_{NZDSF}L_{NZDSF} + S_{DCF}L_{DCF})]. \tag{4.48}$$

FWM in Optical Lightpaths

For each possible FWM mixing term on the route along a probe lightpath, the route is divided into coherent segments. In each coherent segment, the three pump channels belong to three pump lightpaths respectively and co-propagate. Each coherent segment can be treated as an optical link and the FWM noise power is computed using Equation 4.45. The power of the total FWM noise at the end of the probe lightpath is the sum of noise powers generated by all coherent segments. Algorithm 4.2 describes how to compute the FWM noise at the end of a probe lightpath in a WDM network.

Algorithm 4.2 Computing FWM noise on a probe lightpath

```
1: fwm_noise = 0;
2: for each possible FWM mixing term do
3:    Divide route of the probe lightpath into coherent segments;
4:    for each coherent segment do
5:       seg_noise = compute the FWM noise generated by the segment at the end
         of the lightpath;
6:       fwm_noise+=seg_noise;
7:    end for
8: end for
```

The above discussions have assumed that there is no power in the probe channel and all the pump channels are also CW sources. In practical networks, all the signal channels send out optical pulse streams and we are concerned with their signal qualities. Even in such complex cases, the analytical models developed in this section can be used to estimate the Q factor of a signal channel. Its co-propagating channels can be treated as CW pump channels with power equal to the channel average power (i.e. $\frac{1}{2}$ of the peak power). At the space state, the power of FWM noise befor photo-detection can be computed by the developed analytical models and denoted as σ^2_{fwm}. After photo-detection, there is a noise term caused by the FWM noise beating itself with the variance denoted as $\sigma^2_{fwm-fwm}$. At the mark state, the probe channel also works as a CW pump channel with power equal to the channel peak power and there are more FWM mixing terms compared to the space state. At the receiving side, there is a noise term caused by the signal beating the FWM noise after photo-detection with the variance denoted as $\sigma^2_{sig-fwm}$. The variance of this beating term is [52]

$$\sigma^2_{sig-fwm} = 2P_{sig_peak} * \sigma^2_{fwm}. \tag{4.49}$$

Numerical Simulation of FWM

We investigate the FWM effect using PHOTOSS^{TM}. The simulation speed is slow because a small step size has to be used. In some cases, the simplified simulation approach, which decouples the coupled nonlinear Schrödinger equations by assuming that the propagation of pump channels is linear, is used. FWM noise is sensitive to

the initial phases of signal channels and multi-iteration simulation is needed. Both the pump channels and the probe channel use CW sources, and the power of the probe channel at the link end is a constant for each iteration. At the space state, the simulated FWM noise power σ^2_{fwm} is the average of the power of the probe channel across all iterations. At the mark state, the simulated FWM noise power $\sigma^2_{sig-fwm}$ is the variance of the power of the probe channel across all iterations.

Figure 4.9 shows the simulation setup in investigating FWM noise in a single fiber segment. In the simulation, we vary powers of the signal channels and two scenarios are considered: when the probe channel is powered on and when it is powered off.

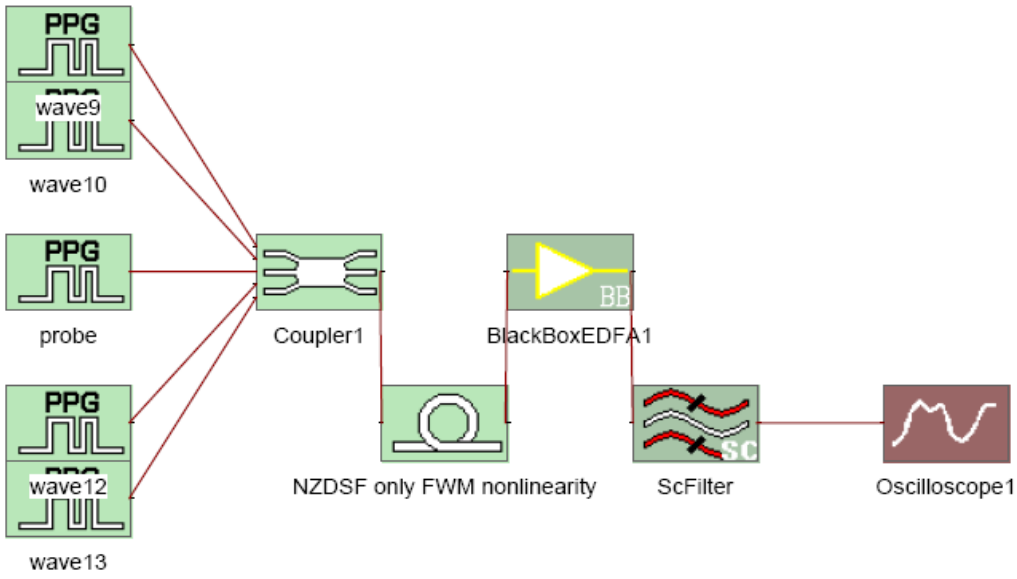

Figure 4.9. FWM simulation setup for a single fiber segment. All used channels are CW sources and the pump channels have equal powers. The probe channel has power 0 when it is powered off and has the same power as pump channels when it is powered on. The frequency comb has spacing 50GHz. The probe channel is at the center of the comb and has frequency 193.1THz. The NZDSF fiber has configurations: L =80 Km, α =0.25 dB/Km, D =4 $\frac{\text{ps}}{\text{Km*nm}}$, γ =2 $\frac{1}{\text{w*Km}}$. The gain of the in-line EDFA amplifier is 20 dB. The signal quality of the probe channel is analyzed at the end of the fiber.

Figure 4.10 and Figure 4.11 compare Q factors of the probe channel computed by the analytical model and by the PHOTOSS^{TM} simulation in the two scenarios respectively. When the probe channel is powered on, the Q factor is defined as $Q = 10\log_{10}\frac{P_{probe}}{\sigma_{sig-fwm}}$. When the probe channel is powered off, a pseudo Q factor is defined as $Q = 10\log_{10}\frac{P_{pump}}{\sigma_{fwm}}$. In the Q factor definitions, only the influence of FWM has been considered.

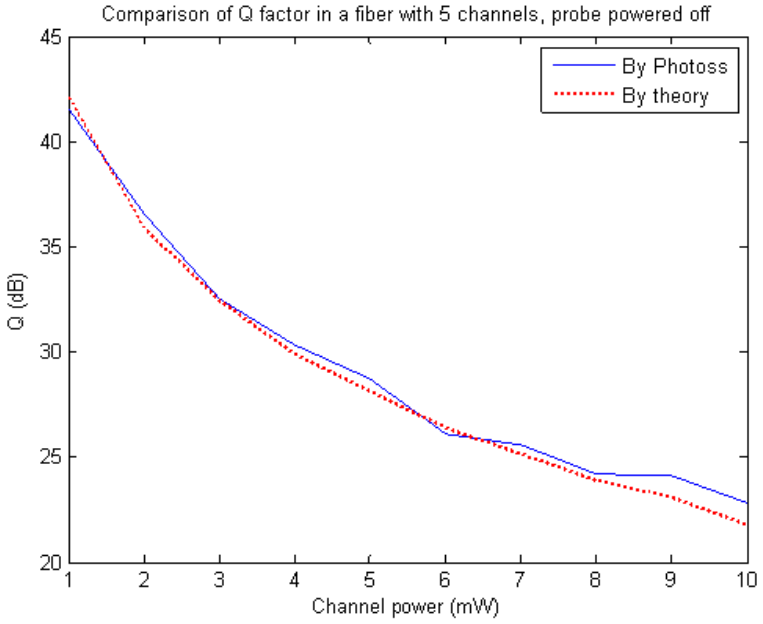

Figure 4.10. Comparison of the Q factor of a powered-off probe channel in a fiber segment with 5 channels. The setup is as in Figure 4.9 with the probe channel powered off. Each point on the curve of 'by Photoss' is obtained using 80 iterations.

We further increase the number of pump channels in the frequency comb of Figure 4.9 to large values. A simplified simulation method is applied to improve the simulation speed. In this method, the propagation of the pump channels is assumed to be linear. Figure 4.12 compares Q factors of the probe channel computed by

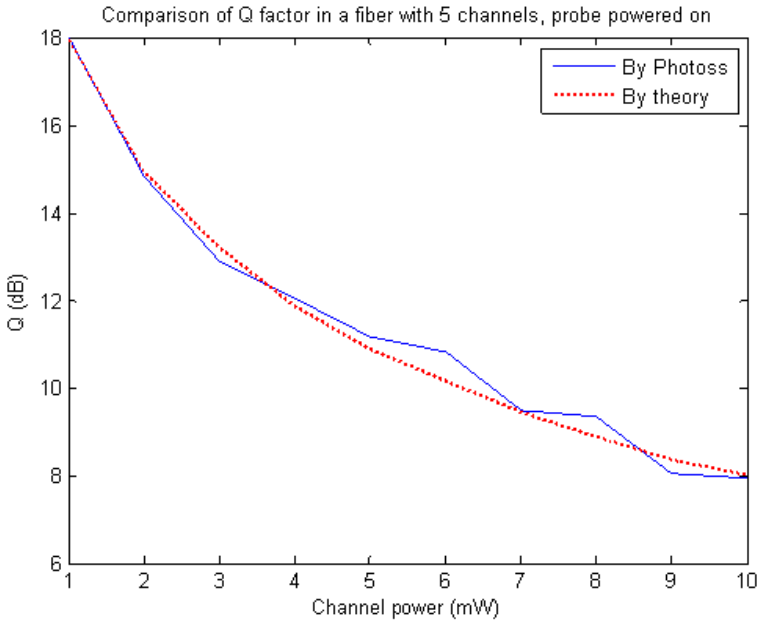

Figure 4.11. Comparison of the Q factor of a powered-on probe channel in a fiber segment with 5 channels. The setup is as in Figure 4.9 with the probe channel powered on. Each point on the curve of 'by Photoss' is obtained using 80 iterations.

the analytical model and by the simplified method 'lin-sim' in the fiber segment of Figure 4.9 when the probe channel is powered on and there are 10 pump channels on both sides of the probe channel.

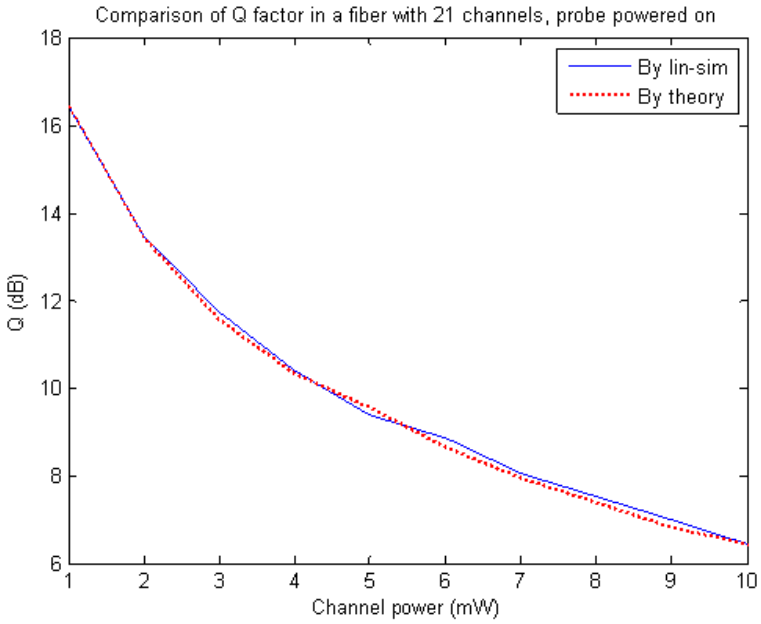

Figure 4.12. Comparison of the Q factor of a powered-on probe channel in a fiber segment with 21 channels. The numbers of pump channels in Figure 4.9 on both sides of the probe channel have been increased to 10. Each point on the curve of 'by lin-sim' is obtained using 200 iterations.

To simulate FWM noise in a multi-span link, the simulation setup in Figure 4.13 is used. In Figure 4.13, there are only two FWM mixing terms ((193.15+193.15-193.2)THz and (193.2+193.2-193.3)THz) generated on the probe channel.

Figure 4.14 and Figure 4.15 compare Q factors of the probe channel in a periodically amplified link computed by the analytical model and by the PHOTOSS^{TM} simulation in two different scenarios respectively.

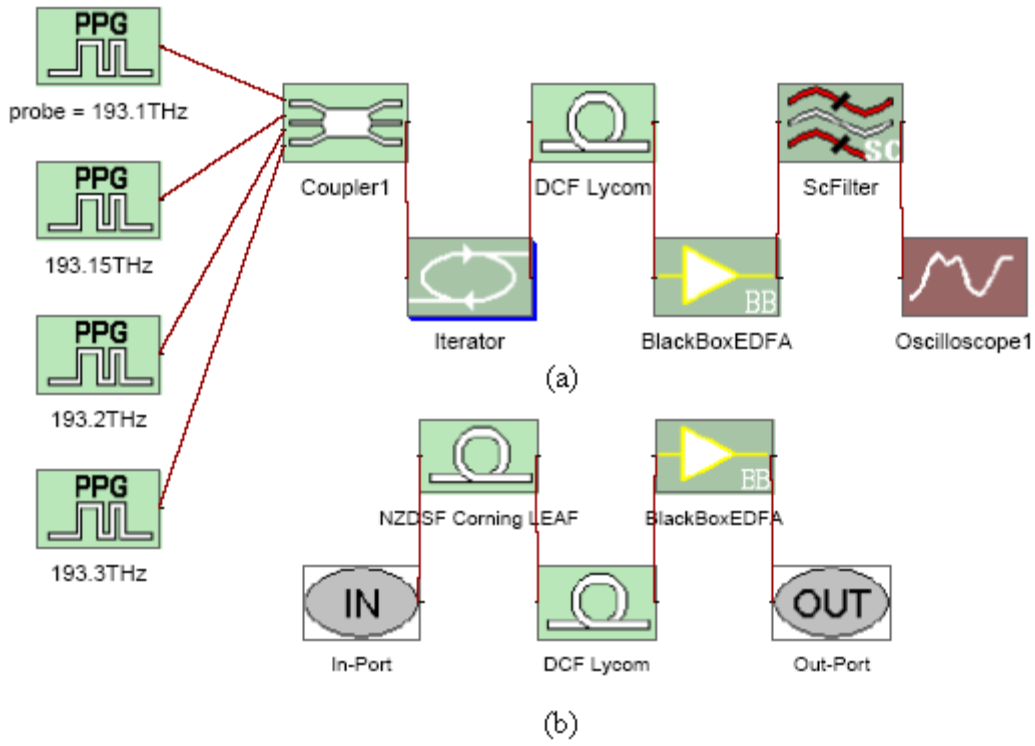

Figure 4.13. FWM simulation setup for an optical link. All used channels are CW sources and the pump channels have equal powers. The probe channel has power 0 when it is powered off and has the same power as the pump channels when it is powered on. The link has 6 identical spans, which is shown in (b). In each span, the NZDSF fiber has configurations: L =80 Km, α =0.25 dB/Km, D =4 $\frac{\text{ps}}{\text{Km*nm}}$, γ =2 $\frac{1}{\text{w*Km}}$. The DCF fiber is linear with configurations: L =3.2 Km, α =0.5 dB/Km, D=−100 $\frac{\text{ps}}{\text{Km*nm}}$. The gain of the in-line EDFA amplifier is 21.6 dB. The post-compensation DCF fiber has length L =0.2 Km and its attenuation is exactly compensated by the following EDFA.

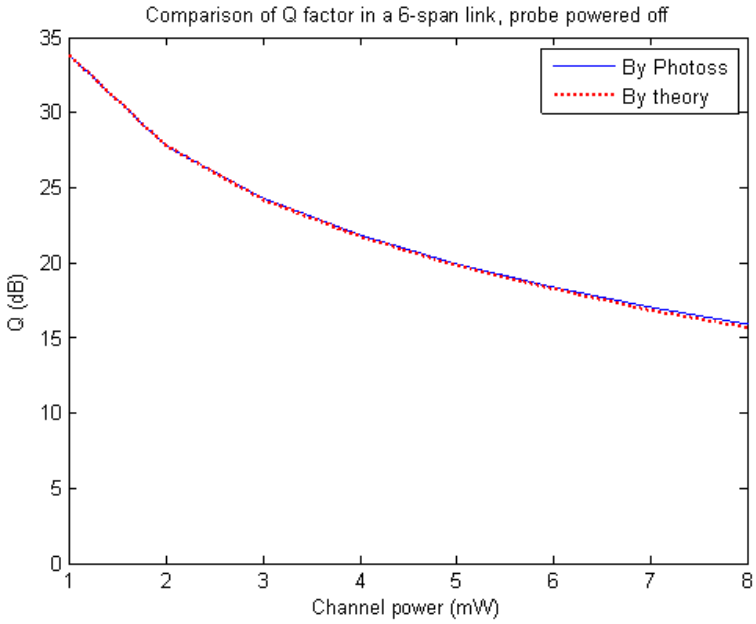

Figure 4.14. Comparison of the Q factor of a powered-off probe channel in the optical link of Figure 4.13. Each point on the curve of 'by Photoss' is obtained using 80 iterations.

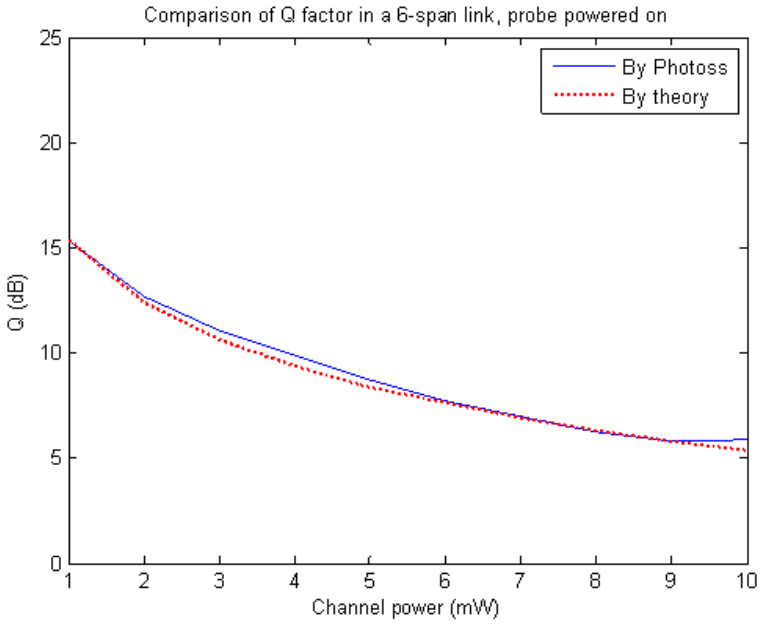

Figure 4.15. Comparison of the Q factor of a powered-on probe channel in the optical link of Figure 4.13. Each point on the curve of 'by Photoss' is obtained using 60 iterations.

For simplicity, we assume XPM and FWM work independently as in [52][60], i.e.

$$\sigma^2_{1/0,total} = \sigma^2_{1/0,XPM} + \sigma^2_{1/0,FWM} + \sigma^2_{1/0,\text{other noises}}, \tag{4.50}$$

where $\sigma^2_{1/0,XPM}$ is the noise power due to XPM only at the mark/space state, $\sigma^2_{1/0,FWM}$ is the noise power due to FWM only at the mark/space state, and $\sigma^2_{1/0,\text{other noises}}$ is the noise power due to other sources at the mark/space state.

We use PHOTOSS$^{\text{TM}}$ simulations to validate Equation 4.50. Three cases have been considered: when FWM dominates, when XPM dominates, and when FWM and XPM have approximately equal influences. In the simulation, only the influences of XPM and FWM have been considered. The PHOTOSS$^{\text{TM}}$ simulation setup is shown in Figure 4.16.

For different cases, only the input channels are changed and the link is fixed with the structure shown in Figure 4.16. The 'probe and pump' approach is applied to study the influence of multiple nonlinear effects (i.e. XPM and FWM) on the signal quality of a probe channel, which is a CW source and has frequency of 193.1THz. All the pump channels are dynamic and send out random bit streams. In the analytical models for predicting the noise power due to FWM, all channels are assumed to be CW sources. When applying these models, the pump channels are treated as CW sources with their power equal to half of the channel peak power. For comparison,

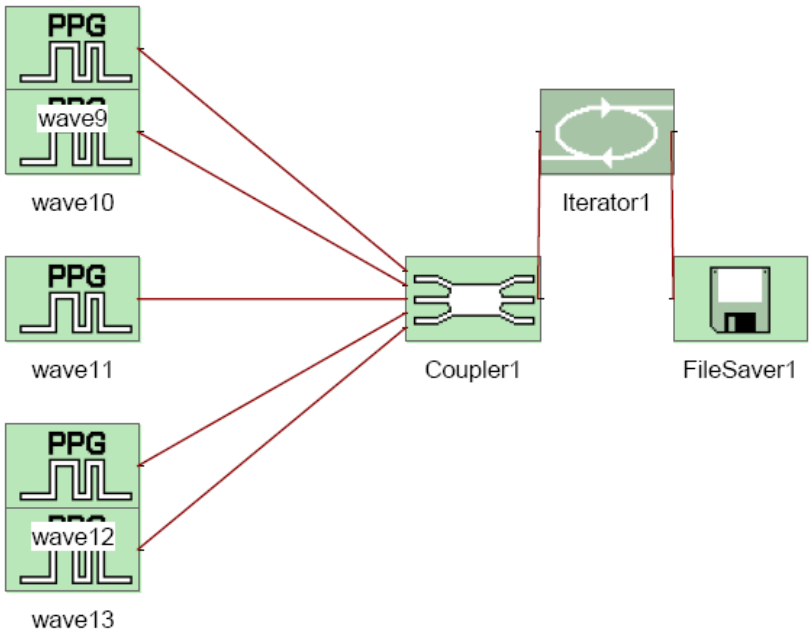

Figure 4.16. Simulation setup for investigating signal quality when both XPM and FWM are active. The structure of each span is the same as in Figure 4.3(b) and compensated using the FOCS scheme as shown in Figure 4.4.

the Q factors of the probe channel when only XPM or FWM is active are also shown in the figures below.

Because the FWM noise power depends on initial phases of the signal channels, for each simulation, multiple (40 iterations in our simulations) iterations are executed, and the output waveforms (saved by the Filesaver component in Figure 4.16) of the probe channel in these iterations are cascaded to determine its signal quality.

Case 1: FWM dominates

When the channels [193.0 193.05 193.1 193.15 193.2]THz are injected into the link of Figure 4.16, the FWM noise dominates according to the analytical model

developed in this chapter. Figure 4.17 compares Q factors of the probe channel computed by the analytical model and by the PHOTOSS^{TM} simulation at the output of each span along the link.

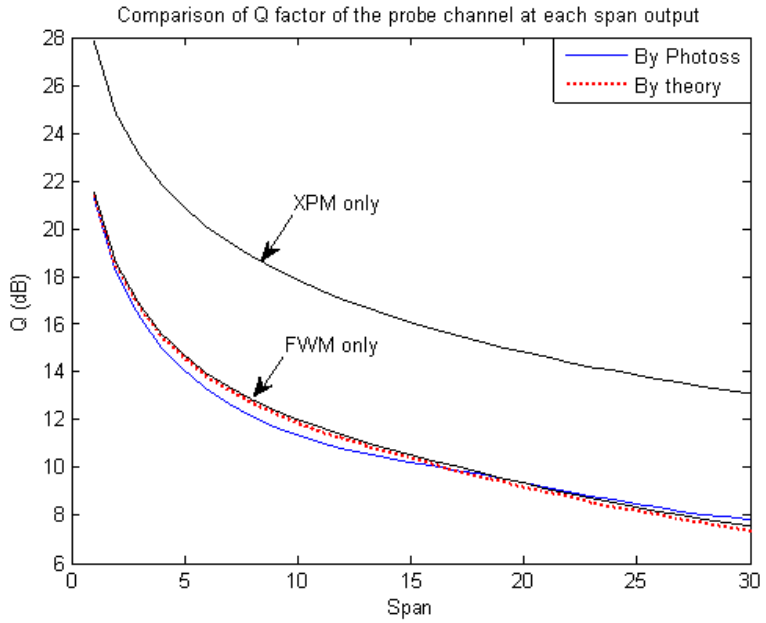

Figure 4.17. Comparison of the Q factor of a probe channel at the output of each span when both XPM and FWM are active (case 1).

Case 2: XPM dominates

When the channels [193.1 193.15 193.2]THz are injected into the link of Figure 4.16, XPM and FWM first have approximately equal influences at the beginning of the link, but later XPM dominates. Figure 4.18 compares Q factors of the probe channel computed by the analytical model and by the PHOTOSS^{TM} simulation at the output of each span along the link.

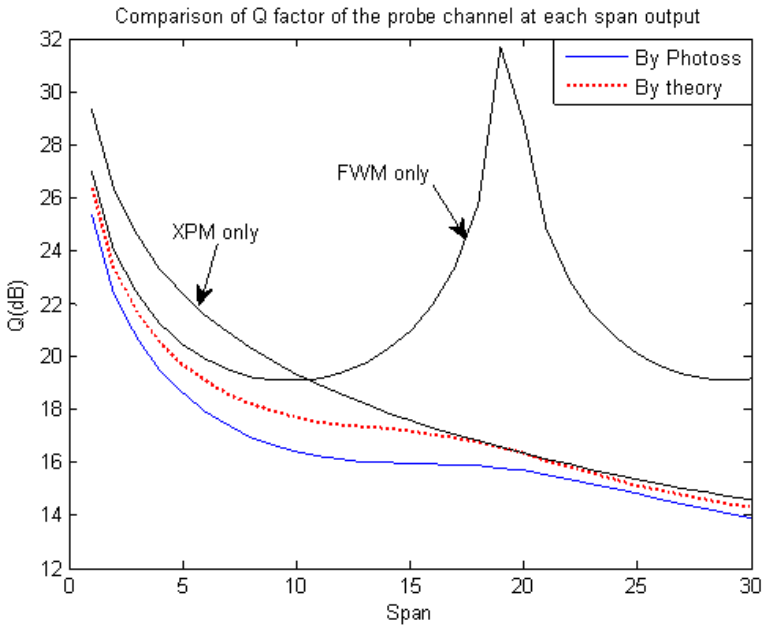

Figure 4.18. Comparison of the Q factor of a probe channel at the output of each span when both XPM and FWM are active (case 2).

Case 3: Equally dominate

When the channels [193.0 193.1 193.16 193.2]THz are injected into the link of Figure 4.16, XPM and FWM approximately have equal influences. Figure 4.19 compares Q factors of the probe channel computed by the analytical model and by the PHOTOSS^{TM} simulation at the output of each span along the link.

The simulation results from different cases show that the proposed analytical model for predicting signal quality of a channel under multiple nonlinear effects works well.

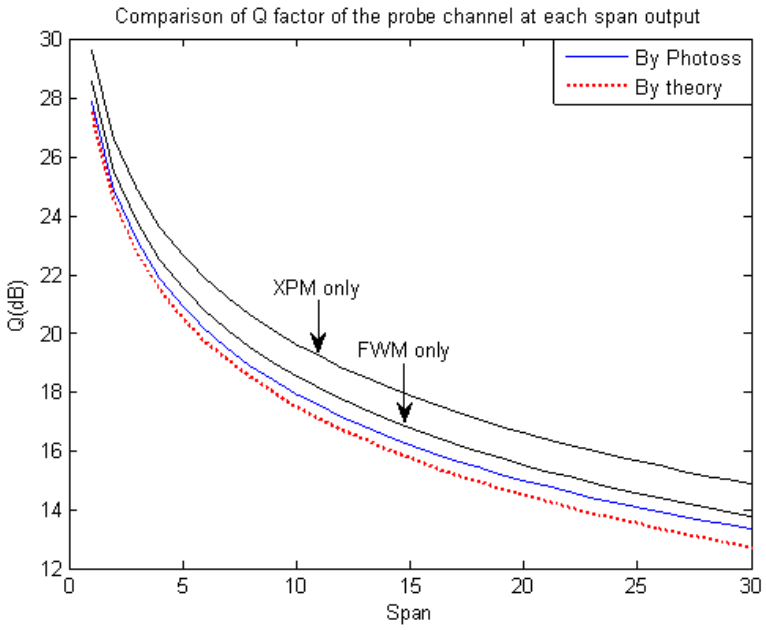

Figure 4.19. Comparison of the Q factor of a probe channel at the output of each span when both XPM and FWM are active (case 3).

Discussion

The proposed analytical models for predicting channel signal quality under the influence of nonlinear effects will be used in in-line RWA algorithms to intelligently choose a lightpath satisfying user QoS requirements. Considering the requirement of in-line computation and the number of different physical impairments, the analytical models should be efficient, flexible, and scalable.

The analytical models for predicting noise power due to XPM have used the assumption that powers of the signal channels are low and the small-signal analysis method can be applied. For this reason, the proposed analytical models in this chapter can only be applied to optical networks where signal channels have low powers.

In Equation 4.19, a numerical integration is needed to compute the noise power due to XPM. Computation efficiency can be improved if this integration is executed off-line in advance and a matrix M is stored in each switch node of a network, with $M(i, j)$ specifying the noise power induced by the pump channel j on the probe channel i through XPM.

The independence assumption, used when computing channel signal quality under multiple nonlinear effects, can greatly simplify the algorithm design of the proposed QoS framework for all-optical networks in Chapter 7. The analytical models for predicting signal degradations caused by different physical impairments can be developed individually and these models can be easily integrated to predict the signal quality of a channel under the influence of multiple physical impairments. This makes the proposed QoS framework flexible and scalable, and can be easily adjusted to take new physical impairments into account as the underlying physical layer evolves.

SUPPRESSION OF NETWORK TRANSIENTS

Introduction

The transients discussed in this chapter include switch transients and amplifier transients. These two have different origins and we propose different strategies to suppress them. Switch transients occur after a controlling signal is applied to a switching fabric and before the fabric stabilizes. The switching time is a function of switch structure. For fast optical switches, the duration of transients lasts only several nanoseconds. But for other switches (e.g. the MEMS switch used in our research) the duration can last several milliseconds. When a controlling signal is applied to a MEMS switch, it causes mirrors to rotate and guide the input light to the desired output port. But before the positions of the mirrors stabilize, oscillations of the mirrors can occur and cause ringing of the signal output power as observed in the measurement shown in Figure 2.12.

Amplifier transients, as shown in Figure 2.13, originate from the effect of cross-gain modulation. A simple two-level model as shown in Figure 5.1 can be used to explain the working principle of EDFA amplifiers. The amplification is provided by the Er^{3+} ions doped in the fiber of an EDFA. When an Er^{3+} ion at the ground state absorbs energy from pumping photons, it jumps to the excited state. From the excited state, the ion can jump to the ground state by spontaneous emission or by stimulated

emission when hit by a signal photon. The spontaneous emission generates the ASE noise and the stimulated emission provides amplification of the signal photons. The effect of cross-gain modulation comes from the fact that photons of all signal channels share the excited erbium ions. In the unsaturated mode of an amplifier, there are far more than enough excited ions for all channels. The gains consumed by one channel will not influence another channel. In the saturation mode of an amplifier, signal channels will compete for the excited ions. If the power of one channel increases abruptly, it will then consume more excited ions, leaving less for other channels, hence the effect of cross-gain modulation. Besides EDFAs, other amplifiers (including SOA, EDWA, and Raman amplifiers) all have the similar transients due to the effect of cross-gain modulation.

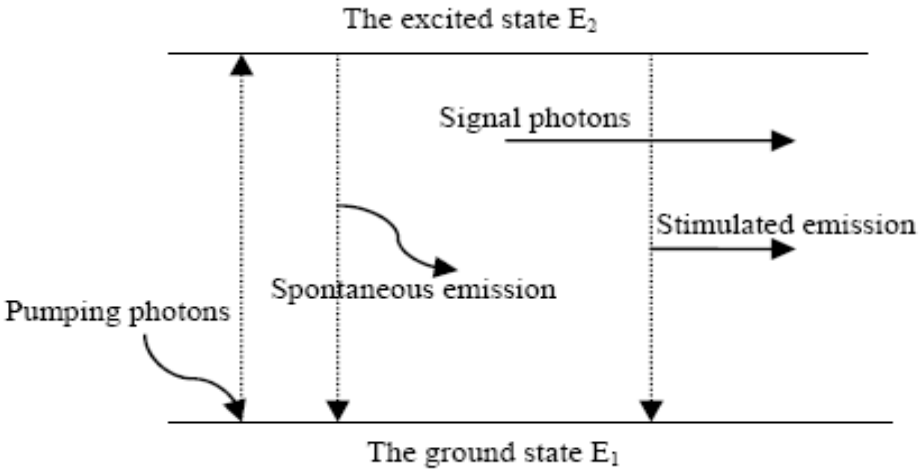

Figure 5.1. Working principle of EDFA amplifiers.

Network transients have detrimental effects on signal quality, resulting in closed eye-diagrams and increased BERs. Different from the reactive approach used in

Chapter 7, where the proposed RWA algorithms try to avoid links with high noise powers, the solutions proposed for suppressing network transients are proactive. In this chapter, we first explain the method for eliminating switch transients and then focus on suppressing amplifier transients. The discussion and simulation of the proposed technique of power shaping use the EDFA as an example. But actually, it is a general solution and can work with other types of in-line amplifiers. The effectiveness of power shaping was verified by my colleagues using experiments in [61]. Finally, we explain a component designed for suppressing amplifier transients at network failures.

Suppression of Switch Transients

Experiment on MEMS transients

The experiment setup used to observe MEMS switch transients is shown in Figure 5.2 [62].

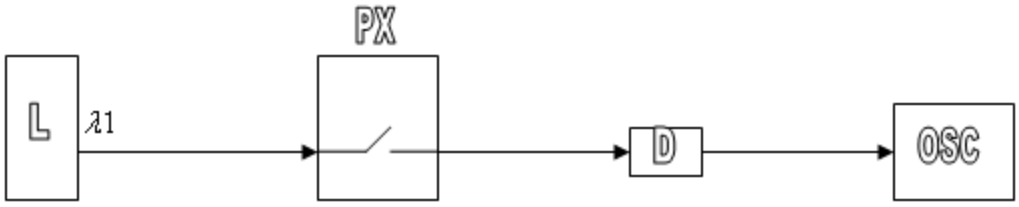

Figure 5.2. Experiment setup for the observation of MEMS switch transients. The laser source (L) has wavelength 1550.92nm (λ_1) and power of 3.8dBm. The MEMS switch (PX) has eight input ports and eight output ports. One of the output ports is connected to the photo-detector (D), which in turn, is connected to the oscilloscope (OSC) [62].

The temporal behavior of the output power is studied by suddenly closing or opening the cross-connection, as shwon in Figure 5.2. When the connection is suddenly closed, the upswing of the output power is shown in Figure 5.3 [62].

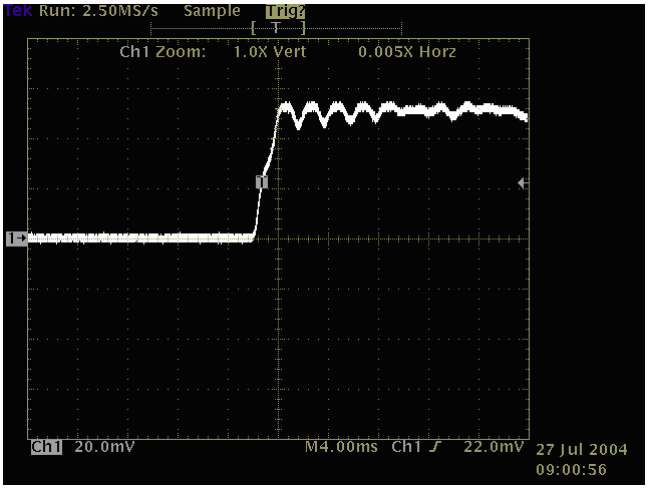

Figure 5.3. Temporal behavior of MEMS switch output power when cross-connection is closed. We observed the average rise time to be approximately 800μs . The resonant frequencies of the ringing are in the range of 1 kHz. The settling time of the ringing is several milliseconds [62].

When the connection is suddenly opened, the downswing of the output power is shown in Figure 5.4 [62]. The reason why the ringing is observed on the upswing and not observed on the downswing can be explained by describing the behavior of the signal as observed from the output port of the PX [62]. When the cross-connection is provisioned, the mirrors move to focus the input light through the required output port. When the mirrors resonate, the focusing is disturbed and the signal coming out of the output port is modulated by the mirror oscillation. When the cross-connection is deleted, the mirrors are moved such that the signal is focused away from the output

port. Even though the mirrors may resonate, the oscillation occurs only when the mirrors are at their final positions, not from the beginning of their movement. So the oscillation can not be seen through the output of the PX.

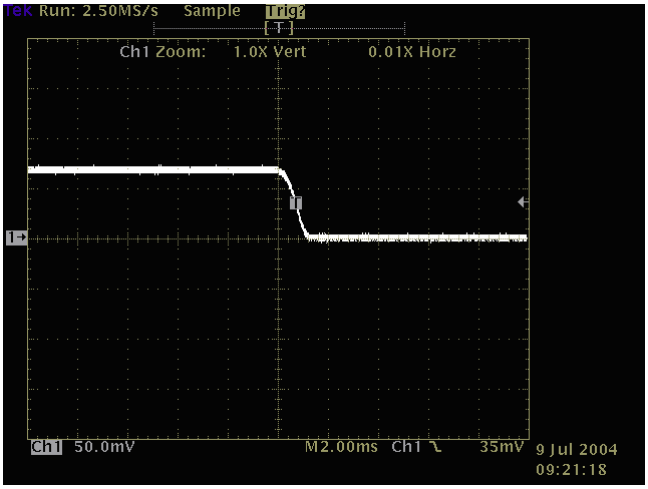

Figure 5.4. Temporal behavior of MEMS switch output power when cross-connection is opened. No ringing is observed [62].

Method for Eliminating Switch Transients

By optimizing the design of optical switches, the duration of transients (i.e. the ringing settling time shown in Figure 5.3) can be decreased, and thus decreasing the influence of switch transients. This requires adjustment of the drive current to the mirror controller and is internal to the switch. We propose a simpler solution implemented at the network layer to totally eliminate the influence of switch transients. The basic idea is to delay sending traffic data until the optical switches on a lightpath all have reached the stable state. Recall in Chapter 1 that the destination node will

send a 'resv' message upstream to the source node in the backward reservation protocol. When a switch node receives the 'resv' message, it needs to allocate necessary resources for the connection and send controlling signals to the switch fabric under its control to create a cross-connection from a wavelength on the input fiber to a wavelength on the output fiber. We add a new field 'required-delay' in the 'resv' message to tell the source node how long it needs to wait. Two approaches with increasing complexities can be applied.

The first one is more conservative. When receiving the 'resv' message, a switch node updates the 'required-delay' field as given by Algorithm 5.1.

Algorithm 5.1 conservative algorithm for Updating 'required-delay'

1: Set 'required-delay' = max('Required-delay', switch settling time of this node);
2: Send the message upstream.

The efficiency of Algorithm 5.1 can be improved by considering the transmission delay, the queuing delay, and the signaling message processing time when the 'resv' message is propagated upstream. Each switch node maintains an estimation of the transmission delays of its incident links. When receiving the 'resv' message, a switch node can update the 'required-delay' field as given by Algortihm 5.2.

Algorithm 5.2 optimistic algorithm for Updating 'require-delay'

1: Set 'required-delay' = max('Required-delay', switch settling time of this node);
2: Set 'required-delay' = 'required-delay' - transmission delay - queuing delay- signal processing time.
3: Send the message upstream.

In Algorithm 5.1 and Algorithm 5.2, the transmission delay and the signal processing time are negligible, the switch settling time depends on the optical switches deployed in a network (in the scale of milliseconds for MEMS switches), and the queuing delay depends on network traffic load.

Suppression of In-Line Amplifier Transients

In-line amplifiers usually work in the saturation mode to maximize gains. At the same time, optical networking is moving towards all-optical networks, designed to support circuit-switched, burst-switched, and packet-switched traffic. In such next-generation networks, the number of channels going through an amplifier can be highly variable. Adding and dropping channels will induce transients and such transients can escalate along the cascade of amplifiers on an optical lightpath. It was reported in [29] that the transient speed, measured by power excursion rise time, in an EDFA amplifier cascade is proportional to the number of amplifiers in the cascade, making suppression by conventional electrical and optical feedback techniques less effective. The amplifier transients can pose a serious problem to the performance of next-generation all-optical networks by affecting the bit error rate. A number of solutions have been proposed to suppress amplifier transients, including using optical feedback to clamp the amplifier gain [50][63], adding a dummy optical signal at burst intervals to maintain constant optical input power [64][65], using electrical feedforward and

feedback to maintain constant gain [66][67]. These solutions are all at the physical layer, attempting to improve the performance of individual amplifiers.

We observed from our simulations of the AOGC EDFA (automatic optical gain-clamped EDFA) performance that when small changes are applied to the amplifier input, both the duration and the amplitude of power transients decrease. We proposed a novel link layer solution to suppress amplifier transients by power shaping [68][69]. The idea is to increase/decrease the power of an added/dropped channel gradually rather than abruptly, thus the in-line amplifiers can respond fast enough to suppress the induced transients. Compared to other solutions, our approach has the advantages of being more economical and general. Because the solution is at the link layer, it does not influence the design of routing algorithms at all.

Working Principle

Power shaping is defined as adjusting and maintaining the temporal behavior of the power of a channel or connection. The application of power shaping in networks using different switching technologies can be explained using Figure 5.5.

Figure 5.5(a) shows the power profile of a channel in a next-generation all-optical network as a function of time t when power shaping is not applied. Notice that there are idle gaps between traffic blocks (each traffic block is a series of continuous data frames). Transients are induced on other co-propagating channels when its power suddenly increases from 0 to the working level, or suddenly drops from the working level to 0.

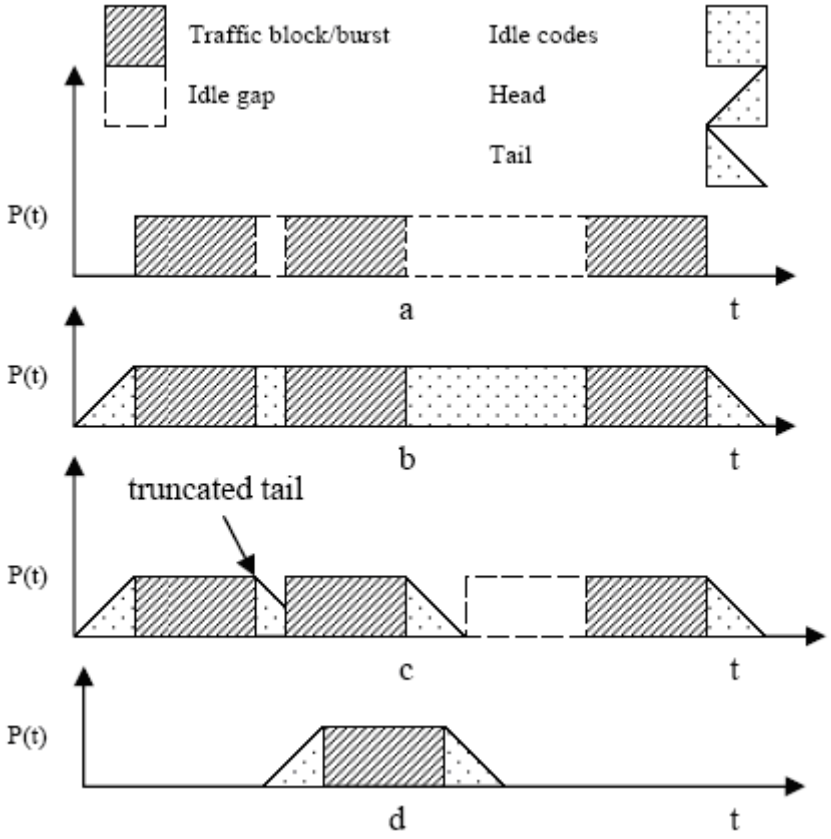

Figure 5.5. Working principle of power shaping. (a) shows the power profile of a channel without power shaping. (b) shows the application of power shaping on a circuit-switched connection. (c) shows the application of power shaping on a packet-switched LSP. (d) shows the application of power shaping on a burst.

Figure 5.5(b) shows power shaping on a circuit-switched connection. Before the first traffic block and after the last traffic block, a *head* and a *tail* are inserted respectively. Both the head and the tail are pseudo-random bit patterns. In the head, the probability of bit '1' is gradually increased to 0.5 (in traffic data, the probability of bit '1' is also about 0.5 after scrambling or block code generation). In the tail, the probability of bit '1' is gradually decreased to 0. Idle codes are used to fill the gaps as in SONET/SDH transmission to keep the power constant.

Figure 5.5(c) shows power shaping on a packet-switched connection (e.g., a label switched path (LSP) in GMPLS [70]). In packet-switched networks, multiple connections can be statistically multiplexed on one channel. Power shaping is performed on a per connection basis. The heads and tails need to be encapsulated in data frames for the purpose of switching at intermediate nodes. Those data frames are assigned low priority and can be discarded if necessary. Compared to Figure 5.5(b), the difference is that a tail is added after each traffic block instead of idle codes to decrease generating extra traffic. Heads are not used during the connection to avoid introducing extra delays for traffic data (this is a design choice). In addition, a tail can be truncated when new arriving data need to be sent.

Figure 5.5(d) shows power shaping on a burst in burst-switched networks. Two important parameters of power shaping are the lengths of head and tail. For the simplicity of implementation, their values are set equal and denoted as *shaping-period*. For efficiency considerations, the application of power shaping in burst switching suggests that size(burst) >> shaping-period. We will discuss its selection and optimum value later in this section.

Performance of Power Shaping in Circuit/Burst-Switched Networks

We first investigate the performance of power shaping in circuit-switched networks. In our simulation, AOGC EDFAs are used as in-line amplifiers. All the

amplifiers are identical and constructed according to the model in [50]. A multi-wavelength network is characterized using a model consisting of two wavelengths (CW1 and CW2), each with a power 5mW and representing 5 channels with an average power of 1mW per channel, going through a cascade of 10 AOGC EDFAs. The amplifiers are tuned and the gain flattening mechanism is used to provide 20dB gain for both wavelengths, exactly compensating the loss in a fiber span. The OptSim^{TM} model is shown in Figure 5.6.

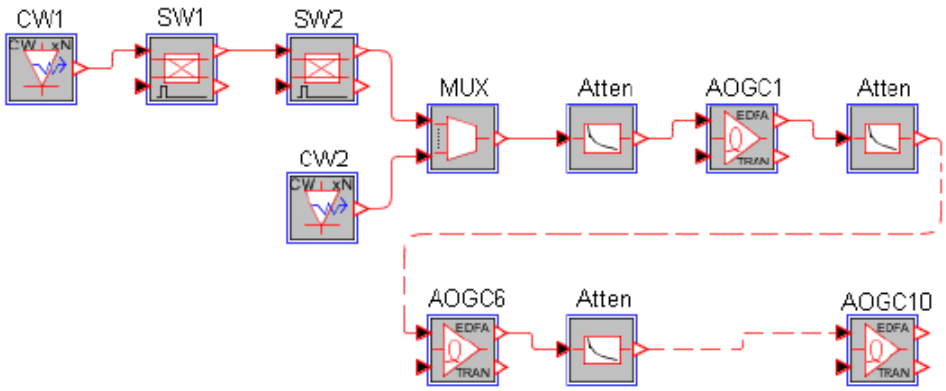

Figure 5.6. OptSim^{TM} model for simulating the application of power shaping in circuit-switched networks. CW: continuous wave, SW: transient switch, MUX: multiplexer, Atten: -20dB attenuator to simulate a fiber span, AOGC: AOGC EDFA with 20dB gain. The two SWs are used to perform power shaping on CW1 (for simplicity, the power of the head and the tail is directly shaped by transient switches instead of using pseudo-random bit patterns).

The transients on CW2 are measured when CW1 is added and then dropped. The transients on CW2 at the output of the 10^{th} amplifier with and without power shaping are compared in Figure 5.7.

It is evident that considerable transients are induced on CW2 when power shaping is not applied. When power shaping is applied on CW1, the speed of the power

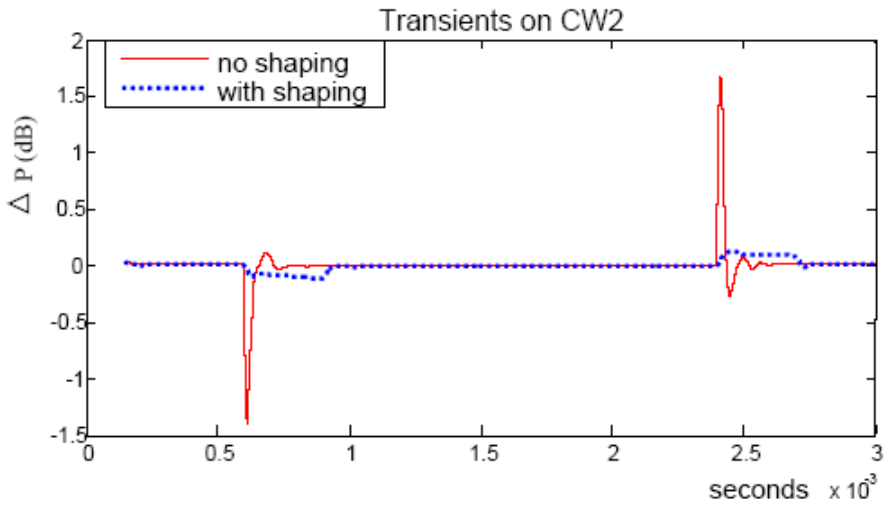

Figure 5.7. Comparison of power transients on CW2 with and without power shaping in circuit-switched networks.

variation is slowed to be comparable to the response time of the in-line amplifiers and the transients on CW2 are successfully suppressed. Although the transient duration slightly increases when power shaping is applied, the major performance deterioration happens when large overshoot and undershoot occur as shown in Figure 5.7 when power shaping is not applied. Better transient suppression can be achieved by using a larger value for the shaping-period at the cost of increasing connection duration. The use of PPP (i.e., point-to-point protocol) has been proposed [71] to bridge the gap between IP and WDM. It would be simple and straightforward to incorporate power shaping into the PPP.

The application of power shaping to a burst has similar effects as shown in Figure 5.7 (Refer to Figure 5.5(b) and Figure 5.5(d) for the similarity of power profiles).

For efficiency considerations, we suggest that the source nodes create bursts with durations in the range of several hundred microseconds or greater. The traffic grooming process will not cause significant end-to-end delay, because there is no buffering at intermediate nodes in optical burst-switched networks. At the same time, the value of shaping-period can be set to several microseconds with state of the art in-line amplifiers. However, if power shaping is applied to a burst, then burst segmentation [72] can not be used. Deflection routing algorithms [73] can be used to decrease burst dropping probability.

Performance of Power Shaping in Packet-Switched Networks

To investigate the performance of power shaping in packet-switched networks, we consider, as in the burst case, appending gradually decreasing tails to the ends of data blocks. Two scenarios are investigated. In scenario A, the average data block inter-arrival time is smaller than the shaping-period, simulating a busy backbone network link. In scenario B, the average data block inter-arrival times of some channels are greater than the shaping-period, characteristic of an optical link where some of the channels are not as busy as other channels. This might occur, for example when the First-fit wavelength assignment algorithm is used in a GMPLS controlled all-optical network, where the data block inter-arrival times of channels with larger indices tend to be greater than that of channels with smaller indices.

A point-to-point WDM optical link consisting of a cascade of 6 AOGC EDFAs is simulated. There are 10 channels on the link. Nine of the channels are dynamically added and dropped, each simulating a packet-switched connection. The 10^{th} channel is fixed and always transmits a traffic stream. The induced power transients on the 10^{th} channel are measured.

The data sources of the nine dynamic channels are identical and independent with a bit rate of 1Gbps each. For each data source, the whole simulation time is divided into a series of alternating "on" and "off" period. In an "on" period, the data source generates pseudo-random bit streams, simulating a traffic block. In an "off" period, the data source is silent. Two traffic patterns are considered. In the self-similar traffic pattern, the lengths of the "on" and "off" periods are controlled by the Pareto distributed random variables T_{on} and T_{off} respectively,

$$T_{on/off} = \left\lfloor \frac{T_0}{U^{\frac{1}{\alpha_{on/off}}}} \right\rfloor, \tag{5.1}$$

where U is a uniformly distributed random variable ranging in (0,1) and T_0, α_{on}, and α_{off} are adjustable parameters. The same method of generating self-similar traffic was also used in [31]. In the Poisson traffic pattern, the lengths of the "on" and "off" periods are controlled by exponentially distributed random variables with mean value μ_{on} and μ_{off} respectively. The 10 channels have uniform wavelength separation of 0.4 nm. The laser sources are externally intensity modulated. Important parameters for components in the simulation are summarized in Table 5.1.

Table 5.1. Power shaping simulation parameters.

channels:		
Channel	Wavelength (nm)	Average power (mW)
1-10	1551-1554.6nm, with 0.4nm separation	1
AOGC EDFA:		
Length	16m	
Pump power	90mW	
Pump wavelength	1480nm	
Feed back loss	18dB	
Lasing wavelength	1563.5nm	
Provided gain[a]	20dB	
The nine dynamic channels:		
Traffic data	Pseudo-random bit stream	
Data transfer rate	1Gbps	
T_0	0.512μs	
α_{on}	Adjustable in (0, ∞)	
α_{off}	Adjustable in (0, ∞)	
μ_{on}	Adjustable in (0, ∞)	
μ_{off}	Adjustable in (0, ∞)	
The 10^{th} channel:		
Traffic data	Pseudo-random bit stream	
Data transfer rate	1Gbps	
Fiber in each span:		
Type	SMF	
Length	80km	
Total loss	20dB	
Power shaping:		
Shaping-period[b]	300μs	
Optsim configuration:		
Iterations[c]	2000	

[a]Provided gains are the same for all channels by gain flattening. We have tuned the AOGC EDFA model such that it will provide 20dB gain for each channel when all are present on the link. All the AOGC EDFAs used on the link are identical. The gain of 20dB will compensate the loss in the fiber span prior to an EDFA.

[b]Shaping-period is set to 300μs because we found that the transient settling time of AOGC EDFA is about 200-300μs.

[c]A simulation has 2000 iterations, with duration of 0.512μs each. So the total simulation time is 1024μs. Each sampling point in the figures below is the iteration average power of the 10^{th} channel.

Scenario A. Using the self-similar traffic pattern and setting α_{on}=1.2, α_{off}=1.64, the output power (optical power at the output of the last amplifier) and the output power probability density function (PDF) of channel 10 with and without power shaping are compared in Figure 5.8.

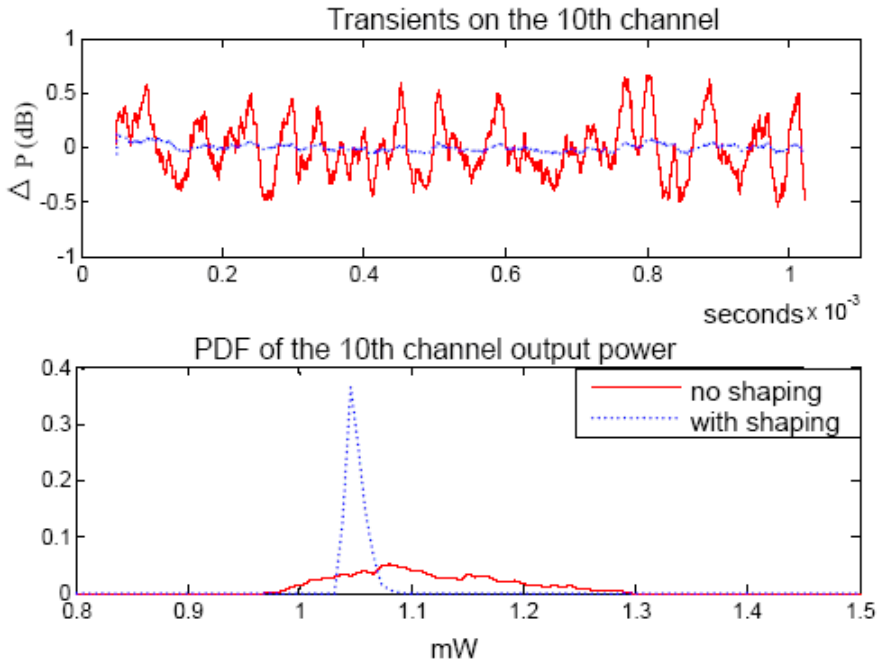

Figure 5.8. Comparison of power transients on channel 10 with and without power shaping using the self-similar traffic pattern.

Notice that when power shaping is not applied, the power excursions of channel 10 can increase to large values, consistent with results reported in [74]. Figure 5.8 shows a pronounced benefit of using power shaping. The generated tails effectively fill the idle gaps in the power profile of a dynamic channel. This decreases the power variation range of a channel, thus decreasing the transients not only due to channel dropping but also due to channel adding.

We have also run simulations with α_{on}=1.2, α_{off}=1.2 and with α_{on}=1.64, α_{off}=1.2 to simulate the link at different traffic loads. In those traffic loads, the application of power shaping also shows similar improvements. These traffic settings were used in [31].

Using the Poisson traffic pattern and setting μ_{on}=3.07μs, μ_{off}=1.31μs, corresponding to the same traffic load as in Figure 5.8, the output power and the output power PDF of channel 10 with and without power shaping are compared in Figure 5.9. Figure 5.9 shows the performance improvement when using power shaping.

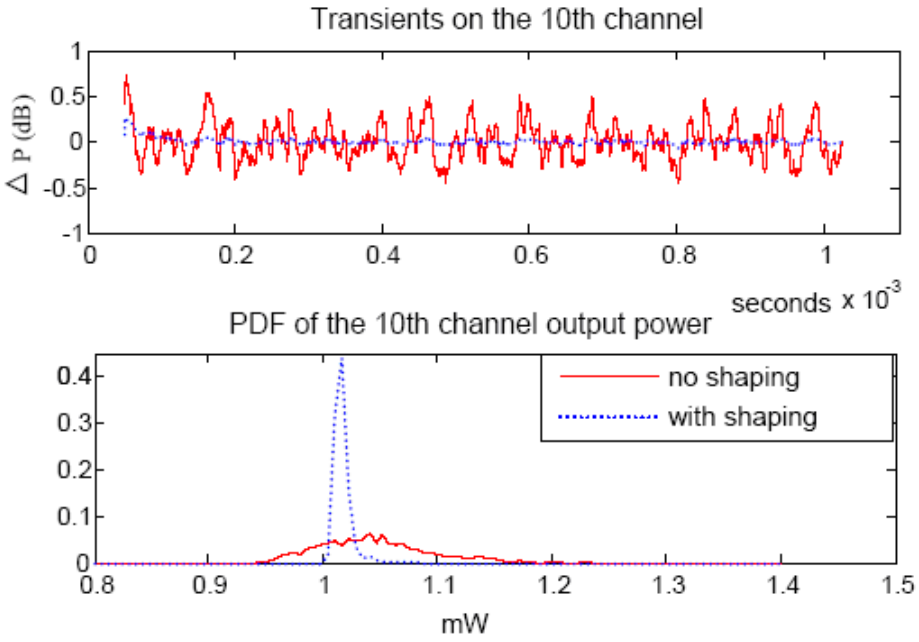

Figure 5.9. Comparison of power transients on channel 10 with and without power shaping using the Poisson traffic pattern.

Scenario B. If the duration of an "off" period is greater than the shaping-period, the power of a dropped channel will then have a finite chance of going to 0. To investigate the performance of power shaping in such a 'bad' situation, we change the durations of the "on" periods and the "off" periods of 3 dynamic channels in scenario A to be controlled by uniformly distributed random variables ranging in [tail length - 100μs, tail length +100μs].

We examine the effect of such a mixed traffic scenario on the performance of a steady state channel with and without power shaping. Figure 5.10 shows the resulting transients on channel 10, when using the self-similar traffic pattern and the same setting for dynamic channels as in Figure 5.8.

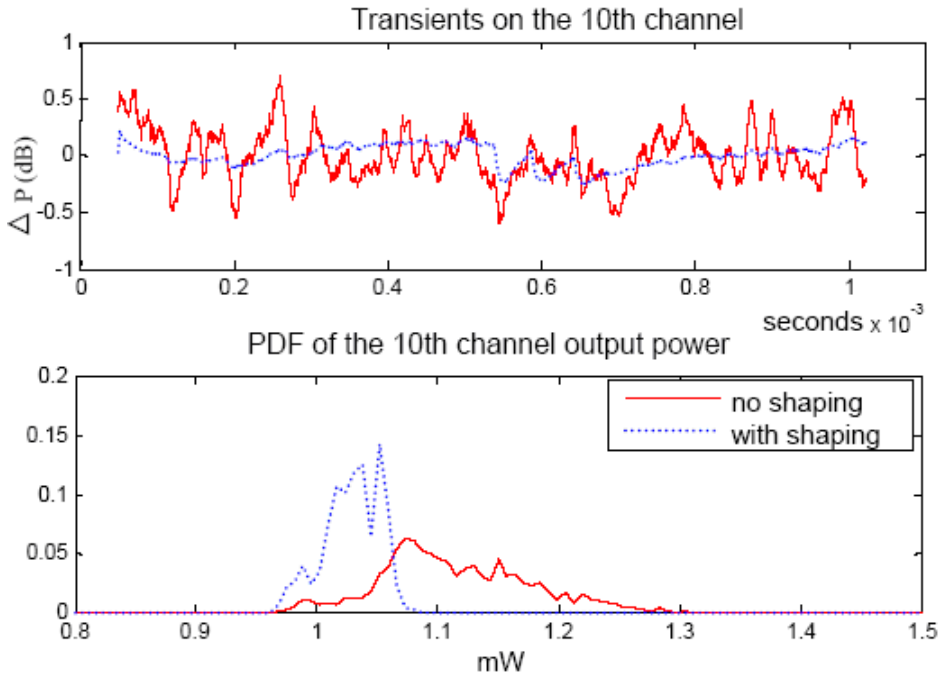

Figure 5.10. Comparison of power transients on channel 10 with and without power shaping using the self-similar traffic pattern in a mixed scenario.

With power shaping applied, the comparatively large undershoots of channel 10 between 0.5 and 0.65 ms in Figure 5.10 are caused by channel adding. This is due to our choice not to insert heads during a connection. The transients induced by channel dropping, including the dropping of the 3 channels which have long "off" periods, have been successfully suppressed by power shaping. The tilting of the output power in Figure 5.10 between 0.2 and 0.5 ms, and between 0.65 and 1.0 ms is due to spectral hole burning effects (SHB) [28] and can be eliminated by tuning the lasing wavelength in an AOGC EDFA. The application of power shaping decreases the excursion range by at least more than one half, because the power excursion caused by channel dropping, which is suppressed by power shaping, is more severe than that caused by channel adding. This has been verified by the simulation shown in Figure 5.10 and by another simulation where we change the durations of the "on" periods and the "off" periods of all dynamic channels to be controlled by uniformly distributed random variables ranging in [tail length-100μs, tail length+100μs].

The performance improvement of using power shaping when using the Poisson traffic pattern and the same setting for dynamic channels as in Figure 5.9 in the mixed scenario is shown in Figure 5.11.

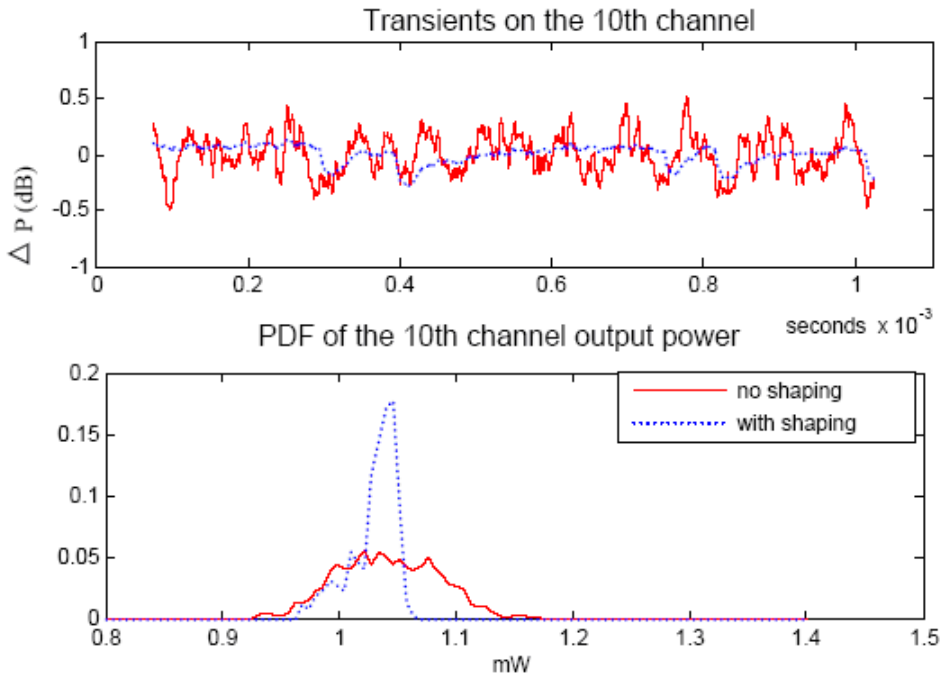

Figure 5.11. Comparison of power transients on channel 10 with and without power shaping using the Poisson traffic pattern in a mixed scenario.

Sensitivity to the Shaping-Period

In packet-switched and burst-switched networks, we want the shaping-period to be as short as possible to minimize the overhead and maximize the throughput. Using the same setting as in Figure 5.10, we vary the value of the shaping-period and compare the effects in Figure 5.12.

We notice in Figure 5.12 that for shaping periods greater than 200μs, the effects of power shaping are not dependent on the shaping-period. When the shaping-period is 100μs or less, the overshoots are pronounced. Our simulations show that for tens of channels each with power in the range of several mW, the transient settling time of an AOGC EDFA is about 200μs (verified in [75]). In practice, the typical power

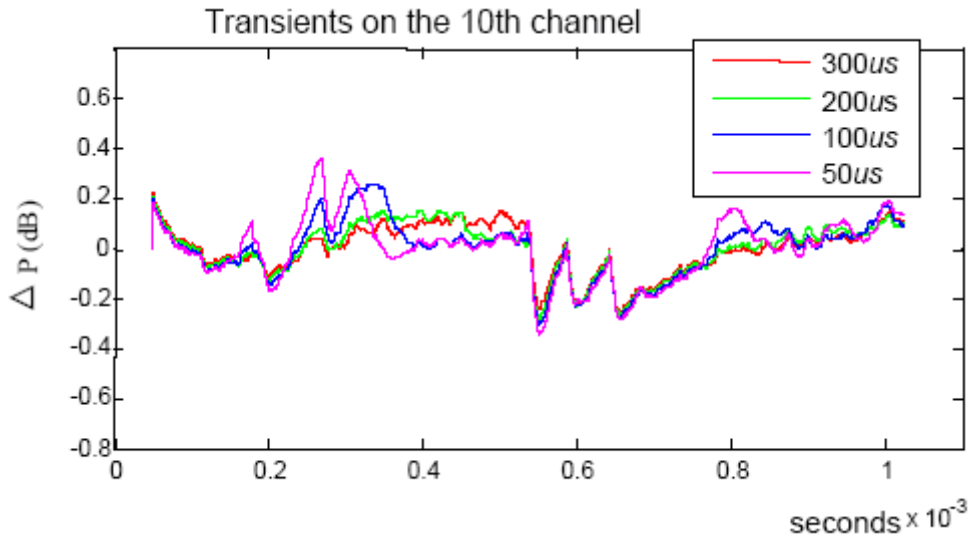

Figure 5.12. Power transients on channel 10 with varying shaping-period.

per channel is also several mW, and is limited by different effects. For example the threshold for SBS onset is about 10mW. This suggests that the value of shaping-period should be greater than the transient settling time of in-line amplifiers. The transient durations of amplifiers using other technologies (such as Raman [75] and EDWA [77]) are usually shorter than that of an EDFA. In a real deployment, the value of shaping-period needs to be tuned and can be chosen based on the characteristics of in-line amplifiers.

Experimental Validation

The experiment setup used to validate power shaping is shown in Figure 5.13 [61]. A CW probe laser with wavelength 1560.67nm and a data laser with wavelength 1554.14nm are coupled (through a 3dB coupler) onto an amplifier chain. The output

power of each laser is set to 5mW to represent 5 channels with average power 1mW each. The Bookham MGMFL-1AEC28 and MGMFL-1AWC28 series EDFAs with internal electronic gain control are used in the amplifier chain. The inter-amplifier attenuators are used to simulate fiber spans and are tuned to make sure that the amplifiers operate in the saturation mode. The probe channel (i.e. the probe laser) is filtered out at the end of the amplifier chain and connected to the oscilloscope. In Figure 5.13, the data laser is switched on and off (controlled by the BERT) and the induced transients on the probe channel is investigated.

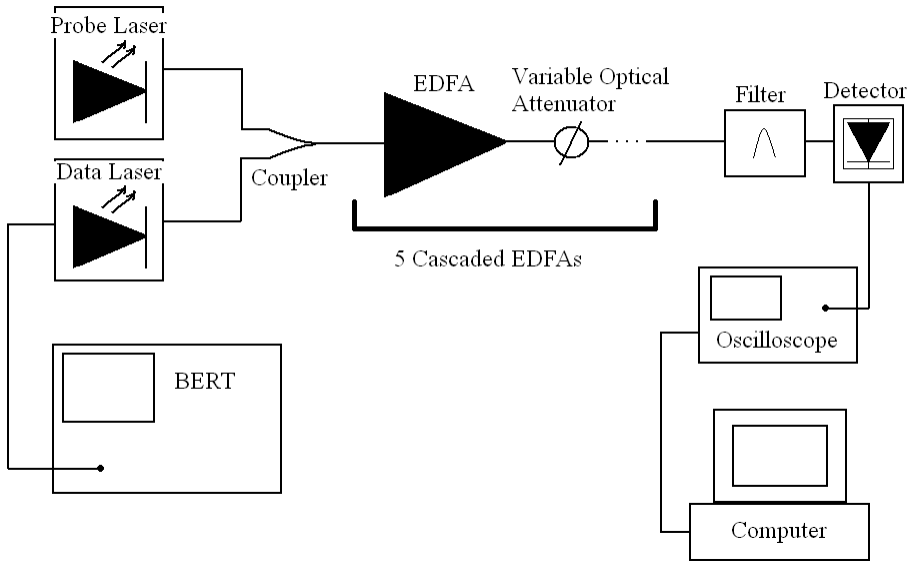

Figure 5.13. Experiment setup for testing the effectiveness of power shaping [61].

When power shaping is not applied on the data laser, Figure 5.14 [61] shows the transients induced on the probe channel when the data laser is turned on and off.

When power shaping is applied on the data laser with the linear shaping profile, Figure 5.15 compares the transient amplitudes when different shaping-periods are

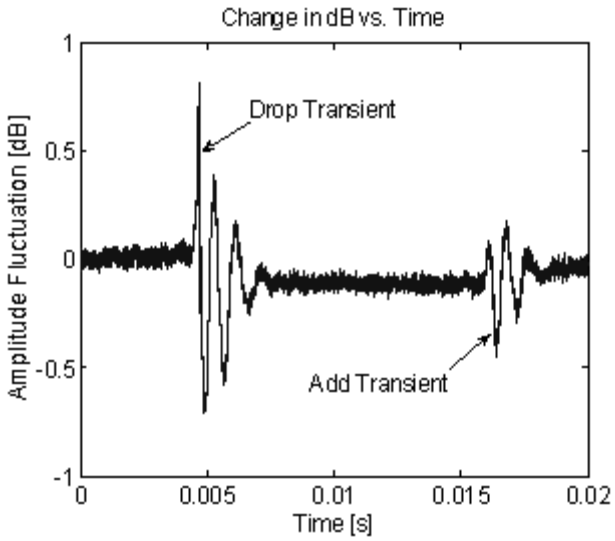

Figure 5.14. Transients on the probe channel when no power shaping is applied [61].

used [61]. We notice that both the peak and the mean of transient amplitudes decrease as the shaping-period is gradually increased regardless of adding or dropping the data laser.

Discussion

Power shaping works at the link layer and can be implemented under software control using FPGAs. This requires direct control of the optical line codes and methods should be provided such that the scrambler or block code generator, if present, can be bypassed or controlled. This can be achieved, for example, by setting the INIT (initializtion) signal of a scrambler [78]. When the INIT signal is set high, the current data word is forwarded unscrambled. For a given network, the parameter shaping-period should be decided by analyzing the behavior of existing in-line amplifiers. Its value can be set to several microseconds with state of the art amplifiers.

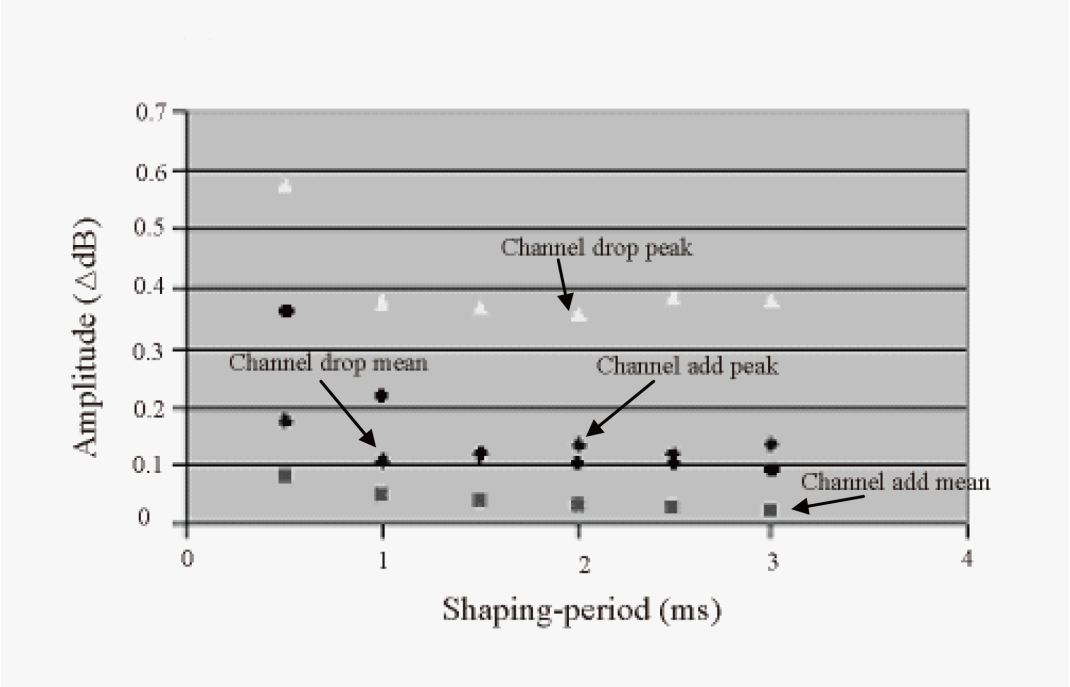

Figure 5.15. Comparison of transient amplitudes for linear shaping profile.

In power shaping, the speed of power changes is slowed by gradually increasing/decreasing the probability of sending bits '1'. The generated pseudo-random bits are treated as traffic data and encapsulated in data frames (including the synchronization bits to ensure correct clock signal extraction). The receiver bit error rate will not be affected. The data frames of power shaping will be discarded by the receiver link layer.

A big concern regarding power shaping is the bandwidth consumed (bandwidth penalty) by sending power shaping heads and tails. This will not be a problem for circuit-switched networks as the entire bandwidth of a connection is exclusively reserved. For an OBS network using an average burst length of 1ms and head and

tail length each of 10μs, the bandwidth penalty by power shaping is just 2%. For a connection-oriented OPS network, a tail is appended only after a traffic block, not each packet. When the users of a connection continuously send traffic data, then only one head at the start and one tail at the end of the connection are sent. In backbone networks where a number of user connections between the same source and destination pair are multiplexed on one GMPLS connection, the bandwidth penalty is negligible. To further decrease bandwidth penalty, power shaping can be disabled for very short bursts and traffic blocks in the case of OBS and OPS networks, because the transients caused by the leading and trailing edges of such a burst/traffic block can cancel each other.

In [61], the effectiveness of power shaping was verified using experiments. In the experiments, different power shaping profiles were tested (including linear as used in the simulations of this section, Gaussian, exponential, and Squared-cosine). The experiment results show that the linear shaping profile has the most pronounced effect on decreasing transient amplitude for both channel dropping and channel adding situations.

The real situations in an OPS network are more complex than in our simulations and experiments, because multiple LSPs can be statistically multiplexed on a channel. To maintain the power profile of a connection as in Figure 5.5(c) requires that some of the bandwidth of each channel should be reserved, such that data frames of a connection can be switched promptly. Fortunately, EDFAs are not sensitive to

extremely fast power variations due to its comparatively long spontaneous emission life time of about several milliseconds.

All-optical networks may use wavelength converters to decrease connection-blocking and packet-dropping probabilities. Power shaping will still be effective as long as all the data frames of a connection still follow the same path. This is because amplifiers are only sensitive to the variations of the total input power.

Although our modeling and simulations are based on the use of EDFAs, power shaping can be applied to other amplifiers. The parameter shaping-period will need to be adjusted to correspond to the inherent temporal behavior of the specific amplifier technology used. In current optical networks, electronic gain controlled EDFAs are commonly deployed. The effect of power shaping is to slow down the speed of power variations and smooth out the traffic. The cooperation of power shaping with electronic gain controlled in-line amplifiers can further improve their performance and decrease design costs.

Suppression of In-Line Amplifier Transients at Network Failures

Current work regarding protection and restoration in optical networks mainly focuses on the efficient re-routing of affected connections after network failures. An important phenomenon usually accompanying network failures is the possible large power excursions induced on the channels that share amplifiers with these re-routed connections. These channels are indirectly influenced by network failures through

the effect of cross-gain modulation. Although such network failures occur rarely, if they do happen there can be large input power drops at amplifiers on the affected paths. In the literature, a number of schemes have been designed to suppress amplifier transients induced by traffic related channel adding and dropping, but typically they have not considered the special case of network failures.

In next-generation WDM all-optical networks, as more wavelengths per fiber are put into use, the range of amplifier input power variations will increase. It will be expensive to implement amplifiers that can efficiently suppress transients induced by possible power variations in the whole range. We observe that, in a short time period under normal operating conditions, the amplifier input power only varies over a comparatively small range. Passive gain control schemes (e.g. AOGC-EDWA) can meet the requirements of most situations except for some special events, such as network failures. We propose that the in-line amplifiers manage transients under normal operating conditions. Rare network failures, such as a fiber cut, should be handled separately, due to their different characteristics. We proposed an efficient and cost-effective protection scheme for suppressing transients induced by network failures [79]. We demonstrate through numerical simulation that such a protection scheme can help a cascade of AOGC EDFAs suppress transients when a network failure occurs. The scheme can also work with other types of in-line amplifiers.

System Design

The proposed protection scheme is performed on a per node basis. A device called the *transient protection controller* (TPC) is installed in each switch node. We do not make any assumptions regarding which transient-suppression scheme is used by the in-line amplifiers. The design of the TPC is schematically explained using Figure 5.16, where 3 input fibers and 3 output fibers are connected to an optical switch. The TPC is composed of a *laser source* and a *generator controller*. The laser source is used to generate a compensation signal. The generator controller has a tap on each output fiber, detecting its power variations. When a network failure occurs and the power drop on one output fiber is greater than a pre-determined threshold beyond which the in-line amplifiers can not efficiently suppress, then the generator controller signals the laser source, through the port labeled O2, to generate a compensation signal which is injected into the optical switch. At the same time, a command is sent, through port O1, to configure the optical switch. The optical signal from the laser source is added to the affected output port to compensate for the power loss due to the network failure. The wavelength of the laser source is fixed and outside the range used for communication. The generator controller is table driven. The controlling table is created based on information from experiments or simulations of output fiber in-line amplifier cascades, and has fields <power drops, compensation power, output port>. After the in-line amplifier cascade stabilizes, the power of the compensation signal is gradually decreased to 0. At last, it can be retracted and be used to protect

against another network failure. In the structure illustrated in Figure 5.16, we have assumed that the amplifier cascades on the three output fibers are identical and that only one output fiber can possibly have transient outage in case of a network failure. Otherwise, multiple laser sources and controlling tables need to be provided.

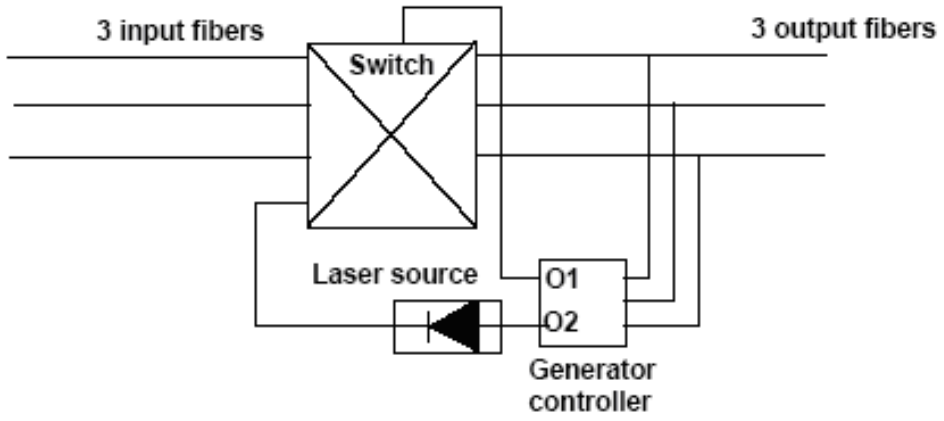

Figure 5.16. Design of TPC.

Numerical Simulation

We investigate our protection scheme by numerical simulations using the software OptSim^{TM}. The simulation model is shown in Figure 5.17, where we simulate a simple scenario: signal channels (with power 1mW per channel) on two input fibers are switched onto an output fiber with a cascade of 10 AOGC EDFAs. Channels on the first input fiber are represented by CW1 (with wavelength 1551nm), with adjustable power to simulate different numbers of working channels. Another single channel on the second input fiber is represented by CW2 (with wavelength 1553nm). We investigate the performance of the proposed protection scheme in suppressing

transients on the output fiber when the working channels on the first input fiber are all suddenly dropped due to a network failure. In Figure 5.17, attenuators with losses of 20dB are used to simulate fiber spans. The AOGC EDFAs (with gain flattening) have been tuned such that CW1 and CW2 will both achieve 20dB gains. The transient switch SW1 is used to simulate network failure (i.e., at the specified moment, its status will suddenly change from bar to cross). The transient switch SW2 is used to simulate the gradual increase of the compensation signal (i.e., after detecting a network failure, its status will change from cross to bar with transition period TP_{cmp}). The transient switch SW3 is used to simulate the gradual decrease of the compensation signal after the amplifier cascade has stabilized. The laser source is simulated by CW_CMP. We assume that each fiber can has 20 wavelengths and when the input power of the amplifier cascade drops more than 10mW, the in-line amplifiers cannot suppress resultant transients efficiently. The output fiber is connected to port 1 of the optical switch. Based on these assumptions, Table 5.2 shows the controlling table used in the simulation.

Simulation results obtained with TP_{cmp}=5μs, are given in Figure 5.18, which shows the power evolution of each wavelength at the output of the 10^{th} in-line amplifier, when using TPC at the worst case (i.e., when 20 channels on the first input fiber are dropped). The transients induced on CW2 with and without TPC are compared in Figure 5.19 when different numbers of channels are dropped. It is evident that

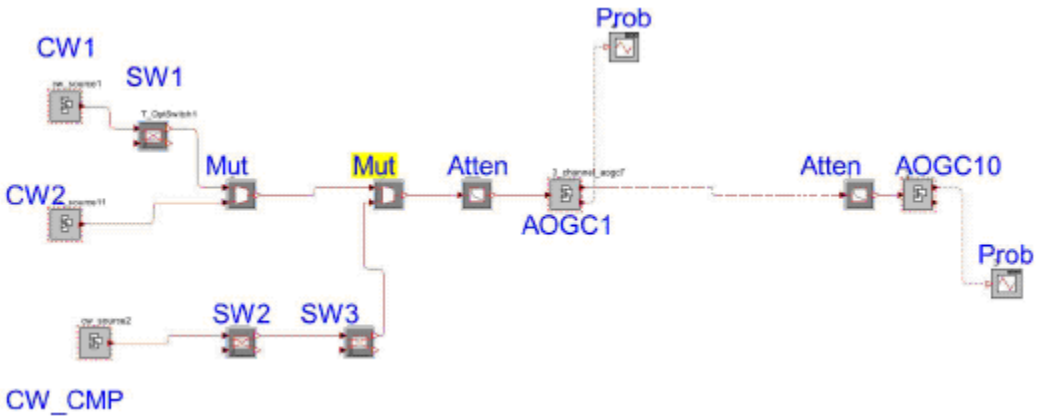

Figure 5.17. OptSim^{TM} simulation model for TPC. CW: continuous wave, CW_CMP: continuous wave compensation signal, SW: transient switch, Mut: multiplexer, Atten: attenuator, AOGC: AOGC EDFA, Prob: optical power probe.

Table 5.2. The controlling table of generator controller used in a simulation.

Power drops (mW)	Compensation power (mW)	Output port
11	7.5	1
12	8	1
13	9	1
14	10.5	1
15	11	1
16	12	1
17	12.5	1
18	13	1
19	14	1
20	15.5	1

the application of TPC not only has decreased the amplitude of power excursions, but also has decreased the duration of transient periods.

We investigate the influence of TP_{cmp} on the performance of TPC. We vary the value of TP_{cmp}, and compare the induced transients on CW2 at the worst case in Figure 5.17. Parameter TP_{cmp} is the sum of the generator controller response time, the

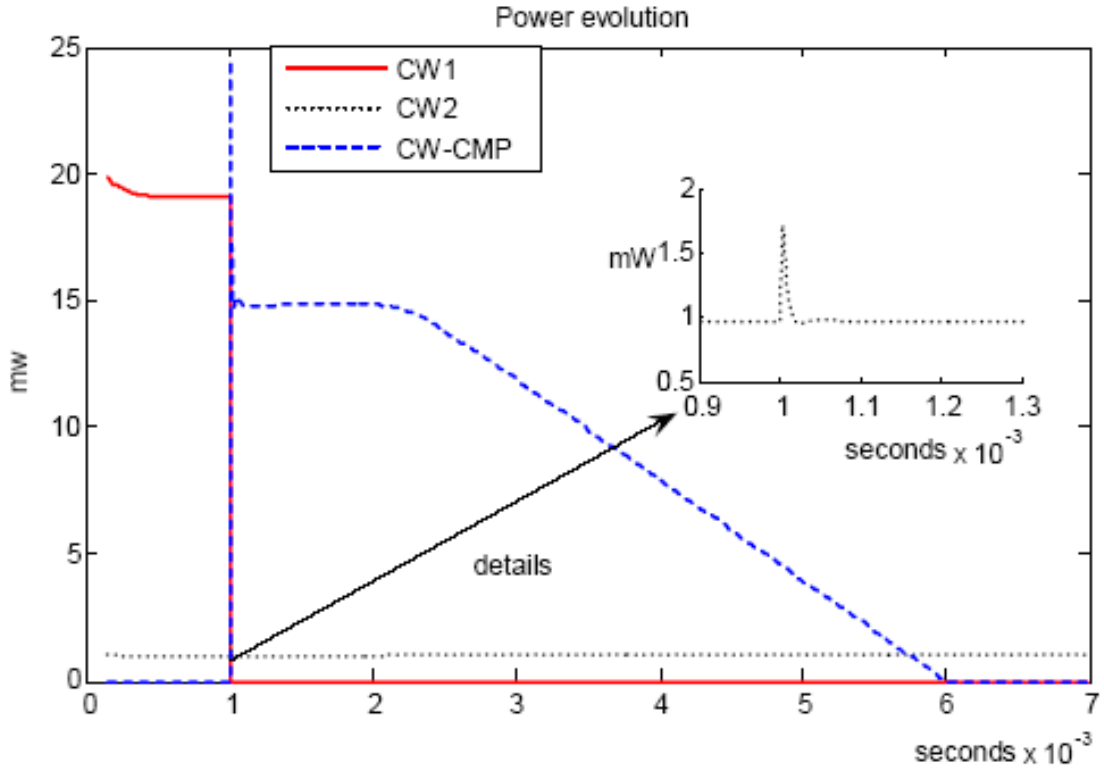

Figure 5.18. Power evolution of each wavelength. Details of the induced transients on CW2 are shown in the embedded small figure.

rise time of the laser source, and the switching time of the optical switch. Decreasing TP_{cmp} will achieve better transient suppression. The difference between the design of TPC and of other schemes applying electrical feedforward/feedback circuits is that the feedback control mechanism is not needed in TPC, and so it is much easier to build. The signal to noise ratio on the power samples taken using taps on the output fibers limits the fault detection time, and thus the response speed of the generator controller.

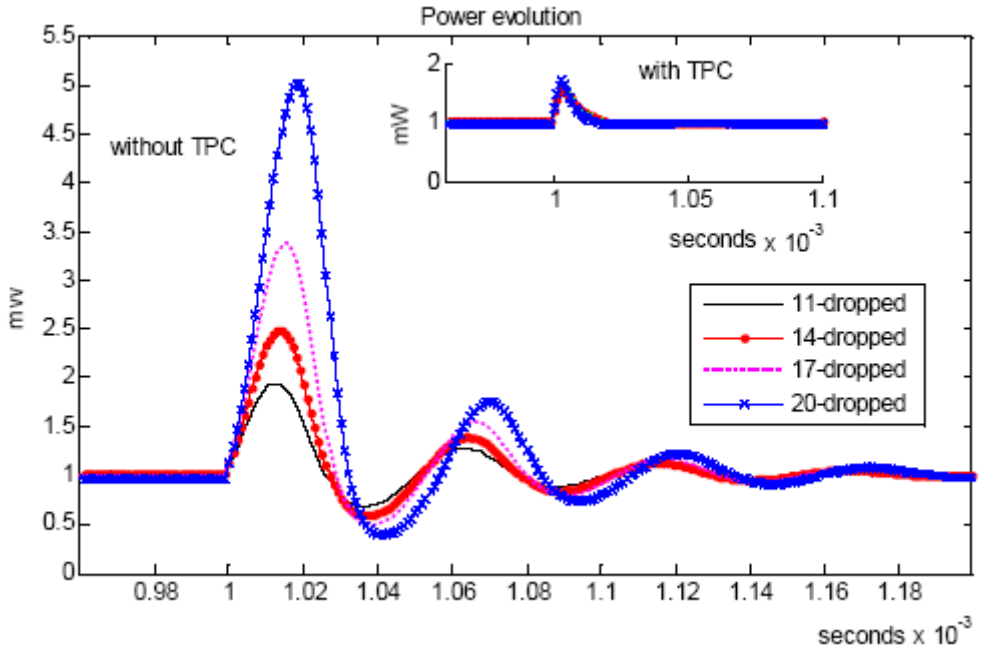

Figure 5.19. Comparison of transients with and without TPC when different numbers of channels are dropped in a network failure.

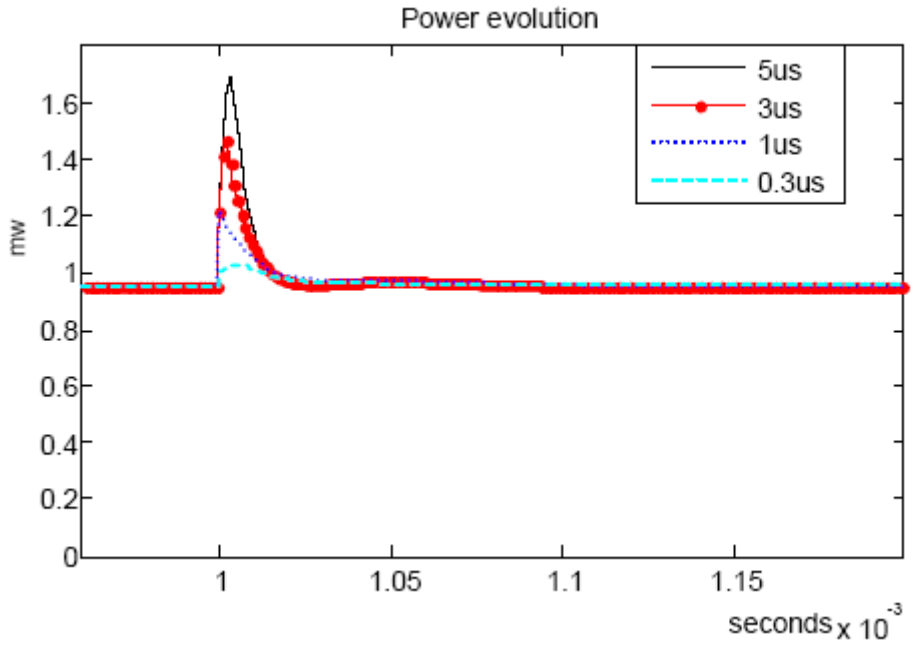

Figure 5.20. Comparison of TPC performance with varying TP_{cmp}.

Discussion

One important issue is the ability of this approach to distinguish between power excursions due to network failures and normal transients induced by temporal traffic fluctuations. We do not want TPC to interfere with in-line amplifiers under normal operating conditions. To prevent false positive fault detections, each traffic source should periodically transmit maintenance packets in case no traffic data are sent.

In the design illustrated in Figure 5.16, the optical switch is assumed to be much faster than the response speed of the generator controller. This is not a problem for switches that would be used in burst or packet switched networks. For slow switches used in circuit switched networks (e.g. MEMS switches), a special component must be designed so that the compensation signal can be coupled to an output fiber fast enough.

Because the time required to complete the proposed protection operation is in the range of several milliseconds, we only consider the case of a single network failure. More than one laser source would be needed to protect multiple output fibers that might have transient outages at the same time. For example, suppose that only one input fiber (with N wavelengths) of a node can suddenly lose all of its power in case of a network failure, the in-line amplifiers can at most handle input power drop P^*(powers per channel), and the node has M output fibers, then $min(M, \lceil \frac{N}{P+1} \rceil)$ laser sources are needed to protect all of the output fibers in the worst case. In

practice, only a few laser sources would be needed. This illustrates a trade off between implementation cost and system performance.

ADAPTIVE RWA ALGORITHMS FOR TRAFFIC ENGINEERING

Introduction

Next-generation all-optical networks will use on-demand resource allocation to increase the overall network performance and meet application requirements for dynamic connection requests. These multi-wavelength, all-optical networks will use optical switches and optical amplifiers to achieve the overall network performance. For their operations, it is necessary that the control planes of such networks can dynamically control traffic flow and make effective use of network resources. In recent years the amount of traffic due to internet-based services has grown significantly [80]. New applications, including the real-time ones which require guaranteeing QoS for a subset of services, have been deployed on IP networks. Next-generation networks, using optical networks as infrastructure, should also have multi-service capability to support different types of services, with different requirements in terms of QoS.

The considerations above motivated the adoption of traffic engineering (TE) in next-generation networks. The definition of TE given by [81] is to improve the efficiency and reliability of network operations while optimizing network resource utilization and traffic performance. More specifically, the application of TE in optical networks includes choosing routes for data flows and the way they are grouped and multiplexed onto optical lightpaths, taking into account traffic load, network state,

and user requirements such as QoS and bandwidth, and to move the traffic from more congested paths to less congested ones. The multi-protocol label switching MPLS (and its generalization GMPLS), constraint based routing, and enhanced link state interior gateway protocol are identified as the key ingredients of TE. It is widely known that the MPLS/GMPLS control plane together with proper constraint based routing solutions will provide the means for achieving TE [80].

The extension of MPLS to include optical routing (e.g. GMPLS) takes into account certain attributes associated with optical networks [82][83][84], and a technique to take these factors into account in routing has been proposed as a modification to SPF algorithms (shortest path first) [85]. However, the lightpath characteristics explicitly identified in the GMPLS framework, including interface switch capability, interface bandwidth, link protection type, traffic engineering metric, hop count limit, priority, preemption, and etc., are logical and ideal. There is currently no inclusion of optical layer behavior and performance factors such as number of wavelengths on a fiber, signal power levels, noise levels, end-to-end bit error rate, etc. in GMPLS, although there is considerable discussion in the IETF (Internet Engineering Task Force) to consider these factors. These factors could be constraints in selecting optical paths and should be considered in RWA algorithms [86].

Our own research on all-optical routing has led to the development of new algorithms for RWA. We have been addressing the problem where a single wavelength must be used end-to-end (i.e., no wavelength conversion is available) and designed

algorithms that are particularly well-suited to enable highly-dynamic RWA anticipated in burst-mode and customer-controlled all-optical networks. In a transparent, all-optical network, an end-to-end path and a free wavelength need to be chosen for each connection request that minimize connection blocking probability and maximize resource utilization. The solution is state dependent, meaning that that the current network state (i.e. assignment of traffic to wavelengths and links) affects the optimum RWA for a particular connection request.

In this chapter, two adaptive algorithms (LORA [87] and MBR [88]) are described. The goal of the algorithm design is to maximize resource utilization and decrease connection blocking probability. Although these algorithms do not take the physical impairments into account, the LORA algorithm will be adapted to enable physically aware constraint based routing discussed in the next chapter.

A Lexicographically Optimized Routing Algorithm (LORA) for All-Optical Networks

For a large network, a common way to solve the RWA problem is to separate it into two sub-problems: first finding a path from the source to the destination, and then assigning a wavelength that is free on each link of the computed path.

Adaptive routing algorithms usually use the Dijkstra algorithm to compute a minimal cost path from source to destination. The link cost function is critical for such algorithms. In [89], the cost of a link L was defined as $\frac{1}{F_l}$, where F_l is the number

of free wavelengths of link L. In [90], the link cost of a link L was defined as $e^{\frac{1}{F_l}}$. In [91] a lexicographic routing algorithm was proposed for distributing the IP traffic load among all links to avoid the bottleneck problem of OSPF routing. However, its time complexity is exponential in network size for a general link cost function. Additionally, for a connection request, its solution usually consists of several paths, so the traffic from the source to the destination can split. This is not applicable to wavelength routing in all-optical networks. Because of its time complexity and the peculiarities of all-optical networks, it can't be applied directly in all-optical networks.

Inspired by [91], we have developed a new adaptive routing algorithm (LORA). We are mainly concerned with how to compute a path based on the current network state to decrease the connection blocking probability.

Network Model

An optical network can be represented as a directed or undirected graph. We use the NSF network topology as the basis for modeling and simulation. This topology has been used in other simulations [92], enabling us to compare our results with those obtained with other RWA algorithms.

Nodes in the topology graph are optical switches and are connected by multi-wavelength optical links. We assume that optical links are directed, so an edge in the graph between two adjacent nodes (e.g. A, B) actually includes two links (A→B and B→A). Each link is assumed to have only one fiber with N indexed wavelengths λ_0, $\cdots$, λ_{N-1} (Different links can have different number of wavelengths, our assumption

of equal number of wavelengths on all links is used to simplify the modelling and implementation). In this chapter, we will not consider physical impairments. The real structure of optical links will not influence the design of the proposed algorithms. We further assume that no wavelength converters are available in the network.

Workstations (traffic generation nodes not shown in the topology graph) attached to the switches send out connection requests randomly and independently according to a random process with arrival rate γ. The duration of each connection is modeled using a random variable with mean μ. Each node in the network periodically broadcasts wavelength-usage information of incident links every T seconds. With the development of DWDM, it is possible that there are hundreds of wavelengths on each fiber, and with dynamic traffic, the states of wavelengths can change in a short period. We assume that in large networks optical switches only broadcast the usage information instead of the state of each wavelength. The network broadcast can be either in-band (signaling messages are transmitted on traffic channels) or out-of-band (signaling messages are transmitted on exclusive channels) depending on the network design.

Source nodes apply a routing algorithm and use the backward reservation protocol to create a connection. The backward reservation protocol is chosen because of its advantages compared to the forward reservation protocol [93]. The source node sends out a 'probe' message to the destination node. The 'probe' message includes the following fields: <source id, destination id, path_info, wave_map, connection id>,

where 'path_info' is the ordered list of nodes on the selected path and 'wave_map' is an array indicating the availability/unavailability of each wavelength. After receiving a 'probe' message, an intermediate node updates the 'wave_map' field by marking wavelengths locked by itself as 'Busy'. Upon receiving a 'probe' message, the destination node picks a free wavelength according to a wavelength assignment algorithm (First-fit, Random, etc.) based on information in the 'wave_map' field, and sends a 'resv' message upstream. The 'resv' message includes the following fields: <connection id, selected wavelength>. All nodes along the lightpath will lock the wavelength specified in the 'resv' message. When a connection finishes, the source node sends a 'release' message downstream to release the used wavelength.

The Design of LORA

Following the lexicographical optimization approach, we define the optimization objective function as follows.

Given the current network state, for each computed path from the source to the destination, a usage vector ν is defined whose elements are the wavelength usage of each link along the path. The optimal path is the one whose usage vector is the lexicographical minimum among all candidate paths with the lexicographical comparison defined by the following Algorithm 6.1.

Algorithm 6.1 Lexicographical comparison of two usage vectors, X and Y

1: Set X^{sort}= sort components of X in the decreasing order.
2: Set Y^{sort}= sort components of Y in the decreasing order.
3: **if** $\exists k, X_1^{sort} = Y_1^{sort}, \cdots, X_{k-1}^{sort} = Y_{k-1}^{sort}$ and $X_k^{sort} < Y_k^{sort}$ **then**
4: **return** $X < Y$;
5: **else if** $\exists k, X_1^{sort} = Y_1^{sort}, \cdots, X_{k-1}^{sort} = Y_{k-1}^{sort}$ and $X_k^{sort} > Y_k^{sort}$ **then**
6: **return** $X > Y$
7: **else**
8: **return** $X == Y$
9: **end if**

As in [91], by using this optimization objective function, we distribute the traffic load among all links. By the definition of lexicographical comparison, the lexicographically optimized routing algorithm should find a path first by using the least used links, then the intermediately used links, and finally the most used links. In other words, links with different usage values have different powers. A natural way to express this idea is to set the link cost function as β^{U_l}, where U_l is the number of used wavelengths of link L and β ($\beta > 1$) is a parameter we want to change dynamically.

We illustrate the lexicographic approach in the following example. Consider a source S and destination D, which could be connected by two paths: P1=S-A-B-C-D and P2=S-E-F-G-H-D, as indicated in Figure 6.1. The number associated with each link in each path indicates the number of wavelengths in use on the link. We then form ordered vectors for P1 and P2 corresponding to the number of wavelengths in use on each link, ordered with the highest number first: P1=<4,3,1,0> and P2=< $3, 2, 1, 1, 0 >$.

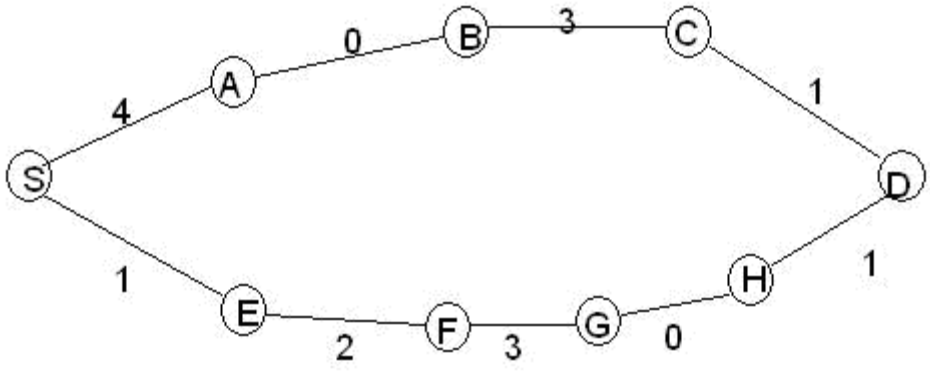

Figure 6.1. Two paths between S and D with different wavelength utilizations.

By the lexicographic approach, we choose P2 as the preferred route, because the highest link usage (4) on P1 exceeds the highest link usage on P2 (3). The preferred route is P2 despite the fact that P2 is longer than P1, in terms of hops.

LORA is described by the following Algorithm 6.2.

Algorithm 6.2 The Algorithm LORA

1: Decide the value of parameter β according to the current network traffic load;
2: Set the cost of each link using $cost(L) = \beta^{U_l}$.
3: Return the minimal cost path by calling the Dijkstra algorithm

The following Theorem 1 clarifies our intuition that by using large β, we can search for a less congested path in a larger area of the network topology graph than when a smaller β is used. We notice that with LORA there are two extreme situations: when $\beta > n-1$ (n is the number of nodes in the topology graph) the algorithm finds a lexicographically minimal path globally, when $\beta = 1$ this algorithm degrades to the shortest-path.

Theorem 1. *For a given network with n nodes, if $\beta > n-1$, then LORA will return the lexicographically minimal path.*

Proof. Let's assume that the minimal cost path returned by LORA is P_1. It has i_k links with usage k, i_{k-1} links with usage $k-1$, $\cdots$, and i_0 links with usage 0. Let's also assume that the lexicographically minimal path P_2 has j_k links with usage k, j_{k-1} links with usage $k-1$, $\cdots$, and j_0 links with usage 0. Notice that P_2 can't have links with usage more than k and $i_k > j_k$, because P_2 is the lexicographical minimum. Also notice that $\sum_{n=0}^{n=k} i_n$ and $\sum_{n=0}^{n=k} j_n$ are the lengths of P_1 and P_2 in number of hops respectively.

We claim $i_k = j_k$. Else $i_k > j_k$, then,

$$\begin{aligned} cost(P_1) - cost(P_2) =& \sum_{n=0}^{n=k} i_n * \beta^n - \sum_{n=0}^{n=k} j_n * \beta^n \\ =& (i_k - j_k) * \beta^k + \sum_{n=0}^{n=k-1} (i_n - j_n) * \beta^n \\ \geq& \beta^k - (\sum_{n=0}^{n=k-1} j_n)\beta^{k-1} \\ \geq& \beta^k - (n-1)\beta^{k-1} \\ >& 0 \end{aligned} \tag{6.1}$$

But this contradicts our assumption that P_1 is the minimal cost path. So $i_k = j_k$. By using the same method, we can prove $i_{k-1} = j_{k-1}$, $\cdots$, and $i_0 = j_0$. □

Dynamically Changing β

In an all-optical network, distributing traffic load among links is not our only consideration. We also need to allocate wavelengths effectively. LORA usually returns a path longer than the shortest path. But a longer path will use more network resources. We can dynamically change β to control the lengths of paths returned by LORA using an off-line method. For a given network topology, we obtain the optimal values of β under several traffic loads by simulation using the Hill-Climbing algorithm [87]. By interpolation, we obtain a curve for the optimal value of β as a function of traffic load. Such a curve can be stored in optical switch control software. When a connection request arrives, an edge optical switch first computes the optimal value of β for the current network traffic load, which can be obtained from historic data or by information broadcast by all edge optical switches.

Numerical Simulation and Analysis

We use the NSF network, which has 16 nodes as shown in Figure 6.2, as our experiment network topology and assume that it is all-optical. We assume that each link has 10 wavelengths. The destination node uses the First-fit algorithm [94] for wavelength assignment in the simulations. The edge node uses explicit source routing. No wavelength conversion is assumed to be available in the network. Figure 6.3 shows the optimal values of β under different traffic loads obtained for the NSF network.

As shown in Figure 6.3 when the traffic load is low (below 30 Erlangs), the optimal value of β is 1. Under such light load conditions, we can also use a larger

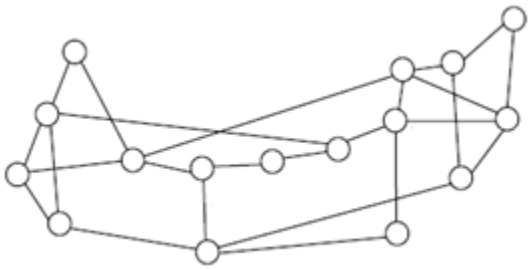

Figure 6.2. The NSF network topology.

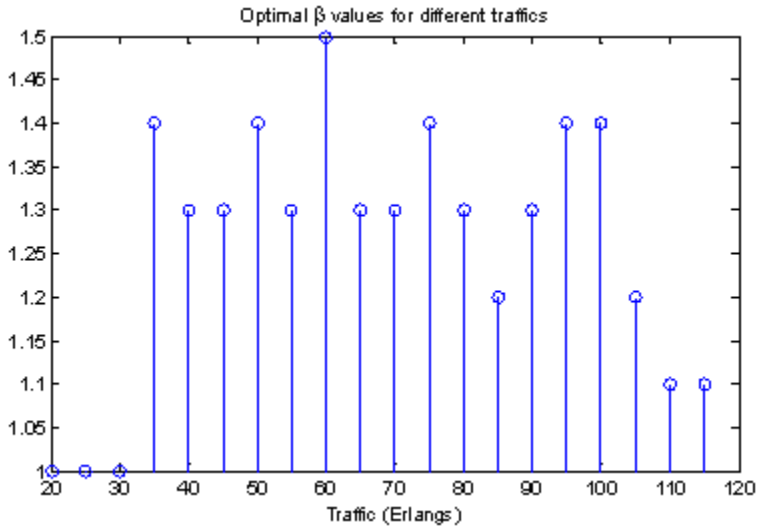

Figure 6.3. Optimal value of β versus traffic load with hill climbing step resolution 0.1.

value for β to achieve low blocking probability. As we increase the traffic, we find that 1.3 is a good value for β. When the traffic load is above 105 Erlangs, we find that using a large value for β doesn't help decrease blocking probability. Based on these simulation results, we use the following Equation 6.2 to adjust β under different traffic loads, which is a piecewise linear function,

$$\beta = \begin{cases} 1.3 & \text{if traffic load} < 105 \text{ Erlangs} \\ 1.1 & \text{if traffic load} \geq 105 \text{ Erlangs.} \end{cases} \tag{6.2}$$

We compare the performance of LORA with three benchmark algorithms: the shortest-path, the minimal-cost-path with $cost(L) = \frac{1}{F_l}$ (denoted as Least Congested (LC)), and the minimal-cost-path with $cost(L) = e^{\frac{1}{F_l}}$ (denoted as Enhanced Least Congested (ELC)). Figure 6.4 shows the results of the comparison. Our simulations show that LORA works well compared to other algorithms. The blocking probability achieved with LORA is at least as low or lower at all network traffic loads than with any of the other RWA algorithms tested. The results obtained with LORA are significantly better than those obtained with the least congested (LC) method, with at least a 25% reduction in blocking probability.

This work forms a foundation for our research designing RWA algorithms under additional constraints such as link performance, transient effects in switches and amplifiers, and other physical layer factors.

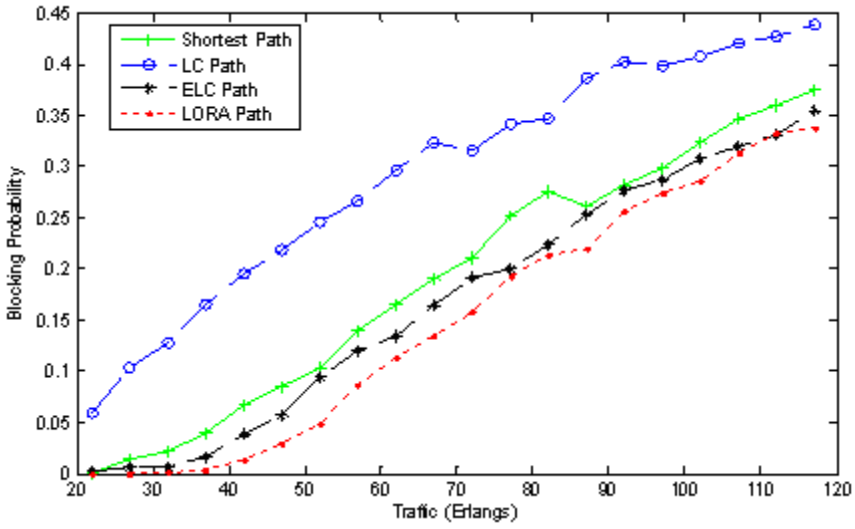

Figure 6.4. Performance comparison of LORA and benchmark algorithms.

Most RWA algorithms only try to decrease the probability of blocking caused by lack of resources (i.e. lack of free wavelengths), without considering blocking caused by reservation confliction. When paths of several connection requests share a common link, confliction can occur if more than one connection request tryies to use the same free wavelength on an optical link. Figure 6.5 illustrates a confliction scenario in the backward reservation procedure. We assume in this simple network, the shortest-path and First-fit algorithms are used for routing and wavelength assignment.

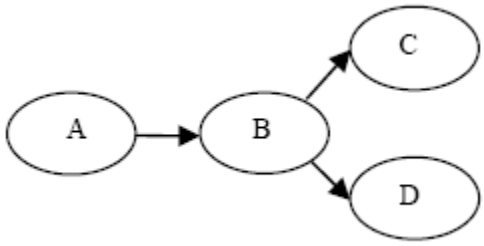

Figure 6.5. An example of reservation confliction.

Assume all wavelengths on all links are initially free. The 'probe' message of connection request Q1 (A→B→C) arrives at C first. Node C will choose λ_0 according to the assumption (First-fit). Before C sends a 'resv' message upstream, the 'probe' message of connection request Q2 (A→B→D) arrives at B, which will still find that all wavelengths on link A→B and B→D are free. When the 'probe' message of Q2 arrives at D, node D will also choose λ_0. One of the connection requests will succeed while the other will be blocked depending on whose 'resv' message arrives at B first.

When the network is not heavily loaded, reservation confliction is the major cause of blocking.

There are a few algorithms reported in the literature that take into account reservation confliction. In [95], a new model was proposed to predict the blocking probability considering both the lack of free wavelengths and reservation confliction. Their assumption (random wavelength selection) and computation method (fixed point) make it impossible to use this model in a real-time routing algorithm. In [96], parallel reservation was used to decrease the reservation confliction probability. The source node uses the forward reservation, but will send 'resv' messages to all nodes on the selected paths at the same time. Compared to backward reservation, the frequency of wavelength-usage information broadcast has to be increased in this algorithm because it lacks a probing procedure. The signaling process is also more complex because a distributed transaction needs to be implemented. In optical burst-switched networks, delayed-reservation, delayed-reservation-without-void-filling, and delayed-reservation-with-void-filling algorithms are used to solve the reservation confliction under the assumption that a switch node knows the start time and duration of each burst [97]. In [98], a wavelength priority table is maintained in each node. Each time a connection is accepted using a free wavelength, the priority of this wavelength is increased, resulting in connection requests from different source nodes tending to use different wavelengths. In [92], wavelengths suggested to be used by connection requests are stored in a flagged pool. The wavelength assignment algorithm first tries

to randomly pick a free wavelength, but if no free wavelength exists, then it randomly picks a wavelength from the set with the lowest priority in the flagged pool. Wavelengths in the flagged pool are prioritized based on the time they have stayed in the pool. In both [92] and [98], although the reservation confliction probability can be decreased, the blocking probability due to lack of free wavelengths will increase when the network is comparatively highly loaded, because it will be more difficult to find a wavelength which is free on all links of a path with a large hop number. A good algorithm should consider both of these factors. On the one hand, it needs to decrease the confliction probability. On the other hand, it also needs to keep the set of used wavelengths compact in the wavelength index space as in the First-fit and the Most-used algorithms.

As described later, we designed a new reservation protocol to decrease the reservation confliction probability. The new protocol is a modification of the backward reservation. Our basic idea is to guess the wavelengths that other competing connection requests will use. Then when a destination node chooses a free wavelength for a connection, it can avoid selecting those wavelengths possibly chosen by competing connection requests. We show below our approach can achieve significant improvements compared to other algorithms.

Markov Modeling of Optical Links

The proposed Markov-Based Reservation protocol (MBR) works much like the backward reservation protocol. To decrease the probability of reservation confliction,

MBR uses a modified version of the First-fit algorithm to avoid selecting the free wavelengths that may be selected by other competing connection requests.

For a given connection request, intermediate nodes can guess the wavelength assignment decision of its destination node if they know the states of wavelengths on links along the path. If the guess results are stored in intermediates nodes, then all competing connection requests arriving later could avoid selecting this wavelength. However, traffics on links are dynamic. Although each switch node can broadcast wavelength-usage information every T seconds, the broadcast information is not necessarily correct during the period between two successive broadcast moments. Instead of using the broadcast information directly, we build a continuous time Markov chain (C-T Markov chain) for each link and use the C-T Markov chain to predict the wavelength usage at any arbitrary time.

Each C-T Markov chain corresponds to one link in the network. There are two ways to define its state space. One method is to use a bit array of length N to represent the state of each wavelength (0: Free, 1: Busy). Each possible combination of the bit array defines one state. The size of the state space is 2^N. Such a state space can be used with any wavelength assignment algorithm. But it can only be used in networks with a small number of wavelengths per fiber because the size of the state space increases exponentially with the number of wavelengths.

Another method can be applied if the First-fit wavelength assignment algorithm is used. The First-fit algorithm was shown to have good performance in [94]. It is

also easier to implement and incurs less system overheads compared to the Most-used algorithm. In First-fit, the destination node will always use the free wavelength with the smallest index. If the destination node chooses λ_i, then $\lambda_0, \cdots, \lambda_{i-1}$ all are busy. Although this assumption does not hold for all links, it is correct for busy links where traffic converges and those links determine the wavelength allocation for connections by First-fit. In this situation, each state of the C-T Markov chain can be defined as the number of used wavelengths on a link (i.e., state i means i wavelengths are used). The size of such a state space is N+1. We use this definition of state space in the design of the proposed algorithm. Figure 6.6 illustrates the state space of a chain.

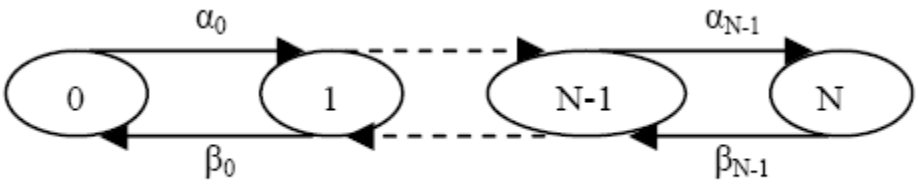

Figure 6.6. The C-T Markov chain of an optical link with N wavelengths. α_i, β_i are transition rates.

The parameters of a chain (transition rate between states) are obtained by network monitoring. For an arbitrary link A→B, we call A the *controlling node* of the link and controlling nodes will do the network monitoring. We denote the transition from state i to j as $tran(i, j)$, the number of times that the transition $tran(i, j)$ happens in a monitoring period as $count(i, j)$. The transition time $time(i, j)$ is defined as the interval from the moment when the chain enters state i until the moment

when the chain leaves i and enters state j. Transition $tran(i,j)$ can happen multiple times in a monitoring period, the sum of their transition times $time(i,j)$ is denoted as $sum(i,j)$. Notice, according to the definition of state, $|i-j|$ is always equal to 1 for valid transitions.

The transition rate $R(i,j)$ of $Tran(i,j)$ is defined as

$$R(i,j) = \begin{cases} \frac{count(i,j)}{sum(i,i-1)+sum(i,i+1)} & \text{if } |i-j|=1, \\ 0 & \text{otherwise.} \end{cases} \tag{6.3}$$

The $R(i,j)$s totally describe the dynamics of an optical link. The controlling node of an optical link will broadcast these transition rates periodically (denote the chain parameter broadcast period as T') or only when significant changes happen depending on network policy. Other nodes will store these parameters in their database as properties of the optical link.

The transition rate $R(i)$ of a state i is defined as

$$R(i) = R(i,i-1) + R(i,i+1). \tag{6.4}$$

This is the transition rate of state i to other states (*leaving rate*).

Every T seconds, switch nodes broadcast wavelength usage of links. Usually, we set $T' >> T$. Each node then knows the exact wavelength allocation on all links at time $0T$, $1T$, $\cdots$, sT, $\cdots$. At an arbitrary time $sT+\tau$ between sT and $(s+1)T$, a node can use C-T Markov chains to guess the free wavelength distribution on non-incident links. In our simulation, we have not considered the propagation delays of network broadcast messages.

The transient analysis of a C-T Markov chain is given in [99]. Given that a chain is at state i at time 0, then the probability $P_{i,j}$ that the chain will be at state j at time t is

$$P_{i,j} = \sum_{n=0}^{n=\infty} e^{-\nu t} \frac{(\nu t)^n}{n!} (\overline{P_{i,j}})^n, \tag{6.5}$$

where n is the number of transitions possibly occurred in the duration t. Equation 6.5 is called the Uniformization method in C-T Markov chain transient analysis. A C-T Markov chain can be viewed as a Poisson process plus a discrete Markov chain. However, the Poisson process has different transition rates when the chain is at different states. The Uniformization method transforms the original chain into an equivalent chain with a uniform rate. The uniform rate ν is defined as

$$\nu = max\{R(i) | i = 0, 1, \cdots, N\}. \tag{6.6}$$

The transition probability $\overline{P_{i,j}}$ (the probability that the embedded discrete chain will transit to state j when it leaves state i) is defined as

$$\overline{P_{i,j}} = \begin{cases} \frac{R(i,j)}{\nu} & \text{if } |i-j| = 1, \\ \frac{\nu - R(i,j)}{\nu} & \text{if } |i-j| = 0, \\ 0 & \text{otherwise.} \end{cases} \tag{6.7}$$

Using Equation 6.5, we can compute the state distribution of a chain (the set of probabilities that the chain will be at each state) at time $sT + \tau$, given that it is at state i at time sT. Figure 6.7 illustrates an example. The traffic of a link in this example is 2 Erlangs. Given that the chain is at state 5 at time 0, we want to predict the state distribution of the chain after 10, 50 and 100 seconds. From the figure, we

see that the chain converges to its steady state quickly. Two wavelengths are in use in the steady state.

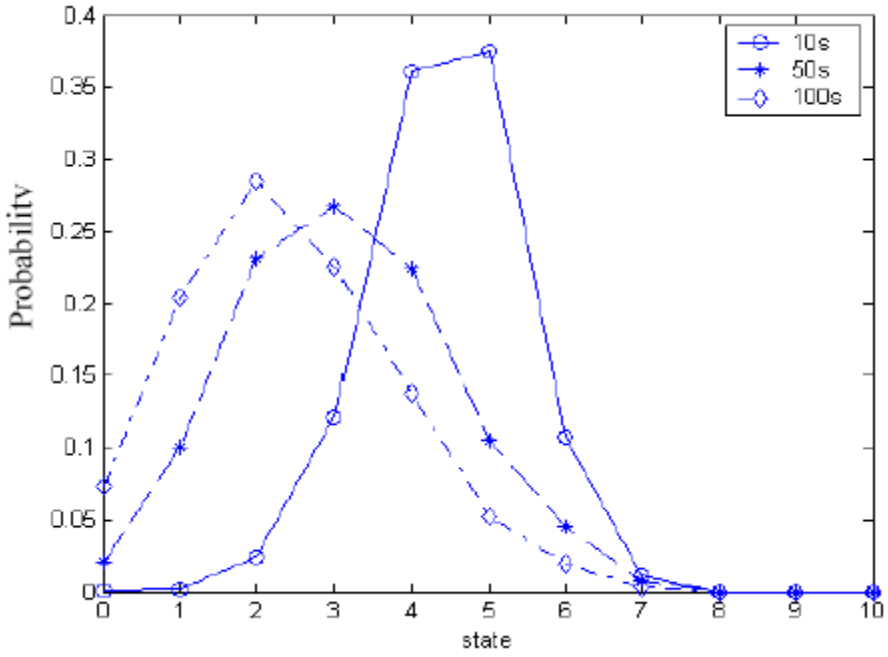

Figure 6.7. Prediction of the behavior of a C-T Markov chain.

According to the First-fit assignment in MBR, the probability that wavelength λ_k is free on link l at time $sT + \tau$, given i wavelengths are used at time sT, is computed by

$$P(\lambda_k \text{ free on } l) = \sum_{j=0}^{j=k} P(i,j), \tag{6.8}$$

where $P_{i,j}$ is defined in Equation 6.5.

Using the assumption that the usages of wavelengths on different links are independent, we can compute the probability that wavelength λ_k is free on a path Z (i.e.

λ_k is free on all links of Z) as

$$P(\lambda_k \text{ free on } Z) = \prod_{l \in Z} P(\lambda_k \text{ free on } l). \tag{6.9}$$

While the independence assumption is not completely valid in reality, we will use it as an approximation. When adaptive routing algorithms are used, the correlation of wavelength usage among links will decrease.

Detecting Interfering Connection Requests

When a connection request arrives at a node, other requests may have arrived at the node earlier, but the node still doesn't know their wavelength assignment decisions because it has not received the 'resv' messages from the destination nodes. We call these requests "ongoing requests". If these ongoing requests share one link with the current request, we call them "interfering requests". The *Interfering Set* of a connection request includes all interfering requests that the request will find when it is propagated from the source to the destination. Note that the *Interfering Set* of a request only includes requests arriving earlier than itself. Figure 6.8 illustrates request Q4 and its interfering requests Q1, Q2, and Q3.

A table (*Ongoing table*) is created at each node in the network. When a connection request arrives at a node, the node will store in the *Ongoing table* information about the connection request. A record of the *Ongoing table* includes the following fields: <source id, destination id, connection id, pri hop id, next hop id, time, guessed_wave>. Interfering connection requests are those which have the same 'pri

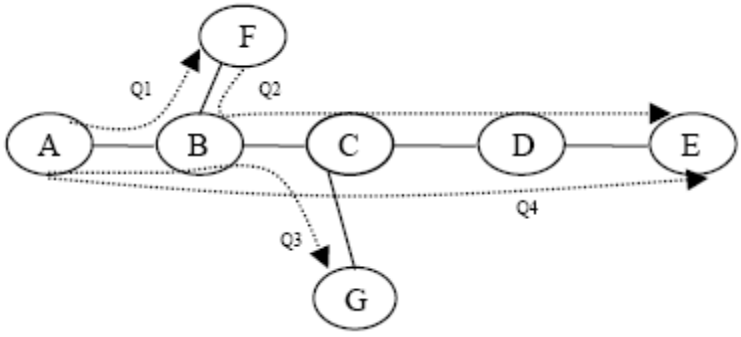

Figure 6.8. Example of interfering connection requests.

hop id' or 'next hop id' as the current request. By checking the *Ongoing table* in each node, a connection request will find all of its interfering connections. For example in Figure 6.8, Q4 will find that Q1 and Q3 are in its *Interfering Set* at node A, Q2 is in its *Interfering Set* at node B. We will explain the field 'guessed_wave' later.

A record in an *Ongoing table* will be deleted when a 'resv' message or a 'release' message upon failure is received. The duration of a record in an *Ongoing table* is bounded by the source-destination round-trip time.

Signaling Procedures of MBR

We explain the signaling procedures of MBR using Figure 6.8 and assume the connection requests arrive in the order of Q1, Q2, Q3, and Q4. When the 'probe' message of any connection request arrives at an intermediate node (node B, for example), the node first updates the 'wave_map' field in the message, marking wavelengths that are locked by this node as 'Busy'. Then it continues as follows.

If node B finds no interfering requests in its *Ongoing table*, for example when Q1 arrives, then for each free wavelength node B will compute the probability that it will be assigned for Q1. The wavelength with the largest probability of being assigned for Q1 is denoted as $\lambda_{most_probable_wave}$. Node B then creates a record about Q1 in the *Ongoing table*, setting the field 'guessed_wave' to $\lambda_{most_probable_wave}$. The 'probe' message is then sent to downstream nodes.

If node B finds interfering requests in the *Ongoing table*, for example when Q4 arrives, it will try to resolve the interference. It needs to update the 'probe' message considering interfering requests and guess which free wavelength will be most probably assigned for Q4. It updates the 'probe' message by marking the wavelengths which are guessed to be chosen by interfering requests (such information is stored in the field 'guessed_wave' of the *Ongoing table* records) as 'Guessed Busy'. Note that interference by competing requests, but with the same next hop, will be left to be handled by downstream nodes. It then guesses which wavelength will most probably be assigned for Q4. Before doing this, it first excludes all wavelengths which are guessed to be chosen by interfering requests. A record about Q4 will be created and stored in the *Ongoing table*, by setting the field 'guessed_wave' to $\lambda_{most_probable_wave}$. The updated 'probe' message will be propagated to downstream nodes.

The destination node will find three sets of wavelengths in the field 'wave_map' of the received 'probe' message: 'Free', 'Busy', and 'Guessed Busy'. The destination

node runs the First-fit algorithm on the set of 'Free' wavelengths. If no 'Free' wavelength exists, a 'release' message is sent upstream to the source node. Otherwise, a 'resv' message is sent.

Upon receiving the 'resv' message, an intermediate node will lock the wavelength chosen by the destination node and delete the record in the Ongoing table about this connection request. In the case of failure, the release procedure will be executed.

Numerical Simulation and Analysis

To evaluate this approach, we have run MBR on the NSF network and another mesh network, shown in Figure 6.9, using OPNET^{TM}. The NSF network has 16 nodes and 25 links with an average lightpath hop number of 3.27. The mesh network has 24 nodes and 43 links with an average lightpath hop number of 4.0. The benchmark algorithms include the backward reservation with First-fit wavelength assignment (FF), the backward reservation with Random wavelength assignment (RND), and the backward reservation with Full-flagging wavelength assignment (FFP) [92]. We choose these three algorithms because they are easy to implement and have comparatively good performance. We have not shown the FF algorithm in the figures below because of its much worse performance compared to RND and FFP. In our simulations, we assume no wavelength converters exist in the network. Workstations (i.e. traffic generation nodes) attached to switch nodes send out connection requests. The source node and destination node of a connection are chosen uniformly at random. The source node uses the shortest-path routing algorithm to select a

path. Each workstation introduces 1 Erlang of traffic to the network (with γ=1/80s, μ=80s). The traffic load is gradually increased by adding more workstations to the network. To make the comparison results more obvious, each destination node delays 2 seconds before sending a 'resv' message to simulate the signal propagation delay in practical networks. The *average load per link* metric of a network is defined as (total traffic load)*(average lightpath length in terms of hop number) / (total number of links in the network), in units of Erlang per link. This metric describes the degree of network congestion. To know to what extent the wavelength assignment guesses by intermediate nodes are actually correct, the *guess correctness probability* metric is defined, which counts the probability of correct guesses whose results are used in resolving conflictions, in other words the probability that $\lambda_{most_probable_wave}$ yields the wavelength chosen by a destination node.

The Poisson traffic and the Pareto traffic models are used in the simulations.

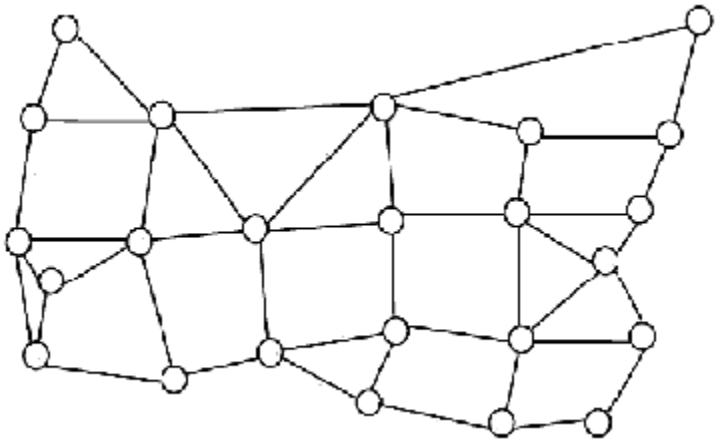

Figure 6.9. The mesh network topology studied in [9].

The Poisson Traffic Model. The inter-arrival time between connection requests and the connection duration are modeled using identical and independent (i.i.d) exponentially distributed random variables with mean 80 seconds.

The performance of different algorithms on the NSF network and the mesh network are compared in Figure 6.10. As the average load per link increases, MBR yields lower blocking probability compared to other algorithms. Algorithm FFP has been used with the optimal values for system parameters as specified in [92].

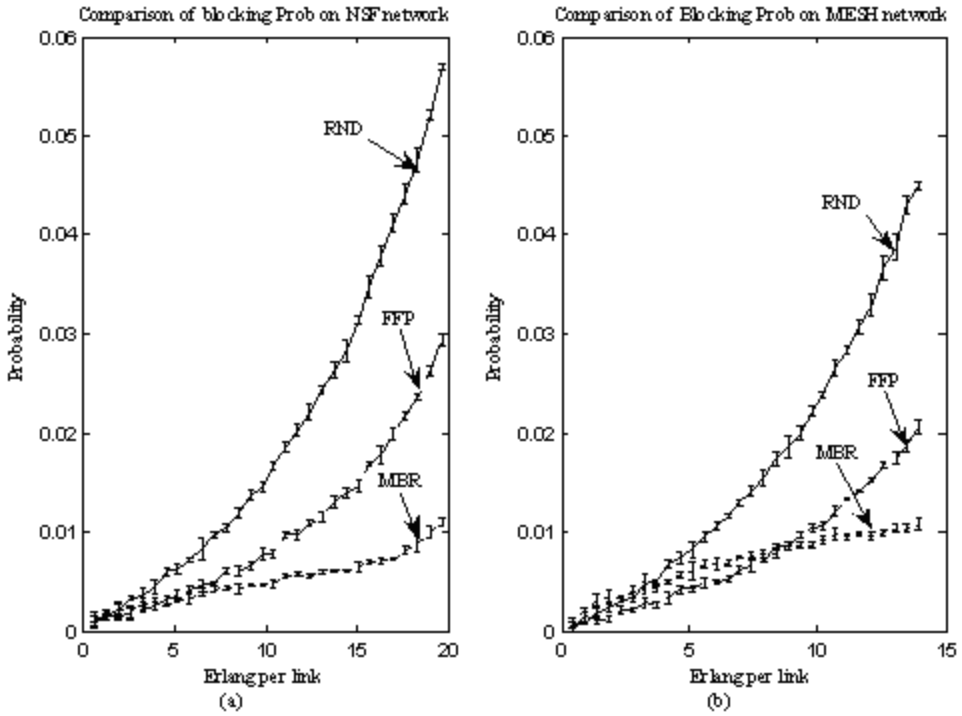

Figure 6.10. Comparison of MBR and benchmark algorithms on the NSF and mesh networks using the Poisson traffic model. Each fiber has 40 wavelengths in both networks. (a) shows the comparison on the NSF network and (b) shows the comparison on the mesh network. Each curve shows the average of several simulations. The short vertical lines represent the error bars. The figures below also use error bars.

The influence of network topology on MBR performance is investigated in Figure 6.11. We notice that the *guess correctness probability* on the NSF network is higher than on the mesh network. As a result, the probability of blocking on the NSF network is lower than on the mesh network for the same link traffic level. The performance of MBR depends on the *guess correctness probability* and the sizes of *Interfering Set*s. In general, networks with larger average lightpath hop number will result in lower *guess correctness probability* and bigger *Interfering Set*s. In this comparison, the mesh network offers the potential of longer source-destination paths (more hops per path) than the NSF topology, resulting in relatively lower performance for MBR.

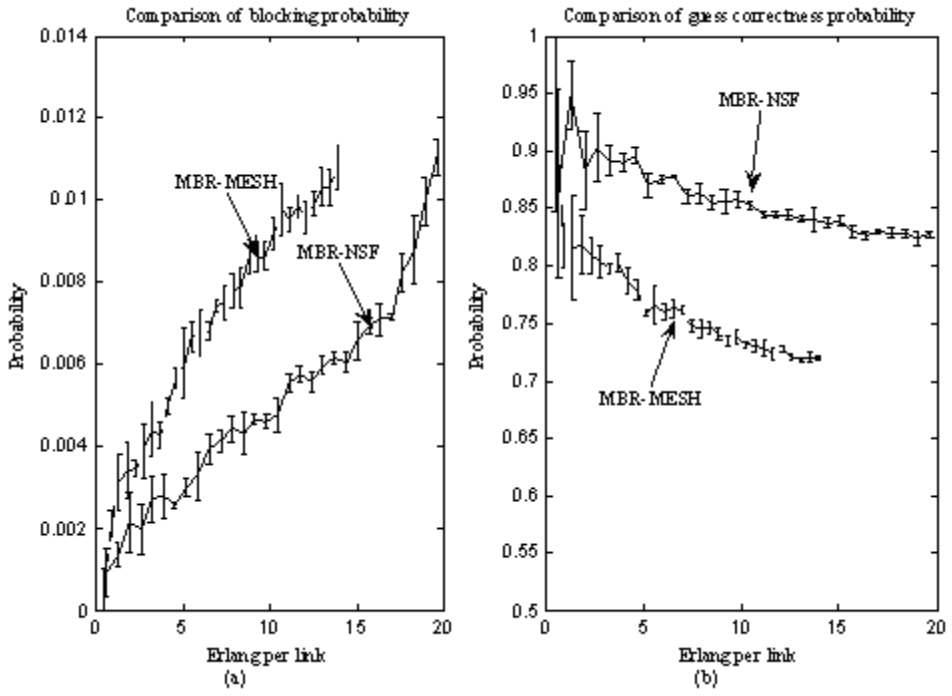

Figure 6.11. Comparison of the performance of MBR on the NSF and mesh networks (both have 40 wavelengths per fiber). (a) shows the comparison of blocking probability and (b) shows the comparison of *guess correctness probability*.

Figure 6.12 shows the influence of the number of wavelengths per fiber on MBR performance. We notice that as the number of wavelengths per fiber increases, the performance of MBR does not improve correspondingly. The sudden increase of blocking probability in MBRNSF-W20 shown in Figure 6.12(a) at a load of about 8 Erlangs per link is attributable to insufficient wavelengths, rather than to reservation confliction.

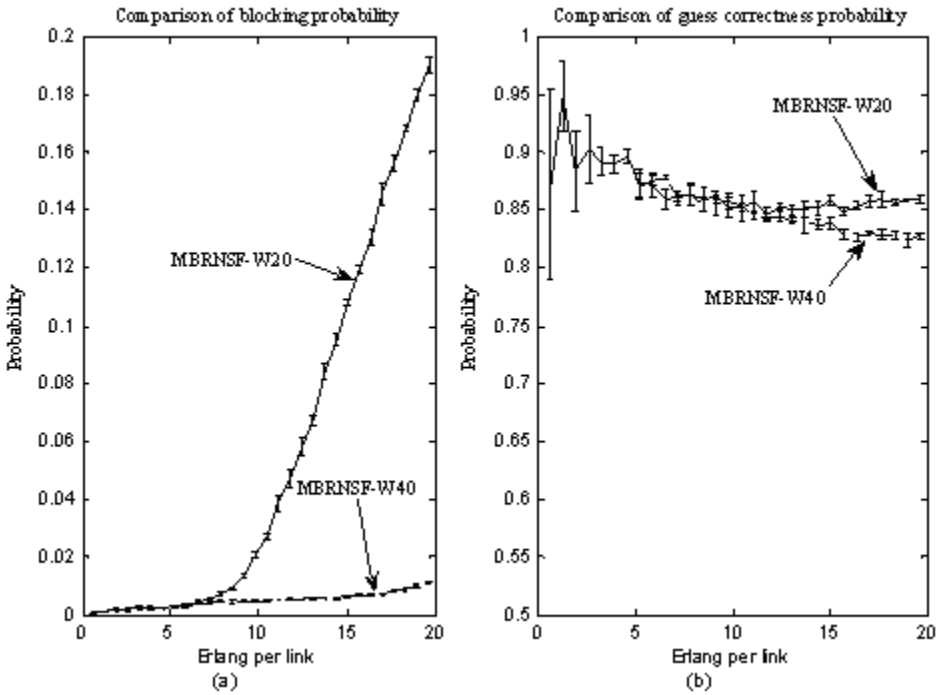

Figure 6.12. Comparison of the performance of MBR on the NSF network in two wavelength configurations (20/40 wavelengths per fiber). (a) shows the comparison of blocking probability and (b) shows the comparison of *guess correctness probability*.

It was noted earlier that at an arbitrary time between two network broadcast moments, a node will use C-T Markov chains to guess the free wavelength distribution on non-incident links. The chain parameter broadcast period T' may influence the

guess correctness probability of MBR. In a T' sensitivity experiment, we fixed the traffic load (about 20 Erlangs per link) on the NSF network with 40 wavelength per fiber and compared the blocking probability and *guess correctness probability* of MBR when varying T' from 500 to 20000 seconds. Using the same traffic load and configuration on the NSF network, in a T sensitivity experiment, we investigate the performance of MBR by varying T from 50 to 2000 seconds. The simulation results are shown in Table 6.1.

Table 6.1. Results of sensitivity experiments using the Poisson traffic model. Normalized standard deviation (normalized to the average value) is denoted by σ.

Experiment	Average Blocking Probability	σ of Blocking Probability	Average Guess Correctness Probability	σ of Guess Correctness Probability
T' sensitivity	1%	3.8%	82%	0.27%
T sensitivity	1%	3.57%	82%	0.43%

The Pareto Traffic Model. The inter-arrival time between connection requests and the connection duration are modeled using i.i.d. Pareto distributed random variables defined as

$$T = \left\lfloor \frac{T_0}{U^{\frac{1}{\alpha}}} \right\rfloor, \tag{6.10}$$

where T_0=10 and α=8/7, resulting in a mean of 80 seconds and an infinite variance.

The performance of different algorithms on the NSF network and the mesh network are compared in Figure 6.13.

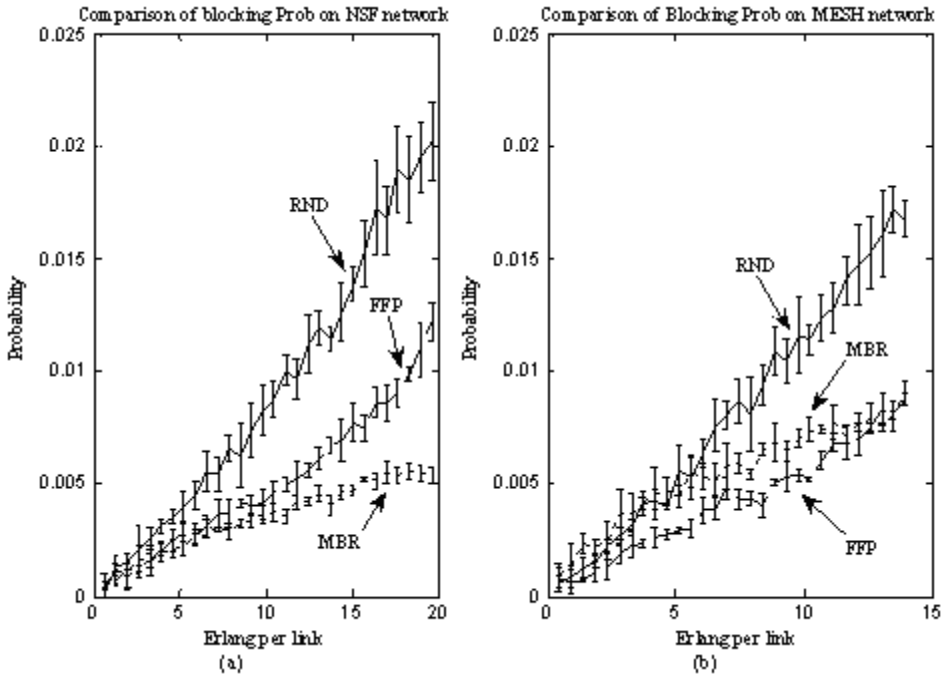

Figure 6.13. Comparison of MBR and benchmark algorithms on the NSF and mesh networks using the Pareto traffic model. Each fiber has 40 wavelengths in both networks. (a) shows the comparison on the NSF network and (b) shows the comparison on the mesh network.

The MBR algorithm still shows low sensitivity to the choice of T and T'. Using the same setting for sensitivity experiments on the NSF network as above except changing the traffic model to the Pareto model, the simulation results are shown in Table 6.2.

Table 6.2. Results of sensitivity experiments using the Pareto traffic model. Normalized standard deviation (normalized to the average value) is denoted by σ.

Experiment	Average Blocking Probability	σ of Blocking Probability	Average Guess Correctness Probability	σ of Guess Correctness Probability
T' sensitivity	0.6%	6.8%	84%	0.53%
T sensitivity	0.6%	6.86%	84%	0.58%

Discussion

From our simulations, we notice that MBR works best in a small-scale network. In such a network, the average hop number of a lightpath is small and the *guess correctness probability* is high. Backbone networks usually satisfy this topology condition. The performance of MBR will not improve as the number of wavelengths per fiber increases. This is a shortcoming of MBR compared to RND and FFP. However, if the number of wavelengths per fiber is relatively small or the number of free wavelengths is comparatively small although the total number of wavelengths per fiber is large, then the use of MBR to decrease reservation confliction is more effective than other algorithms that use random selection mechanisms such as RND and FFP.

We have examined the applicability of the MBR algorithm to networks where the traffic has Poisson characteristics or self-similar characteristics, without temporal or spatial variations. In both cases, the MBR algorithm has good performance. The network has lower probability of reservation confliction when the Pareto traffic model is used. The performance of MBR when the traffic pattern is dynamically changing requires further research. This would require a mechanism to detect when the traffic pattern has changed and a procedure to choose optimal values for the parameters T and T'.

We can use the following heuristics to further improve the performance of MBR.

(H1): In MBR, the size of the state space of each chain is $O(N)$. Notice that the states that a chain can visit during a monitoring period may be only a subset of the

whole state space. We can further decrease the size of the state space by constructing a chain including only those visited states.

(H2): Under the wavelength-continuity constraint, the free wavelength picked for a connection request according to First-fit is decided by links with high traffic load. Consequently, we only need to model these busy links using the Markov chain model.

(H3): Because Markov chains quickly converge to the steady state, we can use their steady state distributions or periodically (with period T") update the state distributions, rather than compute them each time when a connection request arrives. In a simulation on the NSF network topology with traffic load of 20 Erlangs per link, 40 wavelength per fiber, T=2000 seconds and using the Poisson traffic model, we vary the state-distribution update period T" from 50 to 2000 seconds with step interval of 50. The performance of MBR in 40 cases are compared to investigate the influence of T". The average blocking probability is 1% with normalized standard deviation of 3.58% and the average *guess correctness probability* is 81% with normalized standard deviation of 0.5%.

When we use Equation 6.5 to compute the state distribution, the computation requires $O(N^2K)$ time (N is the size of state space, K is the number of terms when computing the partial sum in the formula). Using H1, H2 and H3 can dramatically decrease the overhead of the MBR algorithm.

When the traffic load of a network increases such that the major reason of blocking is the lack of free wavelengths, the confliction resolving mechanism in MBR can be

disabled by setting the Markov chains to be in the state N with leaving rate 0 (i.e., all wavelengths are used). Then MBR is equivalent to the original backward reservation protocol.

QoS FRAMEWORK FOR All-OPTICAL NETWORKS

Introduction

Most RWA algorithms in the literature do not take into account physical impairments that can occur both in network components (e.g. optical switches, multiplexers, demultiplexers, optical amplifiers, etc.) and in optical fibers. In currently deployed commercial optical networks, optical signals may be regenerated at each repeating site. The influences of different physical impairments are eliminated in the regeneration process. As optical networking evolves towards all-optical networks where signals are not regenerated, consideration of QoS in RWA algorithm design becomes necessary and important. In an all-optical network, optical signals are transmitted from source to destination totally in the optical domain. Physical impairments will accumulate along a lightpath and can cause significant signal degradation. It is possible that the signal quality at the destination node is so poor that the bit error rate reaches an unacceptably high value.

In an all-optical network, a lightpath is set up through a cascade of independent fiber links. These links usually have different physical characteristics and thus different influences on signal quality. Moreover, the physical impairments on a lightpath also change with network state. For example, the influences of the nonlinear effects XPM and FWM are both dependent on the number of co-propagating channels and

the spacing between wavelengths of co-propagating channels and wavelength of the channel under consideration. To provide quality of service in an all-optical network, RWA algorithms need to intelligently pick lightpaths satisfying user QoS requirements under the constraints of network physical characteristics and network state.

State of the art QoS routing algorithms for optical networks typically consider two or three types of physical impairments and simplified analytical models are provided to estimate the end-to-end signal quality of a lightpath. In [9], the authors considered attenuation, noise generated by EDFAs and distributed Raman amplifiers (DRAs), and optical switch crosstalk. The proposed routing algorithm in [9] has a hierarchical structure: route computation in a network-layer module and lightpath verification in a physical-layer module. The route computation process is based on the shortest-path algorithm and no information about physical layer characteristics is used to improve the algorithm efficiency. In our view, this is a shortcoming of the algorithm. Fiber nonlinear effects are also not taken into account, which is considered to be important for future optical networks.

The route computation in [60] is similar to [9]. In verifying a lightpath, the authors have considered the nonlinear effects XPM and FWM. After photo-detection, the end-to-end signal quality is defined by the Q factor as [60]

$$Q = \frac{R * P_{s,m}}{\sigma_0 + \sigma_1}, \tag{7.1}$$

where R is the photo-detector responsivity, $P_{s,m}$ is the peak power of a signal channel, and

$$\sigma_0 = \sqrt{\sigma_{th}^2 + \sigma_{shot}^2 + \sigma_{spon-spon}^2}, \tag{7.2}$$

$$\sigma_1 = \sqrt{\sigma_{th}^2 + \sigma_{shot}^2 + \sigma_{sig-spon}^2 + \sigma_{spon-spon}^2 + \sigma_{XPM}^2 + \sigma_{FWM}^2}. \tag{7.3}$$

In Equation 7.1, the photo-current at the space state (when sending bit '0') is assumed to be 0. In Equations 7.2 and 7.3, σ_{th}^2 is the power of the thermal noise, σ_{shot}^2 is the power of the short noise, $\sigma_{sig-spon}^2$ is the power of the signal-ASE beating noise, $\sigma_{spon-spon}^2$ is the power of the ASE-ASE beating noise, σ_{XPM}^2 is the power of the noise generated by the XPM effect, and σ_{FWM}^2 is the power of the noise generated by the FWM effect. The authors have also considered the influence of a new lightpath on existing lightpaths. For a connection request, multiple lightpaths are serially tried. If the insertion of a candidate lightpath can cause existing lightpaths to incur performance outage, then it is discarded and another one is tried. The paper did not provide details of the routing algorithm itself and only considered links compensated using the FOCS scheme.

In [10], the formula $BER = \frac{1}{2}e^{-\eta OSNR}$ was used to compute the bit error rate based on $OSNR$, where η is a coefficient assuming values in the range [0, 1] dependent on photo-detector characteristics and $OSNR$ is the optical signal to noise ratio. The authors considered both linear impairment penalties and nonlinear impairment

penalties. The equation

$$OSNR_{eq,dB} = OSNR_{dB} - OSNR_{pen,l} - OSNR_{pen,nl}, \tag{7.4}$$

was used to compute the end-to-end $OSNR$ of a lightpath, where $OSNR_{dB}$ is the optical signal to noise ratio in units of dB at the detector when only ASE noise is considered, $OSNR_{pen,l}$ is the penalty due to linear impairments, and $OSNR_{pen,nl}$ is the penalty due to nonlinear impairments. For linear impairments, the authors used equations in [11][12] to compute the $OSNR$ penalties. For nonlinear impairments, the authors used a heuristic method to compute their $OSNR$ penalties. They performed a series of Monte-Carlo simulations using OptSim$^{\text{TM}}$. From the simulation results, they deduced an empirical function giving $OSNR_{pen,nl}$ from the knowledge of fiber properties, the number of wavelengths in use, the length of the fiber, and the transmitted power. For each connection request, the proposed routing algorithm first constructs a set $\prod(s,d)$ of candidate lightpaths. The $OSNR$s of all lightpaths in $\prod(s,d)$ are larger than a threshold $OSNR_{min} = 20dB$, when only attenuation and linear impairments are considered. The algorithm then selects one lightpath that satisfies $Max_{\pi \in \prod(s,d),\lambda}\{OSNR(\pi,\lambda)\}$ by further considering nonlinear impairments. The algorithm in [10] is too complex to be implemented as an in-line routing algorithm.

We propose a new framework for QoS routing in all-optical networks. As in [9][60], the framework also has two steps: route computation and lightpath probing to verify signal quality and reserve resources for a connection. Physical impairments are taken into account at the route computation step to improve algorithm efficiency. In the

discussion of this chapter, we consider physical impairments including attenuation, dispersion, ASE noise, and the nonlinear effects XPM and FWM. The proposed algorithms are scalable and flexible due to the assumption that the noises generated by different impairments are independent and the total noise power is the sum of the noise powers generated by individual impairments as in Equations 7.2 and 7.3.

In this chapter, the network model of all-optical networks is explained first. Then the new Physically Aware Routing algorithm (PAR) and the new Physically Aware Backward Reservation protocol (PABR) is discussed in detail, including the route computation step and how to estimate the end-to-end signal quality of a lightpath. The proposed QoS framework can support both single-probing and multi-probing. In multi-probing, multiple candidate paths are probed in parallel to find one satisfying the user QoS requirement, resulting in decreased connection blocking probability but with increased signaling overhead. We also consider and provide new functions in the reservation protocol to preserve the signal quality of a lightpath. This is important for networks with dynamic traffic, where the establishment and release of a lightpath can influence other lightpaths through inter-channel effects (e.g. XPM and FWM). At last, the numerical simulation results in different network topologies and configurations are presented and analyzed.

Network Model

The network under study is an all-optical network, which consists of multiple switch nodes connected by optical links in an arbitrary topology. Because the proposed algorithms need to consider physical characteristics of the network, including fiber properties which are different for the link A→B and the link B→A, the network is represented as a directional graph $G = (V, E)$ with V the set of switch nodes in the network and E the set of optical links between adjacent switch nodes. An optical link consists of several periodically amplified spans. EDFAs are assumed to be used as in-line amplifiers to provide signal amplification. Each link can be compensated using either the FOCS scheme or the DUCS scheme[a], with the link residual dispersion equal to 0. For simplicity, it is assumed that the network is a single-fiber network. In this case, the single edge A→B connecting nodes A and B in the topology graph is actually a cascade of different fibers. There are N wavelengths $(\lambda_0, \cdots, \lambda_{N-1})$ on each fiber for signal transmission. The knowledge of network topology and link ASE noises, which are both fixed and independent of the network state, is stored in all edge nodes of a network for route computation. For the link A→B, we call A the *controlling node*. The physical characteristics of an optical link, including the lumped ASE noise power of amplifiers on the link and properties of its constituent fibers

[a]Refer to Chapter 3 for the definitions of FOCS and DUCS.

(D, S, β_2, β_3), are stored in the controlling node for lightpath verification. Distributing the information about network physical characteristics among nodes in a network makes our design more flexible and scalable.

Every T seconds, the wavelength-usage information of each link is broadcast by its controlling node. Only the number of used wavelength, instead of the state of each wavelength, is broadcast to decrease signaling overhead.

Optical workstations attached to edge switch nodes send out connection requests randomly and independently according to a stochastic process. The edge node executes the routing algorithm to find a path for a connection request from the source to the destination. Then the source node starts the backward reservation protocol by sending out 'probe' messages. The 'probe' message has fields: <source id, destination id, connection id, total probes, sequence id, path_info, wave_map, physical links, co-propagating set>, where 'source id' and 'destination id' are the indices of the source node and the destination node of a connection request respectively, 'connection id' is the id given to the connection request by the source node, 'total probes' is the total number of 'probe' messages sent out for the connection request, 'sequence id' is the id given to the 'probe' message in case multi-probing is used in the reservation protocol, 'path_info' is the ordered list of nodes on the selected path, 'wave_map' is an array indicating the availability/unavailability of each wavelength, 'physical links' is an array recording the physical characteristics of constituent links of a probed path, and 'co-propagating set' is a two-dimensional matrix with each column recording ids

of connections occupying the wavelengths on a constituent link of the probed path. After choosing a lightpath for a connection request, the destination node sends a 'resv' message upstream. The 'resv' message has fields: <connection id, selected wavelength>. If connection request fails (e.g. no free wavelength on the path), a 'release' message is sent upstream.

There are two databases on each network node. The *Established connections* database is used to store information of already established connections in a switch node. Each record in the *Established connections* database has fields: < connection id, link id, wave id>, where 'connection id' is the id of the stored connection, 'link id' is the index of the output link used by the connection, and 'wave id' is the index of the wavelength on the output link which are used by the connection. The *ongoing table* database is used to store ongoing connection requests. Each record in the *ongoing table* database has fields: <connection id, competition time, total probes, sent responses, sequences, sequence size, winning id >, where 'connection id' is the id of a connection request, 'competition time' is a time stamp generated by the destination node upon receiving the first 'probe' message, 'total probes' is the total number of 'probe' messages sent out for the connection request, 'sent responses' is the number of responses (to the 'probe' message) already sent upstream to the source node, 'sequences' is an array recording sequence id of all 'probe' messages which will join the competition (denoted as *lightpath competition*) of being chosen as the lightpath for a connection request, 'sequence size' is the size of the array 'sequences',

and 'wining id' is the sequence id of the 'probe' message which have won the lightpath competition.

QoS Framework for All-Optical Networks

The proposed QoS framework has two parts: the Physically Aware Routing algorithm (PAR) and the Physically Aware Backward Reservation protocol (PABR). The PAR algorithm takes physical impairments into account when computing a path for a connection request. This greatly improves the algorithm efficiency compared to [9][60].

The route computation engine of PAR returns a set of candidate paths which are very likely to satisfy the user QoS requirement. In case of single-probing, only one path is returned. After obtaining candidate paths from the routing algorithm, an edge node starts the PABR protocol. When the 'probe' message is propagated along the computed path from the source node to the destination node, each intermediate node records which wavelengths have already been used in the 'probe' message and checks whether the establishment of this lightpath will cause unacceptable signal degradation to existing lightpaths. If so, this path is discarded and the connection request is also rejected in the case of single-probing. The intermediate nodes also record in the 'probe' message ids of co-propagating lightpaths and the physical characteristics of constituent links of the path. For each received 'probe' message, the destination node

picks one free wavelength which satisfies the user QoS requirement by the Quality-first-fit algorithm and puts the lightpath in a candidate set. After waiting a short period, the destination node randomly chooses one lightpath from the candidate set and sends a 'resv' message upstream. All the other candidate lightpaths are rejected with the reason 'Already_created'. Each part of the framework is explained in more detail in the following.

Physically Aware Routing Algorithm (PAR)

Link Cost Function. We have adapted the LORA algorithm discussed in Chapter 6 for QoS routing in all-optical networks. As in LORA, the cost function of a link l is defined as

$$cost(l) = \beta^{usage(l)}, \tag{7.5}$$

where β is a parameter that needs to be dynamically adjusted according to traffic load, and $usage(l)$ is the number of used wavelengths on link l. The behavior of β as a function of traffic load is obtained using the hill-climbing algorithm. Notice that no physical impairments are considered in the hill-climbing algorithm.

Pruning the Search Space. The PAR algorithm considers physical impairments. For the current and the near-future next-generation optical networks, ASE noise is the dominant physical impairment, which was verified in our numerical simulations

using network configurations of current state of the art optical transmission systems. In our implementation of PAR, only ASE noise is considered.

The objective and constraint of PAR can be formulized as

$$\begin{aligned} Objective: minimize(\sum_{l \in \text{path } P} \beta^{usage(l)}) \\ Constriant: \sum_{l \in \text{path} P} ASE(l) < threshold, \end{aligned} \tag{7.6}$$

where $ASE(l)$ is the lumped ASE noise power on link l and the parameter *threshold* is determined from the QoS requirement of a connection request.

The idea of PAR is explained using Algorithm 7.1.

Algorithm 7.1 Compute a path from S to D using PAR

```
1: while H is not empty do
2:    P=FirstElement(H);
3:    if P==D then
4:       if number of path in the result buffer < required number then
5:          put the path from S to D in the result buffer;
6:       else
7:          return result buffer
8:       end if
9:    else
10:      for each adjacent node a_i of P do
11:         if a_i ∉ S→P && ASE(S→ a_i)< threshold then
12:            a_i.parent = P;
13:            a_i.cost =P.cost+β^{usage(P->a_i)};
14:            insert a_i into H; {H is sorted in the increasing order of the field 'cost'}
15:         end if
16:      end for
17:   end if
18: end while
```

In Algorithm 7.1, nodes in the queue $\mathcal{H}$ are expanded in increasing order of the node cost value, which is defined as the objective value of the partial path from S to

the node. The path from S to D with the minimal objective value is returned first. The pruning operation in Algorithm 7.1 is used to guarantee that only the paths satisfying the constraint are returned. Notice that the idea in Algorithm 7.1 is rather general and can still be used even when ASE noise is not the dominant effect provided that edge nodes know the network state and how to do the pruning operation (e.g. when nonlinear effects like XPM and FWM dominate). The pruning technique can also work with other routing algorithms in the literature to provide QoS assurance.

Physically Aware Backward Reservation Protocol (PABR)

Signaling Procedures of PABR. Once the edge node computes a set of candidate paths for a connection request, it sends out several 'probe' messages to explore these paths and verify their signal qualities. Assuming the size of the set is n, the field 'sequence id' of these 'probe' messages will be set to 0, 1, 2, $\cdots$, $n-1$ respectively and the field 'total probes' will be set to n. When an intermediate node receives a 'probe' message, it first marks the used wavelengths on the chosen output link as 'Busy' in the 'probe' message field 'wave_map' and record identities of all connections which occupy wavelengths on the output link in the 'probe' message field 'co-propagating set'. Properties of the output link are also stored in the 'probe' message field 'physical links'.

Algorithm 7.2 is used for recording connection identities in the 'probe' message.

Algorithm 7.2 Recording connection ids in the 'probe' message at an intermediate node *Inode*

```
1: Find the column id k of the matrix probe.'co-propagating set' corresponding to
   the link from Inode to the downstream node Jnode;
2: for wave = 0 to N − 1 do
3:    if probe.'wave_map'[wave] is occupied then
4:       probe.'co-propagating set'[wave][k] = id of the connection which uses the
         wavelength wave on the link from Inode to Jnode;
5:    else
6:       probe.'co-propagating set'[wave][k] = -1;
7:    end if
8: end for
```

When a destination node receives a 'probe' message, it follows a procedure dependent on whether single-probing or multi-probing is used (this can be detected by checking the 'probe' message field 'total probes').

If single-probing is used, the node first checks whether there is a free wavelength in the field 'wave_map' of the received 'probe' message. If no free wavelength is available, the connection request is rejected, and a 'release' message is sent upstream with reason 'None_resource'. Else, it runs Algorithm 7.3 to pick a free wavelength that has satisfactory signal quality and a 'resv' message is then sent upstream.

Algorithm 7.3 Quality-first-fit

```
1: for wave = 0 to N − 1 do
2:    if probe.'wave_map'[wave]==free then
3:       Q= estimate signal quality of the wavelength wave on the probed path;
4:       if Q > threshold then
5:          return wave;
6:       end if
7:    end if
8: end for
```

The method for estimating signal quality of a wavelength on the probed path is explained in more detail in the following section.

For handling multi-probing, upon receiving the first 'probe' message, the node creates a record in the *ongoing table* to store information of a connection request. The field 'competition time' is set to the arriving time of the first 'probe' message + $local_call_delay$, where $local_call_delay$ is a system parameter.

For probed paths with a satisfactory free wavelength (determined by executing the Quality-first-fit algorithm), the sequence id of the 'probe' message is stored in the field 'sequences' of the *ongoing table* record, and denoted as the *candidate lightpaths*. For each candidate lightpath, a timer is set up, so that it can be considered for being selected as the lightpath for the connection request (the lightpath competition) when the timer expires. All other failed 'probe' messages are rejected immediately. The details are provided in Algorithm 7.4.

Algorithm 7.4 Operation of the destination node upon receiving a 'probe' message (multi-probing)

```
1: wave_dec = Quality_first_fit(probe.'wave_map');
2: current_time = retrieve system clock;
3: search ongoing table whether a record of this connection request exist;
4: if exist then
5:    rec = retrieve record from the ongoing table;
6:    if current_time>rec.'competition time' || wave_dec == -1 then
7:       rec.'sent responses'++;
8:    else
9:       record probe.'sequence id' into rec.'sequences';
10:   end if
11:   if rec.'sent responses' == rec.'total probs' then
12:      delete rec from the ongoing table;
13:   else
14:      update rec in the ongoing table;
15:   end if
16: else
17:   rec = create a empty ongoing table record;
18:   rec.'competition time'= current_time+local_call_delay;
19:   rec.'total probes'= probe.'total probes';
20:   rec.'sent responses'= 0;
21:   rec.'sequences'= empty array;
22:   rec.'sequence size'= 0;
23:   rec.'wining id'= -1;
24:   if wave_dec == -1 then
25:      rec.'sent responses'++;
26:   else
27:      record probe.'sequence id' into rec.'sequences';
28:   end if
29:   if rec.'sent respones'<rec.'total probes' then
30:      store rec in the ongoing table;
31:   end if
32: end if
33: if current_time>rec.'competition time'||wave_dec== -1 then
34:   reject this 'probe' message immediately;
35: else
36:   set a timer timer_competition for this 'probe' message with the timeout time=
      rec.'competition time';
37: end if
```

At the moment of rec.'competition time', a decision is made to determine which 'probe' message wins the lightpath competition by randomly selecting one 'probe' message from the field 'sequences' of the *ongoing table* record. Algorithm 7.5 shows details of the destination node operation when the timer *timer_competition* set for a 'probe' message expires.

Algorithm 7.5 Operation of the destination node upon expiration of *timer_competition*

```
1: rec = retrieve the ongoing table record of this connection request;
2: if rec.'winning id'== -1 then
3:    rec.'wining id'= randomly pick a wining sequence id from the array
      rec.'squences';
4: end if
5: rec.'sent responses'++;
6: if rec.'sent response' == rec.'total probes' then
7:    delete rec from the ongoing table;
8: else
9:    update rec in the ongoing table;
10: end if
11: if probe.'sequenc id' == rec.'wining id' then
12:    send a 'resv' message upstream;
13: else
14:    reject this 'probe' message with reason 'Already_created';
15: end if
```

We notice in Algorithm 7.4 and Algorithm 7.5 that a record in the *ongoing table* will be deleted when the values of the fields 'total probes' and 'sent responses' are equal. This simple mechanism has a potential problem in that some records can become "ghost records" and will stay in the database forever if no extra operation is executed. To prevent this, an *ongoing table* database reclaims its oldest record when receiving a store request and finds that the database is full.

Estimation of Lightpath Signal Quality. The destination node estimates the signal quality of a lightpath (including a path and a given free wavelength) based on the information recorded in the fields 'co-propagating set' and 'physical links' of a received 'probe' message. In our research, only noise generated by spontaneous emission, XPM, and FWM are considered because they have more significant influence on signal quality compared to other effects. We estimate the signal quality after photo-detection (assuming a *pin* detector). At the mark state, the dominant noise power includes $\sigma^2_{sig-spon}$ (i.e. $\sigma^2_{sig-ase}$), σ^2_{xpm}, and $\sigma^2_{sig-fwm}$, and the total noise power $\sigma_1^2 = \sigma^2_{sig-spon} + \sigma^2_{xpm} + \sigma^2_{sig-fwm}$. Because $\sigma_1 >> \sigma_0$ and $I_1 >> I_0$, the Q factor given in Equation 7.1 is approximated as

$$Q = 10 \log (\frac{I_1}{\sigma_1}). \tag{7.7}$$

At the end of a lightpath and before photo-detection, the total ASE noise is given by

$$\sigma^2_{\text{lightpath } P,ase} = \sum_{l \in P} \sigma^2_{l,ase}, \tag{7.8}$$

where $\sigma^2_{l,ase}$ is the lumped noise power generated by amplifiers on a periodically amplified optical link l and the noise power generated by a single EDFA is given by

$$\sigma^2_{ase} = F_n h f_c (G-1) B_w, \tag{7.9}$$

where F_n is the noise figure of an EDFA ($F_n = 2n_{sp}$ for ideal EDFAs), h is Planck's constant, f_c is the carrier frequency of a lightpath under consideration, G is the optical gain, and B_w is the optical bandwidth of the signal channel.

After photo-detection, there exists a noise term due to the beating of the signal channel and the ASE noise. This noise term has power defined as

$$\sigma^2_{lightpath,sig-ase} = 2P_{ch}\sigma^2_{lightpah,ase}, \tag{7.10}$$

where P_{ch} is the peak power of a signal channel.

To compute the noise power generated by the XPM effect, for each possible co-propagating wavelength the lightpath is divided into a series of coherent segments. The powers of the XPM noise before photo-detection and after photo-detection are equal and are the sum of component powers generated in all coherent segments. Details are provided in Algorithm 7.6.

Algorithm 7.6 Computing XPM noise of a lightpath after photo-detection

```
1: xpm_noise = 0;
2: probed_wave = wavelength chosen by the lightpath;
3: for wave = 0 to N − 1 do
4:    if wave != probed_wave then
5:       scan the row probe.'co-propagating set'[wave] and divide the lightpath into
         coherent segments according to the wavelength wave;
6:       for each coherent segment cs do
7:          if cs is used by a co-propagating lightpath then
8:             segment_noise = noise generated by cs at the end of the lightpath;
9:          else
10:            segment_noise = 0;
11:         end if
12:         xpm_noise += segment_noise;
13:      end for
14:   end if
15: end for
```

To compute the noise power generated by the FWM effect, for each possible FWM mixing term which can generate FWM noise on a lightpath, the lightpath is divided

into a series of coherent segments. Algorithm 7.7 provides details of computing FWM noise at the end of a lightpath and before photo-detection.

Algorithm 7.7 Computing FWM noise of a lightpath before photo-detection

```
1: fwm_noise = 0;
2: for each possible FWM mixing term mix do
3:    i = wavelength index of the pump λ_i of mix;
4:    j = wavelength index of the pump λ_j of mix;
5:    k = wavelength index of the pump λ_k of mix;
6:    scan the rows i, j, k of prob.'co-propagating set' and divide the lightpath into
      coherent segments;
7:    for each coherent segment cs do
8:       if cs is used by three co-propagating lightpaths then
9:          segment_noise = noise generated by cs at the end of the lightpath;
10:      else
11:         segment_noise = 0;
12:      end if
13:      fwm_noise += segment_noise;
14:   end for
15: end for
```

In Algorithm 7.7, a coherent segment is defined by three pump channels [i,j,k]. For a coherent segment, three co-propagating lightpaths use the wavelength i, j, and k respectively. Appendix C provides Matlab code to count all the possible FWM mixing terms which can generate noise on a lightpath.

We denote the noise power returned by Algorithm 7.7 as $\sigma^2_{lightpah,fwm}$. After photo-detection, there exists a noise term due to the beating of the signal and the FWM noise generated on this channel. The noise term has power defined as [52]

$$\sigma^2_{lightpath,sig-fwm} = 2P_{ch}\sigma^2_{lightpah,fwm}. \tag{7.11}$$

To improve algorithm efficiency, a system parameter *nonlinear_window* is defined. For a given lightpath with wavelength index f_{id}, only wavelengths with indices in the range $[f_{id} - \frac{nonlinear_window}{2}, f_{id} + \frac{nonlinear_window}{2}]$ are considered when computing noise power generated by nonlinear effects.

Preserve Lightpath Signal Quality. Preserving lightpath signal quality is important for an optical network with dynamic traffic. The establishment of a new lightpath and the release of an existing lightpath both can influence the signal qualities of other lightpaths through inter-channel effects (e.g. XPM and FWM). In [60], the author mentioned the idea of preserving lightpath signal quality without providing an efficient algorithm. In our research, only the dominant nonlinear effects XPM and FWM are considered and we notice that under the assumption that each optical link has zero residual dispersion, preserving lightpath signal quality can be efficiently achieved.

Figure 7.1 shows an example where the establishment of *ligthatph3* can increase the XPM noise and the FWM noise generated on *lightpath1* and *lightpath2*. On the coherent segment B→C, the XPM transfer function of the wavelength λ_3 (the pump channel λ_k in the 'probe and pump' approach) on another wavelength (the probe channel λ_c in the 'probe and pump' approach), e.g. λ_1 or λ_2 in Figure 7.1, is given

by small changes to Equation 4.23 as

$$\begin{aligned} H(w) =& \sum_{n=1}^{N} \int_{z=0}^{z=L} cos(D_B + Q_n^k + q_n z) e^{-\alpha_n z} e^{-jwzd_{ck,n}} e^{-jwD_n^k \triangle\lambda_{ck}} e^{-jw\triangle T_B} * \\ & 4\gamma\overline{P_c(0,T)} e^{-\alpha_n z} sin[C - Q_n^c - b_n z + D_c] e^{-\alpha_n (L-z)} e^{\alpha_n L} dz \\ =& e^{-jw\triangle T_B} \sum_{n=1}^{N} \int_{z=0}^{z=L} cos(D_B + Q_n^k + q_n z) e^{-\alpha_n z} e^{-jwzd_{ck,n}} e^{-jwD_n^k \triangle\lambda_{ck}} * \\ & 4\gamma\overline{P_c(0,T)} e^{-\alpha_n z} sin[C - Q_n^c - b_n z + D_c] e^{-\alpha_n (L-z)} e^{\alpha_n L} dz, \end{aligned} \tag{7.12}$$

where D_B is the accumulated phase-lag from the source of *lightpath3* to node B, $\triangle T_B$ is the difference between the delay from the source of the probe lightpath to node B and the delay from the source of *lighpath*3 to node B, D_c is the accumulated phase-lag from node C to the end of the probe lightpath, and other terms are consistent with those in Equation 4.23.

Under the assumption that each link has zero residual dispersion, Equation 7.12 can be simplified as

$$\begin{aligned} H(w) =& \sum_{n=1}^{N} \int_{z=0}^{z=L} cos(Q_n^k + q_n z) e^{-\alpha_n z} e^{-jwzd_{ck,n}} e^{-jwD_n^k \triangle\lambda_{ck}} e^{-jw\triangle T_B} * \\ & 4\gamma\overline{P_c(0,T)} e^{-\alpha_n z} sin[-Q_n^c - b_n z] e^{-\alpha_n (L-z)} e^{\alpha_n L} dz \\ =& e^{-jw\triangle T_B} \sum_{n=1}^{N} \int_{z=0}^{z=L} cos(Q_n^k + q_n z) e^{-\alpha_n z} e^{-jwzd_{ck,n}} e^{-jwD_n^k \triangle\lambda_{ck}} * \\ & 4\gamma\overline{P_c(0,T)} e^{-\alpha_n z} sin[-Q_n^c - b_n z] e^{-\alpha_n (L-z)} e^{\alpha_n L} dz. \end{aligned} \tag{7.13}$$

At node C, we can use Equation 4.19 to compute the noise components contributed by *lightpath3* on the coherent segment B→C on other co-propagating lightpaths (e.g. *lightpath1* and *lightpath2* in Figure 7.1), with information about link

physical characteristics and co-propagating lightpaths stored in the 'probe' message, and

$$|H(w)|^2 = |\sum_{n=1}^{N} \int_{z=0}^{z=L} cos(Q_n^k + q_n z) e^{-\alpha_n z} e^{-jwzd_{ck,n}} e^{-jwD_n^k \triangle \lambda_{ck}} * 4\gamma \overline{P_c(0,T)} e^{-\alpha_n z} sin[-Q_n^c - b_n z] e^{-\alpha_n (L-z)} e^{\alpha_n L} dz|^2. \quad (7.14)$$

Notice the terms in Equation 7.14 are only related to the fiber properties of the link B→C. We can also predict the noises at node C contributed by FWM mixing terms involving *lightpath3* on *lightpath1* and *lightpath2* using the analytical models developed in Chapter 4. The FWM analytical models only require information about the link B→C.

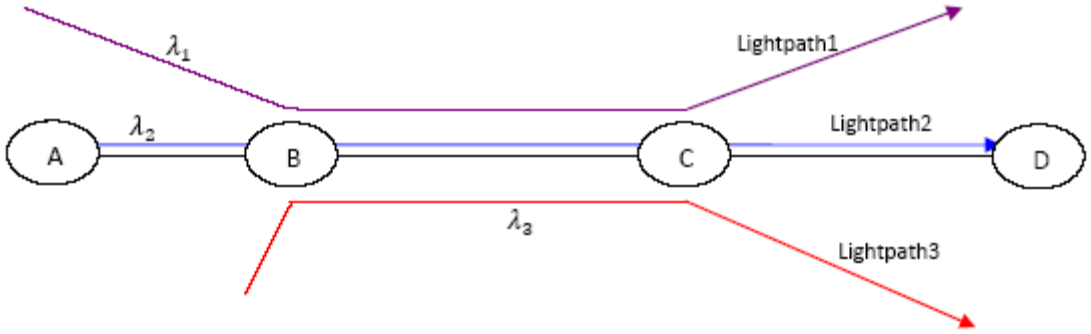

Figure 7.1. Lightpath3 and co-propagating lightpaths.

To preserve the signal quality of a lightpath, a record of the end-to-end noise power and the threshold Q value for the lightpath can be stored in the *established connections* database of each node along the lightpath. When an intermediate switch node receives a 'probe' message, it estimates the influence of a new lightpath (a path + a free wavelength) on existing lightpaths using Algorithm 7.8. Because the intermediate

node doesn't know which wavelength will be chosen for the new connection request by its destination node, it needs to execute Algorithm 7.8 for each possible lightpath by scanning all the free wavelengths. If all the possible lightpath are rejected by Algorithm 7.8, then the 'probe' message is also rejected.

Algorithm 7.8 Estimate the influence of a new Lightpath on existing Lightpaths

1: λ = wavelength of the new lightpath N_p;
2: **for** each existing co-propagating lightpath P **do**
3: new_noise = additional XPM and FWM noise powers introduced by N_p;
4: **if** new_noise + end-to-end-noise-power(P) > threshold for noise power **then**
5: reject N_p and mark λ as 'Busy' in the 'probe' message;
6: **end if**
7: **end for**

When a connection is released, it may decrease the noise powers on other lightpaths. The end-to-end noise powers of these lightpaths should be updated to allow the acceptance of more connection requests. To simplify the algorithm design, we use a delayed update strategy. At the moment of connection release, no update is executed. Instead, the source node of each existing connection periodically sends out 'update' messages to update the information (e.g. the end-to-end noise power) stored on nodes along the lightpath.

Numerical Simulation and Analysis

We use OPNET^{TM} simulations to study the performance of the proposed QoS framework. Because OPNET^{TM} is a network layer simulator, the physical characteristics of a simulated network are provided in an XML configuration file. When a

simulation starts, the physical layer information is loaded into memory and used by the OPNET^{TM} modules developed to implement the PAR and PABR algorithms.

For simplicity, all optical spans in the network are assumed to have the same structure, shown in Figure 7.2, and compensated using the FOCS scheme. The number of spans in an optical link is configurable and specified in the XML configuration file. Parameters specifying physical characteristics of a span is summarized in Table 7.1.

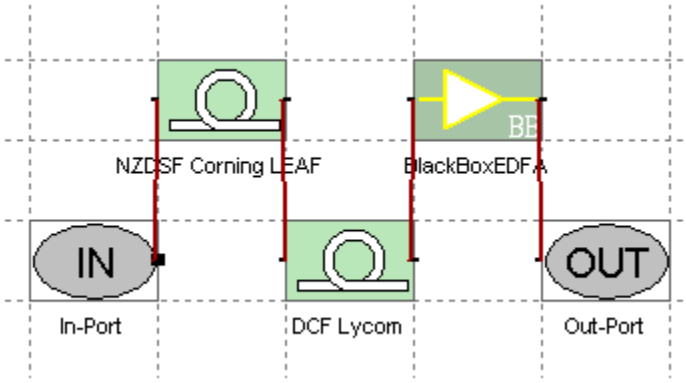

Figure 7.2. Structure of an optical span.

Table 7.1. Physical characteristics of an optical span.

NZDSF parameters		DCF parameters		EDFA parameters	
Mode:	nonlinear	Mode:	linear	NF:	configurable
Alpha:	0.25dB/Km	Alpha:	0.5db/Km	Gain:	21.6dB
D:	4ps/(Km*nm)	D:	-100ps/(Km*nm)		
S:	0.08ps/(km*nm2)	S:	0		
f_0 :	193.1THz	f_0 :	193.1THz		
Length:	80km	Length:	3.2Km		
Gamma:	2/(Km*W)	Gamma:	0		

In the optical span as shown in Figure 7.2, we have considered the nonlinear effects XPM and FWM in the NZDSF transmission fiber, while the DCF fiber is assumed to be linear due to the fact that the generated nonlinear effects are negligible in the DCF fiber.

We further assume that there are 2N+1 wavelengths ($\lambda_0, \cdots, \lambda_{2N}$) with frequency step f_{step} =50GHz on each fiber of the network, with the center frequency f_c = f_N=193.1THz. The peak power of a signal channel is specified by the parameter *channel_power*. Inside a photo-detector, the optical filter has bandwidth B_0 and the electrical filter has bandwidth B_e. For simplicity, the photo-detector responsivity R is set to 1. The nonlinear window used to improve efficiency is specified by the parameter *nonlinear_win*. These related simulation parameters are summarized in Table 7.2.

Table 7.2. PABR simulation parameters.

Parameters		Parameters	
f_c:	193.1THz	R:	1
f_{step}:	50GHz	*nonlinear_win*:	10
B_o:	20GHz	*channel_power*:	1mW
B_e:	10GHz	TH_Q:	configurable
N:	configurable		

The values listed in Table 7.1 and Table 7.2 are used throughout the simulations described in this chapter. The parameter N used in defining number of wavelengths per fiber is varied to achieve different network configurations. The Q factor threshold TH_Q for a simulation is set to be slightly smaller than the Q factor of a lightpath

created on the diameter of the topology graph with edge distance equal to the number of deployed EDFAs on the corresponding link (denoted as *EDFA diameter* later) and when only ASE noise is considered.

Workstations attached to switch nodes send out connection requests randomly and independently according to the Poisson process, with request inter-arrival time of 150 seconds, and average connection duration time of 150 seconds. In our simulations, two network topologies, the NSF network and a mesh network, are considered. The benchmark algorithms include the backward reservation with shortest-path (SP), the backward reservation with lexicographically optimized path (LORA), and the backward reservation with Least-EDFA path (not shown in the following figures due to its poor performance compared to other algorithms). In the simulations, only single-probing is used in PABR. Algorithms proposed in [9][60] are not considered due to the fact that serial multi-probing is too inefficient (in terms of connection provisioning time) compared to the proposed PABR.

The NSF Network Topology

The NSF network topology is shown in Figure 7.3. In the graph, the number in a circle indicates the index of a switch node and the number on an edge indicates the number of spans assumed in the corresponding optical link. The structure of an optical span is shown in Figure 7.2.

We first set $N = 5$, so there are 11 signal channels per fiber. The power of the signal-ASE beating noise of an EDFA $\sigma^2_{sig-spon}$ is set to 10^{-9}W (in the same order of

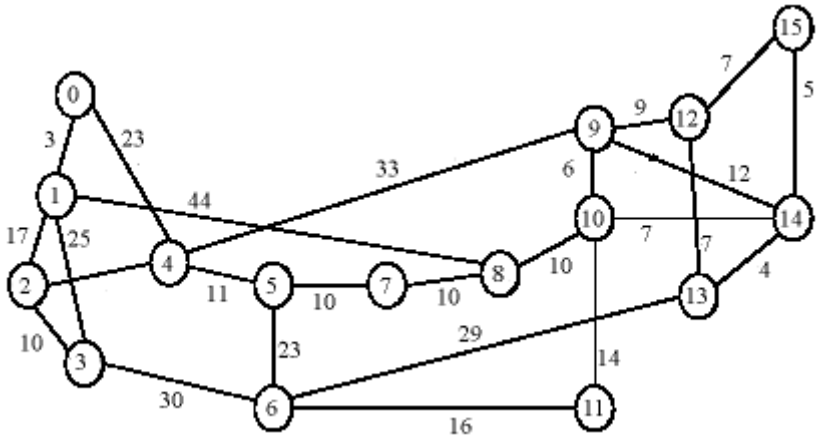

Figure 7.3. The NSF network topology with numbers of spans for edges.

noise power as when the EDFA noise figure is set to 5dB) and assumed the same for all EDFAs in the network. The parameter TH_Q is set to 5.6.

Figure 7.4 compares the performance of different algorithms on the NSF network with 11 channels per fiber.

For the LORA and PABR algorithms, Equation 6.2 is used to adaptively adjust β under different traffic loads. The sudden decrease of blocking probability at a traffic load of about 105 Erlangs is due to the change of β from 1.3 to 1.1. The benchmark algorithms SP and LORA use the First-fit algorithm for wavelength assignment, but PABR uses the proposed Quality-first-fit algorithm for wavelength assignment.

To analyze the performance of PABR, we have categorized the reasons of blocking. The major reasons include bad lightpath signal quality and lack of free wavelengths. Figure 7.5 compares the blocking probabilities due to 'None_resource' (i.e. lack of free wavelengths) of different algorithms. Due to the pruning operation in PAR, LORA

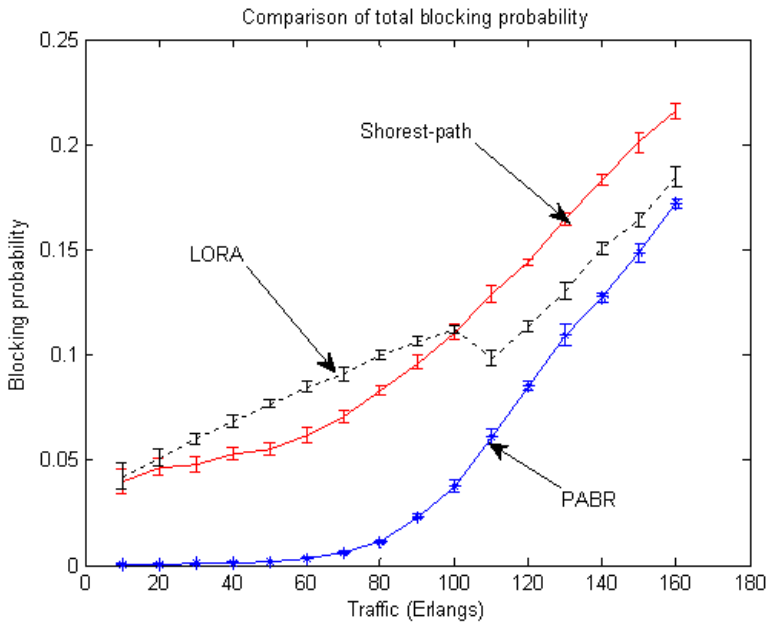

Figure 7.4. Comparison of the blocking probabilities of different algorithms on the NSF network with $N = 5$.

is more effective in distributing traffic and avoiding congested links. But PABR still inherits the merits of LORA in distributing traffic.

Figure 7.6 compares the blocking probabilities due to 'Bad_quality' of different algorithms. The sudden decrease of blocking probability at a traffic load of about 105 Erlangs is due to the decrease of β from 1.3 to 1.1. When the smaller value is applied, LORA tends to use shorter paths and thus decreases the blocking probability due to 'Bad_quality'.

To investigate the performance of PABR in a network with more wavelengths, we increase the value of N to 10, resulting in 21 channels per fiber. The parameter TH_Q is still set to 5.6. Using the hill-climbing algorithm, Equation 7.15 is used to

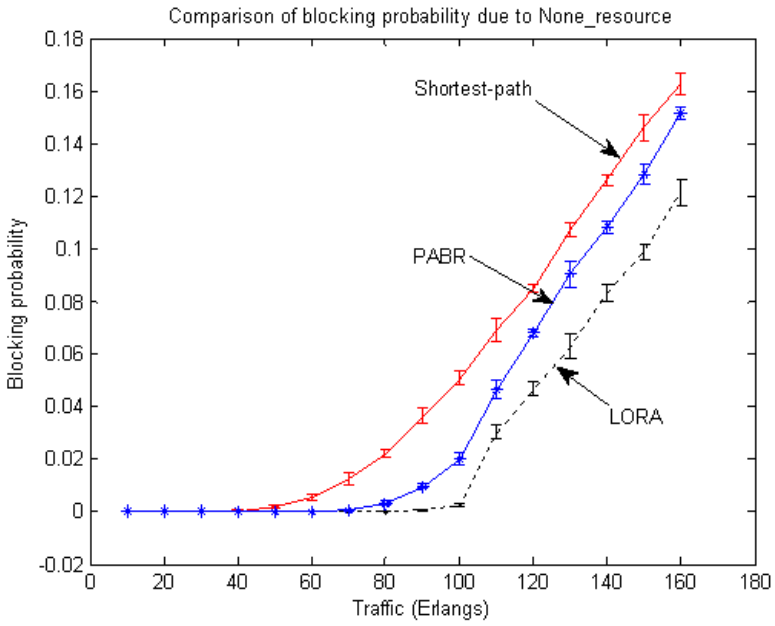

Figure 7.5. Comparison of the blocking probabilities due to 'None_resource' of different algorithms on the NSF network with $N = 5$.

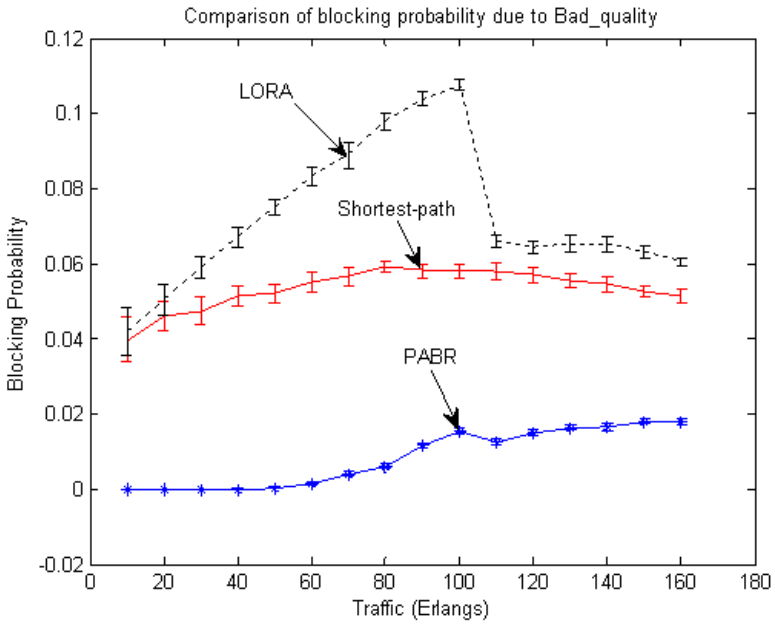

Figure 7.6. Comparison of the blocking probabilities due to 'Bad_quality' of different algorithms on the NSF network with $N = 5$.

adjust β under different traffic loads.

$$\beta = \begin{cases} 1.2 & \text{if traffic load} < 280 \text{ Erlangs} \\ 1.1 & \text{if traffic load} \geq 280 \text{ Erlangs.} \end{cases} \tag{7.15}$$

Figure 7.7 compares the performance of different algorithms on the NSF network with 21 channels per fiber.

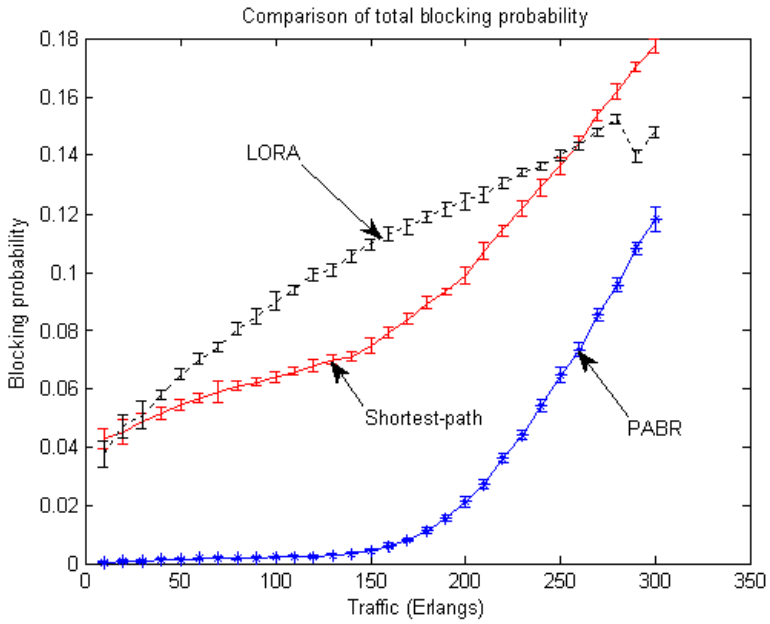

Figure 7.7. Comparison of the blocking probabilities of different algorithms on the NSF network with $N = 10$.

Figure 7.8 and Figure 7.9 respectively compare the blocking probabilities of different algorithms due to the two major reasons.

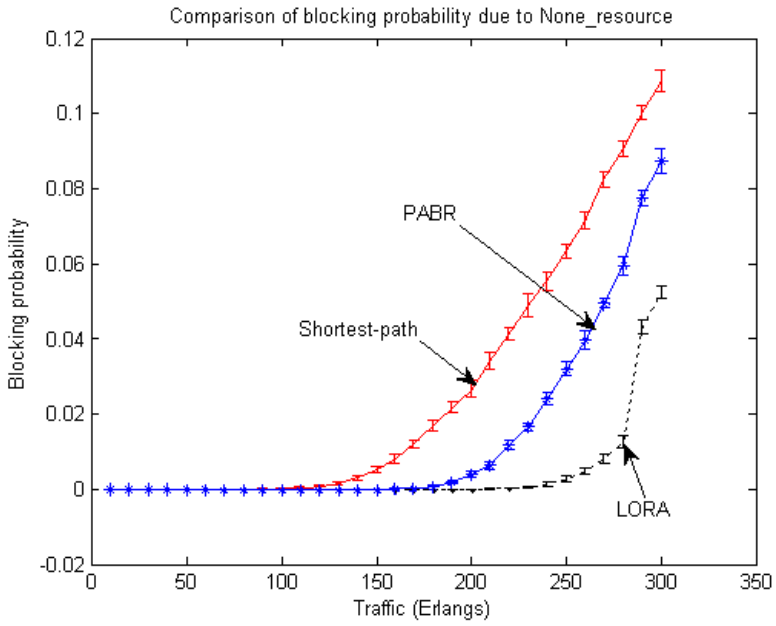

Figure 7.8. Comparison of the blocking probabilities due to 'None_resource' of different algorithms on the NSF network with $N = 10$.

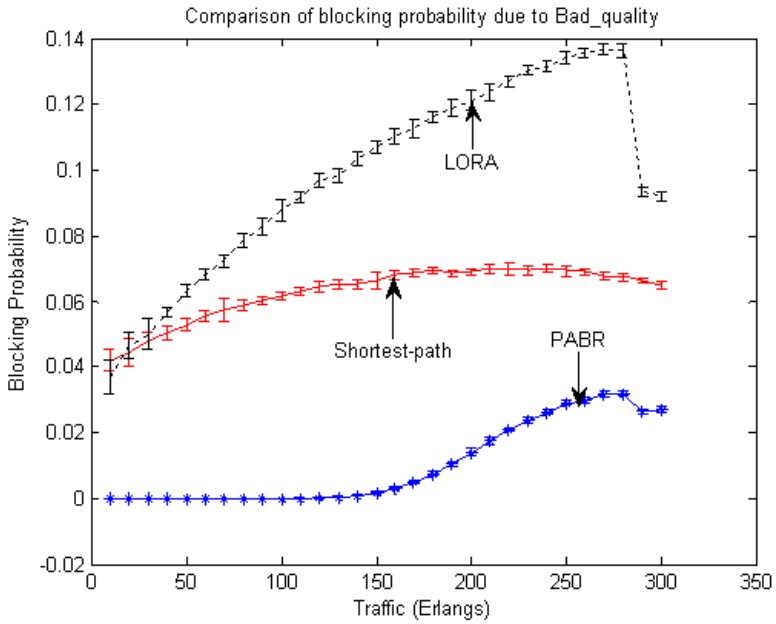

Figure 7.9. Comparison of the blocking probabilities due to 'Bad_quality' of different algorithms on the NSF network with $N = 10$.

We then study the sensitivity of PABR to the number of wavelengths per fiber. We vary the parameter N and compare the performance of different algorithms in these wavelength configurations. The traffic load is fixed to 250 Erlangs and the parameter β is fixed to 1.2.

Figure 7.10 compares the blocking probabilities (total blocking probabilities) of different algorithms. Figure 7.11 and Figure 7.12 respectively compare the blocking probabilities due to the two major reasons. We notice in the figures that when the number of wavelengths is smaller than 21, the blocking probabilities due to 'None_resource' of three algorithms all decrease when more wavelengths are put into use, while the blocking probabilities due to 'Bad_quality' increase. We can explain this phenomenon by considering the implementation of PABR. In PABR when a destination node receives a 'probe' message, it first checks whether there is any free wavelength on the probed path. If so, it then checks whether there is a free wavelength with satisfactory signal quality. When the number of wavelengths increases (in the range [11,21]), more connection requests pass the first checking and are probably rejected with the reason 'Bad_quality'. When the number of wavelengths further increases (greater than 21), situations for the three algorithms are different. For LORA, the blocking probability due to 'None_resource' stays almost the same, and the blocking probability due to 'Bad_quality' dominates. For SP, the blocking probability due to 'None_resource' still decreases but with a slower speed. For both LORA and SP, the blocking probability due to 'Bad_quality' will not decrease as more wavelengths

are used because the First-fit algorithm is applied which always chooses the free wavelength with the smallest index without considering signal quality. LORA tends to use longer lightpaths (in terms of hop count) than SP, so the blocking probability due to 'Bad_quality' of LORA is higher than SP. For PABR, the Quality-first-fit algorithm has more chance to find a free wavelength with satisfactory signal quality when the number of wavelengths increases and the blocking probability due to 'Bad_quality' will further decrease.

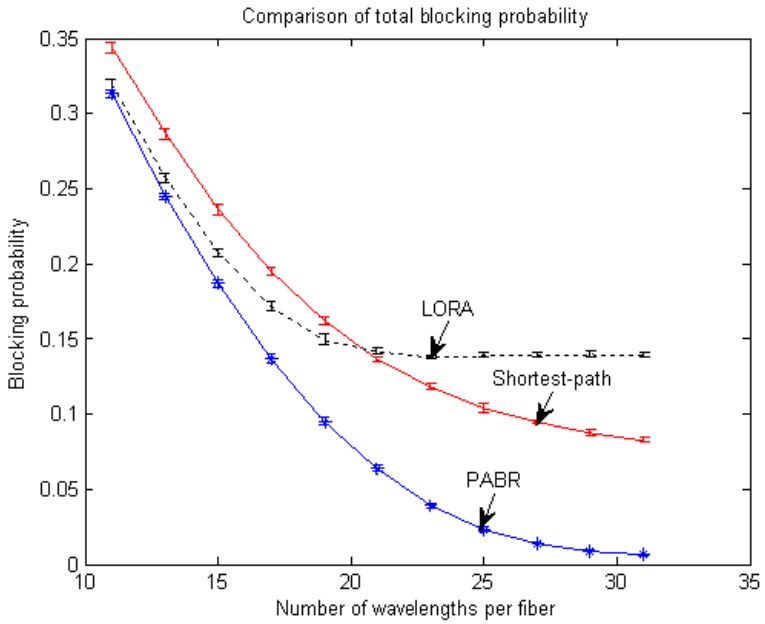

Figure 7.10. Comparison of the blocking probabilities of different algorithms on the NSF network when varying N .

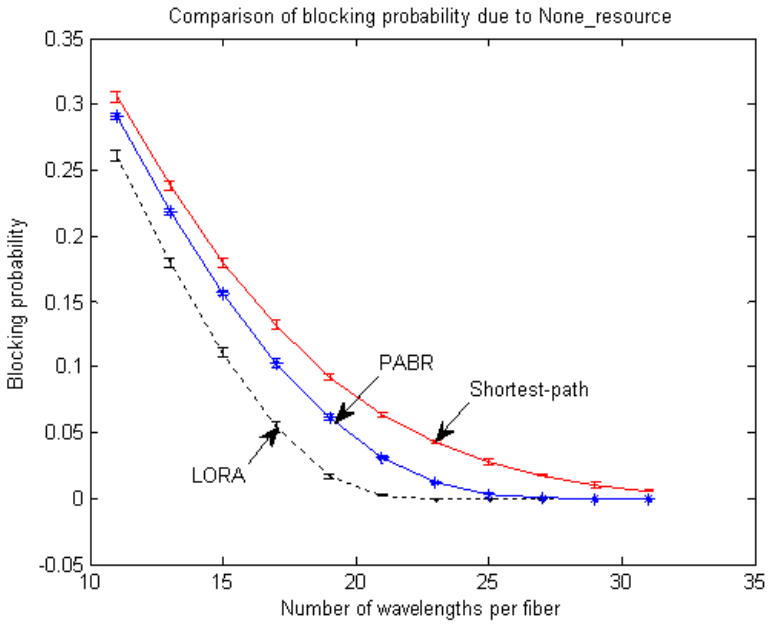

Figure 7.11. Comparison of the blocking probabilities due to 'None_resource' of different algorithms on the NSF network when varying N.

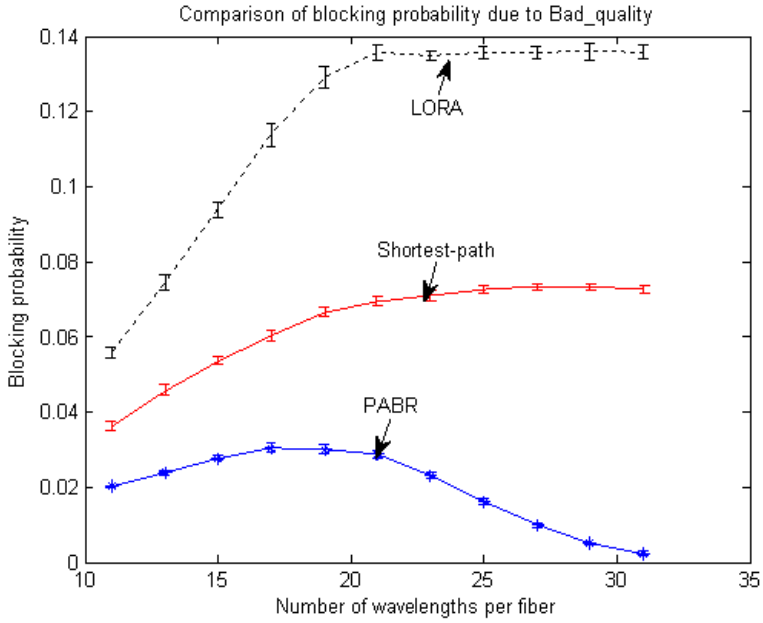

Figure 7.12. Comparison of the blocking probabilities due to 'Bad_quality' of different algorithms on the NSF network when varying N.

The Mesh Network Topology

The mesh topology with switch node indices and numbers of spans for edges is shown in Figure 7.13. For simplicity, we assume that all spans of the mesh network have the same structure as in Figure 7.2 and the values in Table 7.2 are used for simulation parameters. We further assume that there are 21 (N=10) channels per fiber and the parameter TH_Q is set to 5.3. The parameter β is fixed to 1.1 under the considered traffic loads.

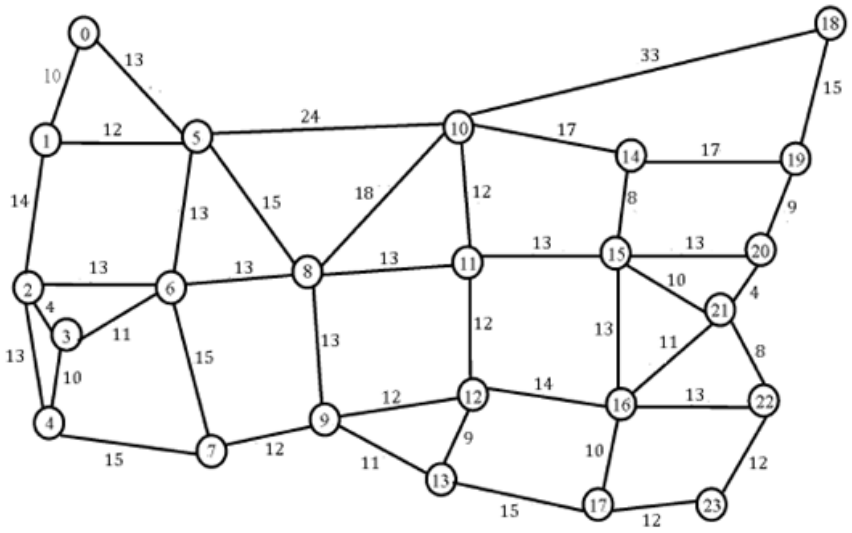

Figure 7.13. The mesh network topology with numbers of spans for edges.

Figure 7.14 compares the performance of different algorithms on the mesh network with 21 channels per fiber.

Figure 7.15 and Figure 7.16 respectively compare the blocking probabilities of different algorithms due to the two major reasons.

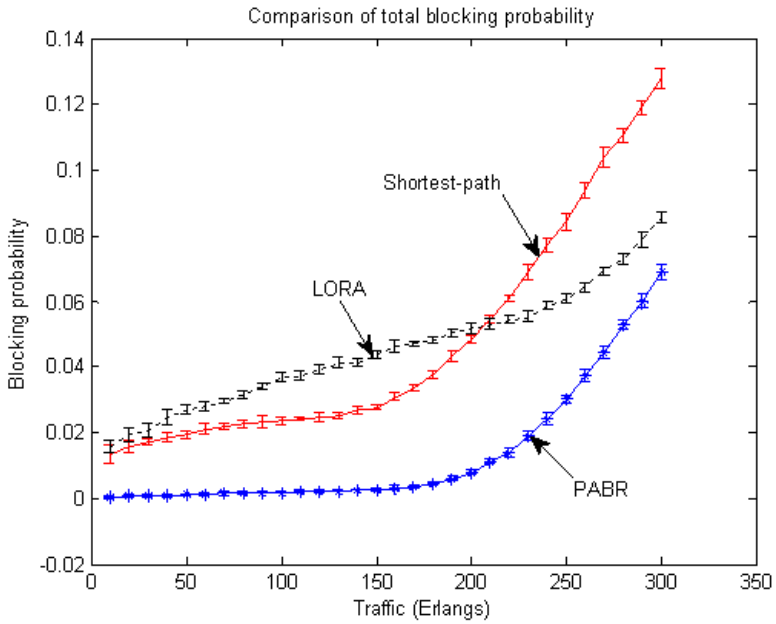

Figure 7.14. Comparison of the blocking probabilities of different algorithms on the mesh network with $N = 10$.

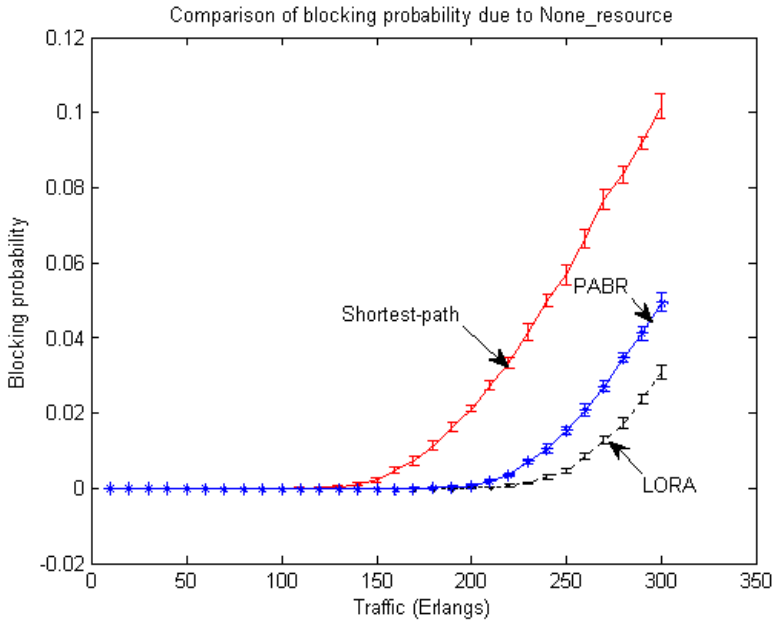

Figure 7.15. Comparison of the blocking probabilities due to 'None_resource' of different algorithms on the mesh network with $N = 10$.

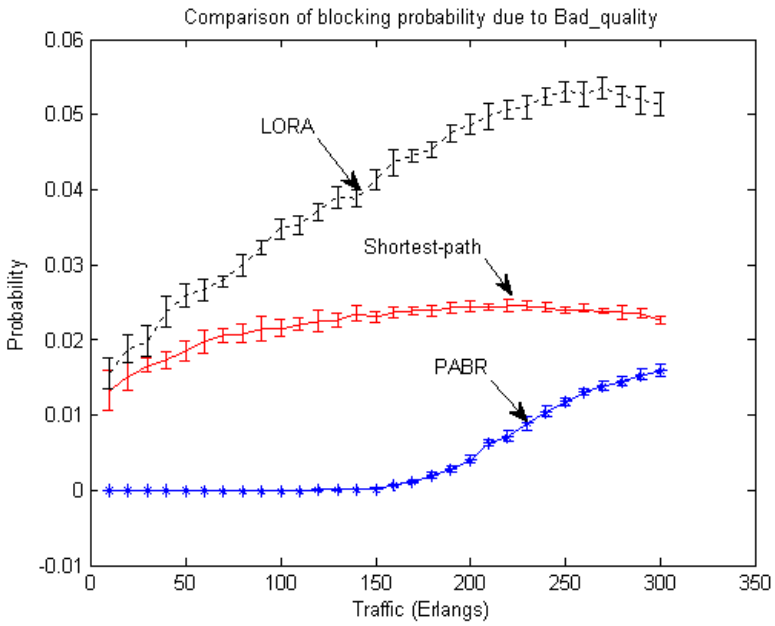

Figure 7.16. Comparison of the blocking probabilities due to 'Bad_quality' of different algorithms on the mesh network with $N = 10$.

Simulation results show that the PABR algorithm has better performance than other benchmark algorithms in different network topologies and network configurations.

Discussion

The simulation results suggest that PABR has better performance compared to other benchmark algorithms. It is efficient and can be implemented by adapting the widely used backward reservation protocol. In PABR, important physical impairments (e.g. ASE noise) are taken into account to choose the candidate paths in the route computation step. This can greatly improve the algorithm performance

compared to other algorithms as in [9][60], in which the set of candidate paths are selected according to criteria totally unrelated to physical constraints (e.g. the shortest path). The optimization goal of PAR is to distribute traffic and avoid congested links, and the pruning operation guarantees that only the paths likely to satisfy the user QoS requirement are returned and later probed. We observe from simulation results that PABR has inherited the merits of LORA in avoiding congested links. PABR is flexible, supporting both single-probing and multi-probing. When multi-probing is applied, multiple candidate paths are probed in parallel, decreasing the connection provisioning time compared to [9][60] and collision probability.

The Quality-first-fit algorithm is used in PABR for wavelength assignment to compact the indices of used wavelengths. As we noted from previous studies, this is important for decreasing blocking probability due to the lack of free wavelengths.

Preserving the signal quality of a lightpath is important for dynamic networks. Some physical impairments depend on network state. For example, when a new lightpath is established, the noise powers due to XPM and FWM will both increase. Without some protection mechanism, it is possible that a lightpath can incur performance outage during some intervals of its lifetime. Under the assumption that each optical link has zero residual dispersion, PABR has provided efficient functionalities to preserve the signal quality of a connection.

To take the physical impairments into account at the network layer, the physical characteristics of different network components and fibers need to be available to

network layer algorithms. Considering the large number of components that may be deployed in a network, the design of the database storing these information needs to be efficient and scalable. In our framework, a distributed database is used. The information about network components and properties of optical fibers on an optical link is stored in the controlling node of the link. Such information is not broadcast in the network to decrease signaling overhead. The destination node can find the characteristics of a probed path in the 'probe' message.

In our research, spatial and temporal traffic variations across a network have not been considered. When applied on a practical network, where traffic variations can frequently occur, the proposed simple mechanism for dynamically adjusting the parameter β needs to be improved and deserves further research.

CONCLUSIONS AND FUTURE WORK

In recent decades, the demands for bandwidth have increased exponentially. With the technology development of cheap laser sources, fiber amplifiers, photo-detectors, and other components, optical networking is a promising approach that can meet such demands. In addition to providing enormous bandwidth, optical networks provide a common infrastructure that can deliver a variety of services. The trend of optical network development is to move towards dynamic all-optical networks, including circuit-switched, burst-switched, and packet-switched networks. In all-optical networks, traffic data are transmitted from source to destination totally in the optical domain without OEO conversion. Compared to the current-generation commercial networks which use the OEO conversion, all-optical networks have the advantage of being more financially favorable, flexible, scalable, and easier to manage and upgrade.

This dissertation has explored some interesting topics in both the physical layer and the network layer of all-optical networks. Our studies investigated the impairments which can adversely influence network performance. Both novel proactive and reactive approaches have been proposed to optimize network design, improve network performance, and provide QoS assurance for users.

The conclusions of the research work reported in this dissertation and the possible future work are summarized as follows.

Conclusions

Numerical simulations are important for studying fiber nonlinear effects. In our research, simulation results are used to validate the analytical models developed for predicting signal degradations induced by fiber nonlinear effects. However, simulation is also very time-consuming considering the possible length (thousands of kilometers) of a lightpath in an all-optical network. We proposed a new simulation system in Chapter 3 based on grid computing technology. This system can automatically distribute simulation tasks to available computing resources across an organization and effectively improve simulation speed.

Analytical models were proposed in Chapter 4 to predict signal degradations due to fiber nonlinear effects. By comparing theoretical predications to numerical simulation results, these analytical models were shown to have good precision. From these analytical models, we observed that under the assumption that each optical link has zero residual dispersion, the models proposed in [55][56] can be extended to predict signal quality of a lightpath in a complex dynamic all-optical network.

Proactive approaches were proposed in Chapter 5 to eliminate or decrease network transients. The MEMS switch transients can be eliminated by simply adding a 'required-delay' field in the 'probe' message of backward reservation and letting the source node wait a short period of time. A novel power shaping technique was proposed to decrease EDFA transients. Experiments have verified the effectiveness of

power shaping. Our approaches are more economical, general, and easier to implement than other methods proposed in the literature.

In Chapter 6, two new algorithms were described that avoid congested links and decrease blocking probability. Distributing traffic and avoiding congested links is an important goal for traffic engineering. LORA was shown by simulation results to be efficient in avoiding congested links and decreasing blocking probability. The MBR algorithm was designed to decrease blocking probability due to confliction. Reservation confliction occurs when several connection requests try to reserve the same wavelength on an optical link. When traffic load is low, confliction is the major cause of blocking. Extensive simulation suggests that MBR works best in small-scale networks. In such networks, the average hop number of a lightpath is small and the *guess correctness probability* is high. Backbone networks usually satisfy this topology condition. The performance of MBR will not improve as the number of wavelength per fiber increases. This is a shortcoming of MBR. However, if the number of wavelengths per fiber is relatively small or the number of free wavelengths is comparatively small, although the total number of wavelengths per fiber is large, then the use of MBR to decrease reservation confliction is more effective than other algorithms that use the random selection mechanism.

In Chapter 7, the LORA algorithm was adapted to provide QoS assurance in all-optical networks. Analytical models developed in Chapter 4 were incorporated into the network layer RWA algorithms to predict the signal quality of a lightpath

under the influence of fiber nonlinear effects and ASE noise. In PAR, important physical impairments are taken into account when choosing candidate paths in the route computation step. When multi-probing is applied, multiple paths which can possibly satisfy the user QoS requirement are probed in parallel. New functionalities were designed in PABR such that the signal quality of a lightpath can be guaranteed during its life time. This is critical for providing QoS assurance in a network with dynamic traffic. Simulation results proved that PABR has better performance than other benchmark algorithms proposed in the literature in terms of decreased blocking probability and connection provisioning time.

Future Work

In Chapter 3, a prototype optical transmission simulation system based on grid computing technology (Grid_sim) was proposed and implemented. The development of such a system can be very useful for studying optical pulse propagation, fiber linear and nonlinear effects, network design optimization, etc. For the research of this dissertation, only two nonlinear effects, XPM and FWM, have been investigated. Studying pulse propagation under other nonlinear effects (e.g. SPM, SRS) and new algorithms which can be used to speed up simulation require further research.

In the analytical models used to predict the signal quality of a lightpath under nonlinear effects XPM and FWM, these two effects are assumed independent. A new analytical model which considers the influence of the phase shift caused by XPM

on FWM can further improve model precision. Our preliminary simulation results suggested that this new model is effective. More systematic simulations are needed to prove that this new model is effective in different network configurations.

For a network with temporal and spatial traffic variations, new mechanisms for dynamically adjusting β under different traffic loads need to be designed. For example, the source node can use multi-probing, with paths computed by using different values for β. In another new method, the source node adjusts β according to the detected blocking probability. Implementation and effectiveness of these new approaches need to be examined.

REFERENCES CITED

[1] M. Wrage, A. Kirstaedter, and H.Rohde, "The evolution to transparent optical networking," Proc. APOC 2004 Conference, vol.5626-46, Beijing, 2004.

[2] C.Murthy and M.Gurusamy, "WDM optical networks, concepts, design and algorithms," Prentice Hall, pp.67-69,85-90, 2001.

[3] H.Zang, J.P.Jue and B.Mukheriee, "A review of routing and wavelength assignment approaches for wavelength-routed optical WDM networks," Optical Networks Magazine, vol.1, no.1, Jan. 2000.

[4] K,Chan and T.P.Yum, "Analysis of least congested path routing in WDM lightwave networks," Proc. IEEE INFOCOM'94, vol.2, pp.962-965, Toronto, Canada, Apr. 1994.

[5] G.Jeong and E.Ayanoglu, "Comparison of wavelength-interchanging and wavelength-selective cross-connects in multiwavelength all-optical networks," Proc. IEEE INFOCOM'96, vol.1, pp.156-163, San Francisco, CA, Mar. 1996.

[6] E.Karasan and E.Ayanoglu, "Effects of wavelength routing and selection algorithm on wavelength conversion gain in WDM optical networks," IEEE/ACM Trans. Networking., vol.6, no.2, pp.186-196, Apr. 1998.

[7] S.Subramaniam and R.A.Barry, "Wavelength assignment in fixed routing WDM networks," Proc. ICC'97, vol.1, pp.406-410, Montreal, Canada, June 1997.

[8] X.Zhang and C.Qiao, "Wavelength assignment for dynamical traffic in Multi-Fiber WDM networks," Proc. 7th International Conference on Computer Communications and Networks, pp.479-485, Lafayette, LA, Oct. 1998.

[9] Y. Huang, P. Heritage and B. Mukherjee, "Connection provisioning with transmission impairment consideration in optical WDM networks with high-speed channels," Journal of Lightwave Technology, vol.23, no.3, March 2005.

[10] R.Cardillo, V.Curri, M.Mellia, "Considering Transmission Impairments in Wavelength Routed Networks," Proc. of Conference on Optical Network Design and Modeling, pp.421-429, Italy, 2005.

[11] L.Moura, N.Karafolas,P.Lane, A.Hill and J.O'Reilly, "Modeling of interferometric crosstalk in optical networks," in Proc. GLOBECOM'96, London, England, pp.333-337, Nov. 1996.

[12] E.Iannone and R.Sabella, "Performance evaluation of an optical multicarrier network using wavelength converters based on FWM in semiconductor optical amplifiers," J.Lightwave Technology. vol.13, pp.312-324, Feb. 1995.

[13] G. P. Agrawal, "Lightwave Technology: Telecommunication Systems," Wiley-Interscience, pp.347, 2005.

[14] B. E. A. Saleh and M. C. Teich, "Fundamentals of Photonics," Wiley-Interscience, pp.632, 1991.

[15] G. P. Agrawal,G. P. Agrawal, "Fiber-optical Communication Systems," 3th edition, Wiley-Interscience, pp.345, 2002.

[16] D. K. Mynbaev and L. L. Scheiner, "Fiber-optical Communications Technology," Prentice Hall, pp.617, 2001.

[17] H. J. R. Dutton, "Understanding Optical Communications," International Technical Support Organization, 1998.

[18] R. Ramaswami and K. N. Sivarajan, "Optical Networks: A Practical Perspective," 2th edition, Morgan Kaufmann Publishers, pp.74, 2004.

[19] P. C. Becker, N. A. Olsson, J. R. Simpson, "Erbium-doped Fiber Amplifiers: Fundaments and Technology," Academic Press, pp.266, 1999.

[20] L. Y. Lin and E. L. Goldstein, "Micro-electro-mechanical systems (MEMS) for WDM optical crossconnect networks" (Invited), IEEE Conference on Military Communications, Atlantic City, NJ, October 1999.

[21] S. O. Kasap, "Principles of Electronic Materials and Devices," 3rd edition, McGraw Hill, pp.565, 2006.

[22] J. Hecht, "Understanding Fiber Optics," 4th edition, Pearson Education, pp.101, 2003.

[23] G. P. Agrawal, "Lightwave Technology: Telecommunication Systems," Wiley-Interscience, pp.186, 2005.

[24] R.S.Wolff, S. Achar "Transient Effects in MEMS-switched All-optical Networks with EDFAs," OCSN2005, Banff, Alberta, Canada, July 2005.

[25] G. P. Agrawal, "Nonlinear Fiber Optics," 3th edition, Academic Press, pp.19, 2001.

[26] G. P. Agrawal, "Nonlinear Fiber Optics," 3th edition, Academic Press, pp.355, 2001.

[27] M. Kar'asek and J. A. Vall'es, "Analysis of Channel Addition/Removal Response in All-Optical Gain-Controlled Cascade of Erbium-Doped Fiber Amplifiers," Journal of Lightwave Technology, vol.16, no.10, Oct. 1998.

[28] G. Luo, J.L.Zyskind,J.A.Nagel, and M.A.Ali, "Experimental and Theoretical Analysis of Relaxation-Oscillations and Spectral Hole Burning Effects in All-Optical Gain-Clamped EDFA's for WDM Networks," Journal of Lightware, vol.16, no.4, 1998.

[29] J. L. Zyskind, Y. Sun, A. K. Srivastava, J. W. Sulhoff, A. J. Lucero, C. Wolf, and R. W. Tkach, "Fast power transients in optically amplified multiwavelength optical networks," Proc. OFC '96, San Jose, CA, post deadline paper PD31.

[30] M. Kar'asek, M. Menif and Leslie, "Output Power excursions in a Cascade of EDFAs Fed by Mulitchannel Burst-Mode Packet Traffic: Experimentation and Modeling," Journal of Lightwave Technology, vol.19, no.7, July 2001.

[31] L.Tancevski and Leslie A.Rusch, "Output power and SNR Swings in Cascade of EDFA's for Circuit- and Packet-Switched Optical Networks," Journal of lightwave technology, vol.17, no.5, Dec. 1999.

[32] R.Ramaswami and K.Sivarajan, "Optical networks—-A practical perspective," second edition, Morgan Kaufmann publishers, pp.285, 2002.

[33] G. P. Agrawal,G. P. Agrawal, "Fiber-optical Communication Systems," 3th edition, Wiley-Interscience, pp.164, 2002.

[34] A. Farbert, C. Scheerer, J. P. Elbers, C. Glingener, and G. Fischer, "Optimized dispersion management scheme for long-haul optical communication systems," IEEE Electron. Lett., vol.35, no.20, pp.1865-1866, 1999.

[35] G. P. Agrawal, "Nonlinear Fiber Optics," 3th edition, Academic Press, pp.49, 2001.

[36] A. Carena, V. Curri, R. Gaudino, P. Poggiolini, and S. Benedetto, "A Time-Domain Optical Transmission System Simulation Package Accounting for Nonlinear and Polarization-Related Effects in Fiber," Journal on Selected Areas in Communicatin, vol.15, pp.751-765, May 1997.

[37] E. Iannone, F. Matera, A. Mecozzi, and M. Settembre, "Performance Evaluation of Very Long Span Direct Detection Intensity and Polarization Modulated Systems," J. L. T, vol.14, pp.261-272, March 1996.

[38] P. I. Systemtechnik company,"Component Manual," version 4.0, pp.43, 2007.

[39] L. G. L Wegener, M. L. Povinelli, A.G.Green, P. P. Mitra, J. B. Stark, and P. B. Littlewood, "The effect of propagation nonlinearites on the information capacity of WDM optical fiber systems: cross-phase modulation and four-wave mixing," Journal of Physica D: Nonlinear Phenomena, vol.189, pp.81-99, 2004.

[40] G. P. Agrawal, "Nonlinear Fiber Optics," 3th edition, Academic Press, pp.283, 2001.

[41] J. H. Lee, "Analysis and Characterization of Fiber Nonlinearities with Deterministic and Stochastic Signal Sources," Ph.D thesis, 2000.

[42] O. V. Sinkin, R. Holzlohner, J. Zweck, C.R. Meyuk, "Optimization of the Split-Step Fourier method in modeling optical-fiber communications systems," J.L.T, vol.21, no.1, 2003.

[43] M. Jaworski, M. Chochol, "Split-Step-Fourier-Method in Modeling Wavelength-Division-Multiplexed links," Proc. of 9th international conference on transparent optical networks, vol.4, pp.47-50, 2007.

[44] G. J. Pendock and W. Shieh, "Fast Simulation of WDM Transmission in Fiber," IEEE Photon. Technol. Lett., vol.18, no.15, 2006.

[45] M. Plura, J. Kissing, M. Gunkel, J. Lenge, J. P. Elbers, C. Glingener, D. Schulz, and E. Voges, "Improved split-step method for efficient fiber simulations," Electronics Lett., vol.37, no.5, 2001.

[46] P. I. Systemtechnik company,"Component Manual," version 4.0, pp.47, 2007.

[47] A. Averbuch, E.Gabber, B. Gordissky, and Y. Medan, "A Parallel FFT on an MIMD machine," Parallel Comput., vol.15, pp.61-74, 1990.

[48] A. Dubey, M. Zubair, and C.EGrosch, "A general purpose subrouting for fast Fourier transform on a distributed memory parallel machine," Parallel Comput., vol.20, pp.1697-1710, 1994.

[49] Rsoft Company, "Model Reference, VII Block Mode," version 4.6, pp.92, 2006.

[50] M. Karasek, A. Bononi, L. A. Rusch, and M. Menif, "Gain stabilization in gain clamped EDFA cascades fed by WDM burst-mode packet traffic," J. Lightwave Tech., vol.18, pp.309-313, 2000.

[51] Rsoft Company, "Model Reference, VII Block Mode," version 4.6, pp.357, 2006.

[52] S. Pachnicke, T. Gravemann, M. Windmann, and E. Voges,"Physically Constrained Routing in 10-Gb/s DWDM Networks Including Fiber Nonlinearities and Polarization Effects," J.L.T, vol.24, pp.3418-3425, 2006.

[53] R. Hui, K. R. Demarest, and C. T. Allen, "Cross-Phase Modulation in Multispan WDM Optical Fiber Systems," J.L.T, vol.17, pp.1018-1026, 1999.

[54] J. Wang and K. Petermann,"Small signal analysis for dispersive optical fiber communication systems," J.L.T, vol.10, pp.96-100, 1992.

[55] A. V. T. Cartaxo,"Cross-Phase Modulation in Intensity Modulation-Direct Detection WDM Systems with Multiple Optical Amplifiers and Dispersion Compensators," J.L.T, vol.17, pp.178-190, 1999.

[56] S. Pachnicke, J. Reichert, S. Spälter, and E. Voges, "Fast Analytical Assessment of the Signal Quality in Transparent Optical Networks," J.L.T, vol.24, pp.815-823, 2006.

[57] K. O. Hill, D. C. Johnson, B. S. Kawasaki, and R. I. MacDonald, "CW three-wave mixing in single-mode optical fibers," J.App.Phys, vol.49, pp.5098-5106, 1978.

[58] N. Shibata, R. P. Braun, and R. G. Waarts,"Phase-Mismatch Dependence of Efficiency of Wave generation Through Four-Wave Mixing in a Single-Mode Optical Fiber," Journal of Quantum Electronics, vol.QE-23, pp.1205-1209, 1987.

[59] W. Zeiler, F. D. Pasquale, P. Bayvel, and J. E. Midwinter, "Modeling of Four-Wave Mixing and Gain Peaking in Amplified WDM Optical Communication Systems and Networks," J.L.T, vol.14, pp.1933-1942, 1996.

[60] C. Politi and V. Anagnostopoulos, "Physical Layer Impairment Aware Routing Algorithms based on Analytically Calculated Q-factor," Proc. Of OFC2006, Anaheim, CA 2006.

[61] T. Jackson, M. Lee, T. Hahn, W. Lin, R. S. Wolff, B. Mumey, and K. Repasky, "EDFA Transient Reduction using Power shaping," WOC'08, Quebec, Canada, May 2008.

[62] Saritha Achar, "Test bed for Measuring Transients in Multi-wavelength All-Optical Communications Networks," Master thesis, 2004.

[63] M. Karasek, M. Menif, and Leslie, "Output power excursions in a cascade of EDFAs fed by multichannel burst-mode packet traffic: experimentation and modeling," J. Lightwave Tech., vol.19, no.7, 2001.

[64] T. Shiozaki, M. Fuse, and S. Morikura, "A study of gain dynamics of erbium-doped fiber amplifiers for burst optical signals," Proc. ECOC 2002, Copenhagen, Denmark, Paper P4.02, 2002.

[65] A. V. Tran, C. J. Chae, R. S. Tucker, and Y. J. Wen, "EDFA transient control based on envelope detection for optical burst switched networks," IEEE Photon. Technol. Lett., vol. 17, pp.226-228, 2005.

[66] C. Tian, and S. Kinoshita, "Analysis and control of transient dynamics of EDFA pumped by 1480- and 980-nm lasers," J. Lightwave Tech., vol.21, pp.1728-1733, 2003.

[67] C. Tian, and S. Kinoshita, "Elimination of power and OSNR swings of EDFA in the amplification of burst WDM traffic," Technical Digest of 9th OptoElectronics and Communication Conference /3rd International Conference on Optical Internet, pp.500-501, 2004.

[68] W. Lin, R. S. Wolff, and B. Mumey, "Suppression of Optical Amplifier Transients by Channel Power Shaping," WOC'07, Montreal, Canada, May 2007.

[69] W. Lin, R. S. Wolff, and B. Mumey, "Decreasing EDFA Transients by Power Shaping," to appear in Journal of OSN, vol.5, no.4, October 2008.

[70] T. Koonen, S. Sulur, I. Monroy, J. Jennen, and H. Waardt, "Optical Labeling of Packets in IP-over-WDM Networks," Proc. Eur. Conf. Optical Communications, 2002.

[71] B. D. Theelen, J. P. M. Voeten, P. H. A. Van der Putten, and M. P. J. Stevens, "Concurrent Support of Higher-Layer Protocols over WDM," Photonic Network Communications, vol.4, no.1, pp.47-62, 2002.

[72] V. M. Vokkarane, J. P. Jue, and S. Sitaraman, "Burst Segmentation: An Approach For Reducing Packet Loss In Optical Burst Switched Networks," Proceedings, IEEE, ICC 2002.

[73] C. Hsu, T. Liu, and N. Huang, "Performance analysis of deflection routing in optical burst-switching networks," in IEEE Infocom 2002, pp.66-73, 2002.

[74] D. H. Richards, J. L. Jackel, and M. A. Ali, "A Theoretical Investigation of Dynamic All-optical Automatic Gain Control in Multichannel EDFA's and EDFA Cascades," J. Selected Topics in Quantum Electronics, vol.3, no.4, Jan. 1997.

[75] D. H. Richards, J. L. Jackel, and M. A. Ali, "Multichannel EDFA Chain Control: A Comparison of Two All-Optical Approaches," J. Lightwave Tech., vol.10, no.1, Jan. 1998.

[76] G. Bolognini, and F. Di Pasquale, "Transient Effects in Gain-Clamped Discrete Raman Amplifier Cascades," J. Lightwave Tech., vol.16, no.1, Jan. 2004.

[77] K. Ennser, G. D. Valle, D. Mariani, S. Taccheo, and J. Shmulovich, "Erbium-doped waveguide amplifier for reconfigurable WDM metro networks," Photonics Technology Letters, IEEE, vol.17, Issue 7, pp.1468-1470, July 2005.

[78] Nick Sawer, "Application notes of Virtex and Virtex-II families' scrambler/descrambler", 2002. http://direct.xilinx.com/bvdocs/appnotes/xapp651.pdf

[79] W. Lin, R. S. Wolff, and B. Mumey, "Protection against Large Power Excursion in Network Failures," WOC'07, Montreal, Canada, May 2007.

[80] R. Sabella and P. Iovanna, "Taffic engineering in next generation multilayer networks based on the GMPLS paradigm," Proc. HET-NETs '04, West Yorkshire, U.K, July 2004.

[81] D. Awduche et al. , "Requirements for Traffic Engineering Over MPLS," IEEE Communications Magazine, IETF RFC 2702, September 1999.

[82] IETF RFC 3471,"Generalized Multi-Protocol Label Switching (GMPLS) Signaling Functional Description," January 2003.

[83] IETF RFC 3472,"Generalized Multi-Protocol Label Switching (GMPLS)Signaling Constraint-based Routing Protocol Extensions (CRLDP)," January 2003.

[84] E. Oki, K. Shiomoto, and D. Shimazaki, "Dynamic Multilayer Routing Schemes in GMPLS-Based IP+Optical Networks," IEEE Communications Magazine, pp.108-113, January 2005.

[85] B. Gao, Y. Yang, C. Chen, "Implementing A Constraint-based Shortest Path First Algorithm in Intelligent Optical Networks," Mahi Networks White Paper, May 2003.

[86] R. S. Wolff, K. Repasky, B. Mumey, A. Green, W. Lin, "Performance optimization of dynamic all-optical networks," posted in OFC 2006, Anaheim, CA, 2006.

[87] W. Lin and R. S. Wolff, "A Lexicographically Optimized Routing Algorithm for All-Optical Networks," Proc. of OCSN 2005, pp.138-141, Banff, Alberta, Canada, 2005.

[88] W. Lin, R. S. Wolff, and B. Mumey, "A Markov-based Reservation Algorithm for Wavelength Assignment in All-optical Networks," Journal of Lightwave Tech., vol.25, pp. 1676-1683, 2007.

[89] Arjan Durresi et.al., "Quality Based Optical Routing Protocols," Proc. of Optical Transmission System and Equipment for WDM Networking II, SPIE vol. 4247, pp. 410-420, September 2003.

[90] Yan Zhang, "Virtual Circuit Routing," Class Report, October 2003.

[91] L. Georgiadis, P. Georgatsos, S. Sartzetakis, K. Floros, "Lexicographically Optimal Balanced Networks," IEEE Infocom 2001, April 2001.

[92] T. Ozugur, M. Park, and J. Jue, "Label prioritization in GMPLS-centric all-optical networks," Proc. ICC, pp.1283-1287, 2003.

[93] Feifei Fang, Xiaoping Zheng, Hanyi Zhang, "Performance Study of Distributed Wavelength Reservation Protocols within both Single and Multi-Fiber WDM Networks," Photonic Network Communications, vol.6, no.2, September 2003.

[94] Hui Zang, Jason P. Jue, Biswanath Mukheriee, "A review of Routing and Wavelength Assignment Approaches for Wavelength-Routed Optical WDM networks," Optical Networks Magazine, vol.1, no.1, January 2000.

[95] K. Lu, G. Xiao, and I. Chlamtac, "Analysis of blocking probabilities for distributed lightpath establishment in WDM optical networks," IEEE/ACM Trans. Networking, vol.13, no.1, Feb. 2005.

[96] R. Ramaswami and A. Segall, "Distributed network control for optical networks," IEEE/ACM Trans. Networking, vol.5, pp.936-943, Dec. 1997.

[97] J. Teng and G. N. Rouskas, "A comparison of the JIT, JET, and Horizon wavelength reservation schemes on a single OBS node," in Proc. The First International Workshop on Optical Burst Switching, 2003.

[98] X. Wang, H. Morikawa, and T. Aoyama, "Priority-based wavelength assignment algorithm for burst switched photonic networks," IEICE Trans. Communications, vol. e86-b, pp.1508-1514, May 2003.

[99] H. C. Tijms, "A first course in stochastic models," Wiley, pp.166-168, 2003.

APPENDICES

APPENDIX A

Matlab Code for Simulating Pulse Propagation

Linear propagation

```
function out_waveforms = ssprop_linear(E_waveforms,fs,fc,z,alpha,beta2,beta3,D,dt)
  c            = 2.99792457778e+8;             %[m/s] speed of light
  [E_num, nt]   = size(E_waveforms);
  out_waveforms = zeros(E_num,nt);

  w       = 2*pi*[(0:nt/2-1),(-nt/2:-1)]/(dt*nt);
  w0      = 2*pi*fc;
  beta1   = 0;

  for i=1:E_num
    cw        = 2*pi*fs(i);     %carrier frequency
    mybeta1   = beta1 + beta2*(cw-w0) + beta3/2*(cw-w0)^2;
    mybeta2   = beta2 + beta3*(cw-w0);
    mybeta3   = beta3;
    tmp       = fft(E_waveforms(i,:));
    djk       = beta1 - mybeta1;
    tmp       = tmp.*exp((-alpha/2+j*w*djk-j/2*mybeta2*w.^2 -j/6*mybeta3*w.^3)*z );
    out_waveforms(i,:) = ifft(tmp);
  end
```

Nonlinear propagation

```
function ret = part_solve(part_E_waveforms,z,dz,ks,gamma,chns,combs)
  global g_ks  g_gamma  g_chns  g_combs;
  g_ks  = ks;  g_gamma = gamma; g_chns = chns; g_combs = combs;

  [E_num, nt]   = size(part_E_waveforms);
  out_waveforms = zeros(E_num,nt);

  options       = odeset('MaxStep',dz);
  for T =1:nt
    [Z B]  = ode45(@NLSE,[z z+dz], part_E_waveforms(:,T),options);
    rows  = size(B,1);
    out_waveforms(:,T) = B(rows,:);
  end
  ret = out_waveforms;


function Aprime = NLSE(z,A)       % z  the absolute
  global g_ks g_gamma g_chns g_combs;

  with_xpm =1 ; with_fwm =1;   % enable and disable fwm and xpm

  Aprime = zeros(g_chns,1);

  all_powers = sum(abs(A).^2);

  for chn =1:g_chns
      xpm_tmp     = all_powers - abs(A(chn))^2;
      xpm_term    = j*g_gamma*2*xpm_tmp*A(chn);

      fs_coms      = g_combs{chn};
      rows         = validrows(fs_coms);
      f_chn_id     = chn;
      fwm_term     = 0;
      for id =1:rows
         fi_id    = fs_coms(id,1);
         fj_id    = fs_coms(id,2);
         fk_id    = fs_coms(id,3);
         d        = fs_coms(id,4);
         diff_k   = g_ks(fi_id)+g_ks(fj_id)-g_ks(fk_id)-g_ks(f_chn_id);
         fwm_term = fwm_term + j*g_gamma*d/3*A(fi_id)*A(fj_id)*conj(A(fk_id))*exp(-j*diff_k*z);
```

```
      end

      Aprime(chn,1) = -(with_xpm*xpm_term + with_fwm*fwm_term);

   end
```

Propagation along a fiber segment

```
function out_waveforms = ssprop(E_waveforms,fs,fc,fc_id,Ks,alpha,beta2,beta3,D,gamma,L,dt,ts)
  max_steps      = 800;
  if (gamma == 0)
      max_steps = 1;
  end
  z  = 0;    const_dz = L/max_steps;   dz = const_dz;
  global_err_delta = 5e-7;

  while(z<L)
    %[z dz]             %for debug
    waveform_onestep  =  ssprop_incremtal(E_waveforms,fs,fc,Ks,alpha,beta2,beta3,D,gamma,z,dz,dt);
    tmp               =  ssprop_incremtal(E_waveforms,fs,fc,Ks,alpha,beta2,beta3,D,gamma,z,dz/2,dt);
    waveform_twostep  =  ssprop_incremtal(tmp,fs,fc,Ks,alpha,beta2,beta3,D,gamma,z+dz/2,dz/2,dt);

    prob_onestep      = waveform_onestep(fc_id,:);
    prob_twostep      = waveform_twostep(fc_id,:);

    err_delta     = norm(prob_onestep - prob_twostep,2)/norm(prob_twostep,2);
    if (err_delta < 0.5*global_err_delta)
       z  = z+dz;
       E_waveforms = 4*waveform_twostep/3-waveform_onestep/3;    % the fields at new z
       dz = min(L-z,2^(1/3)*dz);
    elseif (err_delta < global_err_delta)
       z  = z+dz;
       E_waveforms = 4*waveform_twostep/3-waveform_onestep/3;
       dz = min(L-z,dz);
    elseif (err_delta < 2*global_err_delta)
       z = z+dz;
       E_waveforms = 4*waveform_twostep/3-waveform_onestep/3;
       dz = min(L-z,dz/(2^(1/3)));
    else
      dz = dz/2;
    end
end
  out_waveforms  = E_waveforms;
```

Propagation along an incremental fiber segment

```
function  u_dz = ssprop_incremtal(E_waveforms,fs,fc,Ks,alpha,beta2,beta3,D,gamma,z,dz,dt)
  u_halfdz  = ssprop_linear(E_waveforms,fs,fc,dz/2,alpha,beta2,beta3,D,dt);
  nu_halfdz = kuta_nl(u_halfdz,Ks,gamma,z,dz);
  u_dz      = ssprop_linear(nu_halfdz,fs,fc,dz/2,alpha,beta2,beta3,D,dt);
```

Distribution of simulation tasks onto avaible CPUs

```
function out_waveforms =  kuta_nl(E_waveforms,Ks,gamma,z,dz)
  global  g_chns  g_combs;
  jmr =  findResource('scheduler','type','local');
  all_jobs  = get(jmr, 'Jobs'); list_size = length(all_jobs);
  for j_id =1:list_size
      job = all_jobs(j_id);
      destroy(job);
  end     % clear all other jobs

  [E_num, nt]   = size(E_waveforms);
  core_num = 2;                % configurable
```

```
%partition the job
avgsize  = floor(nt/core_num);
arg1     = cell(1,core_num);   %E_waveform
arg2     = cell(1,core_num);   %z
arg3     = cell(1,core_num);   %dz
arg4     = cell(1,core_num);   %ks
arg5     = cell(1,core_num);   %gamma
arg6     = cell(1,core_num);   %chns
arg7     = cell(1,core_num);   %combs

for id =1:core_num-1
   block_start     = (id-1)*avgsize+1;
   block_end       = block_start+avgsize-1;
   arg1{id}        = E_waveforms(:,block_start:block_end);
end
arg1{core_num}  = E_waveforms(:,(core_num-1)*avgsize+1:nt);

for id =1:core_num
   arg2{id}        = z;
   arg3{id}        = dz;
   arg4{id}        = Ks;
   arg5{id}        = gamma;
   arg6{id}        = g_chns;
   arg7{id}        = g_combs;
end

kuta_success = 0;
while(kuta_success == 0)
   [solutions]   = dfeval(@part_solve, arg1, arg2,arg3,arg4,arg5,arg6,arg7, 'configuration', 'local');
   solutions     = solutions';
   out_waveforms = cell2mat(solutions);
   nt_new        = size(out_waveforms,2);
   if (nt == nt_new)
       kuta_success =1;
   else     % the soluiton of ODE fails, try again.
      msg = strcat('nt is ',int2str(nt),' ','new_nt is ',int2str(nt_new),',','Retry.');
      disp(msg);
      all_jobs  = get(jmr, 'Jobs'); list_size = length(all_jobs);
      for j_id =1:list_size
        job = all_jobs(j_id);
        destroy(job);
      end
      pause(60);
   end
end
```

APPENDIX B

XML Configuration File for the NSF Network

```
<?xml version="1.0" encoding="iso-8859-1"?>
<!DOCTYPE configure SYSTEM "configuration.dtd">
<!-- @version: -->
<configure>
  <system>
    <arrival_interval   value="150"> the inter arrival time on each workstation </arrival_interval>
    <duration           value="150"> the duration time of one connection </duration>
    <nonlinear_halfwin  value="10">  the total nonlinear_win is 2*M+1 </nonlinear_halfwin>
    <halfwavelength     value="5">   the total wavelength is 2N+1 </halfwavelength>
    <Fn_dB              value="5">     noise figure of EDFA </Fn_dB>
    <G_dB               value="21.6">  gain of EDFA </G_dB>
    <Bo                 value="20e+9"> bandwidth of optical filter </Bo>
    <Be                 value="10e+9"> electrical bandwdith of photodector </Be>
    <fc                 value="193.1e+12"> center of the wavelength comb </fc>
    <f_step             value="50e+9">     step of the wavelength comb </f_step>
    <channel_power      value= "1e-3">     power per channel </channel_power>
    <spans              value= "5">        default spans per link </spans>
    <L                  value= "80">       length of the NZDSF in each span </L>
    <alphaDB            value= "0.25">     attenuation of NZDSF in each span </alphaDB>
    <D                  value= "4e-3">     dispersion of NZDSF in each span </D>
    <S                  value= "8e+4">     disperison slop of NZDSF in each span </S>
    <gamma              value= "2">        nonlinear coefficent of NZDSF in each span </gamma>
    <TH_Q               value= "5.6">      nonlinear coefficent of NZDSF in each span </TH_Q>
  </system>

  <topology>
     <edges>
     <edge from="0"  to="1"> define edge Vancouver-Seattle
       <spans value="3"> </spans>
     </edge>
     <edge from="1"  to="2"> define edge Seattle-Palo Alto
       <spans value="17"> </spans>
     </edge>
     <edge from="1"  to="3"> define edge Seattle-San Diego
       <spans value="25"> </spans>
     </edge>
      <edge from="2"  to="3"> define edge Palo Alto-San Diego
       <spans value="10"> </spans>
     </edge>
     <edge from="0"  to="4"> define edge Vancouver-Salt Lake
       <spans value="23"> </spans>
     </edge>
     <edge from="1"  to="8"> define edge Seattle-Urbana
       <spans value="44"> </spans>
     </edge>
     <edge from="2"  to="4"> define edge Palo Alto-Salt Lake
       <spans value="15"> </spans>
     </edge>
    <edge from="3"  to="6"> define edge San Diego-Houston
       <spans value="30"> </spans>
     </edge>
     <edge from="4"  to="9"> define edge Salt Lake-Ann Arbor
       <spans value="33"> </spans>
     </edge>
     <edge from="4"  to="5"> define edge Salt Lake-Boulder
       <spans value="11"> </spans>
     </edge>
     <edge from="5"  to="6"> define edge Boulder-Houston
       <spans value="23"> </spans>
     </edge>
     <edge from="5"  to="7"> define edge Boulder-Lincoln
       <spans value="10"> </spans>
     </edge>
     <edge from="6"  to="13"> define edge Houston-College Park
       <spans value="29"> </spans>
```

```
   </edge>
   <edge from="6"  to="11"> define edge Houston-Atlanta
     <spans value="16"> </spans>
   </edge>
   <edge from="7"  to="8"> define edge Lincoln-Urbana
     <spans value="10"> </spans>
   </edge>
   <edge from="8"  to="10"> define edge Urbana-Pittsburgh
     <spans value="10"> </spans>
   </edge>
   <edge from="9"  to="12"> define edge Ann Arbor-Ithaca
     <spans value="9"> </spans>
   </edge>
   <edge from="9"  to="14"> define edge Ann Arbor-Princeton
     <spans value="12"> </spans>
   </edge>
   <edge from="9"  to="10"> define edge Ann Arbor-Pittsburgh
     <spans value="6"> </spans>
   </edge>
   <edge from="10"  to="14"> define edge Pittsburgh-Princeton
     <spans value="7"> </spans>
   </edge>
   <edge from="10"  to="11"> define edge Pittsburgh-Atlanta
     <spans value="14"> </spans>
   </edge>
   <edge from="12"  to="15"> define edge Ithaca-Boston
     <spans value="7"> </spans>
   </edge>
   <edge from="12"  to="13"> define edge Ithaca-College Park
     <spans value="7"> </spans>
   </edge>
   <edge from="13"  to="14"> define edge College Park-Princeton
     <spans value="4"> </spans>
   </edge>
   <edge from="14"  to="15"> define edge Princeton-Boston
     <spans value="5"> </spans>
   </edge>
</edges>

  <ORs>
     <OR index="0" >
       <adjacent value="1"> adjacent to   OR1 </adjacent>
       <adjacent value="4"> adjacent to   OR4 </adjacent>
     </OR>
     <OR  index="1" >
       <adjacent value="0"> adjacent to   OR0 </adjacent>
       <adjacent value="2"> adjacent to   OR2 </adjacent>
       <adjacent value="3"> adjacent to   OR3 </adjacent>
       <adjacent value="8"> adjacent to   OR8 </adjacent>
     </OR>
     <OR index="2" >
       <adjacent value="1"> adjacent to   OR1 </adjacent>
     <adjacent value="3"> adjacent to   OR3 </adjacent>
     <adjacent value="4"> adjacent to   OR4 </adjacent>
     </OR>
     <OR index="3" >
       <adjacent value="1"> adjacent to   OR1 </adjacent>
       <adjacent value="2"> adjacent to   OR2 </adjacent>
       <adjacent value="6"> adjacent to   OR6 </adjacent>
     </OR>
     <OR index="4" >
       <adjacent value="0"> adjacent to   OR0 </adjacent>
       <adjacent value="2"> adjacent to   OR2 </adjacent>
       <adjacent value="5"> adjacent to   OR5 </adjacent>
       <adjacent value="9"> adjacent to   OR9 </adjacent>
```

```
    </OR>
    <OR index="5" >
       <adjacent value="4"> adjacent to   OR4 </adjacent>
       <adjacent value="6"> adjacent to   OR6 </adjacent>
       <adjacent value="7"> adjacent to   OR7 </adjacent>
    </OR>
    <OR index="6" >
       <adjacent value="3"> adjacent to   OR3 </adjacent>
       <adjacent value="5"> adjacent to   OR5 </adjacent>
       <adjacent value="11"> adjacent to   OR11 </adjacent>
       <adjacent value="13"> adjacent to   OR13 </adjacent>
    </OR>
    <OR index="7" >
       <adjacent value="5"> adjacent to   OR5 </adjacent>
       <adjacent value="8"> adjacent to   OR8 </adjacent>
    </OR>
    <OR index="8" >
       <adjacent value="1"> adjacent to   OR1 </adjacent>
       <adjacent value="7"> adjacent to   OR7 </adjacent>
       <adjacent value="10"> adjacent to  OR10 </adjacent>
    </OR>
    <OR index="9" >
       <adjacent value="4"> adjacent to    OR4 </adjacent>
       <adjacent value="10"> adjacent to   OR10 </adjacent>
       <adjacent value="12"> adjacent to   OR12 </adjacent>
       <adjacent value="14"> adjacent to   OR14 </adjacent>
    </OR>
    <OR index="10" >
       <adjacent value="8"> adjacent to    OR8 </adjacent>
       <adjacent value="9"> adjacent to    OR9 </adjacent>
       <adjacent value="11"> adjacent to   OR11 </adjacent>
       <adjacent value="14"> adjacent to   OR14 </adjacent>
    </OR>
    <OR index="11" >
       <adjacent value="6"> adjacent to   OR6 </adjacent>
       <adjacent value="10"> adjacent to  OR10 </adjacent>
    </OR>
    <OR index="12" >
       <adjacent value="9"> adjacent to    OR9 </adjacent>
       <adjacent value="13"> adjacent to   OR13 </adjacent>
       <adjacent value="15"> adjacent to   OR15 </adjacent>
    </OR>
    <OR index="13" >
       <adjacent value="6"> adjacent to    OR6 </adjacent>
       <adjacent value="12"> adjacent to   OR12 </adjacent>
       <adjacent value="14"> adjacent to   OR14 </adjacent>
    </OR>
    <OR index="14" >
       <adjacent value="9"> adjacent  to   OR9 </adjacent>
       <adjacent value="10"> adjacent to   OR10 </adjacent>
       <adjacent value="13"> adjacent to   OR13 </adjacent>
       <adjacent value="15"> adjacent to   OR15 </adjacent>
    </OR>
    <OR index="15" >
       <adjacent value="12"> adjacent to   OR12 </adjacent>
       <adjacent value="14"> adjacent to   OR14 </adjacent>
    </OR>
 </ORs>

</topology>


<OWs>
  <OW index="0">
  <active           value  ="1">  trigger this workstation </active>
```

```
    <background       value  ="1">   not a background wk </background>
    <target           from ="0"  to ="15"> the set of destinations </target>
    </OW>
  <OW index="1">
    <active           value  ="1">  trigger this workstation </active>
    <background       value  ="1">   not a background wk </background>
    <target           from ="0"  to ="15"> the set of destinations </target>
    </OW>
       ...
  <OW index="159">
    <active           value  ="1">  trigger this workstation </active>
    <background       value  ="1">   not a background wk </background>
    <target           from ="0"  to ="15"> the set of destinations </target>
    </OW>
  </OWs>

</configure>
```

APPENDIX C

Matlab Code for Counting FWM Mixing Terms

Function wave_combines returns all FWM mixing terms which can generate noise on a lightpath

```
function ret_index = wave_combines(fwm_freq,freqs)
 store        = zeros(1,3);
 ret_index    = zeros(1,4);

 size = length(freqs);    full_size = 2*size;
 all_freqs = zeros(1,full_size);
 for i=1:size
    all_freqs(2*i-1)   = -freqs(i);
    all_freqs(2*i)     = freqs(i);
 end;
 all_freqs = sort(all_freqs);

 index  = 1;

 for i=1:full_size
    for j=1:full_size
        for k=1:full_size
            fi = all_freqs(i);
            fj = all_freqs(j);
            fk = all_freqs(k);

            if (fi+fj+fk==fwm_freq)
              if valid_FWM(fi,fj,fk)
                if ~search_store(fi,fj,fk,store)  % check whether already in store
                  store(index,1) = fi;
                  store(index,2) = fj;
                  store(index,3) = fk;
                  [pump_i pump_j pump_k dgen] = FWM_pumps(fi,fj,fk);   %sort them
                  ret_index(index,1)          = search_fs(pump_i,freqs);
                  ret_index(index,2)          = search_fs(pump_j,freqs);
                  ret_index(index,3)          = search_fs(abs(pump_k),freqs);
                  ret_index(index,4)          = dgen;
                  index                       = index+1;
                end
              end
            end
        end
    end
 end
```

Auxiliary functions

```
function suc = valid_FWM(fi,fj,fk)
 suc    = 1;
 vs     = sort([fi,fj,fk]);
 if (-vs(1)==vs(2)|| -vs(1)== vs(3)) %excluding SPM and XPM
    suc =0;
 end


function found = search_store(fi,fj,fk,store)
 found = 0;
 [rows,cols]= size(store);

 for i=1:rows
    if equal_combination(fi,fj,fk,store(i,:))
        found =1;
    end
 end

function equal = equal_combination(fi,fj,fk,record)
 tmp1 = sort([ fi,fj,fk]); tmp2 = sort(record);
```

```
 if (tmp1(1)==tmp2(1)) && tmp1(2)==tmp2(2) && tmp1(3)== tmp2(3))
   equal =1;
 else
   equal =0;
 end

function id = search_fs(f,fs)
  id = -1;
  for i=1:length(fs)
      if (fs(i)== f) id =i;
      end
  end
```